Dissertation zur Erlangung des Doktorgrades
der Fakultät für Chemie und Pharmazie
der Ludwig-Maximilians-Universität München

Synthesis and Characterization of Novel *Tropos*-Systems for Stereodynamic Catalysis

Lena Carina Mayer

aus

Heidenheim an der Brenz, Deutschland

2024

Erklärung:

Diese Dissertation wurde im Sinne von § 7 der Promotionsordnung vom 28. November 2011 von Herrn **Prof. Dr. Oliver Trapp** betreut.

Eidesstattliche Versicherung:

Diese Dissertation wurde eigenständig und ohne unerlaubte Hilfe erarbeitet.

München, den 03.03.2024

_____

(Lena Carina Mayer)

Dissertation eingereicht am:	12.01.2024
Erstgutachter/in:	Prof. Dr. Oliver Trapp
Zweitgutachter/in:	Prof. Dr. Anja Hoffmann-Röder
Mündliche Prüfung am:	28.02.2024

Für meine Eltern.

Abstract

A major challenge for the production of modern pharmaceuticals is the synthesis of enantiomerically pure active substances. Such stereoselective reactions are frequently carried out with chiral catalysts, which often are expensive to produce and require subsequent purification. *Tropos* ligands are an interesting approach to this challenge. The here presented alternative to enantiomerically pure, rigid catalysts combines a flexible biphenyl backbone with an interaction-unit that is able to form non-covalent interactions and thus enables alignment of the ligand. Consequently, asymmetric hydrogenations catalyzed by the presented ligands – complexed with rhodium – are possible. By mimicking naturally occurring hydrogen bonding motives, for example in polypeptides, novel interaction-units based on L-amino acids such as alanine and valine were developed, with which new *tropos* biphenyl-bisphosphinite ligands were synthesized and characterized. Alignment of the interaction-units *via* intramolecular recognition, enabled through non-covalent interactions, leads to diastereomeric enrichment of one ligand rotamer. The orientation of the biphenyl axis, which transfers its chiral information to a rhodium metal complex, controls the stereoselectivity in the subsequent hydrogenation of prochiral olefins. One of the presented ligands made it possible, through spontaneous self-alignment to preferentially produce both the *S*-enantiomer of methyl 2-acetamidoacrylate (MAA) and the *R*-enantiomer of the same compound.

For the unique autocatalytic reaction according to SOAI, the development of a design for self-adaptable catalysts plays a major challenge. Biarylic intramolecular hemiacetals are of particular interest as they are in a dynamic equilibrium between their open (hydroxyaldehyde) and closed (hemiacetal) forms. This class of compounds has the potential to act as both substrate and catalyst in a potential new autocatalytic reaction. Therefore, biphenyl structures decorated with two aldehyde and two hydroxyl functions at the 2,6- and 2',6'-positions were synthesized. These can transition from the *tropos* structure of the biphenyl to the *atropos* form of the hemiacetal by spontaneous intramolecular cyclization and prevent rotation around the σ-axis. Therefore, such a new dynamic biaryl was synthesized and characterized. Analysis by chiral HPLC-MS identified a lactone species in the same measurement as the hemiacetal. The enantiomerization barriers of both were determined by dynamic HPLC (DHPLC) experiments and subsequently the interconversion barriers as well.

Kurzzusammenfassung

Eine große Herausforderung für die Herstellung von modernen Pharmazeutika stellt die Synthese von enantiomerenreinen aktiven Substanzen dar. Stereoselektive Reaktionen werden häufig unter Zuhilfenahme von chiralen Katalysatoren durchgeführt, die aufwendig und teuer hergestellt und anschließend aufgereinigt werden müssen. *Tropos*-Liganden sind ein interessanter Ansatz sich dieser Aufgabe zu stellen. Die hier vorgestellte Alternative zu starren enantiomerenreinen Katalysatoren kombiniert ein flexibles Biphenyl-Rückgrat mit einer Interaktionseinheit, die durch intramolekulare nicht-kovalente Wechselwirkungen eine Ausrichtung des Liganden ermöglicht. Dies ermöglicht die asymmetrische Hydrierungen mithilfe eines Rhodium-Komplexes dieser Liganden. Durch die Nachahmung von Wasserstoffbrückenbindungen, die in der Natur beispielsweise in Polypeptiden vorkommen, wurden neuartige Selektoreinheiten auf Basis von L-Aminosäuren, wie Alanin und Valin, entwickelt, mit denen neue *tropos* Biphenyl-Bisphosphinitliganden synthetisiert und charakterisiert wurden. Die Ausrichtung der Selektoreinheit über Erkennung – vermittelt durch nicht-kovalente Wechselwirkungen – führt zur Anreicherung eines Ligandenrotamers. Die Ausrichtung der Biphenylachse, welche ihre chirale Information auf einen Rhodiumkomplex überträgt, kontrolliert dabei die Stereoselektivität in der anschließenden Hydrierung prochiraler Olefine. Einer der synthetisierten Liganden ermöglichte es durch spontane Selbstausrichtung, sowohl das *S*-Enantiomer von Methyl 2-acetamidoacrylat (MAA) als auch das *R*-Enantiomer der gleichen Verbindung bevorzugt herzustellen.

Für die einzigartige autokatalytische Reaktion nach SOAI spielt die Entwicklung eines Designs für selbstanpassbare Katalysatoren eine große Herausforderung. Biarlyische intramolekulare Halbacetale sind hierbei von besonderem Interesse, da sie sich in einem dynamischen Gleichgewicht zwischen ihrer offenen (Hydroxyaldehyd) und ihrer geschlossenen (Halbacetal) Form befinden. Diese Verbindungsklasse könnte somit sowohl als Substrat als auch als Katalysator in einer potentiellen neuen autokatalytischen Reaktion fungieren. Deshalb wurden Biphenylstrukturen welche je zwei Aldehyd- und Hydroxyfunktionen an 2,6- und 2‘,6‘-Position enthielten, synthetisiert. Diese können von der *tropos* Struktur des Biphenyls durch spontane intramolekulare Zyklisierung in die *atropos* Form des Halbacetals übergehen und somit die Rotation um die σ-Achse unterbinden. Daher wurde ein solches neues dynamisches Biaryl, synthetisiert und charakterisiert. Die Analyse mithilfe von chiraler HPLC-MS offenbarte neben dem Halbacetal auch eine Lactonspezies in derselben Messung. Von Beiden wurde mitels dynamischer HPLC-Experimenten die Enantiomerisierungsbarrieren, sowie anschließend auch die Interkonversionsbarrieren bestimmt.

Scientific Contributions

During this dissertation, scientific contributions in form of publications and poster presentations were made, with parts being represented in this thesis.

Publications:

Lena C. Mayer, Simone Heitsch, Oliver Trapp, *Acc. Chem. Res.* **2022**, *55*, *23*, 3345-3361.

Nonlinear Effects in Asymmetric Catalysis by Design: Concept, Synthesis and Applications.

Simone Heitsch, Lena C. Mayer, Yanis L. Pignot, Oliver Trapp, *Chirality* **2023**, *35*, 549-561.

Synthesis and stereodynamics of intramolecular hemiacetals in biaryl aldehyde-alcohols.

Poster Presentation:

L. C. Mayer, J.-M. Menke, O. Trapp, Chirality, Chicago (USA), July 2022.

Synthesis of L-Amino Acid Based *tropos* Ligand for Transition Metal Catalysis.

List of Abbreviations

Ac	Acetate
acac	Acetylacetone
Ac_2O	Acetic anhydride
ACT	activated
Ala	Alanine
AUX	auxiliary
BINAM	1,1′- binaphthyl-2,2′-diamine
BINAP	2,2′-bis(diphenylphosphino)-1,1′-binaphthyl)
BINOL	1,1′-Bi-2-naphthol
B_2pin_2	Bis(pinacolato)diboron
boc	*tert*-Butyloxycarbonyl
Brine	saturated aqueous solution of NaCl
t-BuLi	*tert*-Buthyllithium
CAT	catalyst
Calc.	calculated
COD	1,5-Cyclooctadien
COMU	(1-Cyano-2-ethoxy-2-oxoethylidenaminooxy)dimethylamino-morpholino-carbenium hexafluorophosphate
Cp*	1,2,3,4,5-Pentamethylcyclopentadien
CPA	chiral phosphoric acids
DCM	Dichloromethane
dg	degassed
DHPLC	dynamic HPLC
DIPEA	*N*,*N*-Diisopropylethylamine
DME	Dimethyl ether
DMEA	Dimethylethanolamine
DMEDA	1,2-Dimethylethylenediamine
DMF	Dimethylformamide
DMSO	Dimethyl sulfoxide

EDCI	1-Ethyl-3-(3-dimethylaminopropyl)carbodiimide
equiv	Equivalent
EtOAc	Ethyl acetate
HOBt	1-Hydroxybenzotriazole
Leu	Leucine
MAA	Methyl 2-acetamidoacrylate
MAC	*N*-acetylphenylalanine methyl ester
MOM	Methoxymethyl ether
$Pd(dppf)Cl_2$	[1,1'-Bis(diphenylphosphino)ferrocene]palladium(II) dichloride
Pent	*n*-Pentane
Prol	Proline
rt	room temperature
SPhos	Dicyclohexyl(2′,6′-dimethoxy[1,1′-biphenyl]-2-yl)phosphane
TBTA	Tris(benzyltriazolylmethyl)amine
Tf	Triflate
TFA	Trifluoroacetic acid
THF	Tetrahydrofurane
Val	Valine

Table of Content

Table of Figures

Table of Schemes

List of Tables

1 Introduction

1.1 Atropisomerism

Optical activity resulting from axial chirality was first identified by CHRISTIE and KENNER in 1922.[1] The term *atropisomerism* originates from the greek *a* = not and *tropos* = turn and was primarily introduced by KUHN in 1933 to describe biaryl compounds exclusively.[2] The requirements for axial chirality in biaryls is a rotational axis as well as the presence of different substituents (see Figure 1) on each side of the axis (**I**).[3] A C_2 symmetry is present, if A≠B and A'≠B' (**II**). Heteroaromatics can induce chirality by the arrangement of the heteroatom alone, even if A = B (**III**).[4] Moreover, axial chirality can be introduced with four identical substituents, if they are bridged, as shown in the D_2 symmetric diether **IV**.[5]

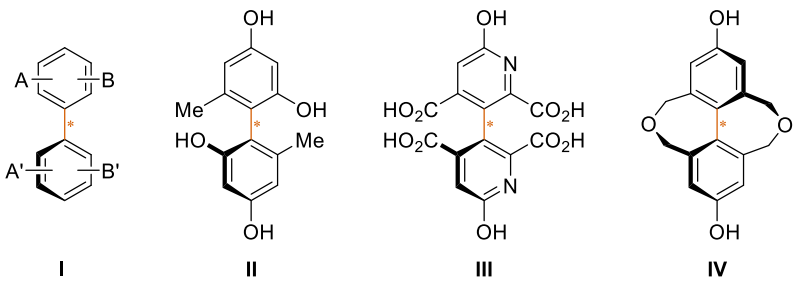

Figure 1: Different biaryl systems showing axial chirality.[3]

On the one hand, the rotational stability of the biaryl axis is another qualification for *atropisomerism*. Low steric hindrance of the substituents and therefore poor rotational stability can be bypassed by cooling to low temperatures, in order to differentiate between the two atropisomers.[6] On the other hand, biaryl species that are stabilized at room temperature (rt) can change into an equilibrium between two atropoenantiomers, when heated.[7] The temperature and the associated interconversion barrier are therefore important components for the definition of atropisomerism[3] A proposed criterion for the separability of atropisomers by ŌKI was a half-life ($t_{1/2}$)>1000 s for rotation around the axis at the set temperature.[8] The following three main factors are fundamental for the configurational stability of axially chiral biaryl compounds: Firstly, the sterical hindrance of substituents close to the axis, secondly, the presence of bridges as well as their length and rigidity and thirdly, physical rotation around the axis, induced by (photo-)chemical atropisomerization mechanisms.[3] For the nomenclature of atropisomers, CAHN-INGOLD-PRELOG rules such as *R* (R_a) and *S* (S_a) are applied, as well as *P* (positive helix) and *M* (negative helix), are used following the chirality rule.[9] Generally, a wider interest regarding atropism arose since the 1980s. The discovery of the BINAP (2,2'-bis(diphenylphosphino)-1,1'-binaphthyl) structure and its application in asymmetric

hydrogenation reactions, catalyzed by rhodium,[10] demonstrated the capability of atropisomers as sole source for stereo control.[11] This stimulated further development of asymmetric catalysis and today a selection of ligands reaching from BINOL (1,1′-binaphthyl-2,2′-diol) over BINAM ((1,1′- binaphthyl-2,2′-diamine) to chiral phosphoric acids derived from BINOL (CPA) are available (see Figure 2).[11]

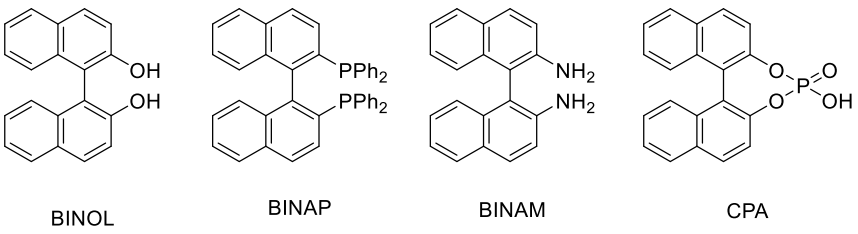

Figure 2: Examples of important binaphtyl molecules.[11]

The variability in applications of atropisomers is very wide. They range from molecular machines[12],[13],[14] over chiroptical switches,[15] host-guest chemistry[16] to atropisomeric receptors.[17]

1.1.1 Classification of Atropisomers

The overall stability of different atropisomers varies depending on their rotational barrier which again correlates to their substitution pattern. Different approaches have been made to further investigate the bond rotation in rotationally restricted compounds. Applied analytical methods for these studies were temperature dependent NMR spectroscopy, HPLC with chiral stationary phases and chromatographic separation with subsequent analysis of epimerization.[18] HUCKE *et al.* proposed a classification system based on the correlation between the rotational barrier and the half-life ($t_{1/2}$) of different compounds.[19]

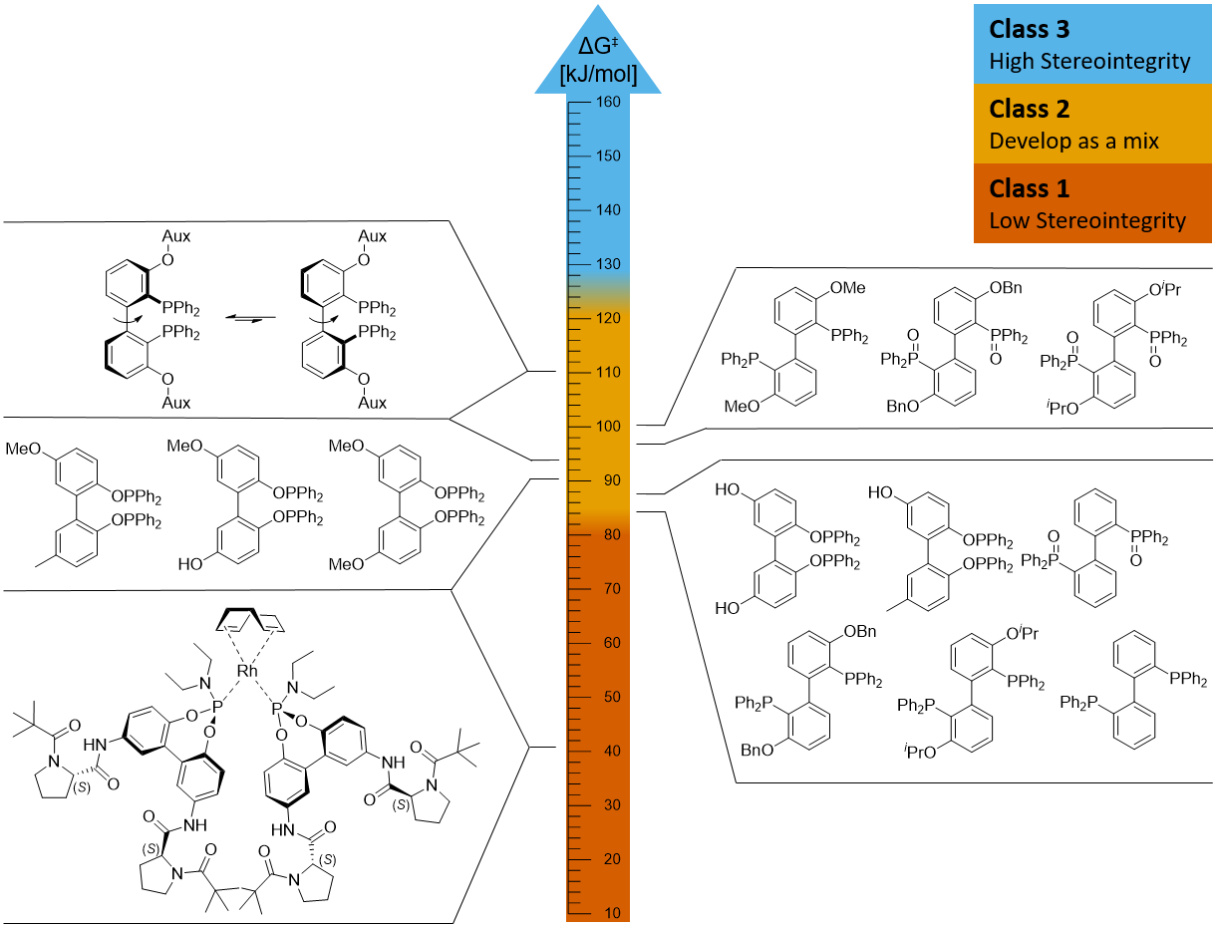

Figure 3: Classification of atropisomers in relation to rotational barriers in accordance to HUCKE.

Class one (see Figure 3) does not show atropisomeric properties due to low stereointegrity. Its compounds have free rotation around the chiral axis, meaning axial rotation in order of seconds or faster and rotational energy barriers (ΔE_{rot}) <≈84 kJ mol^{-1}. Therefore, no axial chirality is exhibited and single compounds are obtained in synthesis. Class two bears potential atropisomers with ΔE_{rot} >≈84 kJ mol^{-1}. They show stability of $t_{1/2}$ in the range of minutes and longer. Based on the stability of one rotamer, a further distinction into class three can be made. Compounds in this class have rotational barriers of ΔE_{rot} >≈125 kJ mol^{-1} which correlates to $t_{1/2}$ in the order of years due to very slow axial rotation and high stereointegrity.[19],[20]

1.1.2 Types of Racemization of Atropisomers

Racemization describes the macroscopic process in which enantiopure/enantioenriched compounds become racemic (see Figure 4), while enantiomerization describes the microscopic process of reversible switching of molecules configuration (e.g. *R* to *S*).[21]

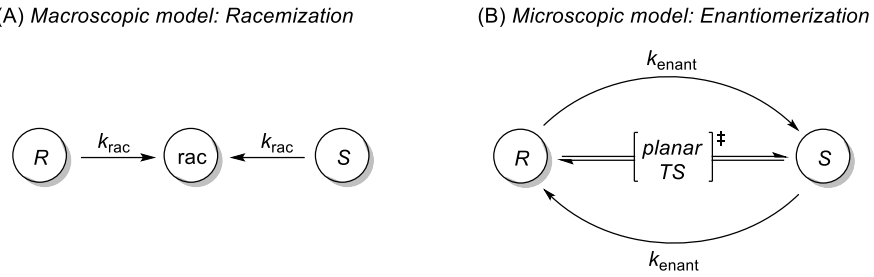

Figure 4: A: Process of racemization with rate constant of racemization k_{rac}; B: Process of enantiomerization with rate constant of enantiomerization k_{enant}.[21]

Atropisomers can rotate around their chiral axis and therefore convert from one atropisomer to the other. Depending on the rotational barrier, they can enantiomerize thermally through bond rotation. If the barrier is too high, compounds will decompose before racemization.[22] Moreover, optical purity of some (biphenyl) atropisomers can be decreased photochemically.[23],[24] CRUMRINE *et al.* showed that the thermally stable 2,2'-dimethyl-6,6'-diethylbiphenyl ($t_{1/2}$=283 and 25 h by temperatures of 345 and 380 °C, respectively) could be racemized by photolysis.[25]

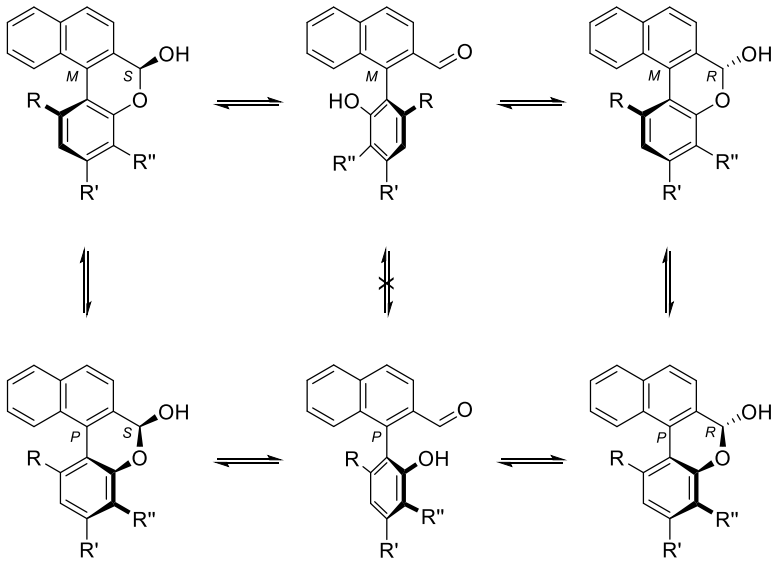

Scheme 1: Atropisomerization via helically twisted lactoles.[26]

Moreover, the formation of a bridge can lead to enantiomerizing biaryl lactones.[27] BRINGMANN *et al.* described lactol-bridged cyclic forms that engage in atropisomerization of helically twisted lactols. The isomerization process between hydroxyl aldehydes and isomeric lactones is shown in Scheme 1. Selective cleavage of these lactones with chiral nucleophils can be utilized as stereoselective synthesis.[26]

An asymmetric synthesis for highly hindered biaryl compounds was thus developed by BRINGMANN *et al.*[3] For this approach, lactone-bridged biaryls are used to induce chiral information. The synthesis starts with the pre-fixation of ortho-bromobenzoic acid and phenols in step (i) in Scheme 2. The resulting bromoester is converted into the

configurationally unstable biaryl lactone by Pd(2)-catalyzed aryl-aryl coupling (ii). The final cleavage of the bridged lactone (iii) by chiral *N*-, *O*- and *H*-nucleophiles enables atropoenantio- or atropodiastereoselective biaryl products.[3]

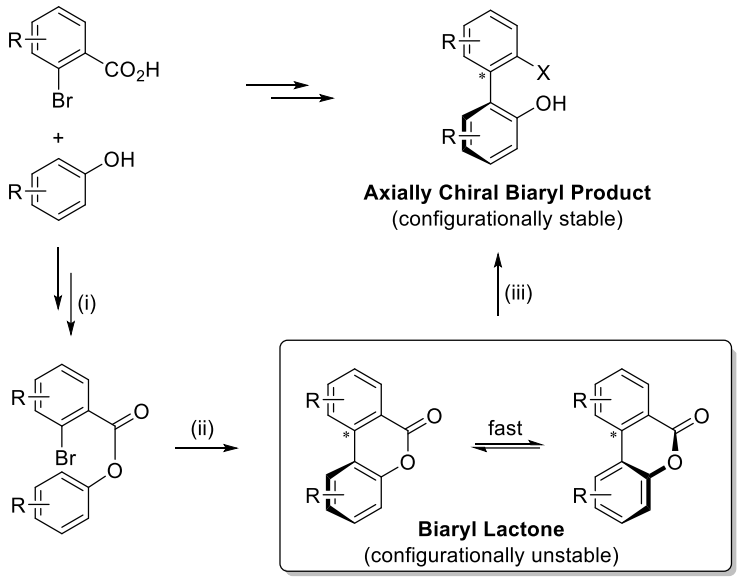

Scheme 2: Lactone concept by BRINGMANN. (i) Pre-fixation, (ii) nonstereoselective biaryl coupling and (iii) atroposelective lactone cleavage.[3]

The *ortho*-substituent next to the axis usually had no influence regarding the direction of the transferred chirality, though different sizes of substituents were tested. This make the ring opening reactions an efficient and optically pure approach to obtain the desired configuration.[3] Furthermore, BRINGMANN´s lactones can undergo atropoenantioselective transesterifications with amine thiourea as promotor.[28]

1.2 Asymmetric Catalysis

For a long time, the selective synthesis of asymmetric centers was not possible, which meant that racemic mixtures had to be resolved. This is not only an elaborate process but also very costly. Therefore, there is a great need of catalysts forming predominantly one isomer.[29] It is still largely impossible to predict the best possible catalyst for a specific reaction, despite the greatest efforts and advances in theoretical chemistry due to the small energy differences in the competing transition states. The design of new catalysts is therefore still somewhat dependent on trial and error.[30]

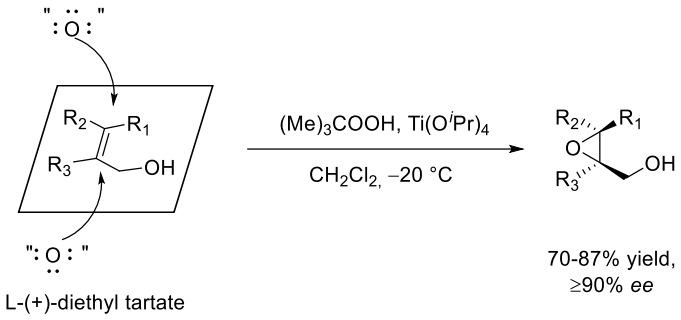

Figure 5: Asymmetric activation by Sharpless.[31]

One of the pioneers in this field was SHARPLESS with a new approach to asymmetric transformations. Specifically, his group designed a new way of catalytic asymmetric epoxidation reactions, illustrated in Figure 5.[31] The theoretical background of asymmetric activation states, that an achiral precatalyst can be transformed into an asymmetric catalyst through ligand exchange with a chiral Ligand L* (see Figure 6). SHARPLESS *et al.* emphasized the necessity of "ligand-accelerated catalysis" in homogeneous catalysis.[32] The analogue in heterogeneous catalysis would be "chiral modification"[33],[34] which is used to describe the modification of an achiral catalyst by applications of a chiral modifier to the surface.

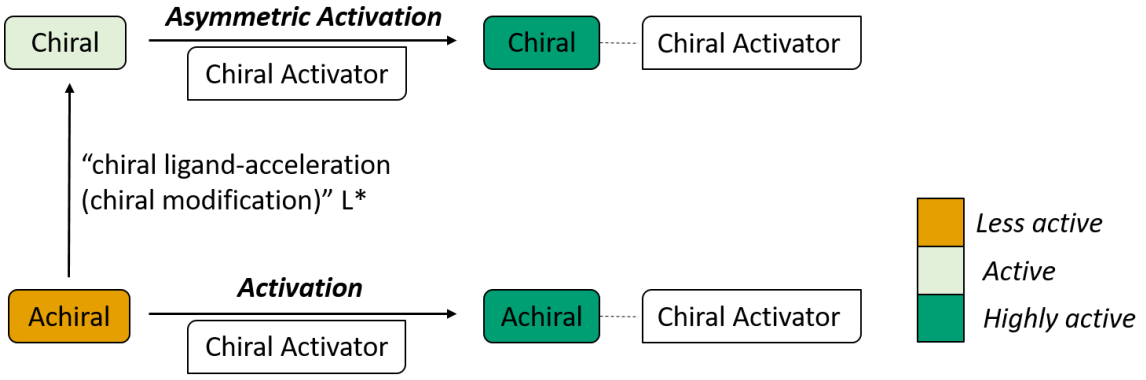

Figure 6: Principle of Asymmetric Activation.

The addition of chiral activators can enhance the activity of both homo- and heterogenous chiral catalysts. The term "asymmetric activation" was coined to describe this process in which e.g. the activation of an achiral reagent, such as activated zinc was achieved.[35],[36] An alternative to enantiopure catalysts is the use of stereochemically flexible ligands. For example the tuning of the flexible *tropos* catalysts with chiral activators leads to a shift from the equilibrium of the racemic mixture of the two ligand enantiomers and the formation of diasteriomeric complexes.[35] Schematic description of the different activation modes of flexible *tropos* catalysts are given in Scheme 3.

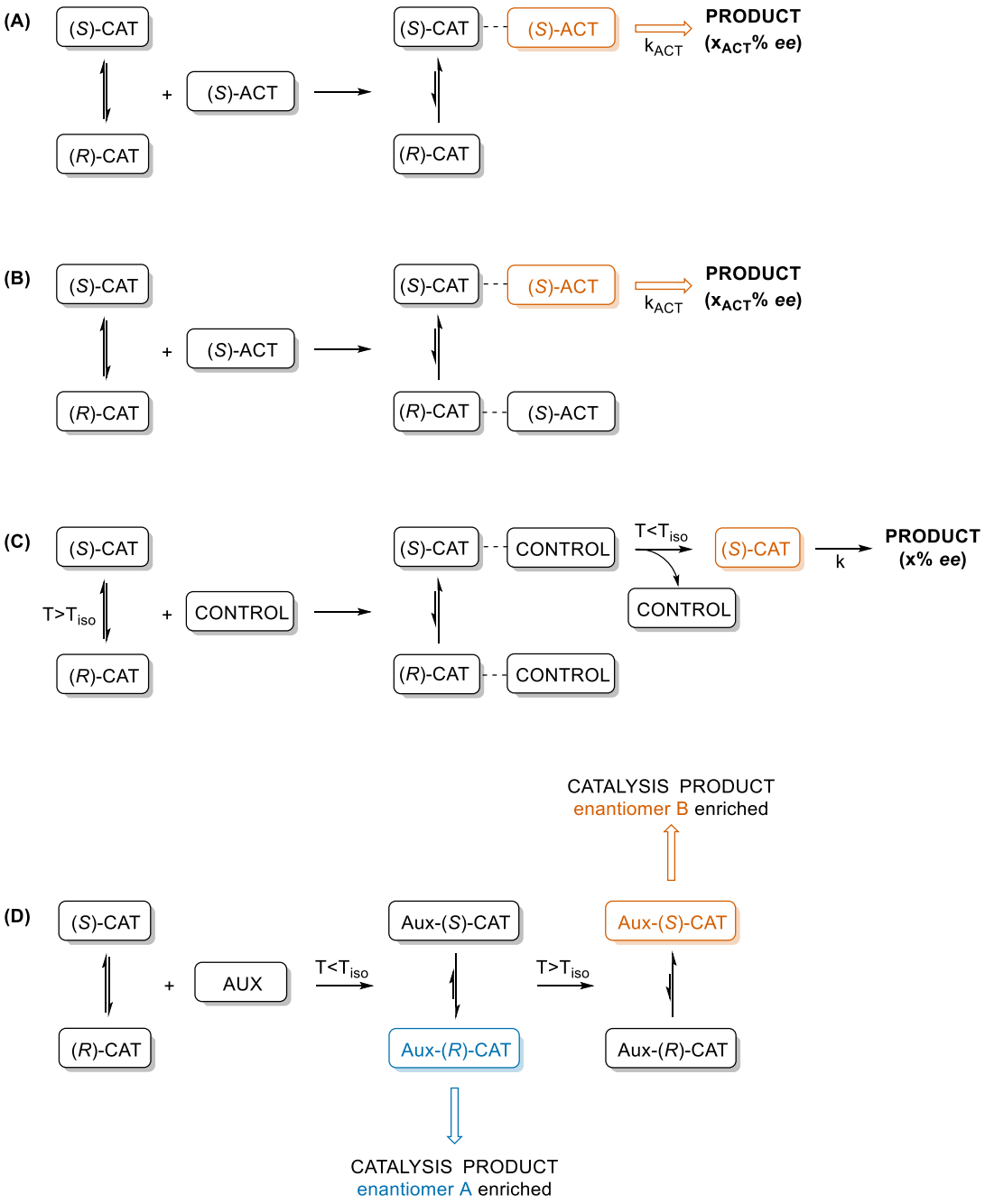

Scheme 3: Overview of chiral activation for *tropos* ligands. (A) Diasteriomeric adduct is formed selectively. (B) Diasteriomeric adducts are formed nonselectively. One adduct is active. (C) Diasteriomeric adducts are formed nonselectively. One enantiomer is enriched before catalysis. (D) Diasteriomeric adducts are formed nonselectively followed by enrichment of one enantiomer depending on reaction condition.

In activation method (A) (Scheme 3) only one enantiomer gets activated by the addition of an additive while both isomers form adducts in method (B). However, in the latter one enantiomer forms more active adducts with the additive resulting in selective product formation. Some additives are able to control enrichment of one enantiomer of the catalysts before its application in catalysis, illustrated in path (C) of Scheme 3. Another

way of chiral activation is the control by complexation with an auxiliary which leads to enrichment of one enantiomer by reaction control see Scheme 3 (D).[37],[38]

1.3 Asymmetric Hydrogenation

Asymmetric hydrogenation is one of the main applications of transition-metal catalysis in industry and has therefore caused high interest in academia.[30] It started during the mid-1960s, when WILKINSON discovered chloro-tris(triphenylphosphine)rhodium [$RhCl(PPh_3)_3$] as a soluble hydrogenation catalyst which was the first competitive catalyst in terms of conversion rates against its heterogenous counterparts (Scheme 4, A).[29],[39] Other optically active phosphines were developed by HORNER[40],[41] and MISLOW[42], for which WILKINSON´s catalyst was replaced by asymmetric phosphines to hydrogenate prochiral olefins.[29] It soon became obvious that the right choice of ligand for each substrate is essential to generate high *ee*s. In 2001, the Nobel Prize in chemistry was awarded in the field of catalytic asymmetric hydrogenation of alkenes,[43] which highlights the importance of the field, especially for industrial application. KNOWLES developed the DiPAMP ligand which upon coordination to Rh was able to hydrogenate olefines highly selectively with quantitative yield and an *ee* of 95% (see Scheme 4, B).[44] Thus, the first targeted asymmetric synthesis has contributed to the industrial scale synthesis of the drug L-DOPA, which is applied in the treatment of Parkinson´s disease.

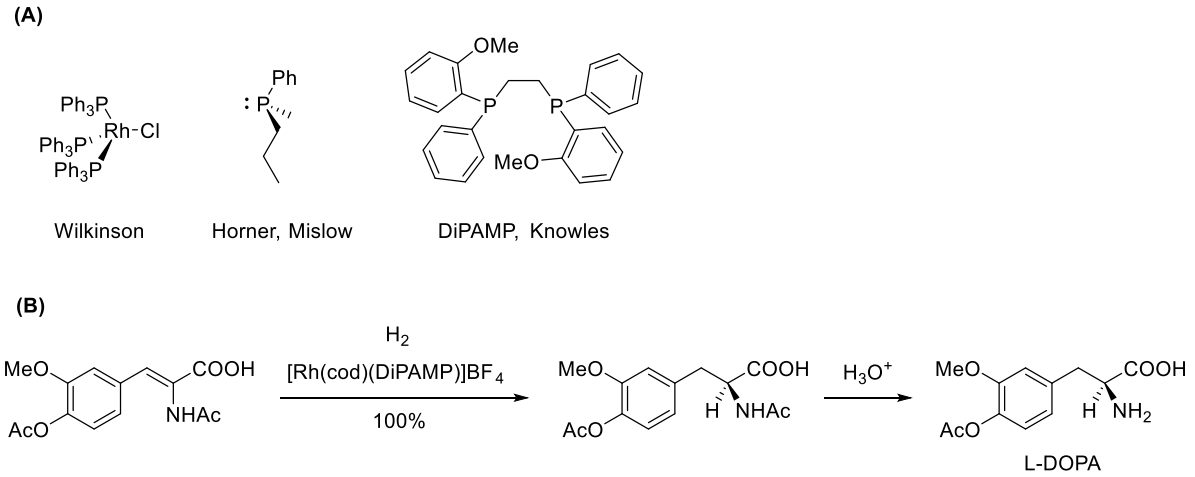

Scheme 4: (A) WILKINSON´S first Rh-catalyst, HORNER and MISLOWS ligand for asymmetric catalysis and KNOWLES DiPAMP and its application shown in (B).

After NOYORI and coworkers published both enantiomers of BINAP (see Figure 2) in 1980,[10] it found application in the industrial synthesis of the chiral menthol. With the exchange of Rh(I) with Ru(II), Ru-BINAP could be used for the industrial production of (*R*)-1,1-propanediol which was further used in the synthesis of the antibiotic levofloxacin.[45]

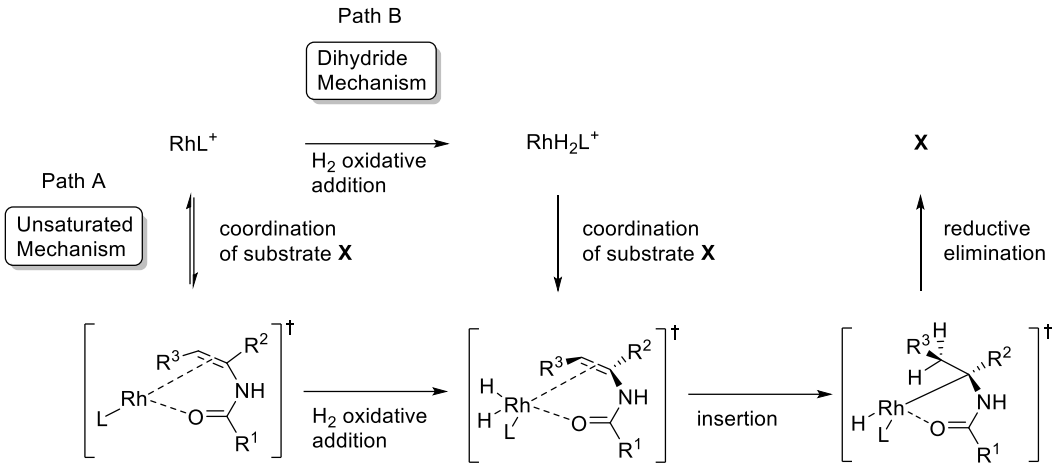

Scheme 5: Mechanism of Rh-catalyzed hydrogenation reactions. Path A: Unsaturated Mechanism, Path B: Dihydride Mechanism.[46]

It is very well investigated, that α-acetamidocinnamic acid and its derivatives can be hydrogenated with excellent enantioselectivity by (*R*)-BINAP ligand and others.[46],[47], The mechanism and the reason behind the high stereoselectivity is still part of current research. There are two proposed reaction mechanisms in the literature. Firstly, the unsaturated pathway (Path A, Scheme 5), also known as the HALPERN-LANDIS-BROWN mechanism, is characterized by the prior chelation of the Rh-catalyst with the enamide, only then H_2 is added to the transition state in an oxidative addition.[48],[49],[50] The second pathway (Pathway B, Scheme 5), the dihydride mechanism starts with the formation of rhodium dihydride with following coordination of the alkene.[51] There are several examples of X-ray crystal structures[52] supporting the unsaturated mechanism, as well as CD analyses[53] and determinations of kinetics and bonding constants between Rh catalyst and enamide through NMR[54] and UV/Vis spectroscopy.[46] The Dihydride Mechanism was supported by GRIDNEV and IMAMOTO were they described a dihydro complex with the catalyst at −95 °C. However, the complex is not proven evidence at room temperature.[55]

1.4 Supramolecular Assembly

In nature, smaller subunits often assemble into large structures as a result of various types of interactions. A well-known example is the double helix of DNA which is made possible by base-pairing.[56] Amino acids forming peptides and proteins are another good example given by nature. While non-covalent interactions are weaker (2–250 kJ mol^{-1}) than most covalent bonds (100–400 kJ mol^{-1})[57] a combination of several interaction sites can lead to stable assemblies capable of determining function and shape of the molecule. Apart from glycine, all natural amino acids have a chiral basic structure and thus are able to transfer chiral information through non-covalent interactions. Additionally, they bring different properties depending on their respective side chain. For instance, aromatic side chains can engage in π-π stacking, neutral polar ones can form hydrogen bonds.[57] Inspired by

these non-covalent interactions, chemists searched for different ways to apply them in supramolecular systems similar to nature. Supramolecular chemistry benefits from specially designed subunits that are able to selectively reorganize. This can lead to spontaneous self-assembly into organized structures.[58] Self-assembly is the spontaneous formation of ordered structures[59] through various non-covalent interactions such as VAN DER WAALS and electrostatic forces, π--π stacking as well as hydrogen bonds.[58] These types of interactions form the basis of supramolecular chemistry. The general information on how greater entities are assembled lies within the structural motifs of the respective building blocks.[57]During the 1970s CRAM, PEDERSEN and LEHN showed first examples in the field of supramolecular chemistry[58] with self-assembling systems like cryptands[60] and crown ethers[61]. Since then, multiple examples of complementary pairs of subunits have been designed and synthesized.[58]

1.5 Chiral Induction Through Non-Covalent Interaction

The enrichment of one ligand rotamer for asymmetric catalysis requires a chiral axis with a stereochemical bias.[62] This means, the racemic catalyst can interact with a chiral additive or a chiral environment. The rotamer distribution after system re-equilibration is controlled by the energy difference of the diasteriomeric adducts. A chiral trigger of re-equilibration can be inserted either by a chiral moiety which is covalently bound to the ligand or by the addition of chiral co-ligands which induce their chiral information across the shared complexed metal.[63]

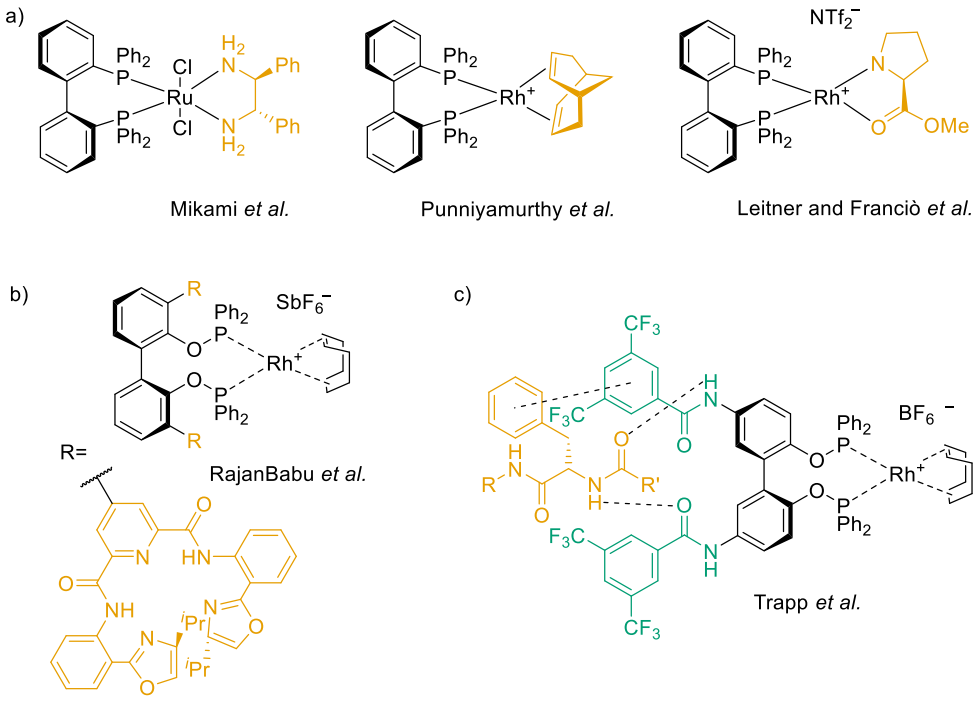

Figure 7: Different systems showing stereoinduction to be applied in asymmetric catalysis. Given examples are (a) a chiral co-ligand, (b) an auxiliary group which is chiral and (c) non-covalent interactions between a ligand-bound interaction-unit and a chiral additive inducing chiral alignment of the ligand.[63]

At a macromolecular perspective, the axial chirality of helical polymers has been modified in a similar manner, using the sergeant and soldier effect to align chiral and achiral copolymer units, [64],[63] or by tuning the stereoflexible polymers with the attachment of chiral terminal groups,[65] or *via* inclusion of chiral guest molecules.[66] The TRAPP group saw great benefits in the combination of non-covalent interactions with the concept of *tropos* biphenyl ligands. Therefore, interaction sites, directly bound to the ligand are introduced to the system and act as selector-units. When presented with matching chiral molecules (additives) the selector units interact with them non-covalently in a directed manner. Resulting diasteriomeric adducts of the two respective ligand rotamers and the additives (chiral molecules) differ in their free energy shifting the ligands equilibrium of the rotamers to re-equilibrate which results in the enrichment of one ligand rotamer. This system is beneficial because the stereoinduction and the actual catalytic side are located at opposite ends of the molecule. The non-covalent nature of the transferred chiral information further ensures its dynamic adaptation by the ligand depending on its surroundings like stereoinducing molecules and their concentration.[63] The selector units have to be well designed to provide the best possible interaction with chiral additives which enables chirality transfer and ultimately induces the spatial alignment of the whole ligand. Here, state-of-the-art selector units used in HPLC or GC columns are used as inspiration. In 2014, TRAPP *et al.* presented their first successful chirality transfer based on on-column deracemization experiments, applying chiral HPLC columns *Daicel* IA-3 and IA. Selector units were positioned at 5,5'-position of the biphenyl, because placement at the 3,3'-position would further increase the rotational barrier of the *tropos* ligand

(buttressing effect)[67] and at the 6,6′-position would make it *atropos*.[68] Directly modifying the selector units of the stereodynamic biphenyl-based ligands with interaction groups based on selectors of HPLC columns lead to further improvement of the additive-selector interactions. An applied example for the selector unit which originates from the stationary phases of *Chiralpak* IC and IE is 3,5 dichlorobenzamide.[69],[70] To further improve the system, the chiral additives are also adapted to the interaction of the chiral stationary phases (CSP). Small molecules that are known to separate well on these were used to generate a better ligand rotamer distribution. The obtained enantioselective catalyst can be used for asymmetrical hydrogenation.[71],[63]

1.6 Self-Alignment *via* Intermolecular Recognition

In nature, reoccurring privileged structures formed by amino acids in peptides and other biomelecoles are a good source of inspiration for supramolecular interactions and intermolecular recognition. Analogous coordination between amino acids has been investigated for other stereodynamic frameworks for the realization of defined supramolecular structures stabilized by non-covalent interactions.[63] Non-covalent interactions were best achieved by amino acid-based secondary diamides. They can be found in systems for chiral separation such as the CHIRASIL-Val, a high performing chiral stationary phase for GC.[72],[73] It was postulated, that the CSP mechanism works in a pincer-like manner for the coordination of small molecules like amino acid derivatives during enantioselective separation (see Figure 8).

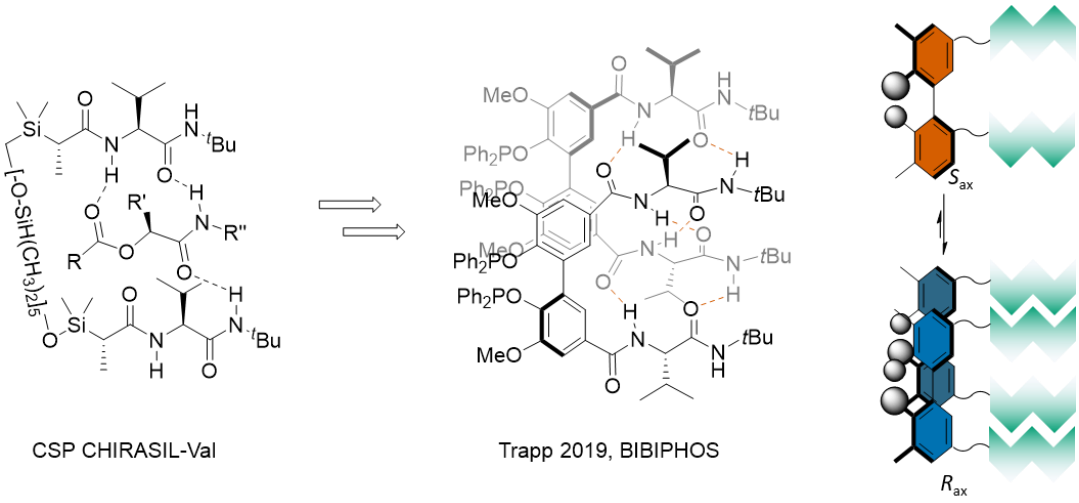

Figure 8: Interaction between CSP CHIRASIL-Val and a chiral analyte and the application of the selector-units in the BIBIPHOS ligand by Trapp.

In theory, stereoinduction should happen by chirality transfer through amino acid-derived selector units which are directly connected to a stereochemically flexible ligand backbone. In praxis, this was achieved by valine-derived selector units acting as the interaction pattern which are covalently bound to a biphenyl backbone.[63],[74] TRAPP *et al.*

developed a ligand (see Figure 8) for asymmetric hydrogenation which was able to assemble into dimers through intermolecular interactions and thus achieve an enrichment of one ligand rotamer. No further addition of chiral additives was needed. The occurring non-covalent interactions between the selector units were efficient enough to trigger spontaneous enrichment of the R_{ax} ligand rotamer for all compounds. Responsible for the highly ordered ligand dimers was an intermolecular interlocking between the selector sites of two different ligands. Selector-sites with their self-recognitive properties lead to chiral induction *via* selective stabilization and therefore cause the rotameric enrichment. The flexible ligand backbone reacts stereoconvergently. Different types of ligands, namely biphenol, bisphosphinite and phosphoramidite ligands were tested and differences between the respective self-alignment processes were found. The phosphoramidite ligands showed quantitative R_{ax}-dimer enrichment whereas bisphosphine only showed rotameric ratios of 16:84 (S_{ax} monomeric/ R_{ax} dimeric). Suitable additives were able to selectively switch that equilibrium.[75] The generated system spontaneously caused stereochemical purity, however neither in an autoinductive process, nor in a linear fashion. Rather, the concept is driven by self-origanization due to mutual alignment induced by the selectors.[63, 74-76]

1.7 Self-Alignment *via* Intramolecular Recognition

As a consequence of the previously mentioned forms of ligand alignment through non-covalent interactions by chiral additives derived by CSPs, [77] or reactions products,[75b, 78] as well as intermolecular interlocking[74] to continue the idea and further develop a system in which spatial alignment can be achieved by intramolecular interlocking.[56] TRAPP *et al.* presented a dynamic biphenyl ligand with amino acid-derived selector-sites as their selector-unit at 5,5′-position and phosphinite moieties for metal complexation (see Figure 9).

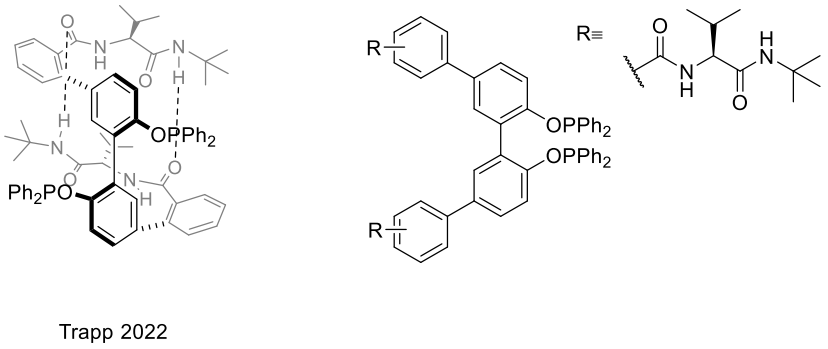

Figure 9: Phosphinite ligand which aligns through intermolecular interlocking.

By mimicking the non-covalent interactions in proteins, especially hydrogen bonding between amino acids, intramolecular recognition lead to enrichment of one axial rotamer of the ligand. Following Rh-catalyzed hydrogenation reactions with the finished catalyst

showed enantiomeric ratios of up to 96:4 (*S*:*R*) for the transformation of olefins. The ligand was further investigated and enrichment of the S_{ax} rotamer was identified. This stands in contrast to the enrichment of R_{ax}-rotamer for the BIBIPHOS ligand mentioned in chapter 1.6. Consequently, the two different ligands show inverted results for their converted olefins in hydrogenation reactions. The elongation of the ligand backbone by a phenylene bridge could cause this inversion. H-D exchange experiments supported the anticipated strong hydrogen bond formation. The importance of the right substitution pattern was proven by the introduction of the selector unit at the phenylene bridge in ortho-, metha-, and para-position. The ortho-substituted ligand was the only one which was able to align through intramolecular interactions and therefore the only one which was geometrically able to form strong hydrogen bonds. The enrichment of one diastereomer is thus not only depending on the interaction site but also on correct substitution of the whole ligand. The catalyst as a whole is only able to interlock, if the chiral axis can be fixated through interlocking and only then good *ee*s can be expected. [20],[56]

1.8 Temperature Controlled Catalysis

Due to the high flexibility of stereodynamic ligands, they can have unusual functions which need detailed kinetic investigation to identify their specific properties.[37],[38] The epimerization of different enantiomers can be controlled by different factors, as mentioned above (see Scheme 3). An example for temperature dependent catalysis was made by LEITNER and FRANCIÒ. They were able to develop an enantioselective system using *tropos* BIPHEP and combining it with a chiral ionic liquid for Rh-catalyzed hydrogenations.[79] [Rh(BIPHEP)(acac)] was combined with the enantiopure ionic liquid [HProlOMe][NTf_2] and showed a 1:1 mixture of the two rotamers at −30 °C. After heating to 50°C leads the (S_{ax})-atropisomer disappear and the irreversible formation of (R_{ax}) rotamer is enforced.[80] Another example was presented by TRAPP and STORCH, in which both enantiomers of an asymmetric hydrogenation reaction were made accessible solely by changing the applied temperature. They presented a diasteriomeric stereochemically flexible rhodium(I) catalyst which was applied in asymmetric hydrogenation of of prochiral (*Z*)-α-acetamidocinnamates and α-substituted acrylates.[37] The enantioselectivity can be changed depending on the applied temperature to generate enantiomerically pure compounds in high yield. At low temperatures, the catalyst produces (*R*)-phenylalanine derivatives in enantiomeric ratios of 87:13 (*R*/*S*) and after reequilibration of the catalyst at elevated temperatures it showed a complete shift of the formation of the corresponding (*S*)-enantiomer in ratios up to 3:97 (*R*/*S*). The design of a ligand that can be influenced by temperature requires a stereochemically flexible core, in this case a biphenyl backbone (see Scheme 6). This acts as a chiral switching unit of the whole catalyst. Moreover, it is decorated with chiral auxiliaries and a phosphinite as coordination cite for the metal. Enrichment of one diasteriomer of the ligand is achieved by bonding with a chiral auxiliary (see (I) Scheme 6). Important requirements that have

to be fulfilled by the chiral residue are the stereogenic center close to the carboxy group (linking group) in order to generate better influence on the stereoselective interaction. In addition, the enlarged aryl group helps to align the neighboring phenyl rings of the diphenylphosphine group.[81] The final catalyst is formed upon complexation with a Rh(I)-metal (see (II) Scheme 6). By exposing the catalyst to elevated temperatures, it changes the diastereomeric ratio of the rotamers and is therefore able to convert substrate into the opposite enantiomer (see (III) Scheme 6).

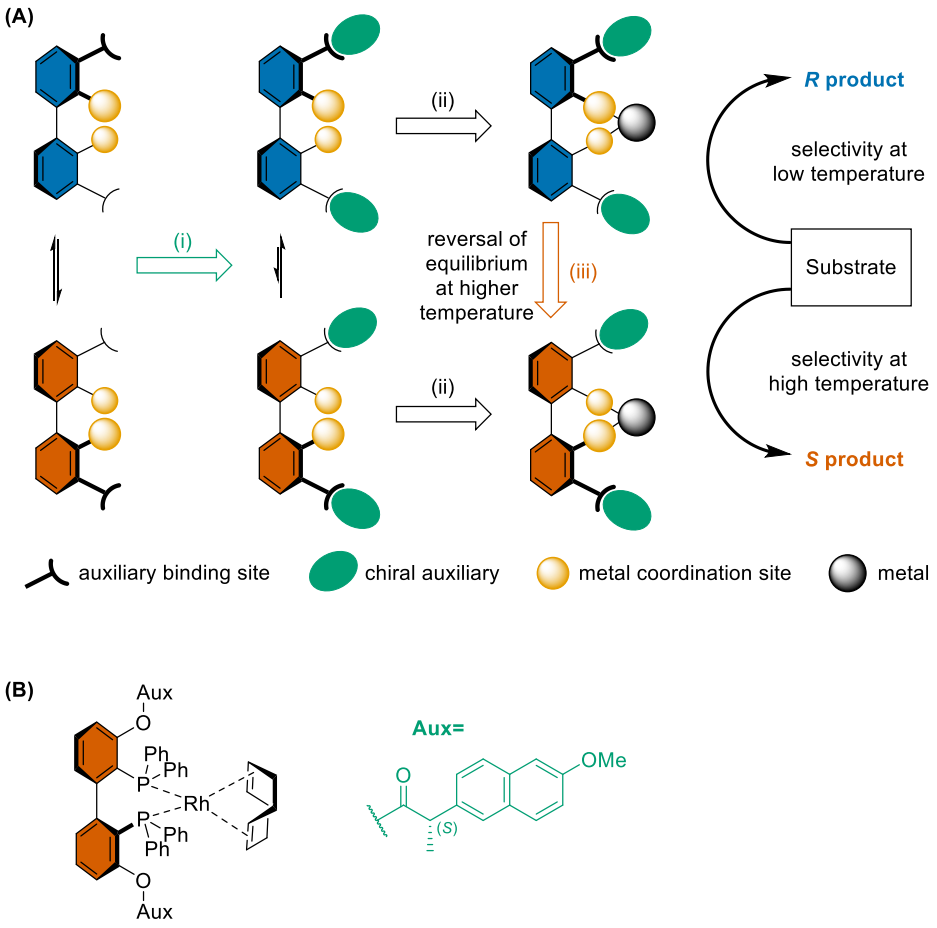

Scheme 6: Temperature depending enantioselective catalyst. (A) overall design and function: (i) enrichment of one diasteriomer by interaction with chiral auxiliary, (ii) formation of the catalyst by metal complexation, (iii) change of temperature alters the diasteriomeric ratio of the catalyst, (B) structure of the bidirectional enantioselective catalyst.

1.9 Nonlinear Effects

Not every chiral catalyst is prepared from enantiopure ligands. Sometimes, the linear relationship between the optical purity of the product and the enantiomeric purity of the catalyst can deviate, which is called a non-linear effect (NLE). In linear correlation racemic catalysts give chiral products as a racemic mixture. If there is a nonlinear relationship

between the enantiomeric excess of the product and the catalyst, a diastereomeric deviation can for example be caused by self-assembly of nonracemic catalysts. As a result, the *ee* of the catalysis product varies from linearity (schematically illustrated in Figure 10).

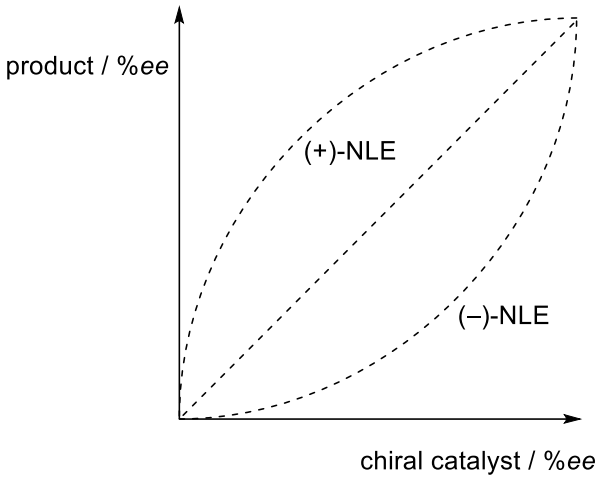

Figure 10: Correlation between enantiomeric purity of ligands and the optical purity of the product in asymmetrically induced reactions. NLE positive (+) and negative (−) are put in relation.

Thus, a higher enantiomeric enrichment of one chiral product compared to the catalyst can be achieved.[82] KAGAN *et al*.[83] as well as MIKAMI *et al.*[84] were the first to describe a convex deviation as a positive nonlinear effect ((+)-NLE). This means a higher asymmetric induction, the preference for one enantiomer to be formed, can be achieved, than with enantiopure, nonracemic catalysts.[35] Additionally, the term asymmetric amplification was introduced in the context of asymmetric addition of dialkylzinc to carbonyls which were catalyzed by chiral amino alcohols by OGUNI *et al.* for (+)-NLE (see Figure 11 Eq. (A)).[85] In the same manner, NOYORI *et al.* showed that the amino alcohol catalyst DAIB is even more efficient in producing high *ee*s for this reaction (see Figure 11 Eq. (B)).[86]

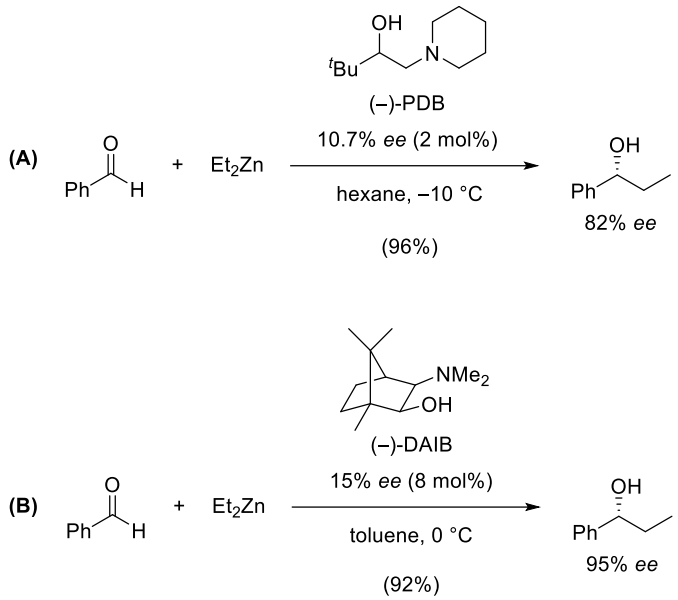

Figure 11: Two asymmetric amplifications. (A) Asymmetric carbonyl addition with 1-piperidino-3,3-dimethyl-2-butanol (PDB). (B) Use of (2S)-3-exo-(dimethylamino)-isoborneol (DAIB) for the same reaction.[35]

Moreover, they also reported the asymmetric amplification and its mechanism proposing a heterochiral dimer of the zinc amino alcohol with focus on its stability compared to the homochiral dimer. Other examples for (+)-NLE reactions are observed with BINOL-derived complexes with metals such as titanium which were published by groups of BOLM,[87] KANEMASA,[88] EVANS,[89] and KAGAN.[35, 90]

1.10 Autocatalytic Processes

The scientific community is fascinated by the origin of homochirality and its role in the origin of life on early earth. Asymmetric organo-catalytic processes could be an explanation for this phenomenon. Essential for an auto-inductive asymmetric reaction is the role of its own reaction product as participant in its formation.[75b] Additionally, a self-amplifying reaction relies a non-linear effect, otherwise the autocatalytic process would have to be 100% enantioselective.[91] As early as 1953 FRANK proposed spontaneous asymmetric synthesis by showing theoretically how two "mutually antagonistic" systems lead to instability. The undesired reaction is suppressed by the intervening product and simultaneously, the desired reaction is enhanced.[92] The growth of enantiomeric excess was successfully demonstrated by KAGAN[83] and NOYORI[93]. Other early examples were given by MIKAMI *et al.* who achieved stereoselective activation and deactivation by addition of chiral co-ligands to racemic ligands.[62] WYNBERG and FERINGA showed stereospecific phenol coupling with enantiomeric recognition and interaction and obtained homochiral dimers *via* dimerization of camphor.[94],[95] One very famous example of self-amplification and autocatalysis is the SOAI reaction in which the reaction product acts as ligandwhich forms the chiral catalyst with the zinc species (see Figure 12).[96] Pyrimidine-5-carbaldehydes are converted with diisopropylzinc into the corresponding chiral pyrimidyl alcohol.

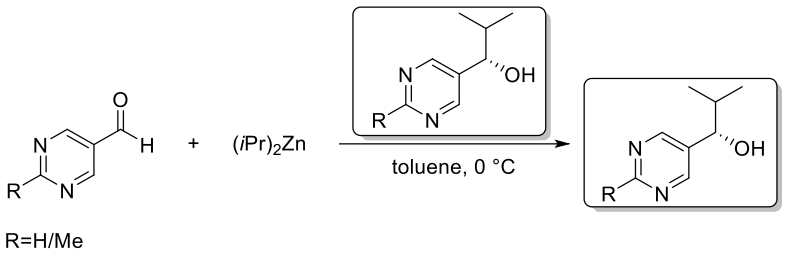

Figure 12: The first example of an autocatalytic reaction, the SOAI reaction.[96]

This catalytic automultiplication shows *ee*s of up to 98.2% and with the right conditions, the enantiomeric purity of the compound does not decrease during the automultiplication.[96] Very small enantiomeric excesses in the original ligands are sufficient to obtain high alkylation selectivities after several cycles.[75b]

Very recently, TRAPP *et al.* presented their own autocatalytic process.[78] With the interaction of reaction products at chiral recognition sites, the highly flexible phosphoramidite-based catalyst can adapt to the produced chiral information and induce enantioselectivity. The dynamic of this catalyst was enabled by its high flexibility and the ability to respond to the reaction product´s chirality resulting in a shift out of equilibrium and enable Δ*ee*s of up to 76% for the hydrogenation of prochiral olefins.[78] The enantioselective non-covalent interaction between the ligand (*S*)-*N*-pivaloylproline 3,5-dimethylanilide and the additive (*S*)-*N*-(3,5-dinitrobenzoyl)leucine dimethylamide are shown in Figure 13, (C), this characteristic was used to install the product interaction-site. The chiral recognition system is based on PIRKLE and MURRAYS.[97],[98],[99] The designed catalyst (see Figure 13, (B)) consists of two phosphoramidite ligands coordinating to the Rh-center giving. Mechanistically, in the first turnover no or no significant amount of *ee* is formed. Afterwards, the catalyst is able to interact with the formed product which induces orientational / alignment changes in the catalyst. Leading to an increased enantioselectivity for the next turnover, which ultimately results in self-amplification. The adaptation process between catalyst-interaction-site and product is repeated after each turnover until the substrate is fully converted.[78]

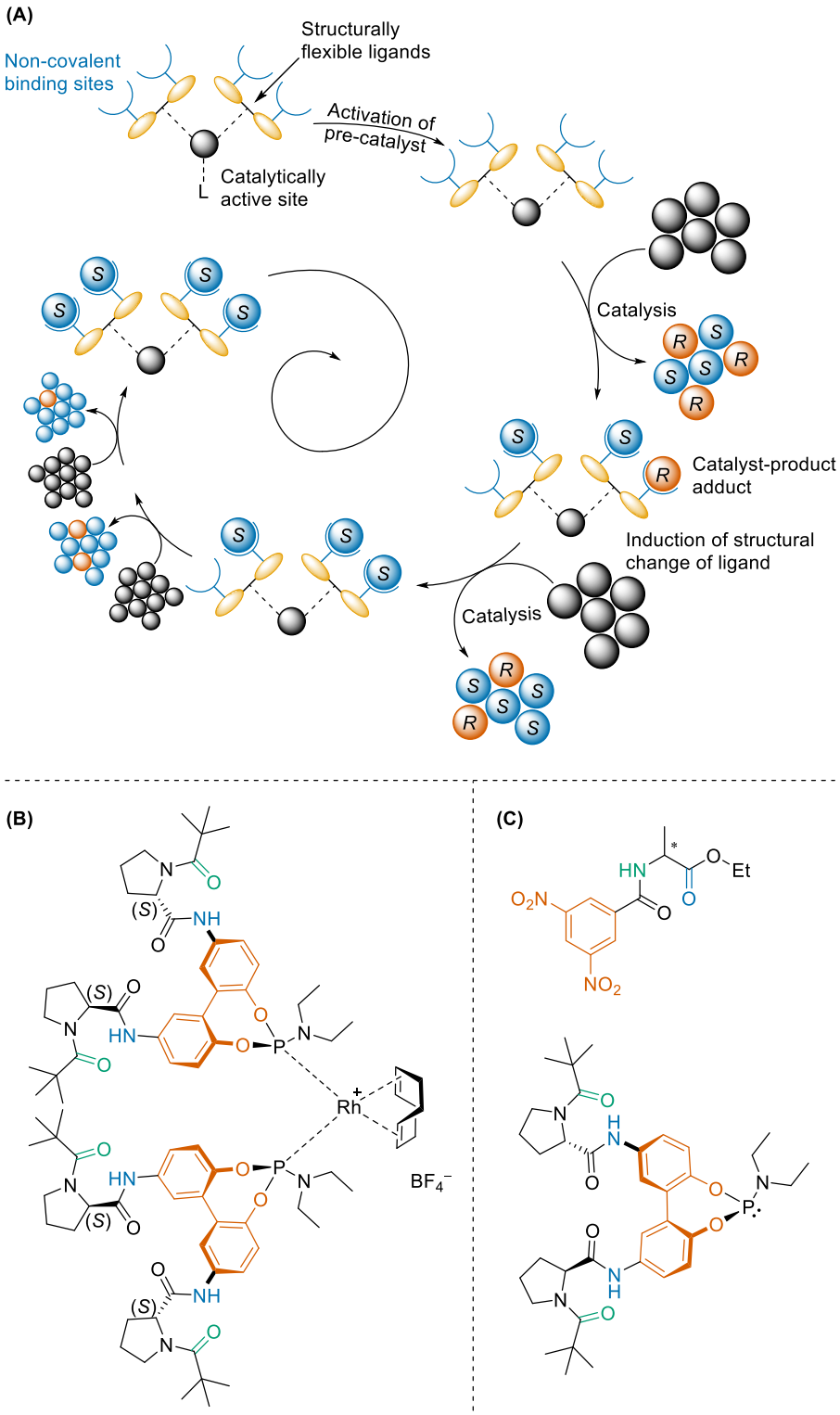

Figure 13: The autocatalytic process by Trapp and Storch (a) General principle of enantioselective self-amplification in catalysis, (b) Structure of the catalyst, (c) Additive and ligand interaction between the units of the same color.

The requirements for such an autoinductive process are:

I) A constant adaptation to the ever changing equilibrium is necessary, which is ensured by non-covalent interactions between ligand and reaction product.

II) Quick absorption into the reaction cycle in comparison the to slow hydrogenation
III) Between ligand and product molecules has to be high enenatioselectivity leading to "mutual antagonism"
IV) Fast stereochemical adaption as response to ligand and product interaction causing realignment of the whole catalyst.[75b]

These requirements were considered to create an autoinductive self-inhibiting system (see Figure 14). Its "inverse nature" leads to the production of the opposite enantiomer.

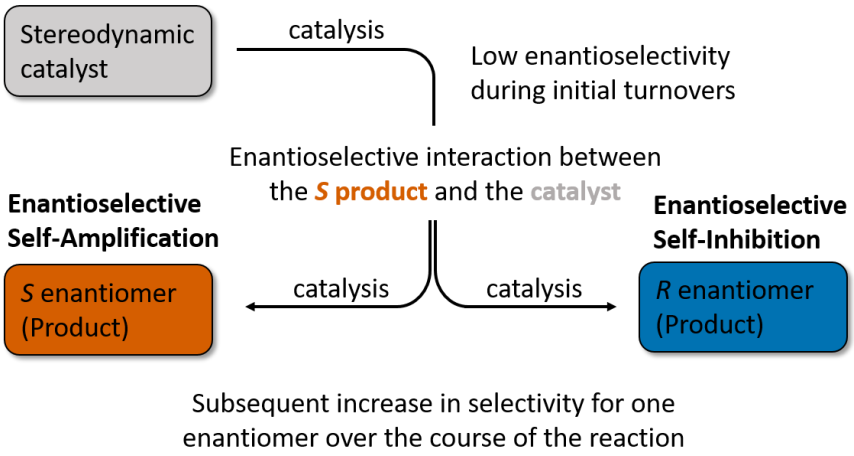

Figure 14: Comparison of autoinductive catalytic reactions: Self-amplification and self-inhibition.

To achieve this TRAPP *et al.* again turned to the phosphoramidite catalyst. This time however, the biphenyl backbone is decorated with (*S*) phenylalanine-based amido ester selector units for supramolecular interaction (see Figure 15). The equilibrium of the two different rotamers was already shifted towards the R_{ax} rotamer. After addition of chiral additives in excess, further enrichment of the R_{ax} rotamer was observed by ^{31}P NMR through peak shifts. Different additives were tested and the most significant stereoinduction was observed with alanine derivatives with electron-deficient aromatics at the *N*-terminus.

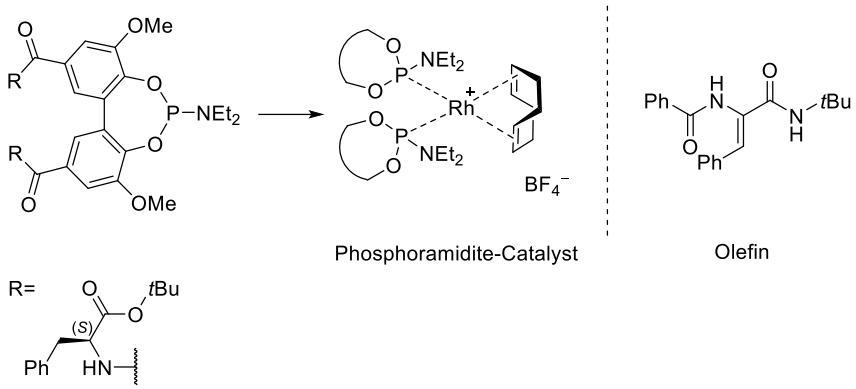

Figure 15: Catalyst for autoinductive self-inhibition by TRAPP *et al*.

Therefore, the olefin derived from PhCO-(*S*)-Ph-NH*t*Bu was applied in asymmetric hydrogenation reactions with the phosphoramidite catalyst (see Figure 15).[75b] It was shown, that the original tendency of the *S*-enantiomer as the product was inverted after interaction with the catalyst and turned into the preferred formation of the *R* enantiomer, thus generating a self-inhibiting system. Ultimately, these two processes can be used to show at the molecular level how biochemical processes could be enantioselectively implemented in nature.[75b]

1.11 Hemiacetals and Their Potential Applications

For the evolution of life, directional recognition processes and reproducible replication was necessary and for this, the presence of homochirality was mandatory.[100], [100b] When prepared without subsequent chiral separation, the direct creation of enantiomerically pure substances can only be achieved through selectively controlled formation. Consequently, this step plays a decisive role in the synthesis of biomolecules in nature. In this regard, the study of asymmetric catalysis, more precisely asymmetric autocatalytic catalysis, is very intriguing due to its potential of bearing non-linear effects which can lead to the amplification of *ee*s.[101],[102] It is widely assumed that this is the reason how homochirality arose in nature. Reactions starting with very low *ee* and the ability to develop high *ee*s in the curse of several turnover rates, are the key to understand and mimic the evolution of homochirality.[103] The asymmetric autocatalytic reaction by SOAI is considered a breakthrough in this research field[104],[104b],[105] and captured the interest of numerous research groups which then focused on mechanistic investigation of the reaction. Only naming a few, who were focused on solving the mechanism experimentally, there are AMEDJKOUH *at al*.,[106],[107],[108] BLACKMOND *et al*.[109] and BROWN *et al*.[110],[111] Very recently, two different mechanistic approaches were proposed by DENMARK *et al*.[112],[113] and TRAPP *et al*.[114],[115]

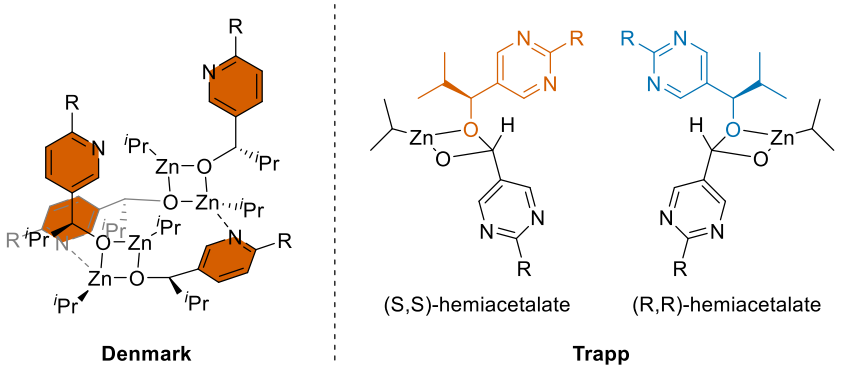

Figure 16: Proposed active species by DENMARK and TRAPP.[116]

While DENMARK claimed the catalytically active species of the SOAI reaction to be a homochiral tetramer of the product alkoxide which is in a square-macrocycle-square conformation, TRAPP identified a transient Zn-hemiacetalate catalyst formed by aldehyde and Zn-alkoxide (see Figure 16).[116] The latter would also explain the long induction period of the reaction due to the determined barrier $\Delta G^{\ddagger}$ of 82.6 kJ/mol for the formation of the transient hemiacetalate catalyst. In doping experiments, it was possible to shift the inflection point of the sigmoidal-shaped curve, which signifies a reduction of the induction phase by 55 seconds compared to the reference measurement as pictured in Figure 17.

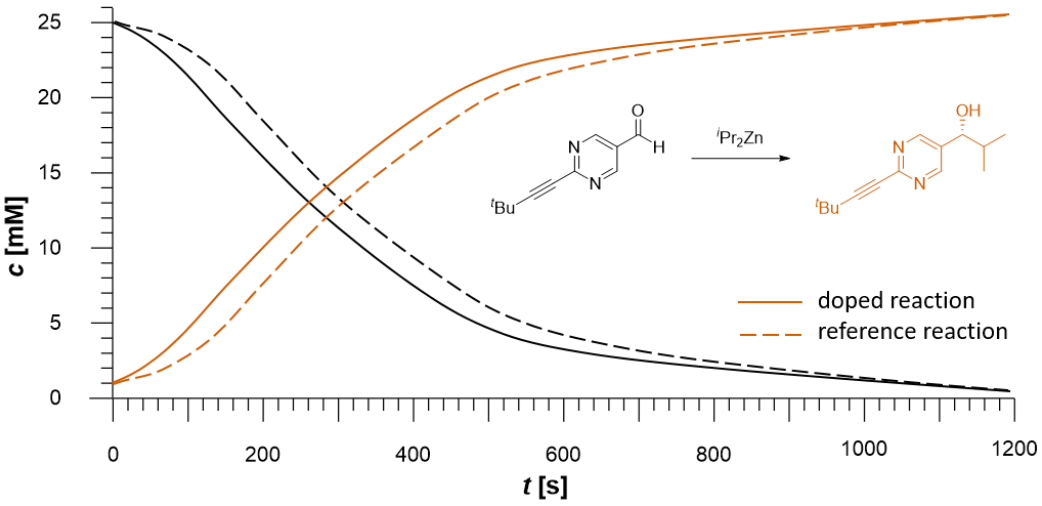

Figure 17: Schematic representation of the reaction process illustrating the decrease in reactant concentration and the increase in product concentration. Doping of the reaction leads to a significant acceleration of product formation.[117]

This doping was achieved by the addition of the transient hemiacetalate catalyst from the apex of its formation from an ongoing SOAI reaction to a freshly prepared one. The same alteration of the induction phase was neither reproducible by doping with a completed SOAI reaction, nor with the addition of the product Zn-alcoholate complex (see Figure 16) which was the proposed catalyst by DENMARK[117]. Giving these results, the investigation

of hemiacetals and their formation as well as their stereodynamic properties is of great interest to further understand spontaneous symmetry breaking.

2 Bisphosphinite Ligands

2.1 Objective – Bisphosphinite Ligands

The previously discussed success in the investigation of stereodynamic chiral *tropos* ligands and their alignment *via* supramolecular interaction through applied interaction units motivates further investigation of similarly configurated structures. Investigations on how their flexibility can be adjusted to facilitate control over the enantioselectivity they induce in asymmetric catalysis are required. After inter- and intramolecular alignment (described in chapter 1.6 and 1.7)[56, 74], further investigations how the alignment can be influenced are conducted. Therefore, the structures previously presented by TRAPP *et al.* form the starting point for the design of possible new ligand systems. The general structure is maintained for all ligand designs as pictured in Figure 18.

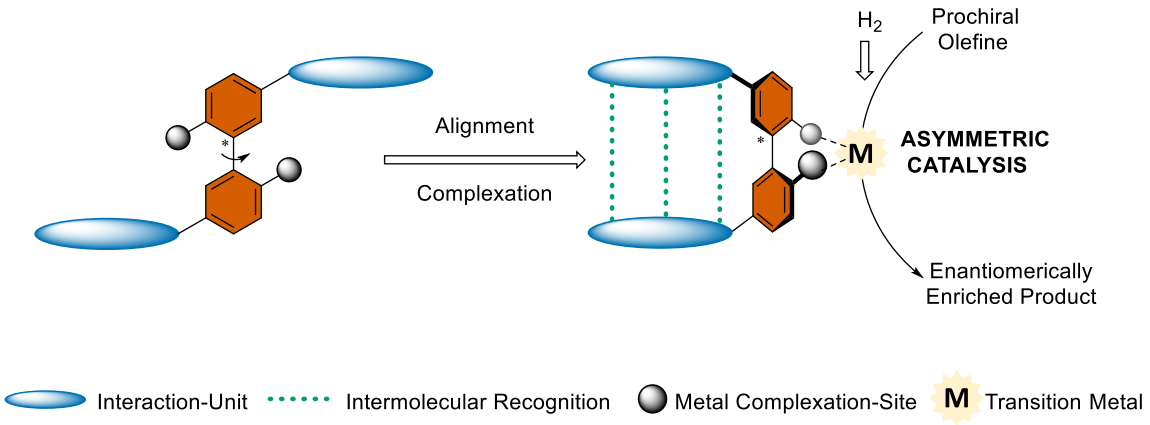

Figure 18: General ligand design to achieve supramolecular recognition, consisting of a flexible biphenyl backbone (orange), interaction units (blue) for non-covalent interaction and a metal complexation site (grey spheres). Through alignment and enrichment of one ligand rotamer, the metal coordinated ligand can be applied in asymmetric catalysis.

The biphenyl backbone is chosen to obtain a stereochemically flexible ligand core with a chiral axis around which axial rotation can occur. Depending on the influence of the interaction-units and their ability to undergo non-covalent interactions, the rotational barrier around the chiral axis can be increased and a shift out of equilibrium can be enforced which results in enrichment of one ligand rotamer. The interaction units themselves are inspired by nature and applied in a biomimetic approach to copy the non-covalent interactions and the alignment occurring in the macromolecular structure of proteins.[56] As previously described, high-performance chiral stationary phases for GC, in particular the CHIRASIL-VAL with their secondary diamines derived from amino acids, seem to be among the most promising inspiration for the design of the interaction-units (see chapter 1.6).[63] The different interaction units should be connected to the biphenyl backbone at 5,5'-position, for the best central-to-axis-chirality transfer while maintaining

the *tropos* properties of the biaryl.[38, 63] The amino acid-based interaction units can be attached in two different ways, namely through attachment at the *N*-terminus or the *C*-terminus of the respective amino acid. For the linker, a phenylene bridge, for more flexibility and the ability to intramolecularly align themselves[56], or a triazole bridge, which should be conveniently prepared by click-chemistry, should be inserted. The latter alteration might generate an easy and fast synthetic route to synthesize the ligand from simple building blocks. The phenylene bridge however was applied before and is hence very promising.[56] The listed variations as well as other amino acid-derived interaction-units based on alanine or *tert*-leucine are planned to be synthesized. Those alterations are expected to exert a significant influence on the non-covalent interactions. For the metal complexation-site, the introduction of phosphinite residues is planned, which are known to act as good coordination sites to transition metals such as rhodium. The epimeric distribution and asymmetric enrichment of the synthesized ligands should be investigated with regard to their temperature dependency. After coordination with transition metals, they are applied in asymmetric hydrogenation reactions of prochiral olefins. The reaction conditions need to be optimized and adapted to the respective catalyst through screening of different reactants, solvents and hydrogen pressures in order to improve enantioselectivity. Moreover, the influence of reaction temperature on the *ee* of the catalyst should be tested. By these measures, an evaluation of the selectivity and stereocontrol of the designed catalysts should be conducted.

2.2 Results and Discussion – Bisphosphinite Ligands

2.2.1 Ligand Design and Synthesis

New amino acid-based diamide bisphosphinite ligands were successfully synthesized. Their design consists of a chiral interaction-unit attached to a highly flexible biphenyl backbone which makes them *tropos*-ligands with a chiral axis (see Figure 19). For the interaction-units of the ligand, different amino acid-derivatives have been investigated. Valine (Val)-based interaction-units were applied previously by MENKE and SCHOLTES in the TRAPP group and were therefore the standard of choice.[56, 74] To further expand the scope of possible interaction-units for non-covalent, intramolecular interaction, alanine (Ala) and *tert*-leucine (^{t}Leu) were applied in a similar manner in design 3. The interaction-units were connected to the biphenyl backbone via a phenylene bridge at 5,5'-position, or with a triazole as for design 2 (see Figure 19). The ligands were further functionalized to bisphosphinites to introduce a metal-complexation site.

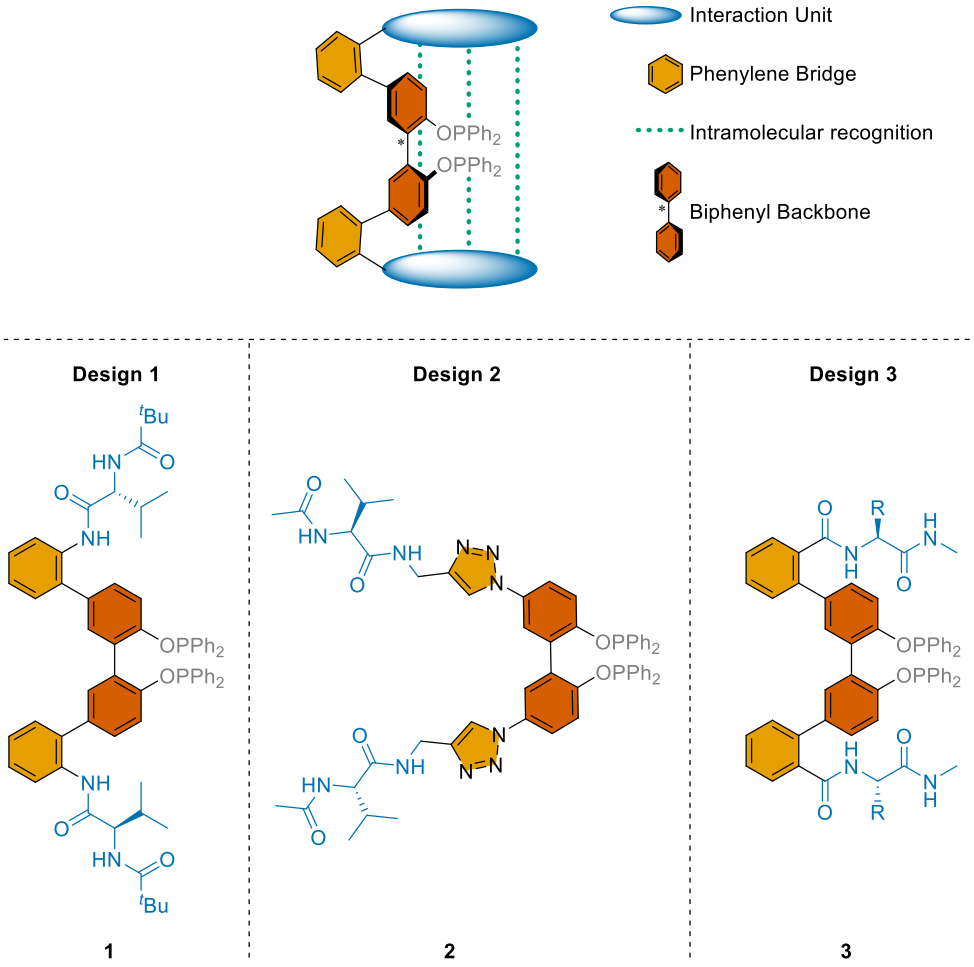

Figure 19: Schematic illustration of the desired ligand designs with two interaction-units (blue) for intramolecular recognition (green) which are connected to the biphenyl backbone (orange) *via* a phenylene bridge (yellow). The different ligand designs of **1**, **2** and **3** are also presented.

2.2.1.1 Ligand Design 1: Biphenyl Backbone with *C*-Terminal Connected Amino Acid Based Interaction-Unit

For the implementation of the ligand design, a functionalized and protected ligand backbone was linked to a valine-based interaction-unit via a cross-coupling. The synthesis for this functionalized ligand backbone was adapted from the procedure of TRAPP *et al.*[56] Boronic acid pinacol ester **5** was obtained (see Figure 20) *via* three steps and gave the desired flexible *tropos* backbone as building block.

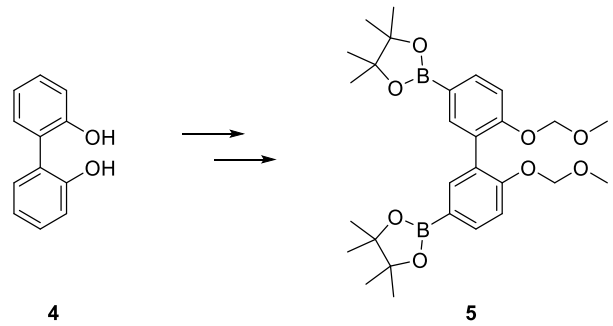

Figure 20: Backbone building block synthesized according to TRAPP *et al.*[56]

The interaction-unit was obtained in a multi-step synthesis (see Scheme 7). Firstly, Boc-protected valine was added to 2-aminophenol **6** *via* peptide coupling. Subsequent functionalization of the free hydroxyl group as the triflate **8** and the following acidic deprotection gave the chloride salt **9**. The interaction-unit building block **10** was obtained through amide formation of the salt **9** (used without further purification) with pivaloyl chloride. Attempts to synthesize the 2-iodo derivative **12** of this interaction-unit were not pursued further than the first step (shown in Scheme 7 **(B)**) due to lower yields.

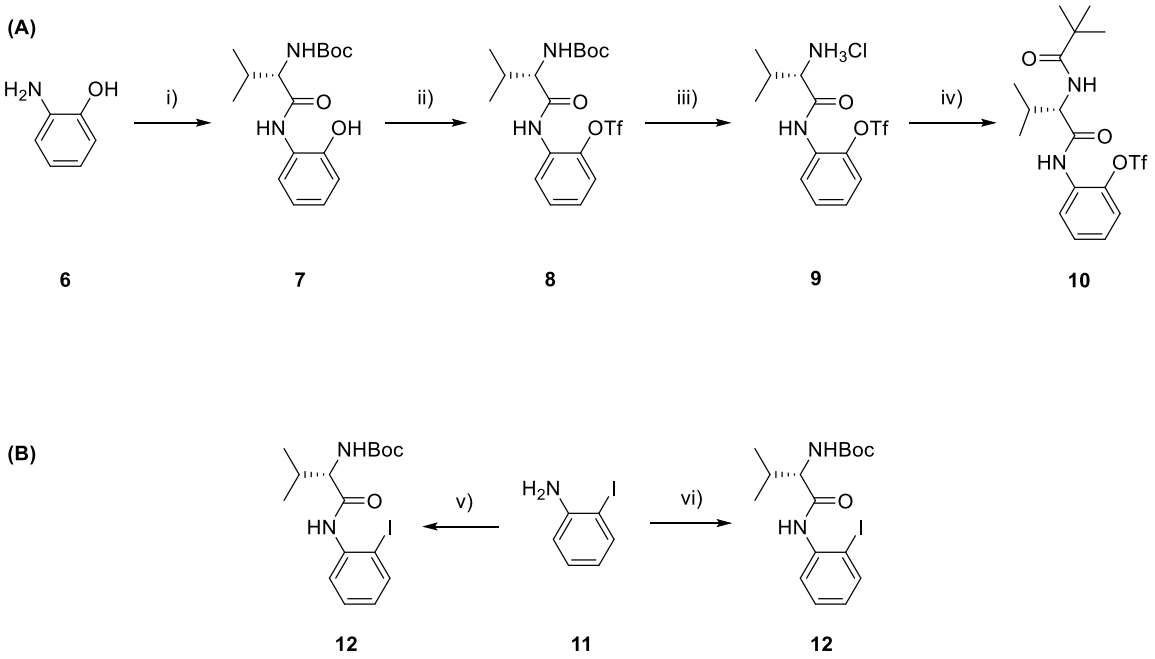

Scheme 7: Interaction-unit **10** synthesis. i) Boc-Val, DME, DIPEA, COMU, DCM; ii) Tf_2O, pyridine, DCM; iii) HCl (5M in isopropanol), $CHCl_3$; iv) pivaloyl chloride, DIPEA, DCM; v) DIPEA, COMU, Boc-Val, DCM; vi) HOBt, DIPEA, EDCI, Boc-Val, DMF.

For the addition of the interaction-unit **10** to the biphenylic core **5**, a SUZUKI-MIYAURA cross-coupling reaction was investigated with different catalysts and bases (see Scheme 8) to obtain compound **13**. Following deprotection of the biphenol´s hydroxyl group gave the biphenol **14**. Addition of chlorodiphenylphosphine gave the final phosphinite ligand **1,** a highly water and oxygen sensitive orange honey-like liquid which proved problematic to handle, even under inert gas. Due to this instability, no investigation of its catalytic potential was performed on this ligand.

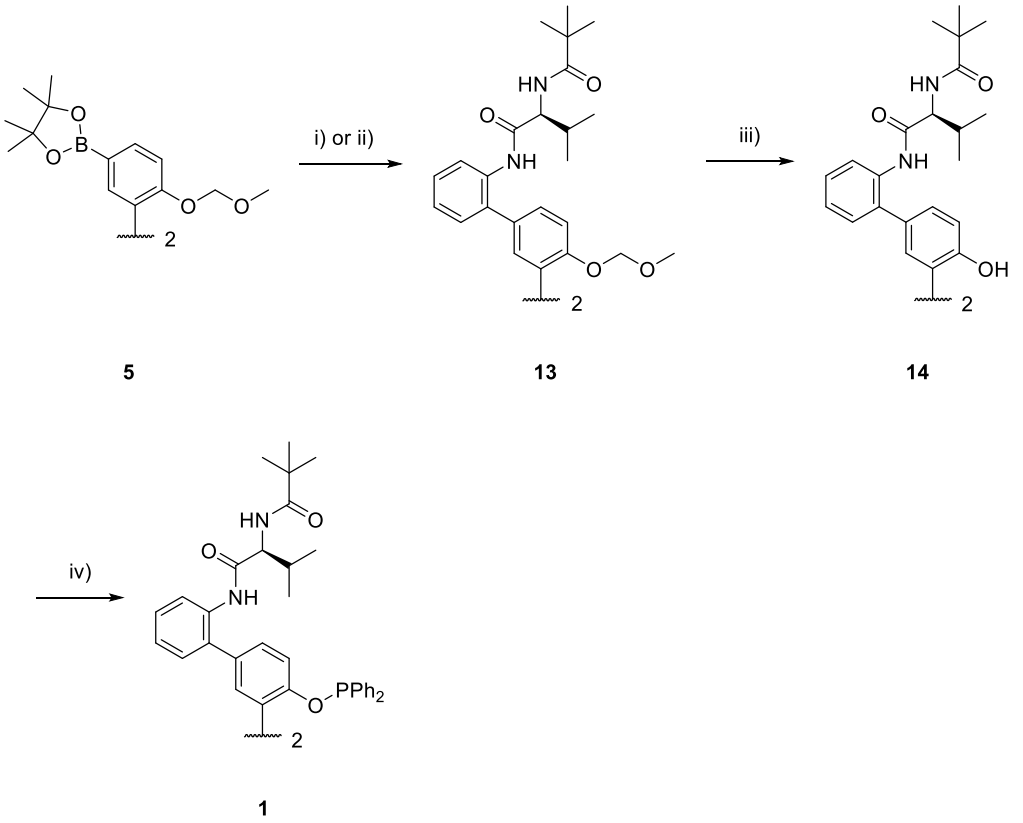

Scheme 8: Synthesis of the phosphinite ligand **1** out of the two building blocks **5** and **10**. i) K_2CO_3, $Pd(PPh_3)_2Cl_2$ and **10**, THF/MeOH; or ii) Cs_2CO_3, $Pd(dppf)Cl_2$, and **10**, DMF; iii) HCl (5M in isopropanol), $CHCl_3$; iv) $ClPPh_2$, NEt_3, DCM.

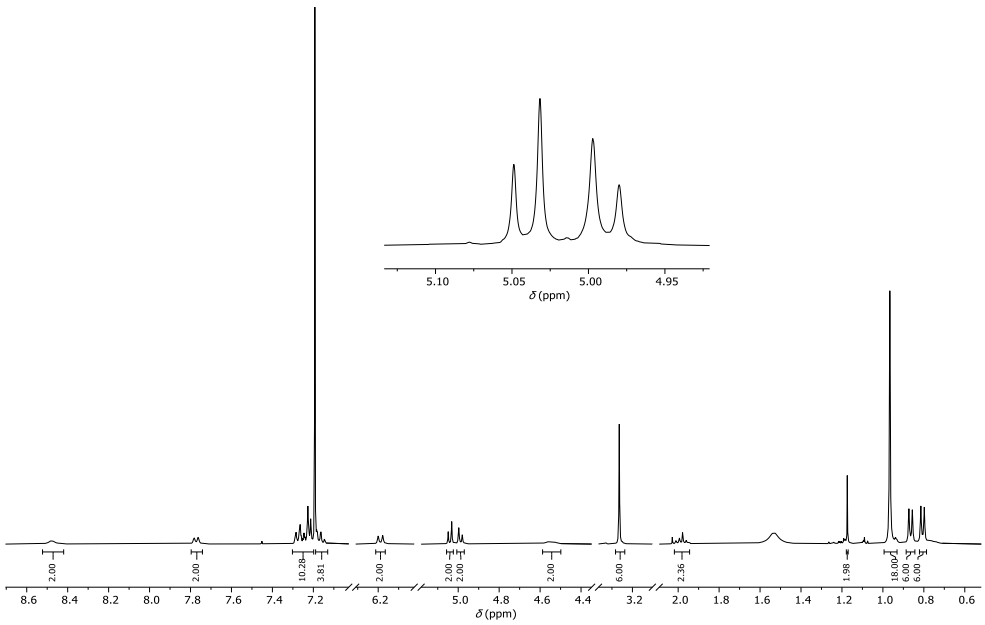

Figure 21: MOM-group splitting of the methylene group in ^1H NMR experiments for **13**.

The ^1H NMR spectrum of the assembled precursor **13** showed a splitting of the methylene group signals of the MOM-protecting group (see Figure 21). This was previously

described as a sign of preorientation of the chiral axis in the biphenyl backbone, induced by the non-covalent intramolecular interaction of the interaction moieties.[56]

2.2.1.2 Ligand Design 2: Synthesis Towards Triazole-Bearing Ligands *via* Click-Chemistry

The simpler, the more elegant is an approach for ligand synthesis. The click reaction, also known as 1,3-dipolar cycloaddition or HUISGEN addition, is a tried-and-true option for linking two molecular units *via* a 1,2,3-triazole. This might be applied to *tropos* ligands to link the interaction-units with the biphenyl backbone, replacing the phenylene bridge used previously (see Section 2.2.1.1.). This would simplify the preparation of the interaction-unit and eliminate the cross-coupling step.

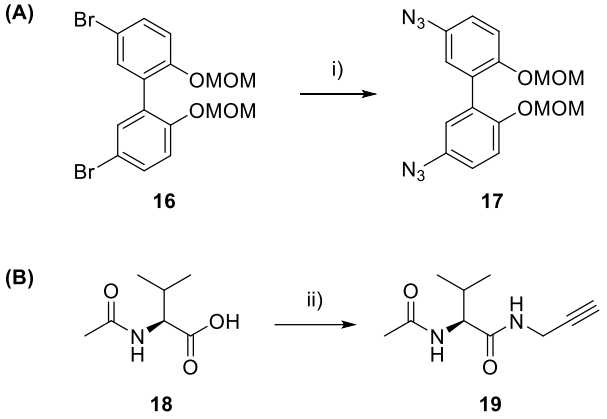

Figure 22: Synthesis of the two precursors for the Click-reaction.**(A)**: synthesis of 5,5′-diazidobiphenol backbone. i) DMEDA, NaN_3, CuI, (+)-Na-L-ascorbate, EtOH/H_2O; **(B):** synthesis of the interaction-unit bearing a propargyl group: ii) HOBt, DIPEA, EDCI, propargylamine, DCM.

Compound **16** was synthesized according to MENKE and TRAPP.[56] The corresponding aryl azide **17** is prepared from the halogen precursor **16** *via* substitution with sodium azide (see Figure 22). [118] The interaction-unit of the ligand should be based on valine and therefore an acyl protected valine derivative **18** was used to prepare the alkyne **19** for the click-reaction.

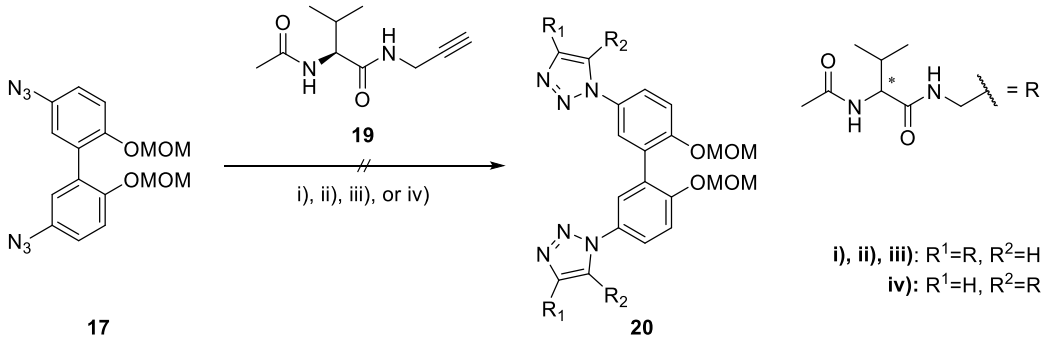

Figure 23: Attempts to link the interaction-unit with the biphenyl backbone via Click-reaction. i)CuI, DIPEA, DCM; ii) Cu/C, NEt3, dioxane; iii) $CuSO_4$, (+)-Na-L-ascorbate, iv) $Cp^*RuCl(PPh_3)_2$, toluene

The linking of the interaction-unit **19** with the biphenyl backbone **17** could not be achieved. Several different approaches were considered, and different copper sources and conditions were tested (see Figure 23). However, neither the coupling with CuI,[119], [119b] nor with Cu/C,[120] $CuSO_4$[120] or the catalyst $Cp^*RuCl(PPh_3)_2$[121] were successful in connecting those two units. It should be mentioned that the use of the catalyst $Cp^*RuCl(PPh_3)_2$ would lead to an inversion of the substituent orientation.[121] Usually, only catalytic amounts of the copper species are applied. To prevent a potential complexation of the catalytic copper species by the MOM-protecting group of the reactant, overstochiometric quantities of copper source were tested in screenings. Further addition of the additive tris(benzyltriazolylmethyl)amine TBTA[122], which was reported to stabilize Cu(I) in its oxidation state by complexation, let to no noteworthy change in the course of the reaction.

2.2.1.3 Ligand Design 3: Biphenyl Backbone with *N*-Terminal Connected Amino Acid Based Interaction-Unit

Similar to ligand design 1, the different building-blocks of a functionalized biphenyl backbone and an interaction-unit based on Ala, Val or *t*Leu derived diamides were linked at their respective *N*-terminus *via* a cross-coupling reaction and the so obtained ligand was further functionalized with the addition of a metal interaction site in form of bisphosphinite residues. The synthesis of the interaction-unit, illustrated in Scheme 9, started with the addition of methylamine to the Boc-protected amino acids alanine, valine, and *tert*-leucine *via* peptide coupling, respectively. Subsequent acidic deprotection gave the desired amino acid-based interaction precursors, **Ala-**, **Val-** and ***t*Leu-23**.

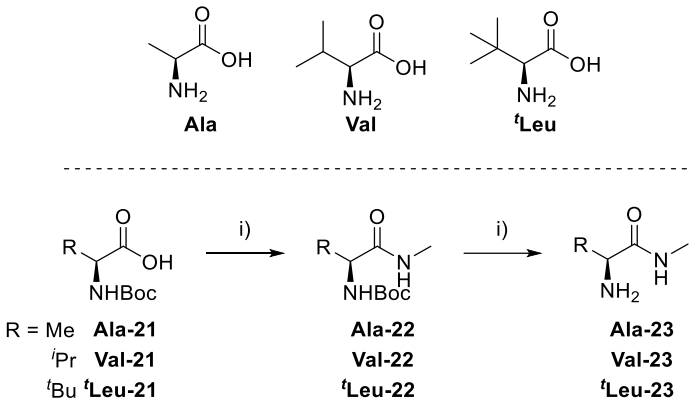

Scheme 9: Interaction-unit **23** synthesis based on alanine, valine, and *tert*-leucine. (i) HOBt, DIPEA, EDCI, $MeNH_2$, DMF; (ii) HCl (3M in MeOH).

The synthesis of the ligand itself (see Scheme 10) started from MOM-protected 5,5'-dibromo biphenol **16** which was synthesized according to TRAPP *et al.*[56] A one-pot sequence of magnesium insertion followed by transmetallation to a zinc species and a subsequent NEGISHI cross-coupling reaction was used to extend the biphenyl-system by an ester substituted phenylene bridge, yielding compound **24**. Subsequent alkaline saponification gave dicarboxylic acid **25**. In the third step, the amino acid derived diamide interaction-units **23** were added to the biphenyl-system *via* amide coupling. This was followed by acidic deprotection to give the biphenol **27**, which was converted to the bisphosphinite-ligand **28** *via* nucleophilic substitution using chlorodiphenylphosphine. The resulting ligand was labile towards oxygen and water and had to be handled under inert conditions.

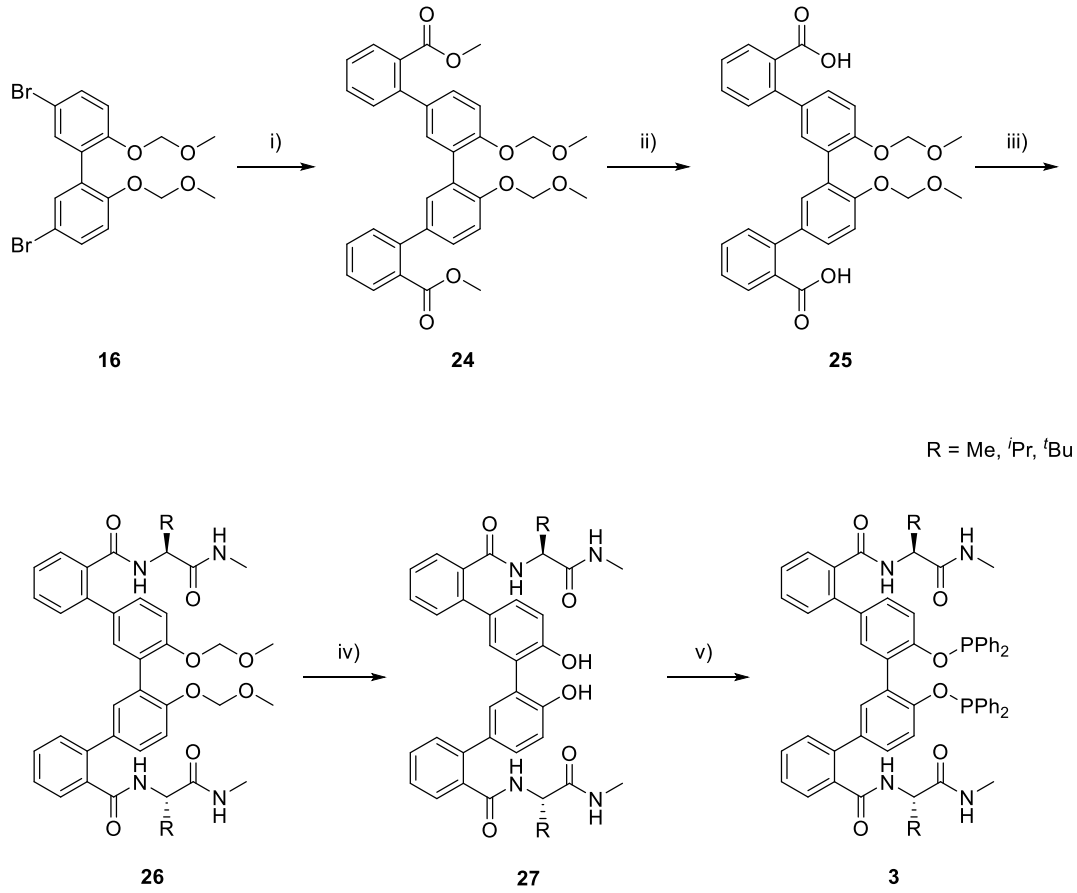

Scheme 10: Synthetic route for ligand **3** synthesis. i) methyl 2-bromobenzoate, Mg, LiCl, $ZnCl_2$, $Pd(Oac)_2$, Sphos, THF. ii) KOH, H_2O/dioxane (1:1) iii) **23**, DIPEA, HOBt, EDCI, DMF. iv) HCl, (5M in isopropanol), $CHCl_3$. V) $ClPPh_2$, NEt_3, DCM.

^{1}H NMR measurements of the protected precursor **26** showed a splitting of the singlet signal corresponding to the methylene group in the MOM-group (see Figure 24). This effect was previously observed in structurally similar *tropos*-ligands for which it indicated a preorientation of the biphenyl backbone due to the non-covalent intramolecular recognition of the interaction groups.[56] This splitting is assumed to originate from the increased rotational barrier of the *tropos* axis locking the isomerization on an NMR time scale.

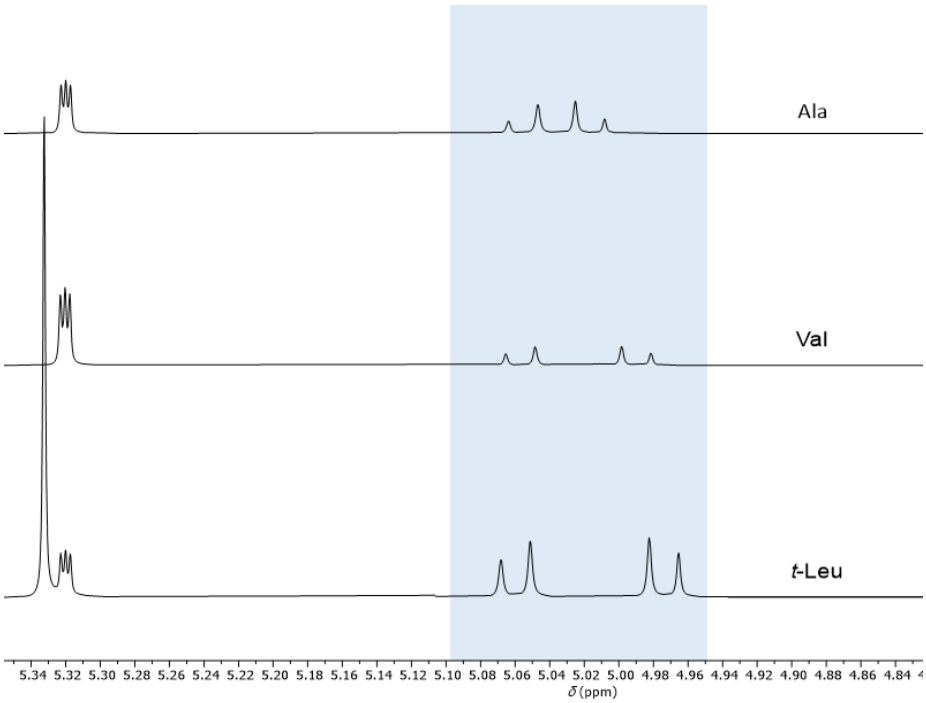

Figure 24: ^{1}H NMR of **26** with the different amino acid-based interaction-units (Ala, Val, *t*-Leu). The MOM methylene groups for the different compounds **Ala-26**, **Val-26** and ***t*-Leu-26** split in CD_2Cl_2, due to non-covalent interactions.

2.2.2 Ligand Study

For further investigation of the self-recognition properties of the ligands, temperature dependent ^{31}P-NMR experiments were performed to assess the influence of temperature on the orientation of the highly flexible *tropos*-ligands. Ligand **Ala-3** was dissolved in CD_2Cl_2 and ^{31}P NMR spectra were recorded between −80 °C and +30 °C in ten degree steps (see Figure 25), showing not only a temperature dependent chemical shift of the phosphinite group but also changes in the proportions of the ligand epimers. The integral ratio of the signals corresponding to the phosphinite group in each of the two diastereomers of the alanine ligand **Ala-3** shifted from 1:1.94 at room temperature to 1:0.28 at −80 °C, revealing the complete inversion of the initial epimeric ratio (see Table 1).

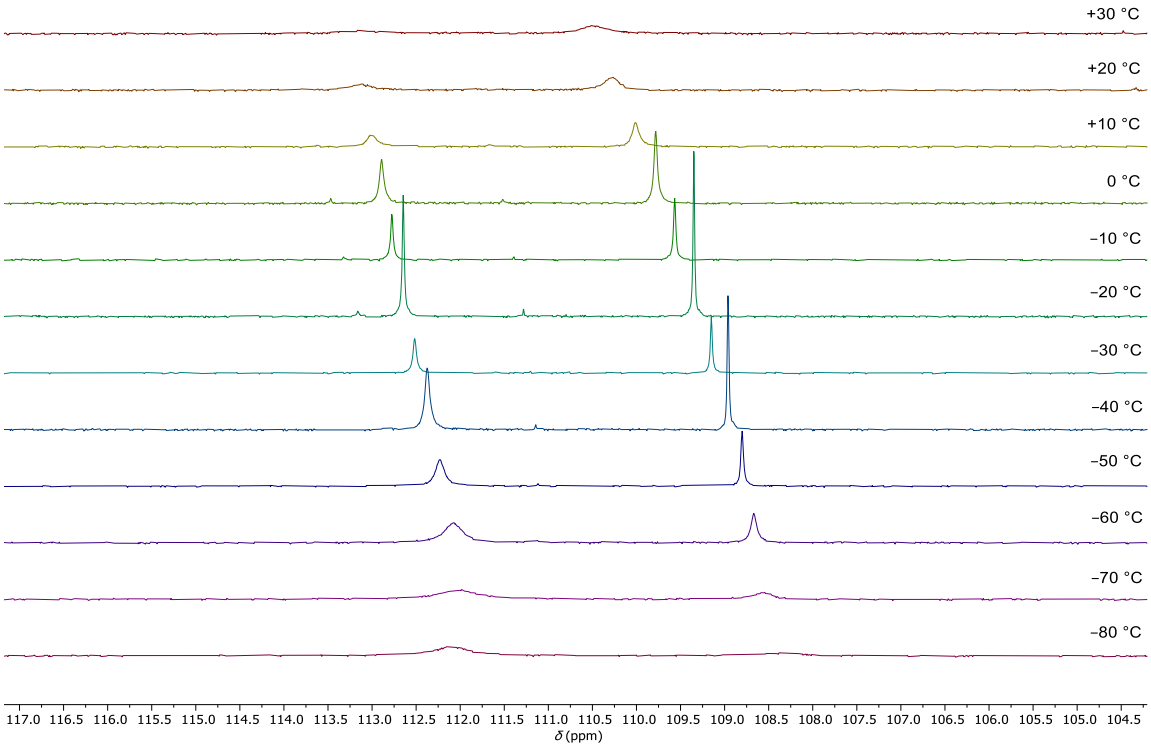

Figure 25: Temperature dependent ^{31}P NMR experiments of **Ala-3** in CD_2Cl_2 from −80 °C to +30 °C in 10 degree steps.

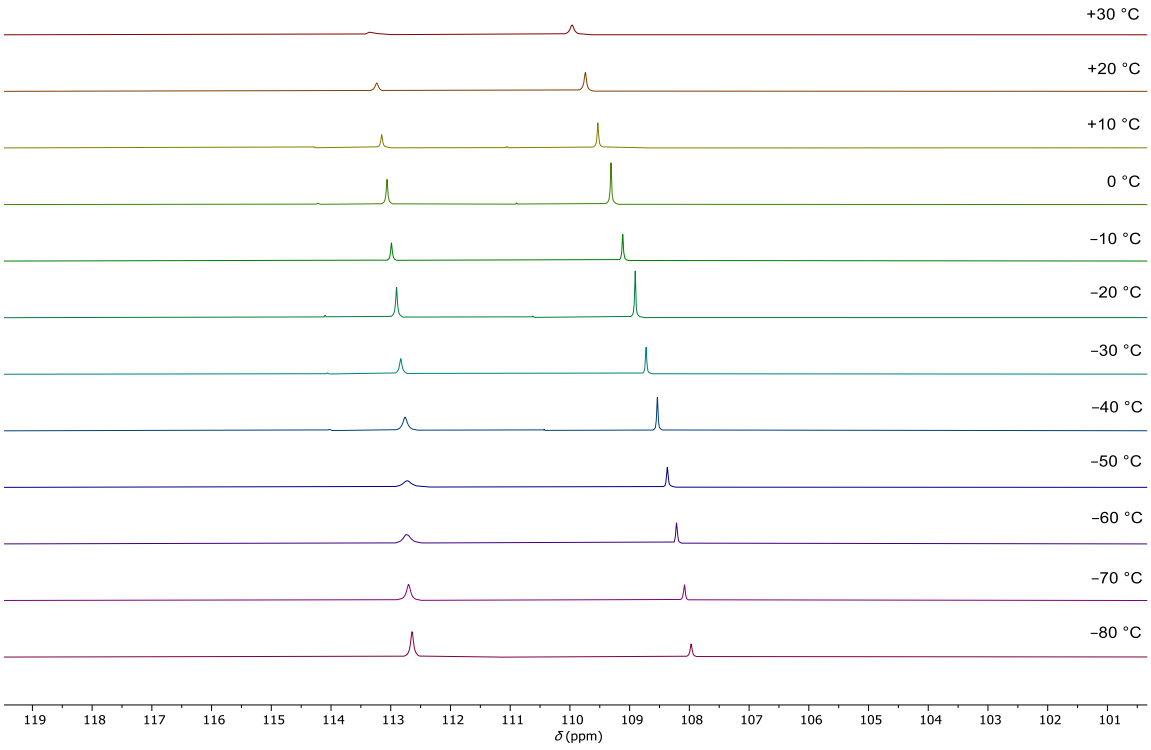

Figure 26: Temperature dependent ^{31}P NMR experiments of **Val-3** in CD_2Cl_2 from −80 °C to +30 °C in 10 degree steps.

In a similar manner, the inversion of the epimeric ratios was also observed in ^{31}P NMR experiments for the valine ligand **Val-3** (see Figure 26) from integrated values of 1:1.82 at room temperature to 1:0.34 at −80 °C. These results indicate a temperature dependence of the conformation around the central axis in the investigated ligands and a temperature-controlled enrichment of one ligand epimer.

Table 1: Calculated equilibrium constant *K*, GIBBS free energy ΔG and epimeric excesses for ligand **Ala-3** and **Val-3** based on the obtained integral ratios of the two epimers of **Ala-3** and **Val-3** in the ^{31}P spectrum in CD_2Cl_2.

			ALA-3			**VAL-3**
***T* [°C]**	***Epimeric Excess* [%]**	***K***	**ΔG [J*mol^{-1}]**	***Epimeric Excess* [%]**	***K***	**ΔG [J*mol^{-1}]**
30	32.0	1.94	−1670	29.1	1.82	−1509
20	16.7	1.4	−820	24.5	1.65	−1221
10	18.4	1.45	−875	19.0	1.47	−907
0	13.4	1.31	−613	12.3	1.28	−561
−10	9.1	1.2	−399	6.10	1.13	−267
−20	1.96	1.04	−82.5	−1.52	0.97	64
−30	−4.17	0.92	169	−8.70	0.84	352
−40	−13.0	0.77	507	−18.3	0.69	719
−50	−23.5	0.62	887	−27.4	0.57	1043
−60	−32.5	0.51	1193	−38.9	0.44	1455
−70	−49.3	0.34	1822	−43.9	0.39	1590
−80	−56.3	0.28	2044	−49.3	0.34	1732

The calculation of the epimeric excess, which is also listed in Table 1, was calculated with equation (1) based on the calculation for the enantiomeric excess.

$$epimeric\ excess\ [\%] = \frac{[major\ epimer] - [minor\ epimer]}{[major\ epimer] + [minor\ epimer]} * 100 \qquad (1)$$

The thus obtained values give the range in the given temperature span in which the ligand can align itself and enrich in one epimer at the measured temperatures. The alanine-interaction unit modified ligand **Ala-3** exhibits a range of 32.0 to −56.3% epimeric excess. If an analogous behavior to the ligands published by TRAPP *et al.* is assumed, the R_{ax} isomer predominates at higher temperatures (T > −20 °C) while the S_{ax} epimer is more

abundant at lower temperatures (T < −20 °C).[56] The valine ligand **Val-3** showed a range of 29.1 to −49.3 epimeric excess in the temperature range of 30 °C to −80 °C.

To get a better understanding of the interconversion dynamics of the epimers of the free phosphinite ligand, detected in the temperature dependent ^{31}P NMR experiments, the equilibrium constant K was calculated applying equation (2).

$$K = \frac{[major\ epimer]}{[minor\ epimer]} \tag{2}$$

The distinction between minor and major epimer was determined based on their integrated values at room temperature, in which the "major isomer" was assigned to the more abundant one and this distinction was kept in for all integrations forward.

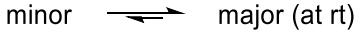

The so obtained equilibrium constants K were then applied in the GIBBS-HELMHOLTZ equation (3) together with the respective temperatures of the measurements to obtain the values of the GIBBS free energy ΔG of the interconversion of the two epimers at a given temperature.

$$\Delta G = -RTln(K) \tag{3}$$

Plotting ΔG against the temperature of the measurement gave a linear progression (fitted to the data points) over the whole range for **Ala-3** (Figure 27) and **Val-3** (Figure 28). Using the GIBBS-HELMHOLTZ equation (4) gives the entropy ΔS (from the slope) and the enthalpy ΔH (from the intersection with the ordinate) of the interconversion.

$$\Delta G = \Delta H - T\Delta S \tag{4}$$

Table 2: Calculated entropy ΔS and enthalpy ΔH values of **Ala-3** and **Val-3** by determination of the equalization line in Figure 27 and Figure 28.

	Ala-3	**Val-3**
Entropy ΔS [J*K^{-1}*mol^{-1}]	28.7	32.1
Enthalpy ΔH [kJ*mol^{-1}]	7.23	8.18

As expected, the values obtained for entropy ΔS and enthalpy ΔH (listed in

Table 2) for the two ligands **Ala-3** and **Val-3** are in good agreement, as already observed for the epimeric ratios. The Values were obtained *via* the determination of the equalization line in Figure 27 and Figure 28.

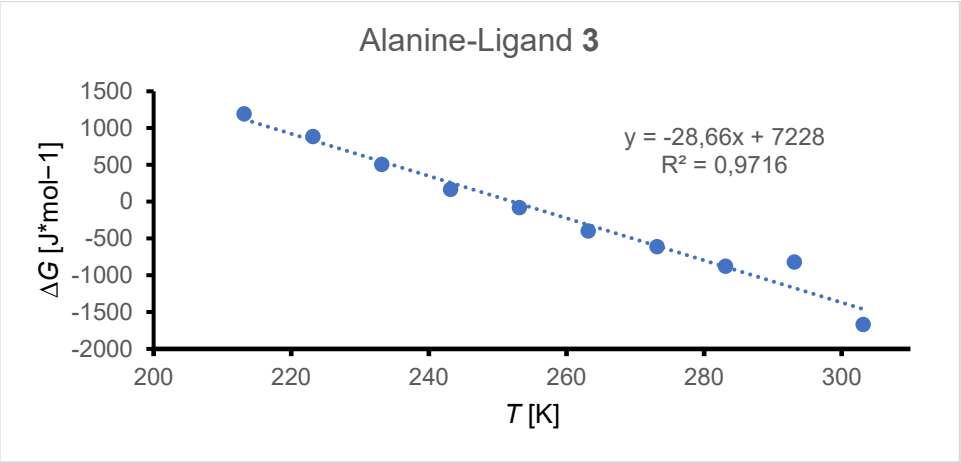

Figure 27: Interconversion of the alanine epimers of the free ligand **Ala-3** put in relation with temperature and the free GIBBS energy ΔG was plotted against the temperature. Giving ΔS=31.3 J*K^{-1}*mol^{-1} and ΔH=7.83 kJ*mol^{-1}.

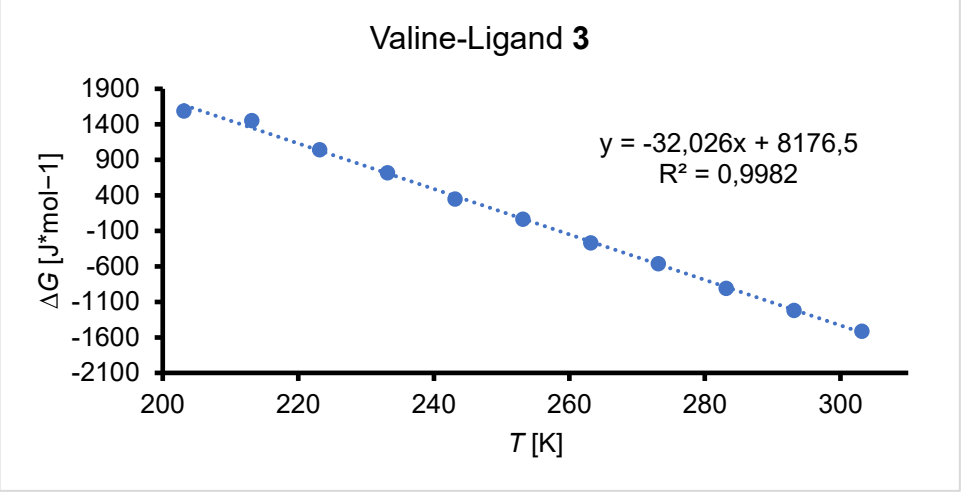

Figure 28: Interconversion of the valine epimers of the free ligand **Val-3** put in relation with temperature and the free GIBBS energy ΔG was plotted against the temperature. Giving ΔS=31.5 J*K^{-1}*mol^{-1} and ΔH=8.04 kJ*mol^{-1}.

2.2.3 Ligand Application in Catalysis

The bisphospinites **28** were applied as ligands for the rhodium catalyzed asymmetric hydrogenation of prochiral olefins, illustrated in Figure 29. The reactions were performed in high pressure autoclaves to test different reaction conditions, namely solvents, H_2 pressure, reaction temperatures as well as different substrates. The specific set-up used for this evaluation was previously described by TRAPP *et al.*[123] $[Rh(COD)_2]BF_4$ was used in all reactions as rhodium source for ligand coordination and *in situ* finalization of the catalyst. The reaction products were then analyzed, and their *ee* determined using chiral HPLC-MS or GC-MS.

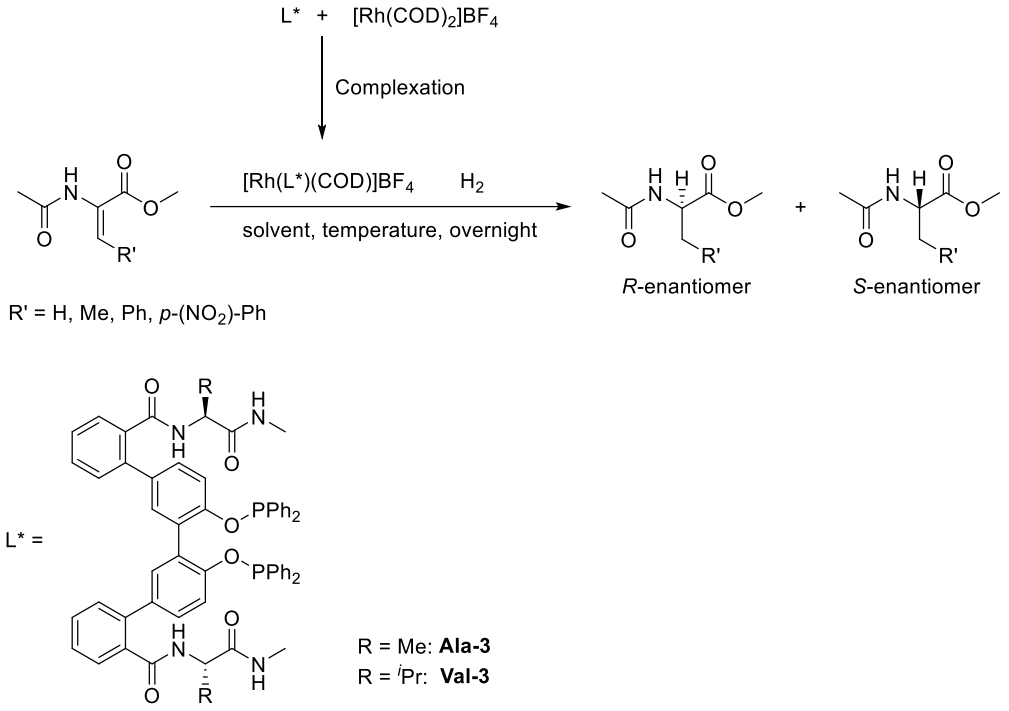

Figure 29: Catalytic application of the ligands in hydrogenation experiments of prochiral olefins with the different parameters that has to be screened.

Before starting the hydrogenation reactions, different stock solutions were prepared beforehand in a glovebox under inert conditions. The olefin methyl 2-acetamido acrylate (**MAA)** and the catalyst, i.e. the rhodium complex $[Rh(L^*(COD)_2]BF_4$ (L* = **Val-3**, see Figure 29), were prepared as stock solutions In order to screen the different reaction conditions, the ligand **Val-3** is first tested with the substrate **MAA** in DCM-d_2 and different H_2 pressures are applied at 20, −20 and −40 °C. These hydrogenation experiments were conducted to determine the H_2 pressure to obtain optimal conversion (see Table 3, Figure 30). The hydrogen pressures tested were 5, 20 and 40 bars. As the best results were obtained at 40 bar hydrogen pressure when averaged over the different temperatures as pictured in Figure 30, all further hydrogenation experiments were carried out at a pressure of 40 bar. It is worth mentioning that in all aforementioned experiments, only the *R*-product of the hydrogenation was observed (identification by comparison of retention times with authentic samples).

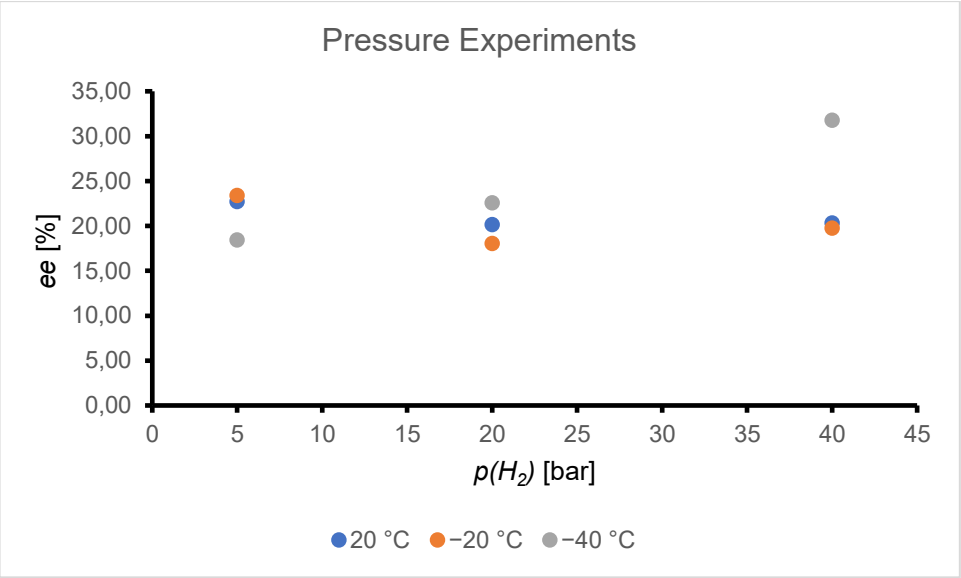

Figure 30: Pressure experiments with **Val-3** in DCM-d_2 with **MAA** at different temperatures (20, −20, −40 °C). The hydrogen pressures tested were 5, 20 and 40 bar.

In the next step, different prochiral olefins, shown in Figure 31, were tested as substrates in hydrogenation reactions and compared to each other. While all tested alkenes are derivatives of 2-acetamido acrylate esters, their different electronic and steric environment is expected to lead to variation in the interaction between the substrate and the chiral ligand system during the reaction which in turn should be observable through differences in the stereoinductions of the hydrogenations.

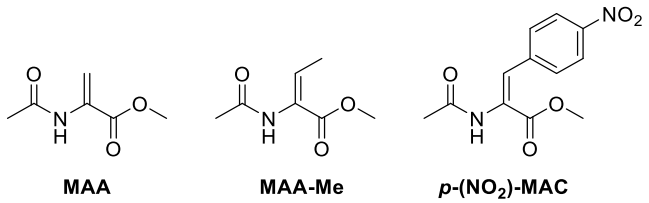

Figure 31: Tested hydrogenation substrates: **MAA**, **MAA-Me**, and ***p*-(NO$_2$)-MAC**.

Another variable to be investigated were different solvents. All applied solvents were deuterated for subsequent NMR analysis of the reaction mixture after the hydrogenation. It was planned to determine the conversion by NMR, however analysis of conversion and reaction products turned out to be more accurate *via* chiral HPLC-MS or GC-MS. As reaction solvents, acetonitrile-d_3, chloroform-d and dichloromethane-d_2 were tested. The reactions in CD_3CN gave racemic mixtures which can be attributed to the coordinating effect of the nitrile to the rhodium metal during the reaction, interfering with the coordination of the chiral ligand to the metal center. As a result, no chiral information could be transferred in the hydrogenation. Comparing the reactions in CD_2Cl_2 (see Figure 32) and $CDCl_3$ (see Figure 33), the best *ee* values were obtained for **MAA** in DCM-d_2. Notably, these reactions all produced the *S*-enantiomer of the product preferentially, which is denoted from here on out by negative *ee* values.

For the preparation of the active catalyst, stock solutions were prepared to add the chiral ligand to the rhodium source in the autoclave. For easier handling, the prochiral olefin was added to the same stock solution as the respective ligand. Afterwards, the Rh-source was added to the mixture of ligand and reactant in the autoclave. Due to all experiments are in favor of the *S*-enantiomer, it cannot be ruled out that the reactant was able to interact with the respective ligand through non-covalent interactions before metal complexation which as a result lead to ligand alignment and enrichment of one ligand rotamer previously to metal complexation. The previously discussed NMR studies of the ligands (see chapter 2.2.2) indicated a different epimeric distribution at different temperatures which ultimately should result in different diasteriomeric enrichment of one ligand rotamer by metal complexation and thus variations in *ee*s (for *S*- or *R*-product enantiomer) at different set temperatures. Therefore, adjustments for the complex preparation were made: the ligand is prepared as a separate stock solution, only mixed with the rhodium stock solution at set temperatures in the autoclave with enough time for complexation and only then, the substrate was added and hydrogen pressure was applied. This procedure of three different stock solutions (ligand, Rh-source, substrate) was applied for all following experiments.

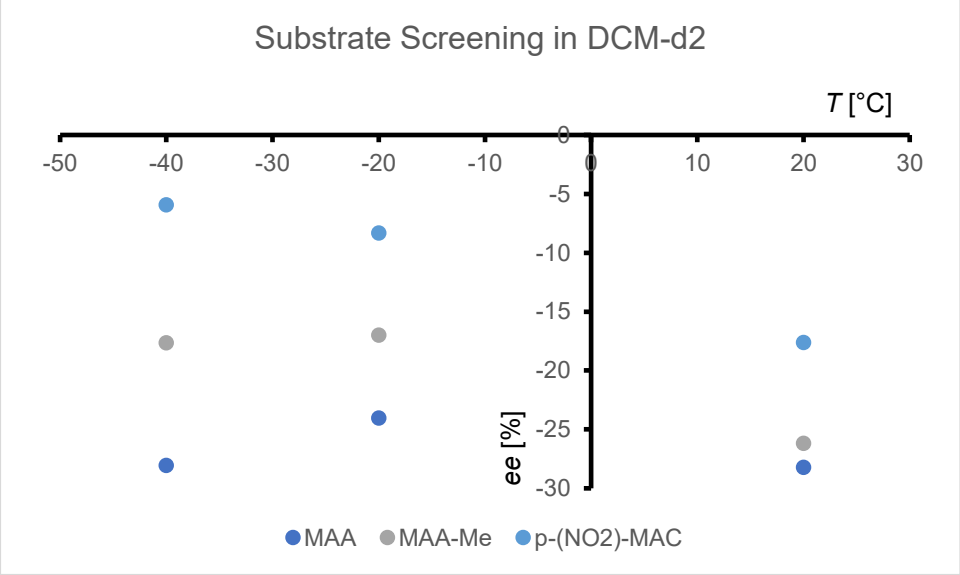

Figure 32: Substrate screening with the ligand **Val-3** and different reactants (**MAA**, **MAA-Me** and ***p*-(NO$_2$)-MAC**) and their *ee* in DCM-d$_2$ at different temperatures.

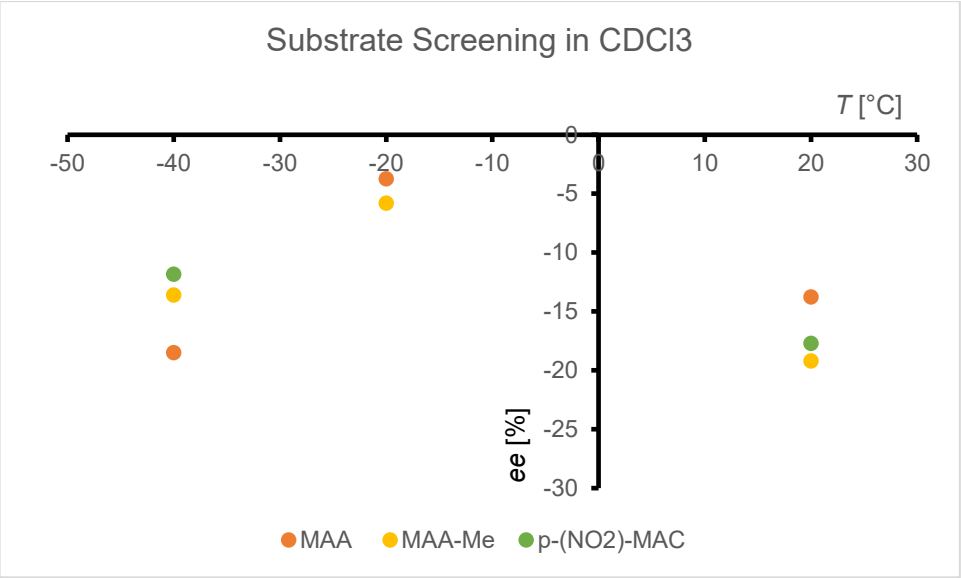

Figure 33: Substrate screening with the ligand **Val-3** and different reactants (**MAA**, **MAA-Me** and ***p*-(NO$_2$)-MAC**) and their *ee* in $CDCl_3$ at different temperatures.

After the ligand **Val-3** itself showed such remarkable temperature dependence of the proportions of the epimers with an inversion of the ratio observed around −20 °C (see Figure 25 and Figure 26), the complexation of the ligand **Val-3** with the metal source $Rh(COD)_2BF_4$ was performed at different temperatures. It is assumed that metal complexation prevents rotation around the chiral biphenyl axis and thus freezes the epimer distribution present at that moment. The idea of having a temperature-dependent ligand system that can be switched to obtain either product enantiomer just by varying the temperature of the complexation step was therefore further investigated. Key to influence the alignment of the ligand in the rhodium metal complex was to prepare different stock solutions of the ligand, the metal complex, and the hydrogenation reactant, as described above. The different solutions were set to the desired complexation temperature over a time of 10 minutes, to assure equilibration of the epimeric ratio of the ligand, followed by mixing the ligand and the rhodium source stock solution.

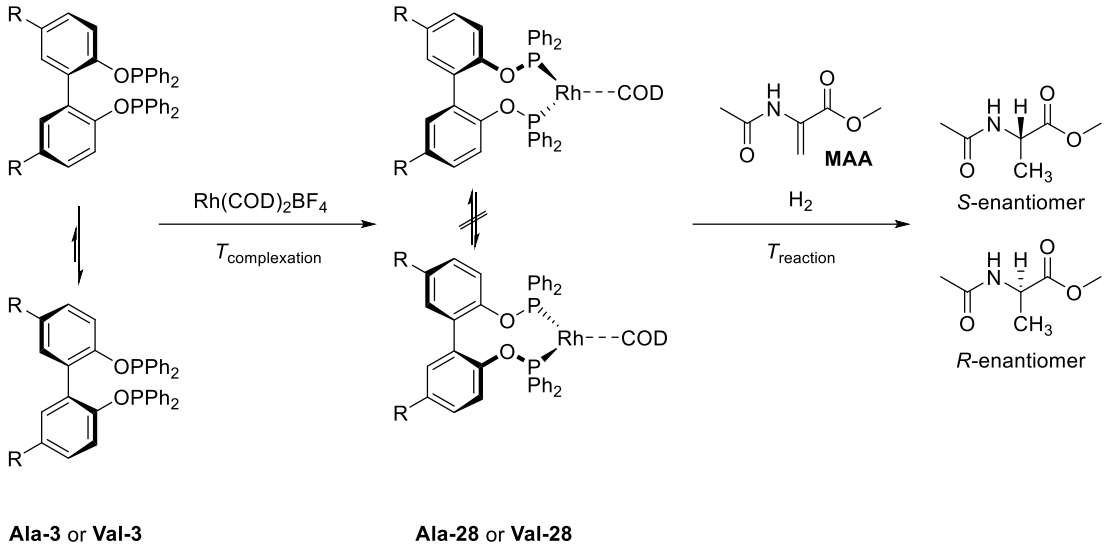

Figure 34: Temperature dependent complexation and subsequent addition of the prochiral olefin (e.g. **MAA**). Reaction temperatures ($T_{reaction}$) can vary from the complexation temperatur ($T_{complexation}$).

Further experiments were conducted in two different ways with the difference between the complexation temperature ($T_{complexatio}$) and the reaction temperature ($T_{reaction}$) (see Figure 34). For dataset one to three (Complex. Temp. (1)-(3)) in Figure 35, the given temperature values of the graph only show the complexation temperature ($T_{complexation}$). The reaction temperature ($T_{reaction}$) was at rt, after complexation and addition of MAA ($T_{complexation} \neq T_{reaction}$). The data set comes as a triplett to average errors. Data set 4 (Const. Temp., in yellow in Figure 35) was kept at set temperatures overnight indicating the same complexation temperature as reaction temperature ($T_{complexation}=T_{reaction}$). After workup of the reaction mixture, the product enantiomers were separated *via* GC-MS. Negative *ee* values again indicate a *S*-enantiomer favoring scalemic mixture while positive values correspond to an abundance of the *R*-enantiomer (see Figure 35). Contrary to the expected behavior however, the conducted experiments indicated that the catalyst system was not reliably controllable *via* simply changing the complexation temperature. It appears that the alignment of the ligand before the complexation step occurs spontaneous and does not consistently favor one or the other rotamer of the ligand even at a set complexation temperature, as indicated by the different signs and magnitude of the enantiomeric excesses of the hydrogenations. It is however noteworthy, that the obtained *ee*s are evenly distributed in the range of the calculated epimeric excesses of the ligand (see Table 1) and had their maximum values for the *S*-enantiomer of the poduct with −32.6% *ee* at −20 °C and −40 °C throughout. The maximum values for the enantiomer excess of the *R*-enantiomer were obtained at 0 °C and −20 °C with an *ee* of 14.6% and 14.0%, respectively.

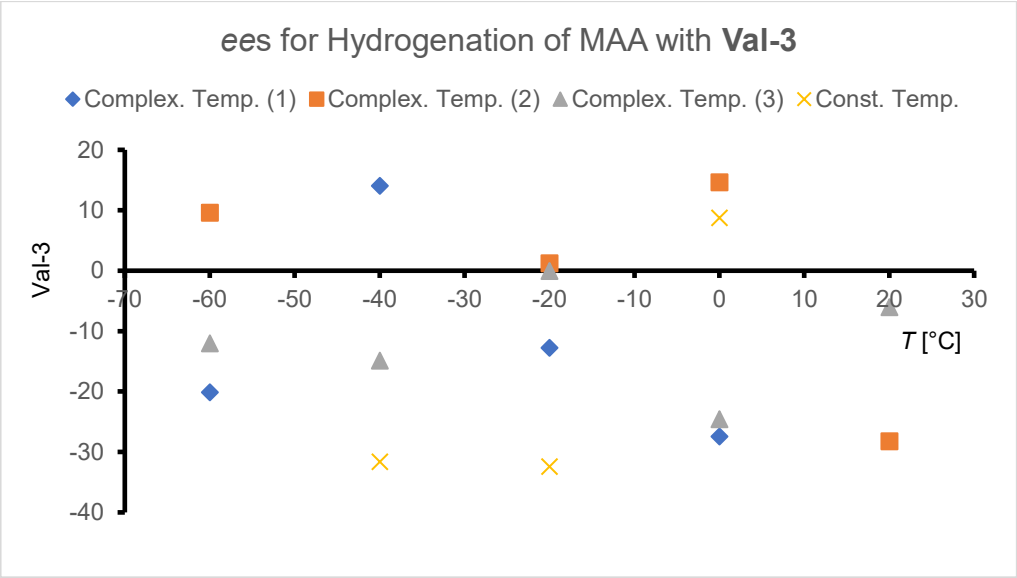

Figure 35: Graphical representation of the obtained *ee*-values after hydrogenation of **MAA** with ligand **Val-3**. For Complex. Temp. (1), (2) and (3), the complexation of the ligand was carried out at the temperatures shown in the graph and the reaction was performed at rt. For data set Const. Temp., the complexation temperature and reaction temperature are the same. Negative *ee*-values correspond to the *S*-enantiomer and positive ones to the *R*-enantiomer.

After an inversion of *ee* was detected for the hydrogenation of **MAA** with **Val-3**, the same experimental setup with different stock solutions for **MAA**, the ligand **Ala-28** and the rhodium source was used to compare **Val-3** with the performance of **Ala-3**. The *ee*s of the obtained hydrogenation products are visualized in Figure 36. No inversion of the stereoinduction was detected with **Ala-3** as chiral ligand. However, it is noteworthy, that with this ligand, only positive *ee* values, meaning the favored formation of *R*-configured dihydro-**MAA**, were observed, which stands in contrast to the mostly negative *ee*s obtained with **Val-3**. The obtained enantiomeric excesses fall in a range between 9.83% and 12.85%. This seems relatively consistent without the above mentioned variations.

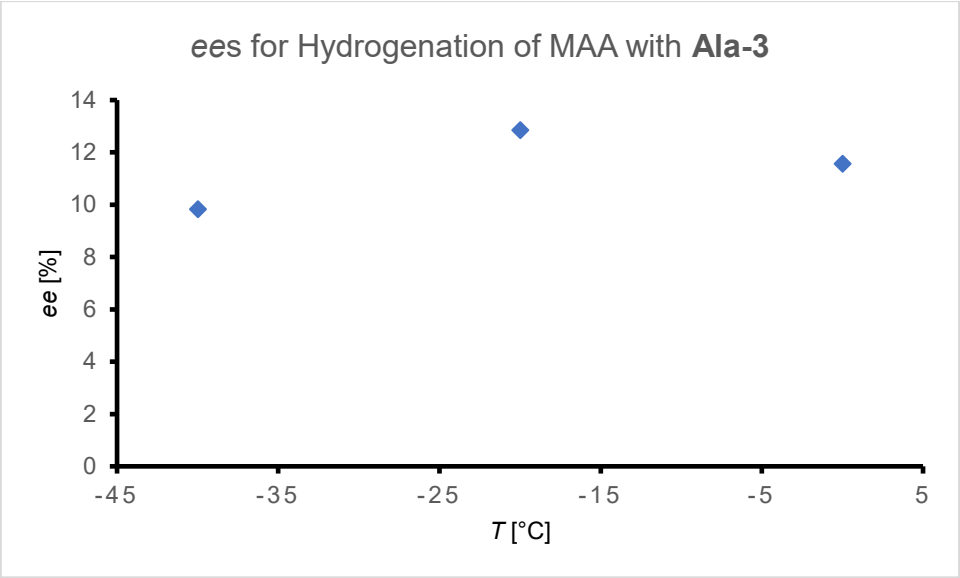

Figure 36: Temperature dependent experiment for the hydrogenation of **MAA** with **ALA-3** in CD_2Cl_2 at 40 bar H_2. Given temperature points indicate the temperature for complexation of the ligand with the Rh-source. The reaction was conducted at rt overnight.

2.3 Summary and Outlook – Bisphosphinite Ligands

Novel biphenyl-based bisphosphinite ligands with amino -acid-derived interaction-units were successfully synthesized and characterized. The interaction-units are connected to a highly flexible biphenyl backbone. The first design for a new ligand included a multistep synthesis for the interaction building block **10** from amino acid-derivatives such as valine based diamides. These interaction-units were connected to the backbone with their *C*-terminus as opposed to earlier work. Already at this stage, promising results in terms of supramolecular interactions could be observed in form of a splitting of the methylene group of the MOM-protective group in ^{1}H NMR experiments. Extreme sensitivity to both oxygen and water made the final bisphosphinite ligand **1** not suitable for catalysis since immediate decomposition reactions were observed.

The synthesis towards ligand **2** started from the same backbone as building block **17** which was slightly modified to an aryl azide. The interaction unit (**19**) chosen based on an amino acid with an alkyne residue as a linker. The intended click-reaction of an azide-alkine [3+2] cycloaddition to form a triazol (as opposed to a phenylene in **1** and **3**) bridge did not yield satisfactory results despite extensive screening. This ligand design was therefore not pursued any further.

Ligand **3** was successfully synthesized with alanine- and valine-based diamide interaction-units. These were transformed to their corresponding methylamides and attached to the biphenyl backbone **5** with their *N*-terminus *via* a bridging phenylene unit. The still MOM-protected ligand precursor **26** showed first signs of non-covalent interactions in ^{1}H NMR spectra in the form splitting of the methylene group in **Ala-26**, **Val-26** and ***t*-Leu-26**. With the introduction of the metal-interaction site, the bisphosphinite ligand was finalized. Due to significant broadening of the signals in the ^{1}H NMR spectra, the temperature dependence of the ligands **Ala-3** and **Val-3** was studied. The ligands were thus investigated regarding their epimeric distribution in temperature dependent ^{31}P NMR, revealing an unexpected inversion of their distribution. The peak ratios of **Ala-3** in ^{31}P NMR ranged from 1:3 at rt to 3:1 at −80 °C with the ligand **Val-3** in a similar range. The peak ratios were to the same extent. These results were used to determine equilibrium constants K and the free GIBBS energy ΔG as well as ΔS and ΔH. Epimeric excesses ranged from 31.97% to −56.25% for **Ala-3** and 29.08% to −49.25% for **Val-3**. In order to investigate the ligands capability to transfer their chiral information to asymmetric catalysis reactions, a subsequent coordination with $Rh(COD)_2BF_4$ was conducted *in situ* to obtain the final catalysts. Different reaction conditions for the hydrogenation were tested to achieve optimal stereoinduction. This screening included variations in H_2 pressure, solvents as well as the substrate. The best results for **Val-3** were obtained with 40 bar H_2 pressure in DCM-d2 with the prochiral olefin **MAA** as substrate. A spontaneous alignment of the ligand **Val-3** was observed, which manifested itself in different *ee*s either favoring the *S*-enantiomer or the *R*-enantiomer in the hydrogenation

reactions of prochiral olefins. After extensive testing, no clear temperature dependence for the alignment of the ligand could be observed. The obtained *ee*s range from −32.6% (in favor of the *S*-enantiomer) to 14.6% (in favor of the *R*-enantiomer).

Variations of the interaction units as well as further screening of conditions in asymmetric catalysis could benefit a deeper understanding of the mode and magnitude of the intramolecular interaction of the system. This study indicates that even small alterations can have a significant impact on the ligand's capability for alignment and recognition. The architecture of the entire ligand has to be precisely arranged in order to achieve self-alignment and non-covalent interactions. Further tuning of the alignment of *tropos* ligands remains a delicate balance between recognition (and therefore fixation) and preserving the flexibility of the ligand. All these delicate factors require further in-depth investigation.

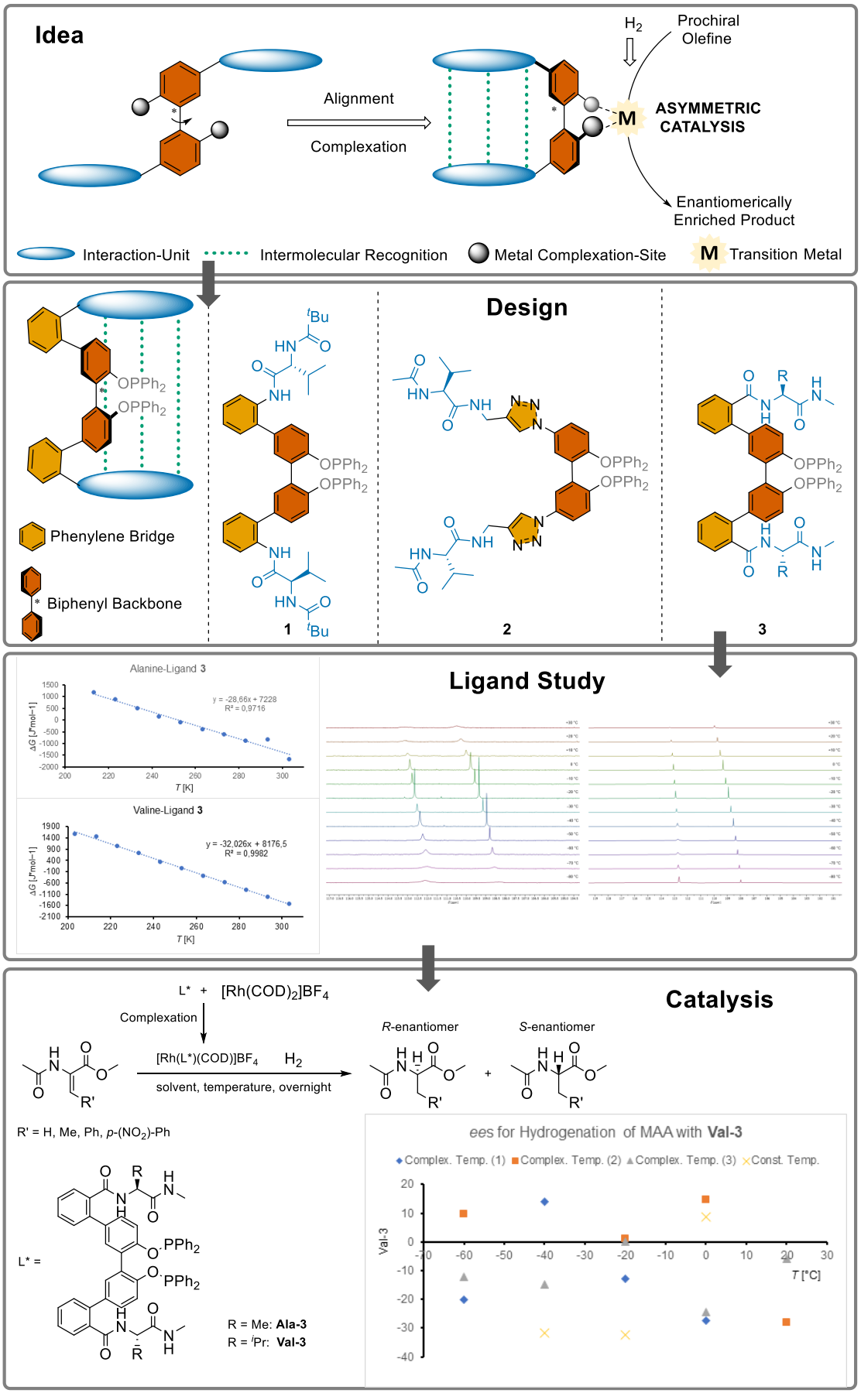

Figure 37: Summary of chapter 2. Design and application of new diamide bisphosphinite ligands.

3 Hemiacetal Investigation

3.1 Objective – Hemiacetal Investigation

As zinc hemiacetalate complexes were identified in high-resolution mass spectrometric measurements to occur in the SOAI reaction,[114] the system of hemiacetals is very important for the design of self-adaptable catalysts in autocatalytic reactions. Additionally, the motif of a dynamic hemiacetal in equilibrium with its ring-opened formation provides the opportunity to simultaneously serve as catalyst and substrate in a SOAI-like type reaction. For a deeper understanding of the behavior of these molecules, further experiments were carried out to synthesize biaryl systems bearing aldehyde and alcohol residues. *Via* spontaneous intramolecular cyclization, they are able to form hemiacetals shifting the biaryl system from *tropos* to *atropos* by stopping the free rotation around the σ-axis. Therefore, a biaryl structure was synthesized with a suitable substitution pattern to enable the formation of hemiacetals pictured in Figure 38.[117] Here the synthesis of a novel dynamic biaryl ligand is described as well as its characterization.

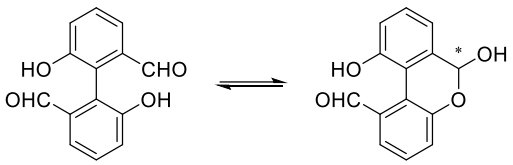

30 **31**

Figure 38: Equilibrium of the hemiacetal with opened and closed form.

Opened and closed form are in equilibrium which should be further investigated in chiral HPLC experiments. These properties make the developed structure a potential ligand in an autocalatysis according to SOAI and thus interesting for further investigations. It is worth mentioning though, that the hemiacetals in the SOAI reaction are formed intermolecularly and the here investigated ones are formed intramolecularly.[117] In the following, the synthesis of a double aldehyde-alcohol and subsequent analysis via HPLC are described in more detail. Further focus is placed on the determination of the interconversion barrier and the activation parameters to compare them with the ones for the formation of the transient hemiacetal catalyst identified by TRAPP *et al*. in the SOAI reaction.[117]

3.2 Results and Discussion – Hemiacetal Investigation

3.2.1 Synthetic Route of the Double Aldehyde-Alcohol System

Compound **32** was prepared according to BOTELHO *et al.*[124] After introduction of the boronic acid pinacol ester to give **34**, **33** and **34** were coupled in a SUZUKI-MIYAURA reaction obtaining **30**, **31**, **32** (see Scheme 11). Giving its very sensitive nature, compound **30** could not be isolated. It occurred only in equilibrium with the intramolecular monohemiacetal **31** and oxidizes to the hemiacetal-lactone **32** which was identified by HPLC-MS. As a result, both the hemiacetal interconversion of **31** as well as the hemiacetal-lactone **32** interconversion was observed in a single chromatographic run by chiral HPLC.

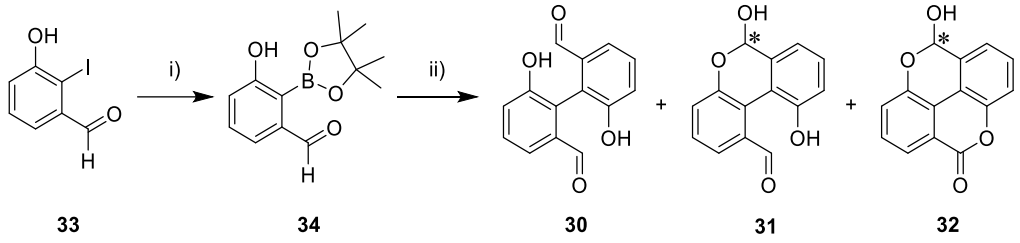

Scheme 11: Synthesis of compounds **30**, **31**, **32** i) B_2pin_2, KOAc, $Pd(dppf)_2Cl_2$ DMSO, 80 °C, 23 h; ii) K_2CO_3, **33**, $Pd(dppf)_2Cl_2$, DMSO, 70 °C, 24 h.[117]

3.2.2 Enantioselective Dynamic HPLC (DHPLC) Analysis

The investigated aldehyde structures are based on a biaryl scaffold and thus providing a free rotatable axis with contained chiral information. They shift between the open *tropos* and the closed six-membered ring form as *atropos*. For the transformation to the closed ring form, the chiral information at the stereogenic axis gets lost by planarization while a stereogenic center occurs at the formation of the hemiacetal.

Upon ring closure, the hemiacetal **31** forms enantiomers as well as the hemiacetal-lactone structure **32**. Additionally, the double aldehyde-alcohol system is present in the meso-isomeric form. The separation of the hemiacetal´s enantiomers was performed by HPLC on immobilized chiral stationary phases[125] and the structures were identified by MS detection (see Figure 39). Slight plateau formation was observed for compound **31** and **32** at room temperature (rt), which already showed the interconversion of the enantiomers. Based on that observation, temperature dependent enantiomeric DHPLC measurements were performed to determine enantiomerization barriers $\Delta G^{\ddagger}$ as well as the activation parameters $\Delta S^{\ddagger}$ and $\Delta H^{\ddagger}$ using EYRING-plot analysis. The constant k_1 standing for the enantiomerization rate was determined by applying the unified equation of dynamic chromatography[126] implemented in the software DCXplorer[127] to analyze the chromatographic peak profiles. For the lactone compound **32** the following parameters were obtained: the activation barrier $\Delta G^{\ddagger} = 89.8$ kJ·mol^{-1} and the activation parameters $\Delta H^{\ddagger} = 35.3 \pm 0.6$ kJ·mol^{-1} and $\Delta S^{\ddagger} = -183 \pm 38$ J·(K·mol)$^{-1}$. A slightly higher

enantiomerization barrier was found for the hemiacetal **31**: $\Delta G^{\ddagger} = 91.2$ kJ·mol^{-1}, $\Delta H^{\ddagger} = 27.8 \pm 1.2$ kJ·mol^{-1} and $\Delta S^{\ddagger} = -213 \pm 40$ J·(K·mol)$^{-1}$ (see Figure 40 and Figure 41). This is on full consistency with the shown interconversion profiles of the lactone form **32** in Figure 39 (B), in which even at slightly elevated temperatures a trend to pronounced plateau formation is visible. The measurement took place simultaneously from the same sample in a temperature range between 20 °C and 60 °C in 10 degree steps.

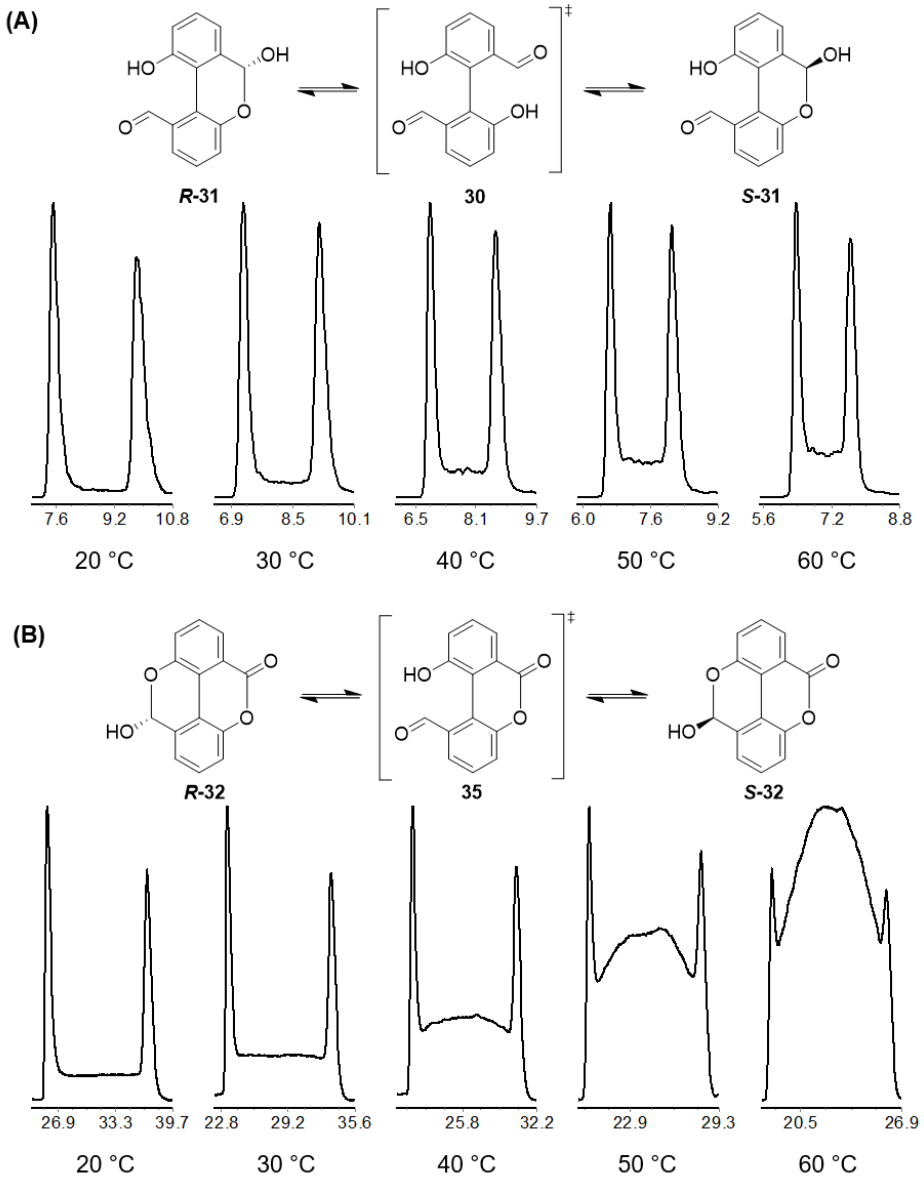

Figure 39: Temperature dependent HPLC measurements of **30**, **31**, **32** on CHIRALPAK IE Daicel (*n*-hexane : isopropanol; 85:15) from 20 °C to 60 °C in 10 degree steps; (A) Hemiacetal **31** interconversion. (B) Lactone **32** interconversion.[117]

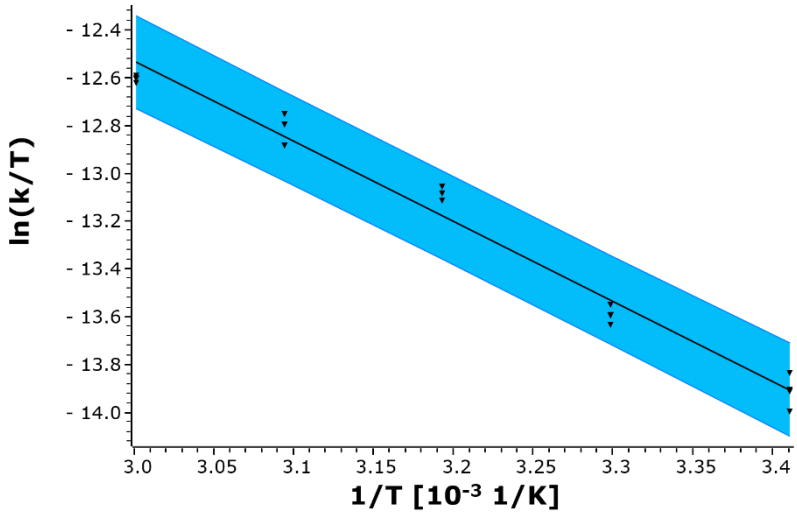

Figure 40: EYRING-plot **31** (hemiacetal) with the resulting values: $\Delta G^{\ddagger}$ = 91.18 kJ/mol; ΔH = 27.76 ± 1.24 kJ/mol; ΔS = −212.7 ± 40.3 J/(K·mol).[117]

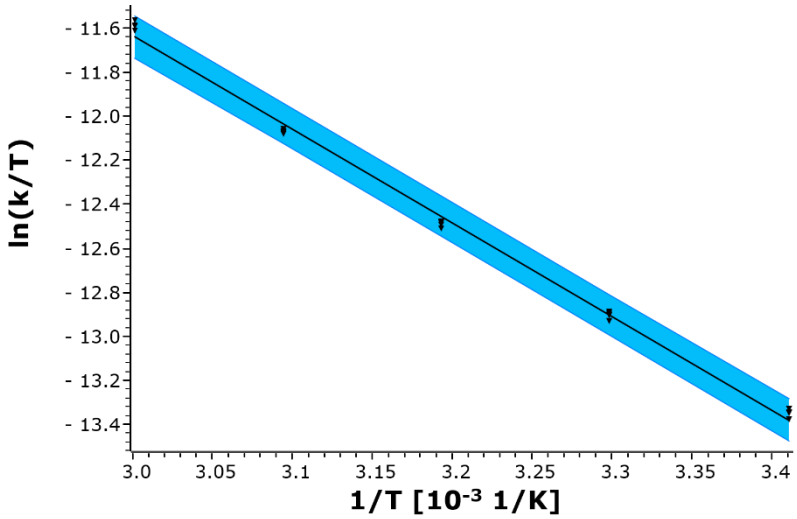

Figure 41: EYRING-plot **32** (lactone) with the resulting values: $\Delta G^{\ddagger}$ = 89.75 kJ/mol; ΔH = 35.33 ± 0.61 kJ/mol; ΔS = −182.5 ± 38.4 J/(K·mol).[117]

3.3 Summary and Outlook – Hemiacetal Investigation

The designed double aldehyde-alcohol structures at the biaryl backbone (**30**, **31**, **32**) could be successfully realized in synthesis. Further analysis of the double aldehyde-alcohol by chiral HPLC-MS detected not only the intramolecular hemiacetal form **31** but also the lactone form **32** during the same measurements. Their enantiomers could be separated by HPLC in the presence of immobilized chiral stationary phases. Further, the enantiomerization barriers could be determined through investigations using DHPLC experiments and subsequent EYRING-plot analysis. Comparison of the determined interconversion barriers with those for the formation of the transient hemiacetal catalyst which was identified to be the highly active species in the asymmetric autocatalytic reaction by SOAI, showed excellent consistency.[117]

The reaction parameter could be further optimized in upcoming experiments just as the scope of the hemiacetal motive should be expanded. Ultimately, these substrates should be implemented in a SOAI–like reaction to see if they can act as substrate and catalyst at the same time.

4 Experimental Section

4.1 General Methods

4.1.1 Analytical Methods

NMR-Spectroscopy

NMR spectra were measured on a Bruker Avance III HD 400 MHz and 800 MHz spectrometer equipped with a CryoProbeTM, Bruker AXR300, Varian VXR400 S and Bruker AMX600 spectrometers operating at 400 MHz, 800 MHz, 300 MHz, 400 MHz, and 600 MHz for proton nuclei (100 MHz, 75 MHz, 100 MHz, 150 MHz for carbon nuclei), respectively. Proton chemical shifts are expressed in parts per million (ppm, δ scale) and are referenced to residual protons in the NMR solvent ($CHCl_3$: δ 7.26, methanol-d_3: δ 4.78, $CHDCl_2$: δ 5.32, THF-d_7: 3.58, 1.72, DMSO-d_5: 2.50, CHD_2CN: 1.94, HDO: 4.79). Carbon chemical shifts are expressed in parts per million (δ scale, assigned carbon atom) and are referenced to the carbon resonance of the NMR solvent ($CDCl_3$: δ 77.16, CD_3OD: δ 49.00, CD_2Cl_2: δ 53.84, THF-d_8: 67.21, 25.31, DMSO-d_6: 39.52, CD_3CN: 1.32, 118.26).[128] ^1H NMR spectroscopic data are reported as follows: Chemical shift in ppm (multiplicity, coupling constants *J* (Hz), integration intensity, assigned proton). The multiplicities are abbreviated with s (singlet), br s (broad singlet), d (doublet), t (triplet), q (quartet) and m (multiplet). In case of combined multiplicities, the multiplicity with the larger coupling constant is stated first. Except for multiplets, the chemical shift of all signals, as well for centrosymmetric multiplets, is reported as the centre of the resonance range. Additionally, 2D NMR techniques such as homonuclear correlation spectroscopy (COSY), heteronuclear single quantum coherence (HSQC) and heteronuclear multiple bond coherence (HMBC) were used to assign signals. All raw fid files were processed, and the spectra analysed using the program MestReNOVA 104.3 from Mestrelab Research S. L.

Mass Spectrometry

Mass spectra were measured by the analytic section of the Department of Chemistry, Ludwig-Maximilians-Universität München and by the TRAPP group. Mass spectra were recorded on the following spectrometers (ionisation mode in brackets): MAT 95 (EI) and MAT 90 (ESI) from Thermo Finnigan GmbH, Q Extractive Plus (ESI) from Thermo Fischer Scientific and Thermo Scientific Q Exactive Plus mass spectrometer (ESI) with direct injection. The method used is reported at the experimental section.

IR Spectroscopy

IR spectra were measured using a Thermo Scientific Nicolet 700 ATR-FT-IR spectrometer and the signals were denoted as s (strong), m (medium), w (weak) and b (broad signal).

High Performance Liquid Chromatography (HPLC)

HPLC and HPLC-MS measurements were performed on Agilent Technologies 1200 equipped with autosampler, G1315D photodiode array detector (DAD) and coupled to a 6120 quadrupole mass spectrometer (APCI). Chiral columns used were chiralpak columns by Daicel Corporation.

Gas Chromatography (GC)

GC analysis was performed on Thermo Trace GC ULTRA, equipped with autosampler, split/splitless injector (20 mL/min splitflow, 250 °C injector temperature) and FID detector and Thermo Polaris Q equipped with autosampler. Chiral columns used (Mosandl-Acetyl: 25 m, i.d. 250 μm, film thickness 250 nm) were prepared and coated in the Trapp group.

4.1.2 Laboratory Methods

Most reactions were performed in flame-dried glassware under a positive pressure of argon, as noted. Air- and moisture-sensitive liquids were transferred *via* syringe or stainless-steel cannula through rubber septa. Solids were added under inert gas counter flow or were dissolved in appropriate solvents. Degassing of solvents was performed with three freeze pump thaw cycles. Dry degassed solvent was stored over molecular shieves 3-4 Å (VWR Chemicals), which were flame-dried under high vacuum for 4 h prior to use. Low temperature-reactions were carried out in a DEWAR vessel filled with a cooling agent: H_2O/ice (0 °C), acetone/dry ice (−20, −40, −60 °C). Hydrogenation reactions were carried out in a Dewar filled with *i*PrOH and cooled to desired temperatures with a gryostat: ministat 230 by huber (−20 °C) and Julaba FT902 (−40 °C). Reaction temperatures above room temperature (rt) were conducted in a heated oil bath. The reactions were magnetically stirred and monitored by analytical thin-layer chromatography (TLC), using poly ester plates precoated with silica gel (0.25 mm, 60 Å pore size, Merck) impregnated with a fluorescent indicator (254 nm). TLC plates were visualized by exposure to ultraviolet light (UV), were stained by submersion in aqueous potassium permanganate solution ($KMnO_4$), ceric ammonium molybdate solution (CAM) or ninhydrin solution and were developed by heating with a heat gun. Flash column chromatography was performed with silica gel (35-70 μm, 60 Å, thermos scientific) and Celite® (545, Macherey-Nagel GmbH &Co. KG) or ISOLUTE® (Biotage) as dryload. Automated flash column chromatography was performed on a puriFlash VS520Plus (interchim). The yields refer to chromatographically and spectroscopically (^1H and ^{13}C NMR) pure material. Autoclaves used were described by Trapp *et al.*[123]

4.1.3 Chemicals

Tetrahydrofuran (THF), diethyl ether (Et_2O), dichloromethane (CH_2Cl_2) and n-pentane were taken from the solvent purification system (MB SPS 5 (MBRAUN) under argon atmosphere. Dimethyl sulfoxide (DMSO), benzene, toluene, and methanol (MeOH) were

purchased from Acros Organics as 'extra dry' reagents and used as received. All other reagents and solvents were purchased from chemical suppliers (Sigma-Aldrich, Acros Organics, Alfa Aesar, TCI, ABCR, Fischer scientific, Deutero) and were used as received. Solvents for extraction, crystallization and flash column chromatography were purchased in technical grade and distilled under reduced pressure prior to use.

4.2 Organic Synthesis

4.2.1 Design 1: Synthesis of the Interaction-Unit

tert-Butyl (*S*)-(1-((2-hydroxyphenyl)amino)-3-methyl-1-oxobutan-2-yl)carbamate **7**

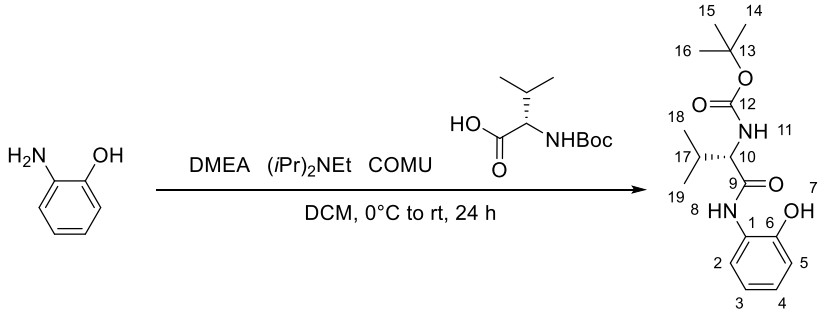

6 **7**

In a flame-dried Schlenk flask under argon, boc-*L*-valine (12.0 g, 55.0 mmol, 3.00 equiv.) was dissolved in anhydrous DCM (180 mL). Subsequently, *N*,*N*-diisopropylethylamine (DIPEA) (9.58 mL, 55.0 mmol, 3.00 equiv.) and 1-cyano-2-ethoxy-2-oxoethylidenaminooxy)dimethylamino-morpholinocarbenium hexafluorophosphate (COMU) (27.5 g, 64.1 mmol, 3.50 equiv.) were added to the solution at 0 °C. After 15 min, *o*-aminophenol **6** (2.00 g, 18.3 mmol, 1.00 equiv.) was added. The reaction mixture was allowed to warm to rt over night. Afterwards, 2-(dimethylamino)ethan-1-ol (DMEA) (40.0 mL, 367 mmol, 20.0 equiv.) was added and the mixture was stirred at rt for 6 h. EtOAc (600 mL) was added and the organic layer was washed with aqueous HCl (2M, 300 mL), saturated aqueous solution of $NaHCO_3$ (300 mL) and H_2O (300 mL). Subsequently, the organic layer was dried over $MgSO_4$ and the solvent was removed *in vacuo*. Afterwards, the crude product was purified by flash column chromatography (silica, pentane:EtOAc 6:1) to afford **7** as off-white powder (3.58 g, 11.6 mmol, 63%).

^{1}H-NMR (400MHz, $CDCl_3$): δ (ppm) = 8.40 (s, 1H, NH7), 7.17 – 7.09 (m, 1H, $H^{2/5}$), 7.02 (td, J = 7.9, 1.5 Hz, 2H, $H^{3,4}$), 6.85 (ddd, J = 8.6, 7.3, 1.5 Hz, 1H, $H^{2/5}$), 5.08 (s, 1H, NH^{11}), 4.17 – 4.04 (m, 1H, H^{10}), 2.28 (h, J = 6.8 Hz, 1H, H^{17}), 1.47 (s, 9H, $H^{14,15,16}$), 1.03 (dd, J = 15.3, 6.8 Hz, 6H, $H^{18,19}$).

^{13}C NMR (101MHz, $CDCl_3$): δ (ppm) = 171.97 (C^9), 149.01 (C^{12}), 127.51 ($C^{2/5}$), 125.23 ($C^{1/6}$), 122.63 ($C^{3/4}$), 120.60 ($C^{2/5}$), 119.87 ($C^{3/4}$), 60.91 (C^{10}), 30.43 (C^{17}), 28.42 ($C^{14,15,16}$), 19.56 ($C^{18/19}$), 18.09 ($C^{18/19}$).

HR-MS (ESI, acetone $[M\text{-}C_5H_{10}NO_2]^+$**)**: $C_{11}H_{14}NO_2^+$, calculated *m*/*z* 192.1019, found 192.0554.

(*S*)-2-(2-((*tert*-butoxycarbonyl)amino)-3-methylbutanamido)phenyl trifluoromethanesulfonate **8**

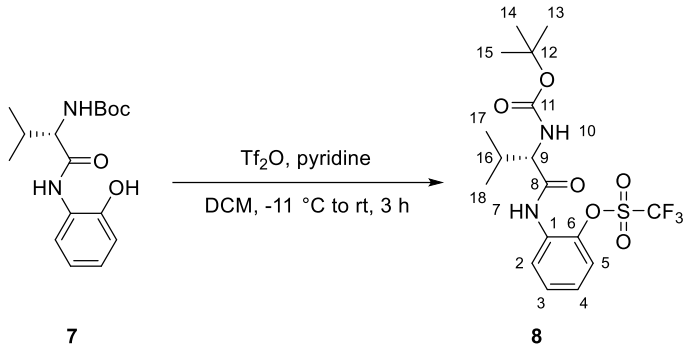

7 **8**

In a flame-dried Schlenk flask under argon, **7** was dissolved in anhydrous DCM (22 mL). Subsequently, pyridine (1.78 mL, 22.1 mmol, 1.90 equiv.) and trifluormethansulfonic anhydride (2.37 mL, 13.9 mmol, 1.20 equiv.) were added to the solution at −11°C. Next, the mixture was stirred for 3 h at rt. Afterwards, the crude product was extracted with EtOAc (480 mL) and was washed with HCl (2M, 3 x 160 mL) and brine(3 x 160 mL). The organic layer was dried over $MgSO_4$ and the solvent was removed *in vacuo*. Next, the crude product was purified by flash column chromatography (silica, pentane:EtOAc 10:1) to afford **8** (3.85 g, 8.74 mmol, 75%) as colourless crystals.

^{1}H-NMR (400MHz, $CDCl_3$): δ (ppm) = 8.33 (dd, J = 8.2, 1.6 Hz, 1H, H^5), 8.26 (s, 1H, NH^7), 7.39 (td, J = 7.8, 1.5 Hz, 1H, $H^{2/5}$), 7.30 (dd, J = 8.3, 1.5 Hz, 1H, H^2), 7.19 (ddd, J = 8.3, 7.4, 1.6 Hz, 1H, $H^{2/5}$), 4.97 (s, 1H, NH^{10}), 4.16 (s, 1H, H^9), 2.40 (hept., J = 6.6 Hz, 1H, H^{16}), 1.47 (s, 9H, $H^{13,14,15}$), 1.04 (d, J = 6.9 Hz, 3H, $H^{17/18}$), 0.95 (d, J = 6.9 Hz, 3H, $H^{17/18}$).

^{13}C NMR (101MHz, $CDCl_3$): δ (ppm) = 170.3 (1C, $C^{8/11}$), 139.1 (1C, C^6) 130.2 (1C, C^1), 129.1 (1C, C^3), 125.4 (1C, C^4), 123.6 (1C, C^2), 121.5 (1C, C^5), 80.8 (1C, C^{12}), 60.9 (1C, C^9), 30.1 (1C, C^{16}), 28.2 (3C, $C^{13,14,15}$), 19.4 (1C, $C^{17/18}$), 17.2 (1C, $C^{17/18}$).

MS (EI, acetone $[M\text{-}C_5H_9O_2]^+$**)**: $C_{17}H_{23}F_3N_2O_6S$, calculated *m*/*z* 340.07, found 340.02.

R_f (pentane/EtOAc 10:1) = 0.33.

(*S*)-2-(2-(chloro-λ⁵-azaneyl)-3-methylbutanamido)phenyl trifluoromethanesulfonate **9**

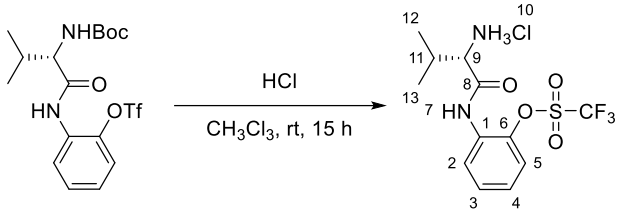

8 **9**

Compound **8** was dissolved in chloroform (25 mL) and hydrochloric acid (5M in isopropanol, 26.22 mL, 122 mmol, 15.0 equiv.) was added. The solution was stirred at rt over night. Afterwards, the solvent was removed *in vacuo* and the crude product was washed with diethylether (200 mL). Compound **9** (3.07 g, 8.15 mmol, 93%) was obtained as colourless powder.

^{1}H-NMR (400MHz, DMSO-*d*$_6$): δ (ppm) = 10.73 (s, 1H, NH^7), 8.39 (s, 3H, NH^{10}), 7.71 (dd, J = 8.4, 1.7 Hz, 1H, H^5), 7.58 – 7.49 (m, 2H, H$^{3/4}$), 7.47 – 7.37 (m, 1H, H^2), 3.93 (d, J = 5.1 Hz, 1H, H^9), 2.36 – 2.22 (m, 1H, H^{11}), 1.02 (dd, J = 29.9, 6.9 Hz, 6H, H$^{12/13}$).

^{13}C NMR (101MHz, DMSO-*d*$_6$): δ (ppm) = 167.85 (C^8), 142.48 (C$^{4/5}$), 129.57 (C$^{1/6}$), 129.32 (C^4), 127.62 (C^2), 127.21 (C^5), 121.96 (C^3), 57.77 (C^9), 29.68 (C^{11}), 18.71 (C$^{12/1}$3), 17.01 (C$^{12/13}$).

(*S*)-2-(3-methyl-2-pivalamidobutanamido)phenyl trifluoromethanesulfonate **10**

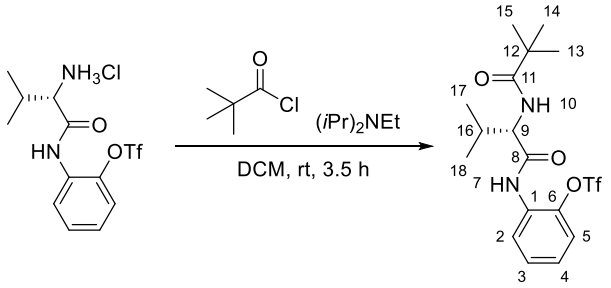

9 **10**

This compound was synthesized to a known procedure.[56] In a flame-driedSchlenk flask under argon, **9** was dissolved in anhydrous DCM (60 mL). The solution was cooled to 0 °C and trimethylacetylchloride (1.00 mL, 8.15 mmol, 1.00 equiv.) and DIPEA (4.26 mL, 24.4 mmol, 3.00 equiv.) were added. Afterwards, the solution was stirred at rt for 3.5 h. Subsequently, DCM (400 mL) was added and the organic layer was washed with HCl (2M, 2 x 200 mL), $NaHCO_3$ (200 mL), H_2O (200 mL) and brine(200 mL). Next, the organic layer was dried over $MgSO_4$ and the solvent was removed *in vacuo*. Compound **10** (3.20 g, 7.54 mmol, 93%) was obtained as colourless powder.

^{1}H-NMR (400MHz, $CDCl_3$): δ (ppm) = 8.17 (dd, *J* = 8.2, 1.6 Hz, 1H, H^5), 8.11 (s, 1H, NH^7), 7.38 (td, *J* = 7.8, 1.5 Hz, 1H, H^4), 7.30 (dd, *J* = 8.4, 1.5 Hz, 1H, H^2), 7.21 (ddd, *J* = 8.6, 7.4,

1.6 Hz, 1H, H^3), 6.17 (d, *J* = 8.2 Hz, 1H, NH^{10}), 4.43 (dd, *J* = 8.2, 6.2 Hz, 1H, H^9), 2.36 (hept., *J* = 6.7 Hz, 1H, H^{16}), 1.26 (s, 9H, $H^{13,14,15}$), 1.01 (dd, *J* = 16.3, 6.8 Hz, 6H, $H^{17,18}$).

^{13}C NMR (101MHz, $CDCl_3$): δ (ppm) = 170.24 (C^{11}), 140.14 (C^8), 130.20 ($C^{1/6}$), 129.18 (C^4), 125.99 (C^3), 124.55 (C^5), 121.64 (C^2), 77.36, 59.35 (C^9), 39.21 (C^{12}), 30.27 (C^{16}), 27.60 ($C^{13,14,15}$), 19.64 ($C^{17/18}$), 17.86 ($C^{17/18}$).

HR-MS (ESI, acetone $[M+H]^+$**):** $C_{17}H_{24}F_3N_2O_5S^+$, calculated *m/z* 425.1353, found 425.1351.

tert-Butyl (*S*)-(1-((2-iodophenyl)amino)-3-methyl-1-oxobutan-2-yl)carbamate **12**

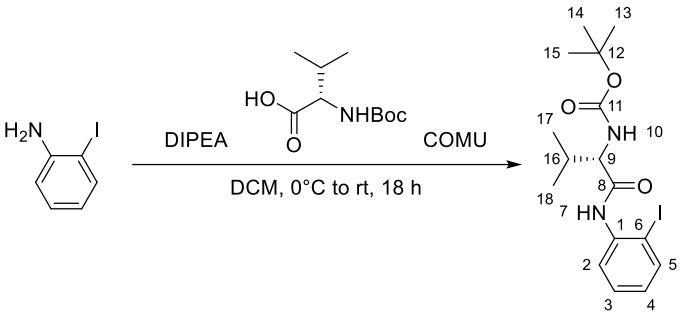

11 **12**

In a flame-dried Schlenk flask under argon, boc-*L*-valine (1.49 g, 6.85 mmol, 3.00 equiv.) was dissolved in anhydrous DCM (30 mL). DIPEA (1.19 mL, 6.85 mmol, 3.00 equiv.) and COMU (3.42 g, 7.99 mmol, 3.50 equiv.) were added to the solution at 0 °C. After 15 min, o-iodoaniline **11** (500 mg, 2.28 mmol, 1.00 equiv.) was added to the solution and the mixture was stirred at rt over night. Afterwards, EtOAc (75 mL) was added and the organic layer was washed with aqueous HCl (2M, 75 mL), a saturated aqueous solution of NaHCO3 (75 mL), H2O (75 mL) and brine(75 mL). Next, the organic layer was dried over MgSO4 and the solvent was removed in vacuo. The crude product was purified by flash column chromatography (silica, pentane:EtOAc 10:1). **12** (268 mg, 640 μmol, 28%) was obtained as yellow powder.

^{1}H-NMR (400MHz, $CDCl_3$): δ (ppm) = 8.30 – 8.23 (m, 1H, H^5), 8.13 (s, 1H, NH^7), 7.78 (dd, J = 8.0, 1.4 Hz, 1H, H^2), 7.35 (td, J = 7.9, 1.5 Hz, 1H, H^3), 6.86 (td, J = 7.7, 1.6 Hz, 1H, H^4), 5.06 (s, 1H, H^{10}), 4.17 (s, 1H, H^9), 2.46 – 2.28 (m, 1H, H^{16}), 1.47 (s, 9H, $H^{13,14,15}$), 1.02 (dd, J = 30.3, 6.9 Hz, 6H, $H^{17,18}$).

^{13}C NMR (101MHz, $CDCl_3$): δ (ppm) = 170.20 (C^{11}), 155.95 ($C^{1/9}$), 138.98 (C^2), 137.93 ($C^{1/9}$), 129.41 (C^3), 126.28 (C^4), 121.92 (C^5), 89.97 (C^6), 80.57 (C^{12}), 61.02 (C^9), 30.62 (C^{16}), 28.52 ($C^{13,14,15}$), 19.61 ($C^{17/18}$), 17.64 ($C^{17/18}$).

HR-MS (ESI, acetone $[M-H]^-$**)**: $C_{16}H_{22}O_3N_2I^-$, calculated *m/z* 417.0681, found 417.0683.

R_f (pentane/EtOAc 10:1) = 0.089.

tert-Butyl (*S*)-(1-((2-iodophenyl)amino)-3-methyl-1-oxobutan-2-yl)carbamate **12**

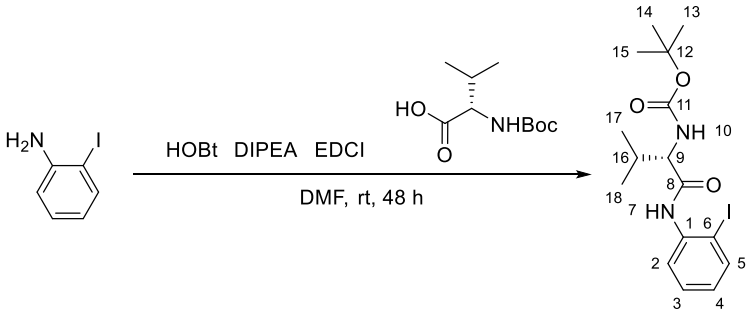

11 **12**

In a flame-dried Schlenk flask under argon, boc-*L*-valine (546 mg, 2.51 mmol, 1.10 equiv.) was dissolved in anhydrous DMF (30 mL). 1-Hydroxybenzotriazol (HOBt) (386 mg, 2.85 mmol, 1.25 equiv.) and *o*-iodoaniline **11** (500 mg, 2.28 mmol, 1.00 equiv.) were added and the solution was cooled to 0 °C. 1-Ethyl-3(3-dimethylaminopropyl)carbodiimide (EDCI) (547 mg, 2.85 mmol, 1.25 equiv.) and DIPEA (497 mg, 2.85 mmol, 1.25 equiv.) were added to the solution. Next, the mixture was stirred at rt for 48 h. Afterwards, EtOAc (400 mL) was added and the organic layer was washed with aqueous HCl (2M, 3 x 300 mL), a saturated aqueous solution of $NaHCO_3$ (3 x 300 mL), H_2O (2 x 300 mL) and brine(300 mL). Next, the organic layer was dried over $MgSO_4$ and the solvent was removed *in vacuo*. The crude product was purified by flash column chromatography (silica, pentane:EtOAc 10:1) to afford **12** (62.3 mg, 149 µmol, 7%) as colourless powder.

^{1}H-NMR (600MHz, $CDCl_3$): δ (ppm) = 8.27 (d, J = 8.3 Hz, 1H, H^5), 8.13 (s, 1H, NH^7), 7.78 (dd, J = 8.0, 1.5 Hz, 1H, H^2), 7.40 – 7.32 (m, 1H, H^3), 6.86 (td, J = 7.6, 1.6 Hz, 1H, H^4), 5.06 (s, 1H, H^{10}), 4.17 (s, 1H, H^9), 2.44 – 2.31 (m, 1H, H^{16}), 1.47 (s, 9H, $H^{13,14,15}$), 1.02 (dd, J = 30.2, 6.9 Hz, 6H, $H^{17,18}$).

^{13}C NMR (151MHz, $CDCl_3$): δ (ppm) = 170.20 (C^{11}), 155.95 ($C^{1/9}$), 138.98 (C^2), 137.93 ($C^{1/9}$), 129.41 (C^3), 126.28 (C^4), 121.92 (C^5), 89.97 (C^6), 80.57 (C^{12}), 61.02 (C^9), 30.62 (C^{16}), 28.52 ($C^{13,14,15}$), 19.61 ($C^{17/18}$), 17.64 ($C^{17/18}$).

HR-MS (ESI, acetone $[M+H]^+$**):** $C_{16}H_{22}O_3N_2I^+$, calculated *m*/*z* 419.0826, found 419.0828.

R_f (pentane/EtOAc 10:1) = 0.260.

4.2.2 Design 1: Backbone Synthesis

5,5′-dibromo-2,2′-bis(methoxymethoxy)-1,1′-biphenyl **16**

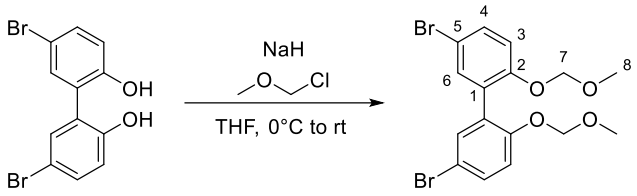

15 **16**

This compound was synthesized to a known procedure.[56] Tetrahydrofuran (250mL, dry, dg) was cooled to 0 °C in a flame-dried Schlenk flask under argon. Afterwards, **15** (34.5 g, 100 mmol, 1.00 equiv.) and sodium hydride (5.56 g, 209 mmol, 2.08 equiv.) were added. After 30 min, MOM-Cl (21.1 g, 2,40 mmol, 2.40 equiv.) was added. After 30 min, the reaction was allowed to warm to rt and stirred for further 3 h. Then, the reaction was quenched with sodium hydroxide (2 M, 100 mL). The aqueous layer was extracted with diethyl ether (3 x 300 mL). The combined organic layers were washed with brine (200 mL) and dried over sodium sulfate. All volatiles were removed *in vacuo* to obtain **16** (38.7 g, 89%) as a yellowish solid. The obtained analytical data were in full agreement with those reported in the literature.

^{1}H NMR (400 MHz, $CDCl_3$) δ = 7.41 (dd, *J*=8.8, 2.6, 2H, H^4), 7.34 (d, *J*=2.5, 2H, H^6), 7.10 (d, *J*=8.8, 2H, H^3), 5.05 (s, 4H, H^7), 3.35 (s, 6H, H^8).

HRMS (ESI) calcd for $C_{16}H_{15}Br_2O_4$ $[M-H]^-$: 428.93426; found: 428.93468.

2,2′-(6,6′-bis(methoxymethoxy)-[1,1′-biphenyl]-3,3′-diyl)bis(4,4,5,5-tetramethyl-1,3,2-dioxaborolane) **5**

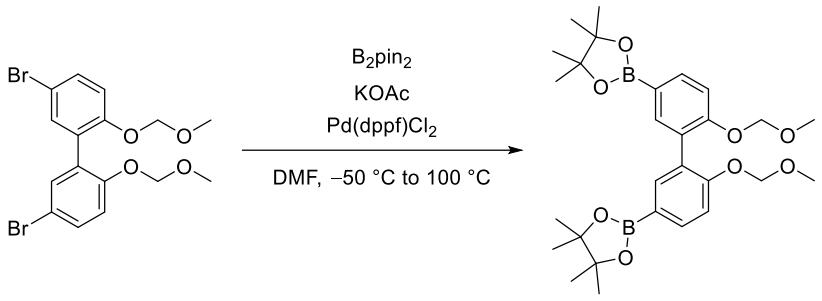

16 **5**

This compound was synthesized to a known procedure.[56] In a flame-dried Schlenk tube under argon, **16** (11.8 g, 27.31 mmol, 1.00 equiv.), B_2pin_2 (15.3 g, 60.1 mmol, 2.20 equiv.), potassium acetate (16.1 g, 164 mmol, 6.00 equiv.) and $Pd(dppf)Cl_2$ (2.00 g, 2.73 mmol, 0.10 equiv.) were dissolved in dimethylformamide (120 mL, dry) at −50 °C. After degassing for 30 min, the reaction was heated to 100 °C overnight. Subsequently, the reaction was cooled to rt and quenched with hydrochloric acid (1 M, 700 mL). The aqueous layer was extracted with dichloromethane (3 x 500 mL). The combined organic layers were dried over sodium sulfate and volatiles were removed *in vacuo.* The crude product was purified by flash column chromatography on silica gel (*n*-pentane ethyl acetate 7:1) to afford **5** (11.5 g, 80%) as a yellowish solid. The obtained analytical data were in full agreement with those reported in the literature.

^{1}H NMR (400 MHz, $CDCl_3$) δ = 7.76 (dd, *J*=8.3, 1.8, 2H), 7.69 (d, *J*=1.7, 2H), 7.18 (d, *J*=8.2, 2H), 5.09 (s, 4H), 3.35 (s, 6H), 1.32 (s, 24H).

^{13}C NMR (101 MHz, $CDCl_3$) δ = 157.75, 138.30, 135.88, 128.48, 114.08, 94.85, 83.71, 77.36, 56.04, 25.01.

4.2.3 Design 1: Ligand Synthesis:

(2*S*,2′*S*)-*N*,*N*′-(4′,6″-bis(methoxymethoxy)-[1,1′:3′,1″:3″,1‴-quaterphenyl]-2,2‴-diyl)bis(3-methyl2-pivalamidobutanamide) **13**

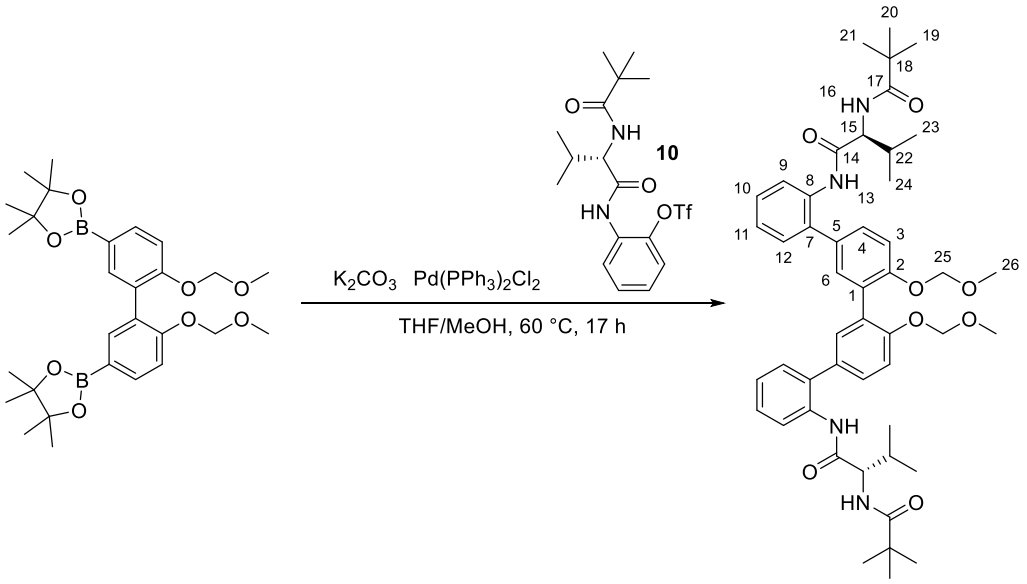

5 **13**

This compound was synthesized to a known procedure.[129] In a Schlenk flask, **5** (620 mg, 1.18 mmol, 1.00 equiv.), **10** (1.00 g, 2.36 mmol, 2.00 equiv.), potassium carbonate (977 mg, 7.07 mmol, 6.00 equiv.) and $Pd(PPh_3)_2Cl_2$ (33.1 mg, 47.1 µmol, 0.04 equiv.) were suspended in a mixture of THF (8 mL) and MeOH (2 mL). The suspension was degassed for 20 min. Afterwards, the reaction mixture was refluxed at 60 °C over night. Next, H_2O (300 mL) was added to the reaction mixture and the aqueous phase was extracted with EtOAc (3 x 300 mL). The combined organic phases were washed with brine(400 mL) and the solution was dried over $MgSO_4$. Subsequently, volatiles were removed *in vacuo*. The crude product was purified by flash column chromatography (silica, pentane:EtOAc 2:1) to afford **13** (445 mg, 541 µmol, 46%) as colourless powder.

H-NMR (800MHz, $CDCl_3$): δ (ppm) = 7.84 (d, ^{4}J=8.1 Hz, 1H, H^{13}), 7.33 (d_d, J=7.7, 1.7 Hz, 2H, $H^{9/12}$), 7.31 (d_d, J=, 8.7, 1.9 Hz, 1H, H^4), 7.30 (d, J=2.1 Hz, 1H, $H^{9/10/11/12}$), 7.27 (d, J=8.6 Hz, 2H, $H^{2,3}$), 7.23 (t_d, J=7.6, 1.3 Hz, 1H, $H^{9/10/11/12}$), 6.27 (d, ^{3}J=8.9 Hz, 1H, H^{16}), 5.11 (d, ^{2}J=6.9 Hz, 1H, H^{25}), 5.06 (d, ^{2}J=7.0 Hz, 1H, H^{25}), 4.60 (s, 1H, H^{15}), 3.33 (s, 3H, H^{26}), 2.05 (h, ^{3}J=6.7 Hz, 1H, H^{22}), 1.04 (s, 9H, $H^{19,20,21}$), 0.93 (d, ^{3}J=6.7 Hz, 3H, $H^{23/24}$), 0.87 (d, ^{3}J=6.9 Hz, 3H, $H^{23/24}$).

^{13}C NMR (201MHz, $CDCl_3$): δ (ppm) = 178.2 (1C, C^{14}), 154.3 (1C, C^2), 146.5 (1C, C^1), 134.6 (1C, $C^{7/8}$), 134.1 (1C, $C^{7/8}$), 132.6 (1C, $C^{3/4/6}$), 131.5 (1C, $C^{5/7}$), 130.7 (1C, $C^{9/10/11/12}$), 129.8 (1C, $C^{3/4,9/10/11/12}$), 128.3 (1C, $C^{5/7}$), 128.0 (1C, $C^{9/10/11/12}$), 125.9 (1C, $C^{9/10/11/12}$), 115.8 (1C, $C^{3/4/6}$), 95.0 (1C, C^{25}), 57.7 (1C, C^{15}), 56.2 (1C, C^{26}), 38.8 (1C, C^{18}), 32.3 (1C, C^{22}) 27.6 (3C, $C^{19,20,21}$), 19.0 (1C, $C^{23/24}$), 18.4 (1C, $C^{23/24}$).

HR-MS (ESI, acetone [M+H]$^+$**)**: $C_{48}H_{63}N_4O_8^+$, calculated *m/z* 823.4640, found 823.4628.

R_f (pentane/EtOAc 2:1) = 0.174.

(2*S*,2′*S*)-*N*,*N*′-(4′,6″-bis(methoxymethoxy)-[1,1′:3′,1″:3″,1‴-quaterphenyl]-2,2‴-diyl)bis(3-methyl2-pivalamidobutanamide) **13**

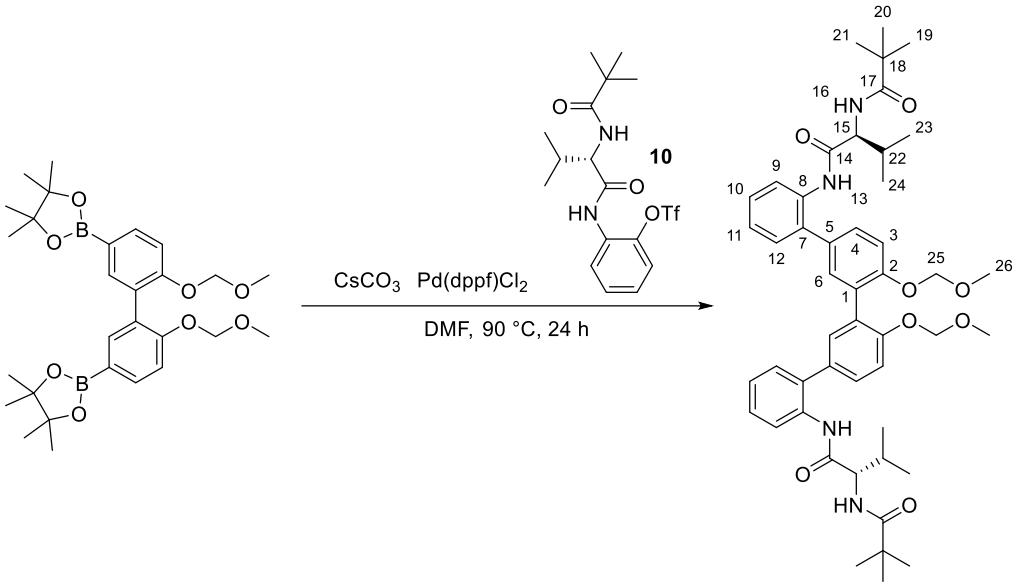

5 **13**

This compound was synthesized to a known procedure.[130] In a flame-driedSchlenk flask under argon, **5** (200 mg, 380 µmol, 1.00 equiv.), **10** (323 mg, 760 µmol, 2.00 equiv.) and caesium carbonate (310 mg, 950 µmol, 2.50 equiv.) were suspended in DMF (8.0 mL). The suspension was degassed for 15 min. Afterwards, $Pd(dppf)Cl_2$ (20.9 mg, 28.5 µmol, 0.07 equiv.) was added to the suspension and the reaction mixture was refluxed at 90 °C for 16 h. Next, EtOAc (100 mL) was added to the reaction mixture and the organic layer was washed with water (3 x 100 mL) and brine(100 mL). The solution was dried over $MgSO_4$ and all volatiles were removed *in vacuo*. Subsequently, the crude product was purified by flash column chromatography (silica, pentane:EtOAc 2:1). Compound **13** (159 mg, 193 µmol, 51%) was obtained as brown solid.

^{1}H-NMR (400MHz, $CDCl_3$): δ (ppm) = 8.17 (d_d, *J*=8.2, 1.2 Hz, 1H, $H^{9/10/11/12}$), 7.78 (d_d, *J*=8.3, 1.7 Hz, 1H, $H^{3/4}$), 7.33 (m, 2H, $H^{9/10/11/12}$), 7.24 (m, 1H, H^6), 7.00 (d_d, *J*=8.2, 1.5 Hz, 2H, $H^{9/10/11/12}$), 6.40 (d, ^3J=8.2 Hz, H^{16}), 5.15 (s, 2H, H^{25}), 4.29 (d_d, ^3J=8.2, 5.8 Hz, 1H, H^{15}), 3.38 (s, 3H, H^{26}), 2.05 (s, 1H, H^{22}), 1.18 (s, 9H, $H^{13,20,21}$), 0.85 (d, ^3J=6.8 Hz, 3H, $H^{23/24}$), 0.77 (d, ^3J=6.9 Hz, $H^{23/24}$).

^{13}C NMR (101MHz, $CDCl_3$): δ (ppm) = 178.9 (1C, C^{17}), 171.3 (1C, C^{14}), 157.6 (1C, C^2), 155.0 (1C, C^1), 148.6 (1C, C^8), 138.2 (1C, $C^{5/7}$), 136.1 (1C, $C^{3/4}$), 132.8 (1C, $C^{3/4}$), 128.2 (1C, $C^{9/10/11/12}$), 127.1 (1C, $C^{5/7}$), 125.6 (1C, $C^{9/10/11/12}$), 122.7 (1C, C^6), 122.2 (1C, $C^{9/10/11/12}$), 119.2 (1C, $C^{9/10/11/12}$),

95.2 (1C, C^{25}), 58.8 (1C, C^{15}), 56.1 (1C, C^{26}), 39.1 (1C, C^{18}), 31.4 (1C, C^{22}), 27.6 (3C, $C^{19,20,21}$), 18.5 (1C, $C^{23/24}$), 17.7 (1C, $C^{23/24}$).

HR-MS (EI, acetone $[M+H+C_3H_6O\text{-}C_{10}H_{18}NO_2]^+$**)**: $C_{41}H_{53}N_3O_7^+$, calculated *m*/*z* 698.3800, found 698.3660.

R_f (pentane/EtOAc 2:1) = 0.367.

Pivalyl (*S*) valine based bis-5,5′-(2-phenylamine)-2,2′-biphenol **14**

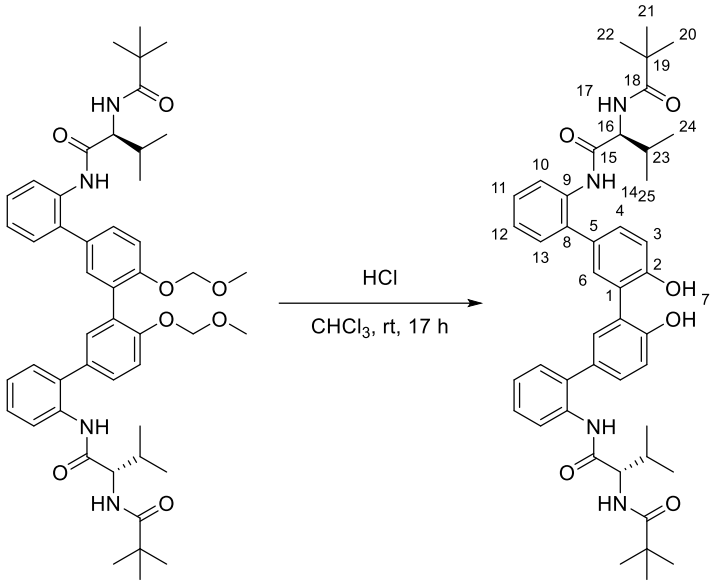

13 **14**

This compound was synthesized to a known procedure.[56] Compound **13** (440 mg, 535 µmol, 1.00 equiv.) was dissolved in chloroform (1.56 mL), before hydrochloric acid (5M in isopropanol, 1.56 mL, 7.81 mmol, 14.6 equiv.) was added. Subsequently, the reaction mixture was stirred at rt over night. Afterwards, EtOAc was added to the solution and the organic layer was washed with water to neutrality. Subsequently, the mixture was dried over $MgSO_4$ and the solvent was removed *in vacuo*. Compound **14** (258 mg, 351 µmol, 66%) was obtained as deep red resin.

^{1}H-NMR (800MHz, DMSO-d_6): δ (ppm) = 7.62 (m, 1H, $H^{10/11/12/13}$), 7.55 (m, 1H, $H^{10/11/12/13}$), 7.36 (d, *J*=8.1 Hz, 1H, $H^{2/3/4}$), 7.27 (m, 1H, $H^{2/5/6}$), 7.16 (m, 1H, $H^{2/3/4}$), 6.98 (m, 2H, $H^{10/11/12/13}$), 3.62 (s, 1H, H^{16}), 2.07 (h, ^3J=6.8, 6.4 Hz, 1H, H^{23}), 1.12 (s, 9H, $H^{20,\,21,\,22}$), 0.88 (d_d, $^{3,\,4}J$=12.3, 6.8 Hz, 6H, $H_{24,\,25}$).

^{13}C NMR (201MHz, DMSO-d_6): δ (ppm) = 177.6 (1C, C^{18}), 171.2 (1C, C^{15}), 153.4 (1C, C^2), 145.0 (1C, C^1), 134.3 (1C, $C^{5/8}$), 132.0 (1C, $C^{10/11/12/13}$), 131.8 (1C, $C^{3/4/6}$), 131.5 (1C, $C^{10/11/12/13}$), 129.8 (1C, $C^{10/11/12/13}$), 128.8 (1C, $C^{8/9}$), 128.4 (1C, $C^{3/4/6}$), 127.0 (1C, $C^{3/4/6}$), 125.2 (1C, $C^{5/8}$), 115.9 (1C, $C^{10/11/12/13}$), 67.5 (1C, C^{19}), 51.5 (1C, C^{16} 29.5 (1C, C^{23}), 27.2 (3C, $C^{20,21,23}$), 19.14 (1C, $C^{24/25}$), 18.8 (1C, $C^{24/25}$).

HR-MS (ESI, acetone [M-H]$^-$**)**: $C_{44}H_{53}N_4O_6^-$, calculated *m*/*z* 733.3971, found 733.397

N,N'-(4',6''-bis((diphenylphosphaneyl)oxy)-[1,1':3',1'':3'',1'''-quaterphenyl]-2,2'''-diyl)bis(3-methyl-2-pivalamidobutanamide) **1**

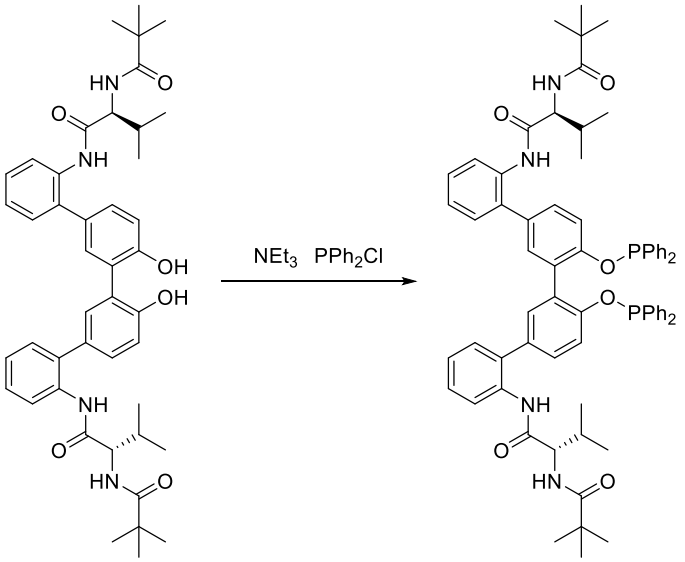

This compound was synthesized to a known procedure.[56]In a flame dried Schlenk tube under argon, BIPOL **14** (157 mg, 214 µmol, 1.00 equiv.) was added and dissolved in tetrahydrofuran (2.2 mL, dry, dg, with stabilizer). NEt_3 (72.7 µL, 854 µmol, 4.00 equiv.) was added and the solution was cooled to 0 °C. Afterwards, PPh_2Cl (259 µL, 854 µmol, 4.00 equiv.) was added dropwise. After 15 min, the mixture was allowed to warm to rt. After the mixture was stirred for 5 h, the suspension was passed through a pad of dry, neutral alumina under inert conditions and eluated with ethyl acetate (25 mL, dry, dg). The combined organic fractions were evaporated *in vacuo*. For further purification, the crude product was dissolved in dichloromethane (1 mL, dry, degassed) and reprecipitated with *n*-pentane (10 mL, dry, dg). The solvent was removed with a filter tipped cannula. Afterwards, volatiles were removed *in vacuo* to obtain **1** (98.6 mg, 42%) as an orange oil.

^{1}H NMR (800 MHz, $CDCl_3$) δ(pmm) = 7.83 – 7.77 (m, 2H), 7.61 (tt, *J* = 8.1, 1.3 Hz, 3H), 7.45 (td, *J* = 7.3, 1.5 Hz, 2H), 7.41 – 7.38 (m, 3H), 7.37 – 7.32 (m, 4H), 7.31 – 7.02 (m, 29H), 6.20 (d, *J* = 8.8 Hz, 1H), 4.68 (s, 1H), 2.05 (dt, *J* = 13.6, 6.7 Hz, 1H), 1.31 – 1.24 (m, 4H), 1.00 (d, *J* = 6.8 Hz, 4H), 0.96 – 0.89 (m, 18H).

^{13}C NMR (201 MHz, $CDCl_3$) δ (ppm) = 135.53, 135.49, 135.43, 135.39, 134.12, 134.11, 131.64, 131.64, 131.63, 131.62, 131.50, 131.47, 131.46, 131.42, 130.64, 130.40, 129.76, 129.75, 129.74, 129.63, 129.42, 128.68, 128.66, 128.62, 128.55, 128.49, 128.44, 128.41, 128.35, 128.33, 128.31,

128.29, 128.29, 128.23, 38.66, 32.47, 27.71, 27.70, 27.68, 27.62, 27.57, 27.50, 27.49, 27.48, 27.47, 19.06, 18.54, 18.52, 1.17.

^{31}P NMR (162 MHz, $CDCl_3$) δ (ppm) = 110.94.

4.2.4 Design 2: Synthesis

Bis-5,5′-diazido-2,2′-di(methoxymethyloxy)-biphenyl **17**

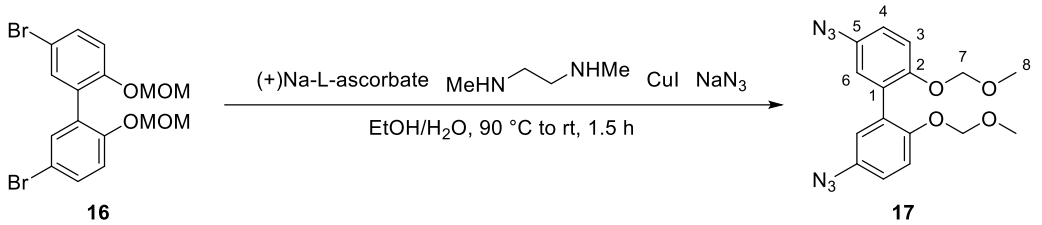

16 **17**

This compound was synthesized to a known procedure.[118] The solvent of this reaction EtOH/H_2O (19.3 mL/8.30 mL; 7:3) was placed in a Schlenk tube under argon. After it was degassed for 10 min, CuI (264 mg, 1.39 mmol, 0.200 equiv.), Na-ascorbate (138 mg, 694 µmol, 0.100 equiv.), NaN_3 (1.81 g, 27.8 mmol, 4.00 equiv.) and 5,5′-dibromo-2,2′-bis(methoxymethyloxy)-biphenyl **16** (3.00 g, 6.94 mmol, 1.00 equiv.) were added under argon. Lastly, the 1,2-dimethylethylenediamine (184 mg, 2.08 mmol, 0.300 equiv.) was added to the mixture and stirred at 90°C for 1 h under reflux. After cooling to rt, the crude product was by extracted with EtOAc (3 x 200 mL). The combined organic layers were washed with brine (1 x 300 mL), dried over $MgSO_4$ and concentrated *in vacuo*. The crude product was purified by flash column chromatography (silica, cyclohexane:EtOAc 12:1, R_F (cyclohexane:EtOAc 12:1) = 0.27) to obtain **17** (1.59 g, 4.45 mmol, 64%) as an orange solid.

^{1}H NMR (400 MHz, CD_2Cl_2): δ (ppm) = 7.21 (d, $^3J_{H\text{-}H}$ = 8.8 Hz, 2H, H^3), 6.99 (dd, $^3J_{H\text{-}H}$ = 8.8 Hz, $^4J_{H\text{-}H}$ = 2.9 Hz, 2H, H^4), 6.92 (d, $^4J_{H\text{-}H}$ = 2.8 Hz, 2H, H^6), 5.05 (s, 4H, H^7), 3.33 (s, 6H, H^8).

^{13}C NMR (101 MHz, CD_2Cl_2): δ (ppm) = 152.59 (C^2), 133.72 (C^5), 129.84 (C^1), 122.05 (C^6), 119.74 (C^4), 117.05 (C^3), 95.82 (C^7), 56.24 (C^8).

HRMS (ESI): m/z: $C_{16}H_{20}N_2O_4Cu^+$ [M+Cu]$^+$: calc.: 367.0714, found: 367.0714.

N-acetyl-L-valine-propargylamide **19**

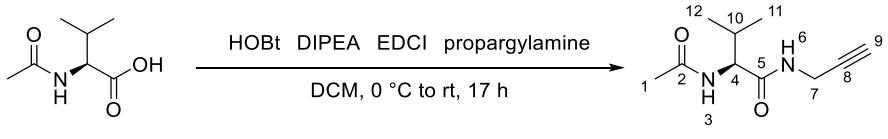

18 **19**

This compound was synthesized to a known procedure.[120] In a flame dried Schlenk tube under argon *N*-acetyl-L-valine **18** (1.00 g, 6.28 mmol, 1.00 equiv.) was dissolved in anhydrous DCM (50 mL). After addition of HOBt (1.06 g, 7.85 mmol, 1.25 equiv.), the mixture was cooled to 0°C and anhydrous DIPEA (1.01 g, 7.85 mmol, 1.25 equiv.) and

EDCI (1.22 g, 7.85 mmol, 1.25 equiv.) were added. After 15 min, propargylamine (433 mg, 7.85 mmol, 1.25 equiv.) was added and the reaction was slowly warmed to rt. The mixture stirred for 17 h. Next, the reaction was diluted with EtOAc (500 mL) and washed with aqueous HCl (2M, 3 x 200 mL), saturated aqueous solution of $NaHCO_3$ (3 x 200 mL) and brine (1 x 200 mL). The organic layer was dried over $MgSO_4$ and concentrated *in vacuo* to obtain **19** (92.3 mg, 470 µmol, 24%) as a white solid.

^{1}H NMR (400 MHz, CD_2Cl_2): δ (ppm) = 6.30 (s, 1H, H^6), 6.06 (s, 1H, H^3), 4.17 (ddd, $^3J_{H\text{-}H}$ = 8.7 Hz, $^3J_{H\text{-}H}$ = 6.9 Hz, $^3J_{H\text{-}H}$ = 3.8 Hz, 1H, H^4), 4.01 (ddd, $^3J_{H\text{-}H}$ = 6.6 Hz, $^3J_{H\text{-}H}$ = 5.5 Hz, $^4J_{H\text{-}H}$ = 2.6 Hz, 2H, H^7), 2.27 (t, $^4J_{H\text{-}H}$ = 2.6 Hz, 1H, H^8), 2.11 – 2.01 (m, 1H, H^{10}), 1.98 (s, 3H, H^1), 0.93 (ddd, $^3J_{H\text{-}H}$ = 5.7 Hz, $^3J_{H\text{-}H}$ = 4.3 Hz, $^4J_{H\text{-}H}$ = 1.4 Hz, 6H, $H^{11,12}$).

^{13}C NMR (101 MHz, CD_2Cl_2): δ (ppm) = 171.24 (C^4), 170.34 (C^{10}), 79.78 (C^7), 71.46 (C^8), 58.73 (C^3), 31.36 (C^2), 29.23 (C^6), 23.39 (C^{11}), 19.31 (C^1), 18.28 (C^1).

HRMS (ESI): m/z: $C_{10}H_{16}N_2O_2Na^+$ $[M+Na]^+$: calc.: 219.1104, found: 219.1104.

4.2.5 Design 3: Synthesis of the Interaction-Unit

Boc-L-alanine methyl amide **Ala-22**

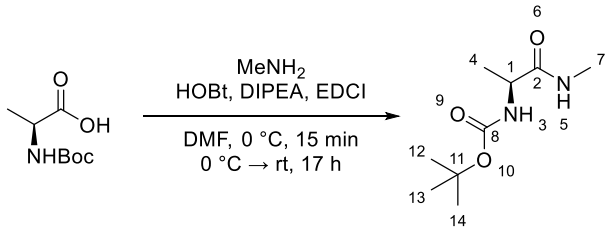

Als-21 **Ala-22**

Boc-L-Ala-OH **Ala-1** (1.89 g, 10.0 mmol, 1.00 equiv.) and HOBt (1.69 g, 12.5 mmol, 1.25 equiv.) were dissolved in DMF (dry, dg, 55 mL) in a flame-driedSchlenk flask under argon. After cooling the mixture to 0 °C, DIPEA (dry, 2.18 mL, 12.5 mmol, 1.25 equiv.) and EDCI (1.94 g, 12.5 mmol, 1.25 equiv.) were added. After 15 min, methylamine (33 wt.% ethanol, 1.56 mL, 12.5 mmol, 1.25 equiv.) was added. The reaction was slowly warmed to rt and stirred for 17 h. The mixture was diluted with EtOAc (750 mL), and the organic layer was washed with aqueous HCl (2M, 3 x 300 mL), a saturated aqueous solution of $NaHCO_3$ (3 x 300 mL) and brine (300 mL). The organic layer was dried over $MgSO_4$, filtrated and concentrated *in vacuo* to obtain **Ala-22** (816 mg, 4.00 mmol, 40%) as a yellow oil.

^{1}H NMR (400 MHz, $CDCl_3$): δ (ppm) = 6.16 (s, 1H, H^3/H^5), 5.05 (s, 1H, H^3/H^5), 4.08 (s, 1H, H^1), 2.76 (d, $^3J_{H\text{-}H}$ = 4.9 Hz, 3H, H^7), 1.42 (s, 9H, $H^{12,13,14}$), 1.30 (d, $^3J_{H\text{-}H}$ = 7.1 Hz, 3H, H^4).

^{13}C NMR (101 MHz, $CDCl_3$): δ (ppm) = 173.4 (C^2), 155.7(C^8), 80.1(C^{11}), 50.5 (C^1), 28.4 ($C^{12,13,14}$), 26.3 (C^7), 18.7 (C^4).

HRMS (ESI): m/z: $C_9H_{19}N_2O_3^+$ [M+H]$^+$: calc.: 203.1390, found: 203.1390.

Boc-L-valine methyl amine **Val-22**

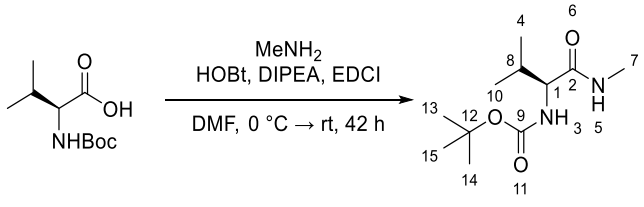

Val-21 **Val-22**

Val-21 (2.03 g, 10.0 mmol, 1.00 equiv.) and HOBt (1.69 g, 12.5 mmol, 1.25 equiv.) were dissolved in DMF (dry, dg, 55 mL) in a flame-driedSchlenk flask under argon. After cooling the mixture to 0 °C, DIPEA (dry, 2.17 mL, 12.5 mmol, 1.25 equiv.) and EDCI (1.94 g, 12.5 mmol, 1.25 equiv.) were added. After 15 min, methylamine (33 wt.% ethanol,

1.55 mL, 12.5 mmol, 1.25 equiv.) was added. The reaction was slowly warmed to rt and stirred for 42 h. The mixture was diluted with EtOAc (750 mL) and the organic layer was washed with aqueous HCl (2M, 3 x 300 mL), a saturated aqueous solution of $NaHCO_3$ (3 x 300 mL) and brine (300 mL). The organic layer was dried over $MgSO_4$, filtrated and concentrated *in vacuo* to obtain **Val-22** (796 mg, 3.70 mmol, 37%) as a yellow oil.

^{1}H NMR (400 MHz, $CDCl_3$): δ (ppm) = 6.45 (s, 1H, H^3/H^5), 4.87 (s, 1H, H^3/H^5), 2.82 (d, $^3J_{H-H}$ = 4.7 Hz, 3H, H^7), 1.48 (s, 6H, $H^{4,8}$), 1.44 (s, 9H, $H^{13,14,15}$).

^{13}C NMR (101 MHz, $CDCl_3$): δ (ppm) = 175.4 (C^2), 155.0 (C^9), 77.4 (C^{12}), 56.9 (C^1), 28.5 ($C^{13,14,15}$), 26.7 (C^7), 26.0 ($C^{4,8}$).

HRMS (ESI): m/z: $C_{10}H_{21}N_2O_3^+$ [M+H]$^+$: calc.: 217.1547, found: 217.1547.

Boc-L-*tert*-leucine methyl amide **^{t}Leu-22**

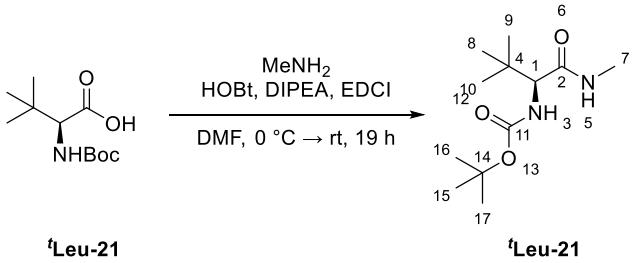

^{t}Leu-21 **^{t}Leu-21**

Boc-L-*tert*-Leu-OH **^{t}Leu-21** (2.31 g, 10.0 mmol, 1.00 equiv.) and HOBt (1.69 g, 12.5 mmol, 1.25 equiv.) were dissolved in DMF (dry, dg, 55 mL) in a flame-driedSchlenk flask under argon. After cooling the mixture to 0 °C, DIPEA (dry, 2.18 mL, 12.5 mmol, 1.25 equiv.) and EDCI (1.94 g, 12.5 mmol, 1.25 equiv.) were added. After 15 min, methylamine (33 wt.% ethanol, 1.56 mL, 12.5 mmol, 1.25 equiv.) was added. The reaction was slowly warmed to rt and stirred for 17 h. The mixture was diluted with EtOAc (750 mL), and the organic layer was washed with aqueous HCl (2M, 3 x 300 mL), a saturated aqueous solution of $NaHCO_3$ (3 x 300 mL) and brine (300 mL). The organic layer was dried over $MgSO_4$, filtrated and concentrated *in vacuo* to obtain **^{t}Leu-22** (2.12 g, 8.67 mmol, 87%) as a yellow oil.

^{1}H NMR (400 MHz, $CDCl_3$): δ (ppm) = 5.70 (s, 1H, H^5), 5.28 (d, $^3J_{H-H}$ = 9.5 Hz, 1H, H^3), 3.78 (d, $^3J_{H-H}$ = 9.3 Hz, 1H, H^1), 2.82 (d, $^3J_{H-H}$ = 4.7 Hz, 3H, H^7), 1.43 (s, 9H, $H^{15,16,17}$), 0.98 (s, 9H, $H^{8,9,10}$).

^{13}C NMR (101 MHz, $CDCl_3$): δ (ppm) = 174.9 (C^{11}), 171.7 (C^2), 79.8 (C^{14}), 62.6 (C^1), 34.7 (C^4), 28.5 ($C^{15,16,17}$), 26.7 ($C^{8,9,10}$), 26.2 (C^7).

HRMS (ESI): m/z: $C_{12}H_{25}N_2O_3^+$ [M+H]$^+$: calc.: 245.1860, found: 245.1860.

L-Alanine methyl amide **Ala-23**[131]

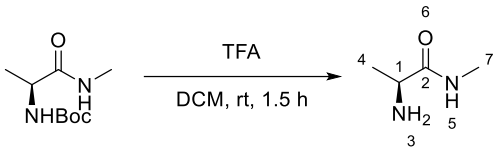

Ala-22 **Ala-23**

Ala-22 (200 mg, 1.00 mmol, 1.00 equiv.) was dissolved in DCM (1.45 mL) and TFA (1.45 mL, 18.8 mmol, 19.0 equiv.). The reaction was stirred for 1.5 h at rt before removing the volatiles *in vacuo*. A saturated aqueous solution of $NaHCO_3$ (5 mL) was added, and the aqueous layer was extracted with DCM (5 x 5 mL). The combined organic layers were dried over $MgSO_4$, filtrated and concentrated *in vacuo* to obtain **Ala-23** (40.1 mg, 392 µmol, 40%) as a white solid.

^{1}H NMR (400 MHz, D_2O): δ (ppm) = 3.81 (q, $^3J_{H\text{-}H}$ = 7.0 Hz, 1H, H^1), 2.74 (s, 3H, H^7), 1.38 (d, $^3J_{H\text{-}H}$ = 7.1 Hz, 3H, H^4).

NH and NH_2 peaks could not be observed in ^{1}H NMR spectrum.

^{13}C NMR (101 MHz, $CDCl_3$): δ (ppm) = 173.4 (C^2), 49.4 (C^1), 25.7 (C^7), 17.5 (C^4).

HRMS (ESI): m/z: $C_4H_{11}N_2O^+$ $[M+H]^+$: calc.: 103.0866, found: 103.0866.

L-Alanine methyl amide **Ala-23**[131]

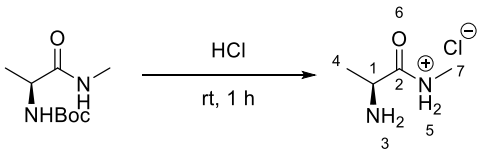

Ala-22 **Ala-23**

Ala-22 (593 mg, 2.93 mmol, 1.00 equiv.) was dissolved in anhydrous HCl (3 M in MeOH, 18.5 mL, 55.4 mmol, 19.0 equiv.). The reaction was stirred for 1 h at rt, before removing the volatiles *in vacuo*. Et_2O (15 mL) was added to the remaining solid and stirred for another 2 h. **Ala-23** (388 mg, 2.77 mmol, 95%) was obtained as an off-white solid by filtration.

^{1}H NMR (400 MHz, MeOD): δ (ppm) = 4.60 (s, 2H, H^3/H^5), 3.86 (qd, $^3J_{H\text{-}H}$ = 7.1 Hz, $^4J_{H\text{-}H}$ = 2.0 Hz, 1H, H^1), 2.76 (s, 3H, H^7), 1.45 (d, $^3J_{H\text{-}H}$ = 7.1 Hz, 3H, H^4).

One NH_2 peak could not be observed in ^{1}H NMR spectrum.

^{13}C NMR (101 MHz, MeOD): δ (ppm) = 171.5 (C^2), 50.2 (C^1), 26.4 (C^7), 17.6 (C^4).

HRMS (ESI): m/z: $C_4H_{11}N_2O^+$ $[M\text{-}Cl]^+$: calc.: 103.0866, found: 103.0867.

L-Valine methyl amide **Val-23**[132]

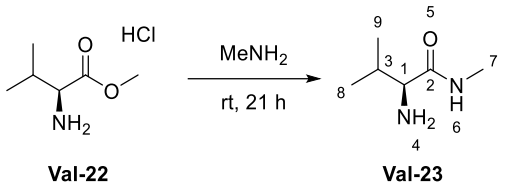

L-Valine methyl ester hydrochloride **Val-22** (8.00 g, 47.7 mmol, 1.00 equiv.) was dissolved in methylamine (33 wt.% ethanol, 23.8 mL, 4.00 equiv.). After stirring for 21 h, ethanol (5 mL) was added, and the solvents were removed *in vacuo*. A saturated aqueous solution of $NaHCO_3$ (45 mL) was added, and extracted with DCM (3 x 55 mL). The combined organic layers were dried over $MgSO_4$, filtrated and concentrated *in vacuo* to obtain **Val-23** (1.43 g, 11.0 mmol, 23%) as yellow oil.

^{1}H NMR (400 MHz, $CDCl_3$): δ (ppm) = 7.31 (s, 1H, H^6), 3.27 (d, $^3J_{H\text{-}H}$ = 3.9 Hz, 1H), 2.82 (dd, $^3J_{H\text{-}H}$ = 5.0 Hz, $^4J_{H\text{-}H}$ = 0.4 Hz, 3H, H^7), 2.31 (heptd, $^3J_{H\text{-}H}$ = 6.9 Hz, $^3J_{H\text{-}H}$ = 3.9 Hz, 1H, H^3), 0.98 (d, $^3J_{H\text{-}H}$ = 6.9 Hz, 3H, $H^{8,9}$), 0.82 (d, $^3J_{H\text{-}H}$ = 6.9 Hz, 3H, $H^{8,9}$).

^{13}C NMR (101 MHz, $CDCl_3$): δ (ppm) = 174.8 (C^2), 60.1 (C^1), 30.8 (C^3), 25.7 (C^7), 19.8 ($C^{8,9}$).

HRMS (ESI): m/z: $C^6H^{15}N^2O^+$ $[M+H]^+$: calc.: 131.1179, found: 131.1179.

L-*tert*-Leucine methyl amide ^{t}**Leu-23**[131]

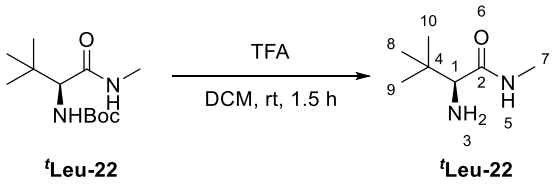

^{t}**Leu-22** (2.10 g, 8.58 mmol, 1.00 equiv.) was dissolved in DCM (12.6 mL) and TFA (12.6 mL, 163 mmol, 19.0 equiv.). The reaction was stirred for 1.5 h at rt, before removing the volatiles *in vacuo*. A saturated aqueous solution of $NaHCO_3$ (5 mL) was added, and the aqueous layer was extracted with DCM (5 x 5 mL). The combined organic layers were dried over $MgSO_4$, filtrated and concentrated *in vacuo* to obtain ^{t}**Leu-23** (344 mg, 2.40 mmol, 28%) as a white solid.

^{1}H NMR (400 MHz, CD_2Cl_2): δ (ppm) = 6.63 (s, 1H, H^5), 3.04 (s, 1H, H^1), 2.75 (d, $^3J_{H\text{-}H}$ = 4.9 Hz, 3H, H^7), 0.96 (s, 9H, $H^{8,9,10}$).

The NH_2 peak could not be observed in ^{1}H NMR spectrum.

^{13}C NMR (101 MHz, CD_2Cl_2): δ (ppm) = 174.1 (C^2), 64.7 (C^1), 34.3 (C^4), 26.8 ($C^{8,9,10}$), 25.7 (C^7).

HRMS (ESI): m/z: $C_7H_{17}N_2O^+$ $[M+H]^+$: calc.: 145.1335, found:145.1335.

4.2.6 Design 3: Backbone Synthesis

Bis-5,5′(2-(methoxycarbonyl)phenyl)-2,2'-di(methoxymethyloxy)-biphenyl **24**[56]

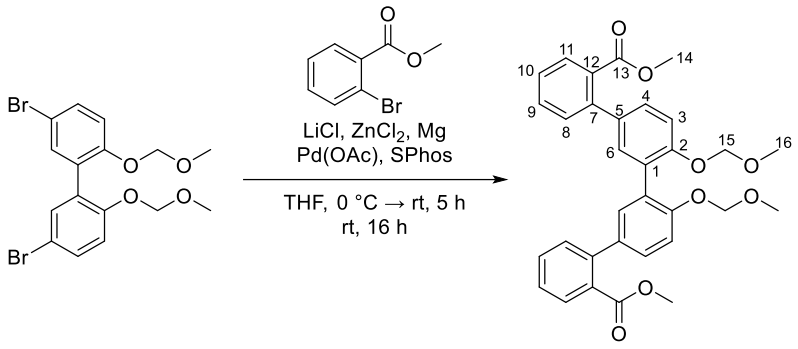

16 **24**

This compound was synthesized to a known procedure. Anhydrous LiCl (2.06 g, 48.6 mmol, 6.00 equiv.) was dried at 450 °C for 15 min under high vacuum in a flame-driedSchlenk tube under argon before $ZnCl_2$ (4.86 g, 35.6 mmol, 4.40 equiv.) was added. The solids were dried at 250 °C for 15 min under high vacuum. After cooling down to rt, magnesium (787.5 mg, 32.4 mmol, 4.00 equiv.) was dissolved in THF (dry, dg, 49 mL) and the mixture was cooled to 0 °C. Methyl-2-bromobenzoate (6.97 g, 32.4 mmol, 4.00 equiv.) was added and the mixture was slowly warmed to rt while stirring for 5 h. The mixture was added dropwise to a stirring solution of 5,5′-dibromo-2,2′-bis(methoxymethoxy)-biphenyl **16** (3.50 g, 8.1 mmol, 1.000 equiv.), Pd(OAc) (53.6 mg, 324 μmol, 0.04 equiv.) and SPhos (266 mg, 648 μmol, 0.08 equiv.) in THF (dry, dg, 35 mL) under argon. The resulting mixture was stirred for 16 h at rt. The reaction was quenched with a saturated aqueous solution of NH_4Cl (105 mL) and extracted with EtOAc (3 x 70 mL). The combined organic layers were dried over Na_2SO_4, filtrated and concentrated *in vacuo*. The crude product was purified by flash column chromatography (silica, pentane:EtOAc 5:1 to 4:1, R_F (pentane:EtOAc 5:1) = 0.34) to obtain **24** (3.28 g, 6.08 mmol, 75%) as a yellow solid.

^{1}H NMR (400 MHz, CD_2Cl_2): δ (ppm) = 7.76 (ddd, $^3J_{H\text{-}H}$ = 7.7 Hz, $^4J_{H\text{-}H}$ = 1.4 Hz, $^5J_{H\text{-}H}$ = 0.5 Hz, 1H, H^{11}), 7.52 (dd, $^3J_{H\text{-}H}$ = 7.7 Hz, $^4J_{H\text{-}H}$ = 1.4 Hz, 1H, H^{10}), 7.43 – 7.35 (m, 2H, $H^{3,4}$), 7.29 – 7.21 (m, 3H, $H^{6,8,9}$), 5.15 (s, 2H, H^{15}), 3.66 (s, 3H, H^{14}), 3.39 (s, 3H, H^{16}).

^{13}C NMR (101 MHz, CD_2Cl_2): δ (ppm) = 169.4 (C^{13}), 154.9 (C^2), 141.9 (C^{12}), 135.0 (C^5), 131.9 (C^8), 131.5 (C^{10}), 131.4 (C^4), 131.1 (C^1/C^7), 130.0 (C^{11}), 129.1 (C^6), 128.9 (C^1/C^7), 127.3 (C^3), 115.3 (C^9), 95.7 (C^{15}), 56.2 (C^{16}), 52.2 (C^{14}).

HRMS (ESI): m/z: $C_{32}H_{30}O_8Na^+$ $[M+Na]^+$: calc.: 565.1833, found: 565.1833.

Bis-5,5′(2-carboxyphenyl)-2,2'-di(methoxymethyloxy)-biphenyl **25**[56]

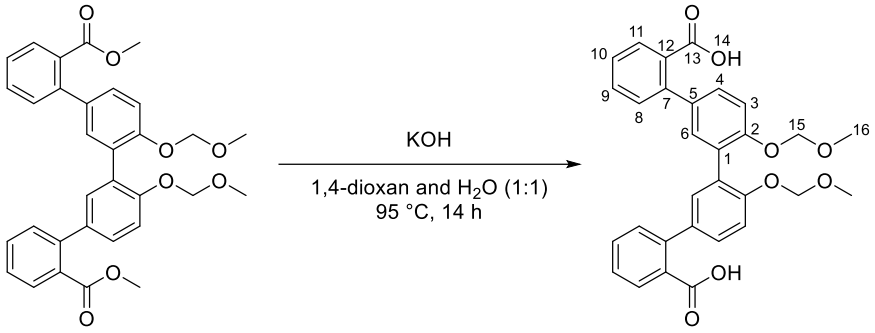

24 **25**

This compound was synthesized to a known procedure. **24** (9.00 g, 16.6 mmol, 1.00 equiv.) was dissolved in 1,4-dioxan (85 mL) and water (85 mL). KOH (9.31 g, 166 mmol, 10.0 equiv.) was added in small portions before the mixture was heated to 95 °C and stirred for 14 h. After cooling to rt, pH was adjusted to 3 with aqueous HCl (6M). By adding EtOAc (3 mL) a third layer could be separated. The crude product was concentrated *in vacuo* to obtain **25** (2.19 g, 4.25 mmol, 75%) as a yellow solid.

^{1}H NMR (400 MHz, $CDCl_3$): δ (ppm) = 7.56 – 7.43 (m, 4H, $H^{4,6,10,11}$), 7.31 – 7.21 (m, 3H, $H^{3,8,9}$), 5.09 (s, 2H, H^{15}), 3.33 (s, 3H, H^{16}).

^{13}C NMR (101 MHz, $CDCl_3$): δ (ppm) = 177.6 (C^{13}), 154.8 (C^{2}), 138.9 (C^{12}), 132.8 (C^{5}), 132.1 (C^{8}), 131.3 (C^{10}), 129.8 (C^{4}), 129.1 (C^{11}), 128.8 (C^{7}), 128.3 (C^{6}), 127.0 (C^{5}), 115.3 (C^{9}), 94.8 (C^{15}), 56.1 (C^{16}).

The C^{1} peak could not be observed in ^{13}C NMR spectrum.

HRMS (ESI): m/z: $C_{30}H_{25}O_8^-$ $[M-H]^-$: calc.: 513.1555, found: 513.1558.

4.2.7 Design 3: Ligand Synthesis

Bis-5,5′(2-(L)-Ala-NHCH$_3$-benzamide)-2,2′-di(methoxymethyloxy)-biphenyl **Ala-26**

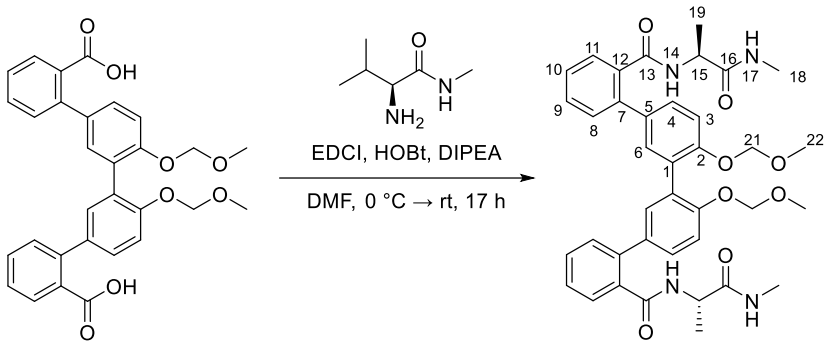

25 **Ala-26**

This compound was synthesized to a known procedure.[56] **Ala-26** (400 mg, 777 µmol, 1.00 equiv.) and HOBt (263 mg, 1.94 mmol, 2.50 equiv.) were added into a flame dried Schlenk tube under argon before anhydrous DMF (11 mL) was added. The mixture was cooled to 0°C and EDCI (373 mg, 1.94 mmol, 2.50 equiv.) and anhydrous DIPEA (251 mg, 1.94 mmol, 2.50 equiv.) were added. After stirring for 15 min, **Ala-23** (199 mg, 1.94 mmol, 2.50 equiv.) was added to the solution. The mixture was slowly warmed to room temperature and stirred for 17 h. Afterwards, the mixture was diluted with EtOAc (150 mL) and washed with aqueous HCl (2M, 3 x 80 mL), saturated aqueous solution of $NaHCO_3$ (3 x 80 mL) and brine (80 mL). The organic layer was dried over $MgSO_4$ and the solvent was removed under reduced pressure to obtain **Ala-26** (436 mg, 639 µmol, 82%) as a white solid.

^{1}H NMR (400 MHz, CD_2Cl_2): δ (ppm) = 7.60 – 7.45 (m, 6H, $H^{14,8,11}$), 7.41 (ddd, $^3J_{H\text{-}H}$ = 8.4 Hz, $^3J_{H\text{-}H}$ = 6.0 Hz, $^4J_{H\text{-}H}$ = 1.9 Hz, 4H, $H^{4,9}$), 7.27 (d, $^3J_{H\text{-}H}$ = 8.5 Hz, 4H, $H^{3,10}$), 7.01 (s, 2H, H^6), 6.60 (d, $^3J_{H\text{-}H}$ = 8.4 Hz, 2H, H^{17}), 5.07 – 5.00 (m, 4H, H^{20}), 4.61 (p, $^3J_{H\text{-}H}$ = 6.8 Hz, 2H, H^{15}), 3.26 (s, 6H, H^{21}), 2.35 (s, 6H, H^{18}), 1.29 (d, $^3J_{H\text{-}H}$ = 6.8 Hz, 6H, H^{19}).

^{13}C NMR (101 MHz, CD_2Cl_2): δ (ppm) = 170.22 (C^{16}), 154.62 (C^2), 139.40 (C^7), 133.71 (C^1), 131.55 (C^6), 130.57 ($C^{8/11}$), 130.45 ($C^{8/11}$), 128.95 (C^{10}), 127.55 ($C^{4/9}$), 116.06 (C^3), 95.28 (C^{20}), 56.13 (C^{21}), 49.69 (C^{15}), 26.26 (C^{18}), 19.79 (C^{19}).

$C^{4/9}$, C^5, C^{12}, C^{13} peaks could not be observed in ^{13}C NMR spectrum.

HRMS (ESI): m/z: $C_{38}H_{43}N_4O_8^+$ $[M+H]^+$: calc.: 683.3075, found: 683.3075.

Bis-5,5′(2-L-Val-NHMe-benzamide)-2,2'-di(methoxymethyloxy)-biphenol **Val-26**

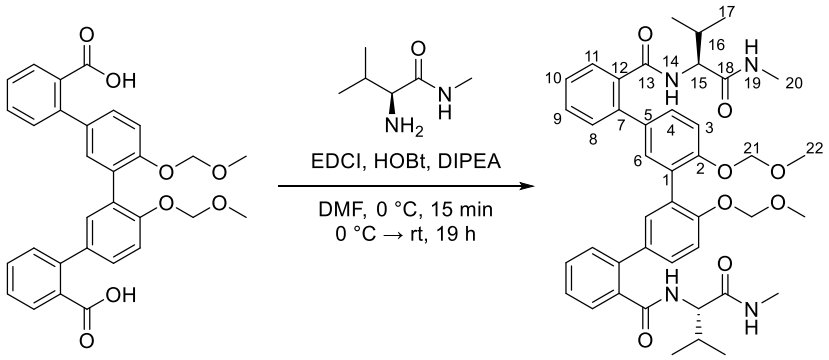

25 **Val-26**

This compound was synthesized to a known procedure.[56] **25** (500 mg, 972 µmol, 1.00 equiv.) and HOBt (328 mg, 2.43 mmol, 2.50 equiv.) were dissolved in DMF (dry, dg, 11 mL) in a flame-driedSchlenk flask under argon. After cooling the mixture to 0 °C, DIPEA (dry, 0.423 mL, 2.43 mmol, 2.50 equiv.) and EDCI (377 mg, 2.43 mmol, 2.50 equiv.) were added. After 15 min, **Val-23** (316 mg, 2.43 mmol, 2.50 equiv.) was added. The reaction was slowly warmed to rt and stirred for 16 h. The solution was diluted with EtOAc (150 mL), and the organic layer was washed with aqueous HCl (2M, 3 x 70 mL), a saturated aqueous solution of $NaHCO_3$ (3 x 70 mL) and brine (70 mL). The organic layer was dried over $MgSO_4$, filtrated and concentrated *in vacuo* to obtain **Val-26** (704 mg, 952 µmol, 98%) as a white solid.

^{1}H NMR (400 MHz, DMSO): δ (ppm) = 8.11 (d, $^3J_{H\text{-}H}$ = 8.3 Hz, 1H, H^{14}), 7.66 (q, $^3J_{H\text{-}H}$ = 4.5 Hz, 1H, H^{19}), 7.47 (ddd, $^3J_{H\text{-}H}$ = 8.4 Hz, $^3J_{H\text{-}H}$ = 6.5 Hz, $^4J_{H\text{-}H}$ = 1.9 Hz, 1H, H^9), 7.39 (m, 3H, $H^{8,10,11}$), 7.34 (dd, $^3J_{H\text{-}H}$ = 8.6 Hz, $^4J_{H\text{-}H}$ = 2.4 Hz, 1H, H^4), 7.25 (d, $^4J_{H\text{-}H}$ = 2.4 Hz, 1H, H^6), 7.15 (d, $^3J_{H\text{-}H}$ = 8.6 Hz, 1H, H^3), 5.15 – 5.06 (m, 2H, H^{21}), 3.99 (t, $^3J_{H\text{-}H}$ = 7.9 Hz, 1H, H^{20}), 3.27 (s, 3H, H^{22}), 2.54 (s, 3H, H^{20}), 1.92 – 1.79 (m, 1H, H^{16}), 0.68 (dd, $^2J_{H\text{-}H}$ = 14.3 Hz, $^3J_{H\text{-}H}$ = 6.7 Hz, 6H, H^{17}).

^{13}C NMR (101 MHz, DMSO): δ (ppm) = 171.2 (C^{19}), 169.2 (C^{13}), 154.0 (C^2), 138.6 (C^7), 136.7 (C^{12}), 133.4 (C^5), 131.1 (C^6), 129.7 ($C^{8/10/11}$), 129.3 (C^9), 128.7 (C^4), 128.1 ($C^{8/10/11}$), 127.9 (C^1), 126.6 ($C^{8/10/11}$), 114.6 (C^3), 94.4 (C^{21}), 58.9 (C^{15}), 55.4 (C^{10}), 29.7 (C^{16}), 25.4 (C^{20}), 19.1 (C^{17}), 18.3 (C^{17}).

HRMS (ESI): m/z: $C_{42}H_{51}N_4O_8^+$ $[M+H]^+$: calc.: 739.3701, found: 739.3701.

Bis-5,5′(2-L-*tert*-Leu-NHMe-benzamide)-2,2'-di(methoxymethyloxy)-biphenol ^{t}**Leu-26**

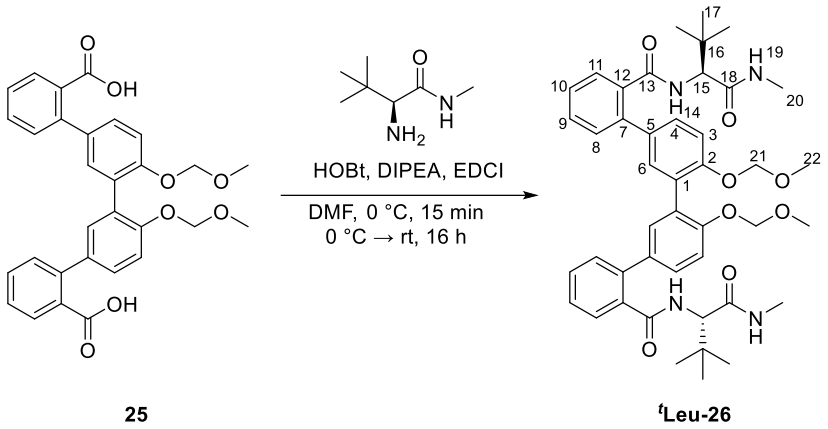

25 ^{t}**Leu-26**

This compound was synthesized to a known procedure.[56] **25** (488 mg, 948 µmol, 1.00 equiv.) and HOBt (320 mg, 2.37 mmol, 2.50 equiv.) were dissolved in DMF (dry, dg, 11 mL) in a flame-driedSchlenk flask under argon. After cooling the mixture to 0 °C, DIPEA (dry, 0.413 mL, 2.37 mmol, 2.50 equiv.) and EDCI (368 mg, 2.37 mmol, 2.50 equiv.) were added. After 15 min, ^{t}**Leu-23** (342 mg, 2.37 mmol, 2.50 equiv.) was added. The reaction was slowly warmed to rt and stirred for 16 h. The solution was diluted with EtOAc (150 mL), and the organic layer was washed with aqueous HCl (2M, 3 x 70 mL), a saturated aqueous solution of $NaHCO_3$ (3 x 70 mL) and brine (70 mL). The organic layer was dried over $MgSO_4$, filtrated and concentrated *in vacuo* to obtain ^{t}**Leu-26** (656 mg, 854 µmol, 90%) as a yellow solid.

^{1}H NMR (400 MHz, DMSO): δ (ppm) = 7.81 (d, $^{3}J_{H\text{-}H}$ = 9.1 Hz, 1H, H^{14}), 7.77 (q, $^{3}J_{H\text{-}H}$ = 4.4 Hz, 1H, H^{19}), 7.51 – 7.43 (m, 1H, H^{9}), 7.42 – 7.36 (m, 3H, $H^{8,10,11}$), 7.33 (dd, $^{3}J_{H\text{-}H}$ = 8.5 Hz, $^{4}J_{H\text{-}H}$ = 2.4 Hz, 1H, H^{4}), 7.27 (d, $^{4}J_{H\text{-}H}$ = 2.4 Hz, 1H, H^{6}), 7.15 (d, $^{3}J_{H\text{-}H}$ = 8.6 Hz, 1H, H^{3}), 5.10 (q, $^{4}J_{H\text{-}H}$ = 6.8 Hz, 2H, H^{21}), 4.15 (d, $^{3}J_{H\text{-}H}$ = 9.1 Hz, 1H, H^{15}), 3.27 (s, 3H, H^{22}), 2.51 (s, 3H, H^{20}), 0.79 (s, 9H, H^{17}).

^{13}C NMR (101 MHz, DMSO): δ (ppm) = 170.2 (C^{18}), 169.2 (C^{13}), 154.1 (C^{2}), 138.6 (C^{7}), 136.7 (C^{12}), 133.4 (C^{5}), 131.2 (C^{6}), 129.8 ($C^{8/10/11}$), 129.3 (C^{9}), 128.8 (C^{4}), 128.1 (C^{1}), 128.0 ($C^{8/10/11}$), 126.6 ($C^{8/10/11}$), 114.7 (C^{3}), 94.5 (C^{21}), 55.4 (C^{22}), 33.6 (C^{16}), 26.7 (C^{17}).

HRMS (ESI): m/z: $C_{44}H_{55}N_4O_8^+$ $[M+H]^+$: calc.: 767.4014, found: 767.4014.

Bis-5,5′(2-(L)-Ala-NHMe-benzamide)-2,2′-biphenol **Ala-27**

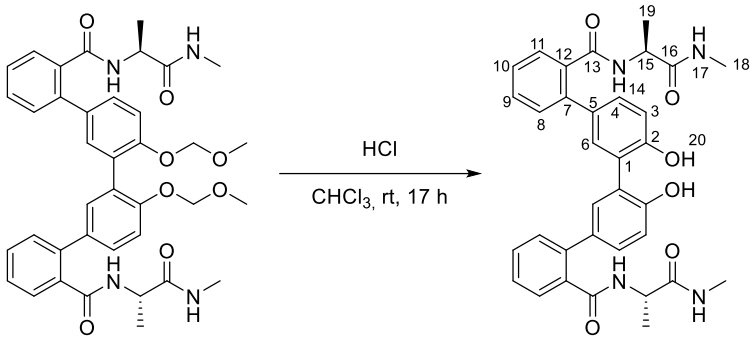

Ala-26 **Ala-27**

This compound was synthesized to a known procedure.[56] **Ala-26** (436 mg, 639 µmol, 1.00 equiv.) was dissolved in $CHCl_3$ (1.3 mL) and aqueous HCl (in *i*-PrOH, 5M, 1.30 mL, 6.39 mmol, 10.0 equiv.) was added. The reaction stirred for 17 h overnight. Afterwards, the solvent was removed *in vacuo* to afford **Ala-27** (358 mg, 601 µmol, 94%) as a white solid.

^{1}H NMR (400 MHz, DMSO): δ (ppm) = 9.39 (s, 2H, H^{20}), 8.15 (d, $^3J_{H\text{-}H}$ = 7.5 Hz, 2H, H^{14}), 7.49 – 7.43 (m, 4H, $H^{9,11}$), 7.42 – 7.33 (m, 6H, $H^{8,10,17}$), 7.21 (dd, $^3J_{H\text{-}H}$ = 6.6 Hz, $^2J_{H\text{-}H}$ = 2.3 Hz, 4H, $H^{4,6}$), 6.94 – 6.88 (m, 2H, H^3), 4.20 (p, $^3J_{H\text{-}H}$ = 7.1 Hz, 2H, H^{15}), 3.63 – 3.56 (m, 6H, H^{18}), 1.01 (d, $^3J_{H\text{-}H}$ = 7.1 Hz, 6H, H^{19}).

^{13}C NMR (101 MHz, DMSO): δ (ppm) = 172.42 (C^{16}), 169.11 (C^{13}), 154.15 (C^2), 139.21 (C^7), 136.32 (C^{12}), 131.49 ($C^{4/6}$), 130.81 (C^5), 129.63 ($C^{8/10}$), 129.48 ($C^{9/11}$), 128.45 ($C^{4/6}$), 128.05 ($C^{9/11}$), 126.29 ($C^{8/10}$), 125.52 (C^1), 115.62 (C^3), 48.76 (C^{15}), 25.63 ($C^{19/19'}$), 25.52 ($C^{19/19'}$).

C^{18} peak could not be observed in ^{13}C NMR spectrum.

HRMS (ESI): m/z: $C_{34}H_{35}N_4O_6^+$ [M+H]$^+$: calc.: 595.2551, found: 595.2551.

Bis-5,5′(2-L-Val-NHMe-benzamide)-2,2'-biphenol **Val-27**

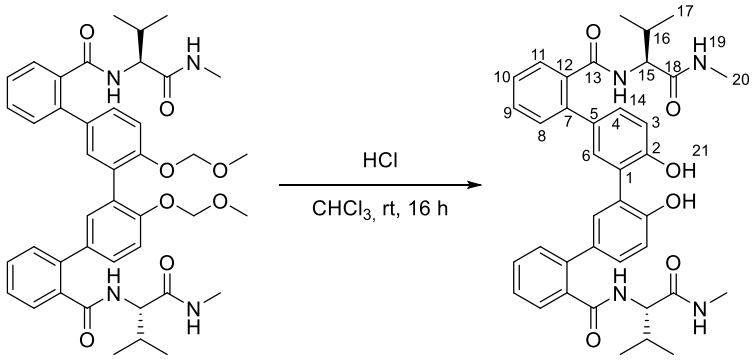

Val-26 **Val-27**

This compound was synthesized to a known procedure.[56] **Val-26** (716 mg, 969 µmol, 1.00 equiv.) was dissolved in HCl (5M in 2-propanole, 1.94 mL, 9.69 mmol, 10.0 equiv.) and chloroform (2 mL) and the solution stirred for 16 h at rt. Cold chloroform (50 mL) and H_2O (38 mL) were added before concentrating *in vacuo* to obtain **Val-27** (506 mg, 775 µmol, 80%) as an off-white solid.

^{1}H NMR (400 MHz, DMSO): δ (ppm) = 9.30 (s, 1H, H^{21}), 8.00 (d, $^3J_{H\text{-}H}$ = 8.5 Hz, 1H, H^{14}), 7.58 (q, $^3J_{H\text{-}H}$ = 4.6 Hz, 1H, H^{19}), 7.48 – 7.40 (m, 1H, H^9), 7.39 – 7.29 (m, 3H, $H^{8,10,11}$), 7.23 (d, $^4J_{H\text{-}H}$ = 2.4 Hz, 1H, H^6), 7.18 (dd, $^3J_{H\text{-}H}$ = 8.3 Hz, $^4J_{H\text{-}H}$ = 2.4 Hz, 1H, H^4), 6.85 (d, $^3J_{H\text{-}H}$ = 8.3 Hz, 1H, H^3), 3.99 (dd, $^3J_{H\text{-}H}$ = 8.5 Hz, 7.3 Hz, 1H, H^{15}), 2.51 (d, $^3J_{H\text{-}H}$ = 4.5 Hz, 3H, H^{20}), 1.84 (hept, $^3J_{H\text{-}H}$ = 6.8 Hz, 1H, H^{16}), 0.69 (dd, $^2J_{H\text{-}H}$ = 10.1 Hz, $^3J_{H\text{-}H}$ = 6.8 Hz, 6H, H^{17}).

^{13}C NMR (101 MHz, DMSO): δ (ppm) = 171.2 (C^{18}), 169.3 (C^{13}), 154.1 (C^2), 139.1 (C^7), 136.6 (C^{12}), 131.5 (C^6), 130.8 (C^5), 129.6 ($C^{8/10/11}$), 129.2 (C^9), 128.3 (C^4), 127.9 ($C^{8/10/11}$), 126.2 ($C^{8/10/11}$), 125.4 (C^1), 115.5 (C^3), 58.8 (C^{15}), 29.8 (C^{16}), 25.4 (C^{20}), 19.16 (C^{17}), 18.3 (C^{17}).

HRMS (ESI): m/z: $C_{38}H_{43}N_4O_6^+$ [M+H]$^+$: calc.: 651.3177, found: 651.3177.

Bis-5,5′(2-L-*tert*-Leu-NHMe-benzamide)-2,2'-biphenol **^{t}Leu-27**

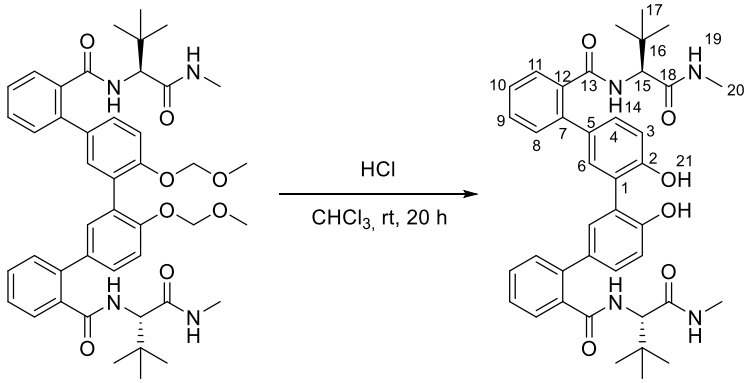

^{t}Leu-27 ^{t}Leu-27

This compound was synthesized to a known procedure.[56] **^{t}Leu-26** (630 mg, 821 µmol, 1.00 equiv.) was dissolved in HCl (5M in 2-propanole, 1.64 mL, 8.21 mmol, 10.0 equiv.) and chloroform (1.64 mL) and the solution stirred for 20 h at rt. Aqueous HCl (1M, 10 mL) was added, the aqueous layer was extracted with DCM (3 x 10 mL) and the combined organic layers were dried over $MgSO_4$, filtrated and concentrated *in vacuo* to obtain **^{t}Leu-27** (604 mg, 804 µmol, 98%) as an off-white solid.

^{1}H NMR (400 MHz, MeOD): δ (ppm) = 7.90 – 7.82 (m, 1H, H^{19}), 7.52 – 7.44 (m, 2H, $H^{9,11}$), 7.45 – 7.30 (m, 2H, $H^{8,10}$), 7.27 (d, $^4J_{H\text{-}H}$ = 2.3 Hz, 1H, H^6), 7.20 (dd, $^3J_{H\text{-}H}$ = 8.3 Hz, $^4J_{H\text{-}H}$ = 2.3 Hz, 1H, H^4), 6.90 (d, $^3J_{H\text{-}H}$ = 8.3 Hz, 1H, H^3), 4.21 (s, 1H, H^{15}), 2.57 (d, $^3J_{H\text{-}H}$ = 4.7 Hz, 3H, H^{20}), 0.83 (s, 9H, H^{17}).

One NH peak and the OH could not be observed in ^{1}H NMR spectrum.

^{13}C NMR (101 MHz, $CDCl_3$): δ (ppm) =172.8 (C^{13}), 172.5 (C^{18}), 155.5 (C^{2}), 141.0 (C^{7}), 137.4 (C^{12}), 133.3 (C^{5}), 132.8 (C^{6}), 131.3 ($C^{8/10}$), 131.1 ($C^{9/11}$), 130.3 (C^{4}), 128.8 ($C^{9/11}$), 127.9 ($C^{8/10}$), 126.8 (C^{1}), 117.5 (C^{3}), 62.7 (C^{15}), 35.5 (C^{16}), 27.1 (C^{17}), 26.1 (C^{20}).

HRMS (ESI): m/z: $C_{40}H_{47}N_4O_6^+$ [M+2HCl]$^+$: calc.: 679.3490, found: 679.3490.

Bis-5,5′(2-(L)-Ala-NHMe-benzamide)-2,2′-biphenol-phosphinite **Ala-3**

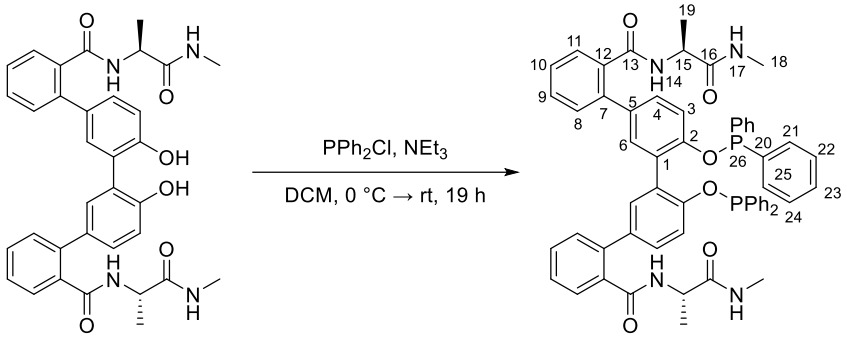

Ala-27 **Ala-3**

This compound was synthesized to a known procedure.[56] In a flame dried Schlenk tube under argon **Ala-27** (340 mg, 501 µmol, 1.00 equiv.) was dissolved in dry and degassed DCM (dry, dg, 10 mL). After that, degassed and anhydrous NEt_3 (203 mg, 2.00 mmol, 4.00 equiv.) and $ClPPh_2$ (442 mg, 2.00 mmol, 4.00 equiv.) were added, after cooling to 0°C. The solution stirred under argon at rt for 19 h. The mixture was purified under argon by flash column chromatography (neutral alumina, EtOAc) to obtain a clear solution. The solution was concentrated *in vacuo* to get a yellow solid. The crude product was purified by precipitation in degassed anhydrous DCM (1 mL) / pentane (10 mL) and filtration under argon. This step was repeated twice to obtain **Ala-3** (384 mg, 367 µmol, 73%) as a white solid.

^{1}H NMR (400 MHz, CD_2Cl_2): δ (ppm) = 12.22 (s, 1H, H^{X}), 7.67 – 7.03 (m, 7H, $H^{3,4,6,8,9,10,11}$), 6.97 (s, 1H, H^{17}), 6.51 (d, $^{X}J_{H\text{-}H}$ = 106.2 Hz, 1H, H^{14}), 4.58 (s, 1H, H^{15}), 3.04 (qd, $^{3}J_{H\text{-}H}$ = 7.3 Hz, $^{3}J_{H\text{-}H}$ = 4.8 Hz, 6H, H^{18}), 1.35 (d, $^{3}J_{H\text{-}H}$ = 7.3 Hz, 6H, H^{19}).

$H^{3',4',6',8',9',10',11'}$, $H^{20\text{-}23}$ peaks could not be observed in ^{1}H NMR spectrum.

^{13}C NMR (101 MHz, CD_2Cl_2): δ (ppm) = 170.32 ($C^{13/16}$), 139.29 (C^{7}), 134.41 (C^{12}), 130.49 ($C^{4/6/8/9/10/11}$), 130.35 ($C^{4/6/8/9/10/11}$), 128.63 ($C^{4/6/8/9/10/11}$), 127.60 ($C^{4/6/8/9/10/11}$), 119.07 (C^{3}), 49.83 (C^{15}), 46.03 (C^{18}), 8.75 (C^{19}).

C^{1}, C^{2}, $C^{4/6/8/9/10/11}$, $C^{4/6/8/9/10/11}$, C^{5}, $C^{13/16}$, $C^{20\text{-}23}$ peaks could not be observed in ^{13}C NMR spectrum.

^{31}P NMR (162 MHz, CD_2Cl_2): δ (ppm) = 113.17, 110.32.

Bis-5,5′(2-L-Val-NHMe-benzamide)-2,2'-biphenol-phosphinite **Val-3**

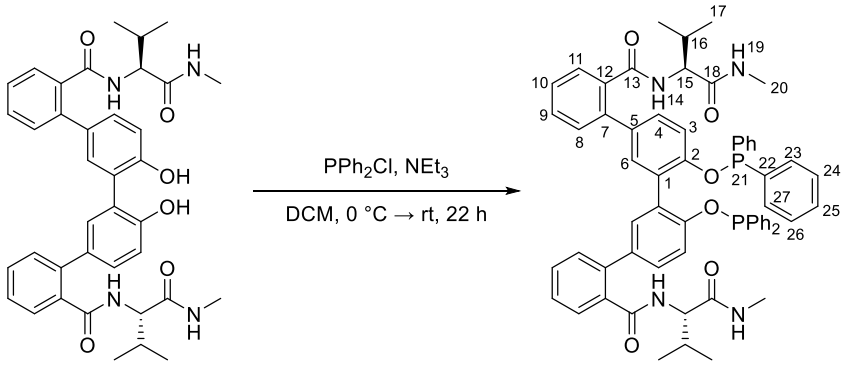

Val27 **Val-3**

This compound was synthesized to a known procedure.[56] PPh_2Cl (dry, dg, 512 µL, 2.77 mmol, 4.00 equiv.) and **Val-27** (450 mg, 692 µmol, 1.00 equiv.) were coevaporated with toluene (dry, dg, 3 x 3 mL) respectively in flame-driedSchlenk tubes. **Val-27** was dissolved in DCM (dry, dg, 15 mL) and the mixture was cooled to 0 °C. NEt_3 (dry, dg, 386 µL, 2.77 mmol, 4.0 equiv.) and PPh_2Cl were added, and the reaction was slowly warmed to rt while stirring for 22 h. The crude product was purified under inert conditions *via* flash column chromatography (neutral alumina, EtOAc) and precipitation from DCM (dry, dg, 3 mL) and pentane (dry, dg, 30 mL). The precipitation was repeated to obtain **Val-3** (436 mg, 428 µmol, 62%) as a white solid.

^{1}H NMR (400 MHz, CD_2Cl_2): δ (ppm) = 7.84 – 6.70 (m, 17H, H^{arom}), 4.55 – 4.34 (m, 1H), 3.04 (qd, $^3J_{H\text{-}H}$ = 7.3 Hz, $^4J_{H\text{-}H}$ = 4.8 Hz, 2H), 2.32 (d, $^3J_{H\text{-}H}$ = 5.1 Hz, 1H), 2.17 – 2.07 (m, 1H), 2.06 – 1.83 (m, 1H), 1.36 (t, $^3J_{H\text{-}H}$ = 7.3 Hz, 3H), 1.04 – 0.79 (m, 6H).

^{31}P NMR (162 MHz, $CDCl_3$) δ (ppm) = 112.67, 108.22.

4.2.8 Enantioselective Hydrogenations

Synthesis of prochiral olefins for hydrogenation:

MAA and **MAA-Me** were purchased.

***p*-NO₂-MAC**

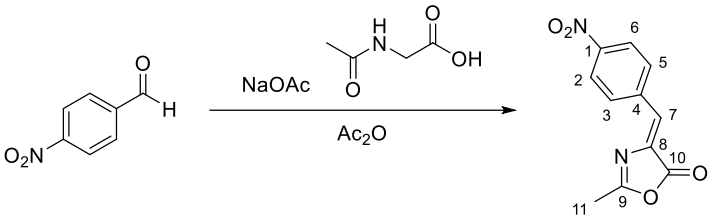

36 **37**

This compound was synthesized to a known procedure.[37] 4-Nitrobenzaldehyde **36** (3.00 g, 19.9 mmol, 1.25 equiv.), *N*-acetyl glycine (1.86 g, 15.9 mmol, 1.00 equiv.), NaOAc (821 mg, 10.0 mmol, 0.630 equiv.) and acetic acid (4.05 g, 339.7 mmol, 2.5 equiv.) were refluxed for 1.5 h. After cooling to rt, the residue was washed with ice water (3 x 100 mL) and extracted with EtOAc (3 x 50 mL) and washed with brine (50 mL). Volatiles were removed *in vacuo*. The crude product **37** (4.69 g, 98%) was used without further purification. The obtained values were in good agreement with the literature.

¹H NMR (400 MHz, DMSO-d₆) δ (ppm) = 8.24 (d, J = 8.9 Hz, 2H, $H^{2,6}$), 7.85 (d, J = 8.9 Hz, 2H, $H^{5,3}$), 7.19 (s, 1H, H^{7}), 2.01 (s, 3H, H^{11}).

¹³C NMR (101 MHz, DMSO-d₆): δ (ppm) 169.70 (C^{10}), 165.48 (C^{9}), 147.12 (C^{4}), 140.60 (C^{1}), 130.90 ($C^{5,3}$), 129.95 (C^{8}), 127.32 (C^{7}), 123.85 ($C^{2,6}$), 22.73 (C^{11}).

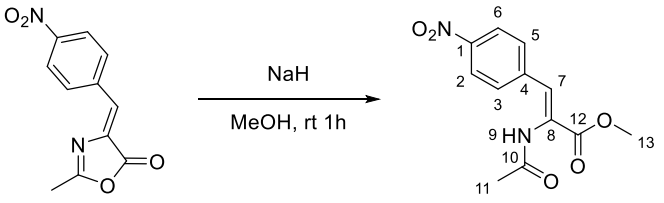

38 ***p*-(NO_2)-MAC**

This Compound was synthesized to a known procedure.[37] **3** (1.91 g, 8.21 mmol, 1.00 equiv.) and NaH (197 mg, 8.21 mmol, 1.00 equiv.) were stirred in methanol (dry, 50 mL) for 1 h. Afterwards, the reaction was quenched with water and the reaction was extracted with EtOAc (3 x100 mL) and the combined organic layer was washed with brine and dried over $MgSO_4$. Volatiles were removed *in vacuo*. The crude product was purified by flash column chromatography (silica, *n*-Pent: EtOAc 5:1) to obtain ***p*-NO₂-MAC** (1.63 g, 75%) as a yellowish solid. The obtained values were in good agreement with the literature.

¹H NMR (400 MHz, CDCl3) δ (ppm) = 8.20 (d, J = 8.8 Hz, 2H, $H^{2,6}$), 7.54 (d, J = 8.4 Hz, 2H, $H^{3,5}$), 7.40 (s, 1H, H^{7}), 7.38 – 7.32 (m, 1H, NH^{9}), 3.90 (s, 3H, H^{13}), 2.14 (s, 3H, H^{11}).

¹³C NMR (101 MHz, $CDCl_3$) δ (ppm) = 167.78 (C^{10}), 165.39 (C^{12}), 147.39 (C^{1}), 141.35 (C^{4}), 129.97 ($C^{4,6}$), 127.49 (C^{7}), 125.75 (C^{8}), 123.72 ($C^{2,6}$), 53.38 (C^{13}), 24.05 (C^{16}).

Set up for Pressure Experiments and for Solvent and Substrate Screening:

For hydrogenation experiments a stock solution of the catalyst and stock solutions of each prochiral olefin were prepared separately. To generate a 6.4mM catalyst-stock solution, the bisphosphinite-ligand **Val-3** (37.0 mg, 36.3 µmol, 1.05 equiv.) and $[Rh(COD)_2]BF_4$ (16.1 mg, 34.6 µmol, 1.00 equiv.) were dissolved in anhydrous and degassed DCM-d_2 (5.4 mL). Second, the stock solutions of each olefin (**MAA**, **MAA-Me**, ***p*-(NO₂)-MAC**) were prepared. **MAA** (22.0 mg, 154 µmol, 4.00 equiv.), **MAA-Me** (24.2 mg, 154 µmol, 4.00 equiv.), MAC (33.7 mg, 154 µmol, 4.00 equiv.) and ***p*-(NO₂)-MAC** (40.6 mg, 154 µmol 4.00 equiv.) were dissolved in anhydrous and degassed DCM-d_2 (1.2 mL). All stock solutions were prepared at the glovebox. Afterwards, 0.3 mL of each stock solution (**MAA**, **MAA-Me**, ***p*-(NO₂)-MAC**) and 0.3 mL of the catalyst-stock solution were united in standard NMR tube located in a nitrogen-filled stainless steel reactor with a small stirring bar. If necessary, a cryostat was used and the reactor was cooled in a bath of *i*-PrOH. The reactor was pressurized with hydrogen gas (40 bar) to initiate the catalysis. The reactor was reopened after 16 h. The solution was passed through a short pipet filled with silica (ca. 3 cm) using ethyl acetate as eluent. The hydrogenation product resulted as a yellow oil by evaporation. Enantiomeric ratio was determined by chiral GC (**MAA** (6-TBDMS-2,3-Ac)-β-CD, 25 m, i.d. 250 µm, film thickness 250 nm, prepared and coated in the Trapp group, 100 kPa helium, 150°C, FID detection, t_R = 5.75 min and t_S = 6.50 min; **MAA-Me**: (6-TBDMS-2,3-Ac)-β-CD, 25 m, i.d. 250 µm, film thickness 250 nm, prepared and coated in the Trapp group, 100 kPa helium, 150°C, FID detection, t_R = 6.01 min and t_S = 6.78 min) an chiral HPLC-MS (***p*-(NO₂)-MAC**: Chiralpak-IC, 1.5 mL/min, rt, 80:10:10 (hexane:methanol:2-propanol), 210 nm t_S = 8.42, t_R = 9.31) product identification was achieved by using couples MS and comparison with literature values. Analog procedure was taken with the anhydrous and degassed deuterated solvents CD_3CN and $CDCl_3$.

Set up for: Hydrogenation (H_2, 40 bar) of MAA with Ala-3 and Val-3 at different Temperatures:

For hydrogenation experiments different stock solutions of the metal source $[Rh(COD)_2]BF_4$, the bisphosphinite-ligand **3** and the prochiral olefin **MAA** were prepared separately in a glovebox. To generate a catalyst-stock solution, $[Rh(COD)_2]BF_4$ (1.00 equiv.) and the bisphosphinite-ligand **3** (1.20 equiv.) were dissolved seperately in anhydrous and degassed DCM-d_2 (each 0.2 mL per batch). The stock solution of the olefin **MAA** (4.00 equiv.) was prepared and dissolved in anhydrous and degassed DCM-d_2 (0.2 mL per batch). The stock solutions and the tube autoclave are set to the desired temperature for 10 minutes. Afterwards, 0.2 mL of ligand stock solution and 0.2 mL of Rh stock solution were united in a standard NMR tube located in a nitrogen-filled stainless steel reactor equipped with a small stirring bar under inert

conditions. The mixture was stirred for 10 min at set temperature, before 0.2 mL of **MAA** stock solution was added to the autoclave. If necessary, a cryostat was used to cool the autoclave The autoclave was pressurized with hydrogen gas (40 bar) to initiate the catalysis. The autoclave was either stirred at rt or at previously set temperature overnight. After opening the autoclave, NMR was measured, to check the reaction progress. Subsequently, the solution was passed through a short pipet filled with silica (3 cm) using ethyl acetate as eluent. The hydrogenation product resulted as a yellow oil by evaporation. Enantiomeric ratio was determined by chiral GC (**MAA** (6-TBDMS-2,3-Ac)-β-CD, 25 m, i.d. 250 μm, film thickness 250 nm, prepared and coated in the Trapp group, 100 kPa helium, 150°C, FID detection, tR = 5.75 min and tS = 6.50 min). The assignment of absolute configuration was accomplished by comparison with literature values, and measurement of the enantiopure compounds.

Results Pressure Experiments:

Table 3: Pressure experiments with **Val-3** ligand and prochiral olefin **MAA** at varying temperatures and pressures.

***pressure* [bar]**	***T* [°C]**	***Conversion* [%]**	***ee***
5	20	5	22.7
5	−20	1	23.41
5	−40	1	18.45
20	20	12	20.16
20	−20	2	18.06
20	−40	1	22.58
40	20	15	20.31
40	−20	4	19.74
40	−40	1	31.78

Results Substrate and Solvent Screening

Table 4: Hydrogenation (H_2, 40 bar) experiments with the ligand **Val-3** and different reactants and their *ee* in CD_2Cl_2 and $CDCl_3$ at different temperatures.

	MAA		**MAA-Me**		***p*-(NO_2)-MAC**	
***T* [°C]**	**DCM**	**$CDCl_3$**	**DCM**	**$CDCl_3$**	**DCM**	**$CDCl_3$**
20	−28.21	−13.77	−26.19	−19.20	−17.63	−17.7
-20	−24.03	−3.73	−16.99	−5.80	−8.34	/
-40	−28.07	−18.49	−17.66	−13.6	−5.93	−11.84

Results Hydrogenation of **MAA** with **Val-3** in DCM-d_2 at different Temperatures:

Table 5: Received *ee* values after hydrogenation (H_2, 40 bar) of **MAA** with ligand **Val-3** in CD_2Cl_2 and the temperature of complexation. The given temperature stands for the temperature of complexation of the ligand with the Rh-source and **MAA** addition for data set: Complex. Temp. (1) – (3). The reaction temperature itself was 20 °C. For data set Const. Temp., the given temperature is the temperature of complexation as well as the reaction temperature overnight.

***T* [°C]**	**Complex. Temp. (1)**	**Complex. Temp. (2)**	**Complex. Temp. (3)**	**Const. Temp**
20	/	-28,22	-6,24	/
0	−28.17	14,59	-24,39	8,85
−20	−12.18	1,21	-0,01	-30,57
−40	14.32	/	-14,26	-32,52
−60	−29.58	8,72	-12,06	/

Results of Hydrogenation of **MAA** with **Ala-3** in DCM-d_2 at different Temperatures:

Table 6: Hydrogenation (H_2, 40 bar) of **MAA** with **ALA-3** with three different stock solutions at different temperatures.

***T* [°C]**	***Conversion* [%]**	***ee***
0	100	22.7
−20	100	23.41
−40	100	18.45

4.2.9 Hemiacetal Synthesis

3-Hydroxy-2-iodobenzaldehyde **33**

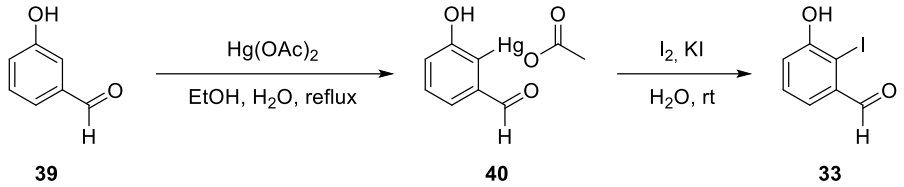

39 **40** **33**

This compound was synthesized to a known procedure.[124] A solution of $Hg(OAc)_2$ (3.00 g, 9.42 mmol, 1.00 equiv.) in ethanol/water/acetic acid (11.5 mL/11.3 mL/0.23 mL) was prepared. A second solution of **39** (1.15 g, 9.42 mmol, 1.00 equiv.) dissolved in ethanol/water (5.75 mL/5.75 mL) was prepared. The combined solutions were heated until reflux for 6 h. After the solution was allowed to cool to rt., it was concentrated to 11 mL. The residue was dried *in vacuo* to give **40** (2.79 g, 78%) as a yellowish solid. The crude product was used without further purification.

40 (2.79 g, 7.32 mmol, 1.00 equiv.) was added to a solution of I_2 (1.99 g, 7.84 mmol, 1.07 equiv.) and KI (1.99 g, 12.0 mmol, 1.64 equiv.) in water (20 mL) and stirred at 0 °C. After 5 h, the mixture was allowed to warm to rt. Afterwards the precipitate was filtered off and recrystallized from ethanol/water (22.5 mL/128 mL) to give the product **33** (1.34 g, 73%) as a yellowish solid.

^{1}H NMR (400 MHz, $CDCl_3$): δ 10.70 (s, 1H, H^8), 7.42 (s, 1H, H^6), 7.39 (t, 1H, H^5), 7.12 (d, 1H, H^4), 5.93 (s, 1H, H^7).

3-Hydroxy-2-(4,4,5,5-tetramethyl-1,3,2-dioxaborolan-2-yl)benzaldehyde[117] **34**

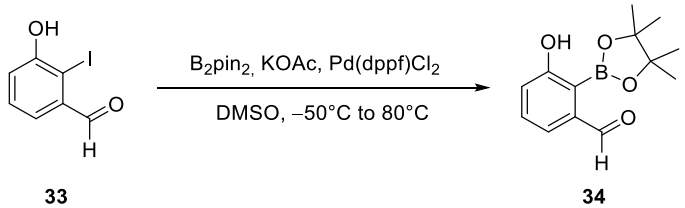

33 **34**

In a flame-dried Schlenk tube under argon, **33** (300 mg,1.21 mmol, 1.00 equiv.), KOAc (356 mg, 3.63 mmol, 3.00equiv.), B_2pin_2(338 mg, 1.33 mmol, 1.10 equiv.), and $Pd(dppf)_2Cl_2$(88.5 mg, 121 μmol, 0.10 equiv.) were dis-solved in DMF (5.6 ml) and stirred at 80 °C. After 19 h, the solution was allowed to cool to rt, HCl (aqueous, 2M, 10 ml) was added, and the solution was extracted with DCM (320 ml). The combined organic layers were washed with saturated aqueous Na/K-tartrate solution (10 ml) and dried over $MgSO_4$. Volatiles were removed *in vacuo*. The crude product was purified by flash column

chromatography (silica, *n*-pentane/EtOAc 9:1 to 5:1) to give **34** (47.0 mg, 16%) as a brown solid.

^{1}H NMR (400 MHz, $CDCl_3$) δ (ppm) = 9.94(s, 1H,), 7.42 (s, 1H), 7.34 (s, 1H), 7.13 (m, 1H), 5.93(s, 1H), 1.25 (s, 12H).

^{13}C NMR (101 MHz, $CDCl_3$,) δ (ppm) = 195.30,164.89, 143.41, 133.40, 129.76, 121.74, 119.27, 85.13,77.48, 24.96.

HR-MS (ESI^+,CH_3CN): [M+H]+:$C_{13}H_{18}BO_4^+$, calc.: m/z 249,1293; found: m/z 249.1288.

IR (KBr):ν =3364.9, 2996.3, 2974.8, 2929.9, 2876.8,1689.0, 1618.8, 1592.8, 1493.5, 1479.6, 1443.4, 1380.6,1370.2, 1304.0, 1278.2, 1233.0, 1000.0, 993.03, 960.8,926.1, 944.6, 894.7, 875.0, 862.7, 803.9, 777.1, 745.5, 698.5,680.7 cm^{-1}.

6,6'-dihydroxy-[1,1'-biphenyl]-2,2'-dicarbaldehyde **30**, 6,10-dihydroxy-6H-benzo[c]chromene-1-carbaldehyde **31**, 10-hydroxychromeno[5,4,3-cde]chromen-5(10H)-one[117] **32**

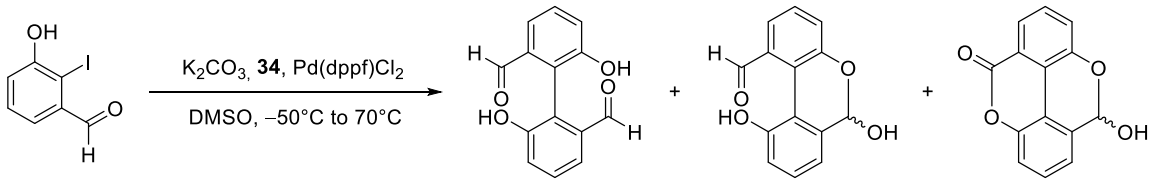

33 **30** **31** **32**

In a flame-dried Schlenk tube under argon, **33** (23.0 mg, 121 μmol, 1.00 equiv.), KOAc (66.9 mg, 484 mmol, 4.00 eq.), **34** (30.0 mg, 121 μmol, 1.00 equiv.) and $Pd(dppf)_2Cl_2$ (885 μg, 1.21 μmol, 0.01 equiv.) were dissolved in DMSO (1 mL, dry, degassed) at –50 °C and then stirred at 70 °C. After 24 h, the mixture was allowed to cool to rt, EtOAc (10 mL) and water (10 mL) were added and the aqueous layer was extracted with EtOAc (2 x20 mL). The combined organic layers were washed with brine (5 mL) and dried over $MgSO_4$. Volatiles were removed *in vacuo*. The crude product was purified by flash column chromatography (silica, pentane:EtOAc 9:1 to 5:1) to give **30**, **31**, **32** (85.0 μg, 0.3%) as a brown oil.

HR-MS (ESI^+, EtOAc): **31** $[M+H]^+$: $C_{14}H_{11}O_4^+$, calc.: m/z 243.0652, found m/z 243.0646. **32** $[M+H]^+$: calc.: m/z 241.0495, found m/z 241.049.

Appendix

Pressure experiments: Val-3, MAA, CD_2Cl_2

5 bar, 20 °C (Val-3, MAA, CD_2Cl_2)

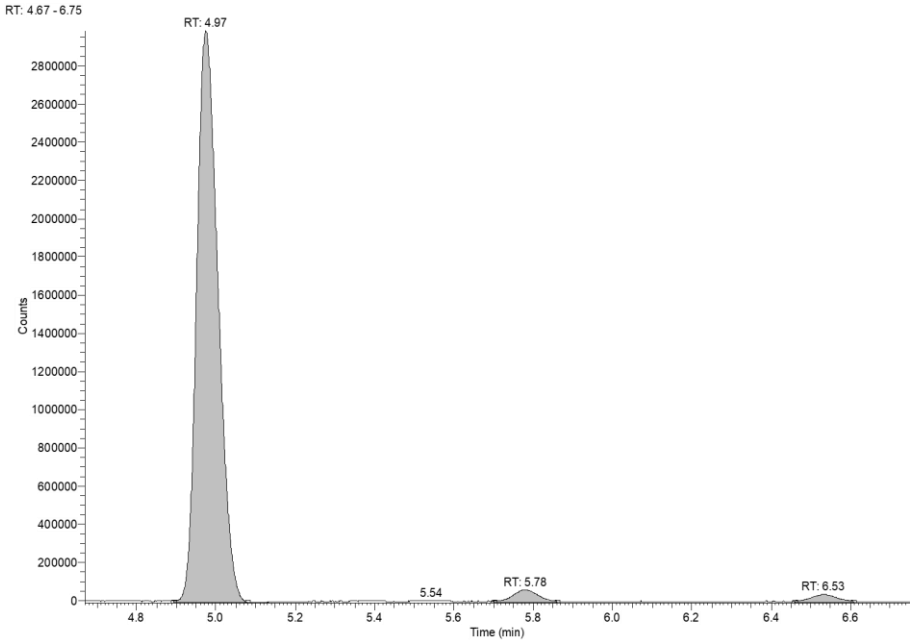

Apex RT	Start RT	End RT	Area	%Area	Height	%Height
4.97	4.89	5.08	11187219.5	95.42	2993300	96.47
5.78	5.7	5.86	318988	2.72	66850	2.15
6.53	6.46	6.61	217765.5	1.86	42750	1.38

5 bar, −20 °C (Val-3, MAA, CD_2Cl_2)

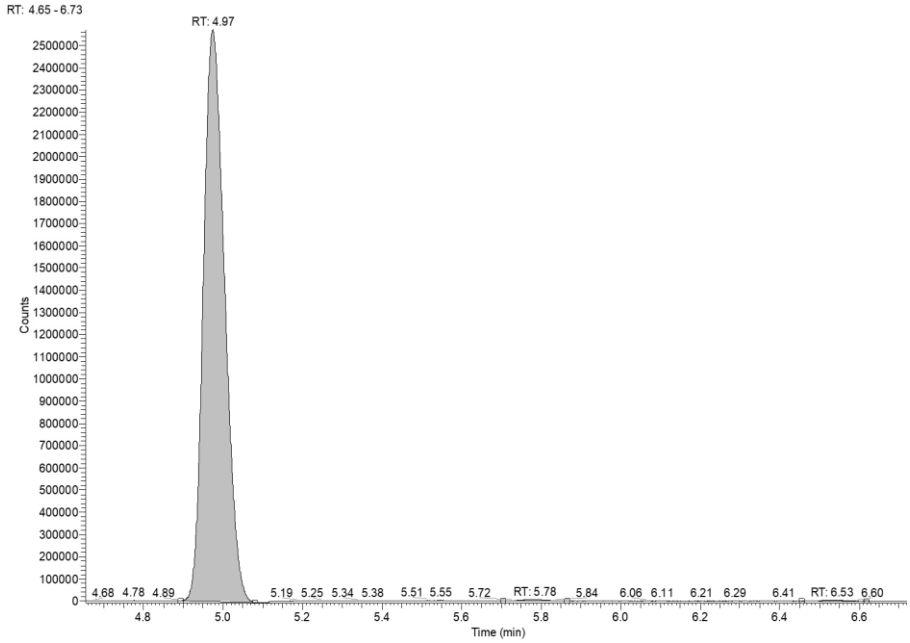

Apex RT	Start RT	End RT	Area	%Area	Height	%Height
4.97	4.89	5.08	9506561.77	99.39	2573248.73	99.44
5.78	5.7	5.86	36189.272	0.38	8719.785	0.34
6.53	6.46	6.62	22328.618	0.23	5741.835	0.22

5 bar, −40 °C (Val-3, MAA, CD_2Cl_2)

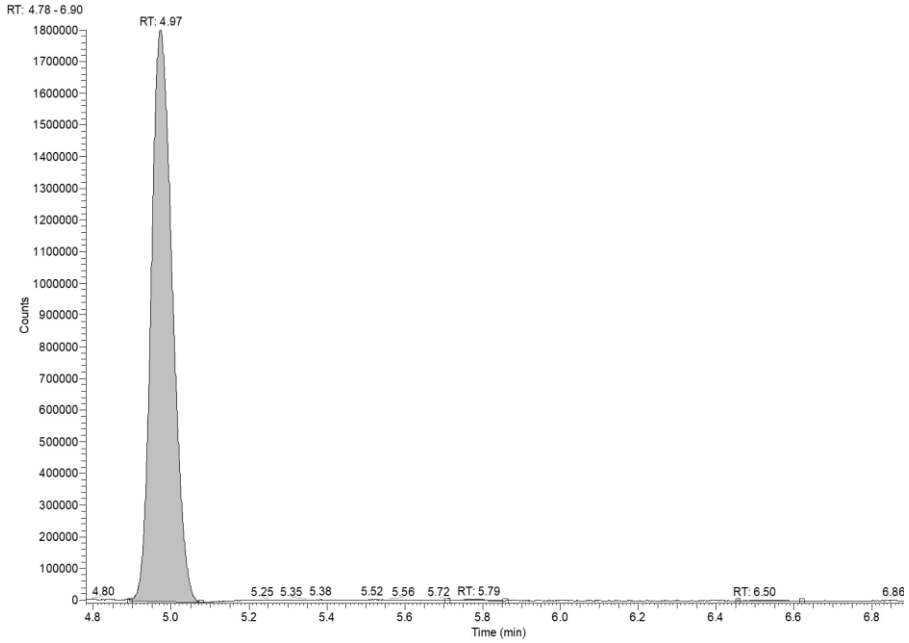

Apex RT	Start RT	End RT	Area	%Area	Height	%Height
4.97	4.89	5.08	6811739.4	99.64	1804915.65	99.65
5.79	5.71	5.86	15444.862	0.23	3940.082	0.22
6.5	6.45	6.62	8909.615	0.13	2471.946	0.14

20 bar, 20 °C (Val-3, MAA, CD_2Cl_2)

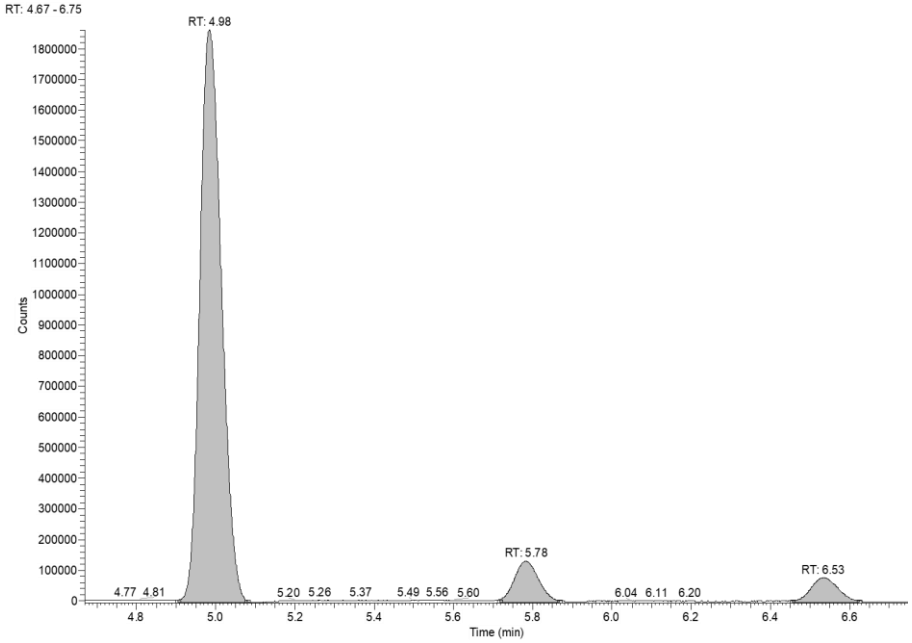

Apex RT	Start RT	End RT	Area	%Area	Height	%Height
4.98	4.9	5.08	7084367	87.72	1867850	89.62
5.78	5.72	5.87	590134.5	7.31	135400	6.5
6.53	6.46	6.62	401817	4.98	80950	3.88

20 bar, −20 °C (Val-3, MAA, CD_2Cl_2)

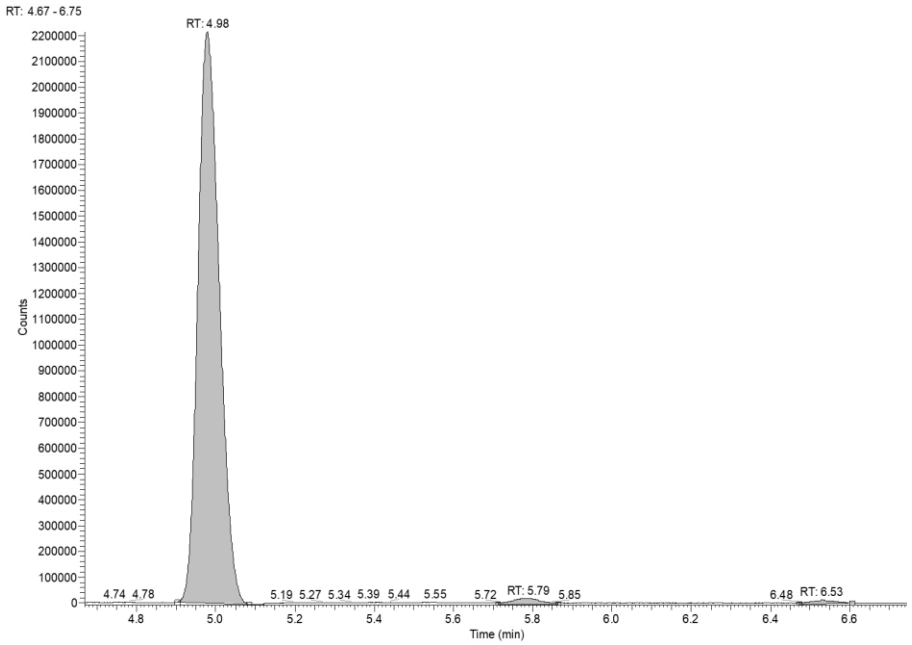

Apex RT	Start RT	End RT	Area	%Area	Height	%Height
4.98	4.9	5.08	8347226.5	97.6	2215520.73	98.22
5.79	5.71	5.86	135196	1.58	25200	1.12
6.53	6.47	6.61	70466.034	0.82	14879.699	0.66

20 bar, −40 °C (Val-3, MAA, CD_2Cl_2)

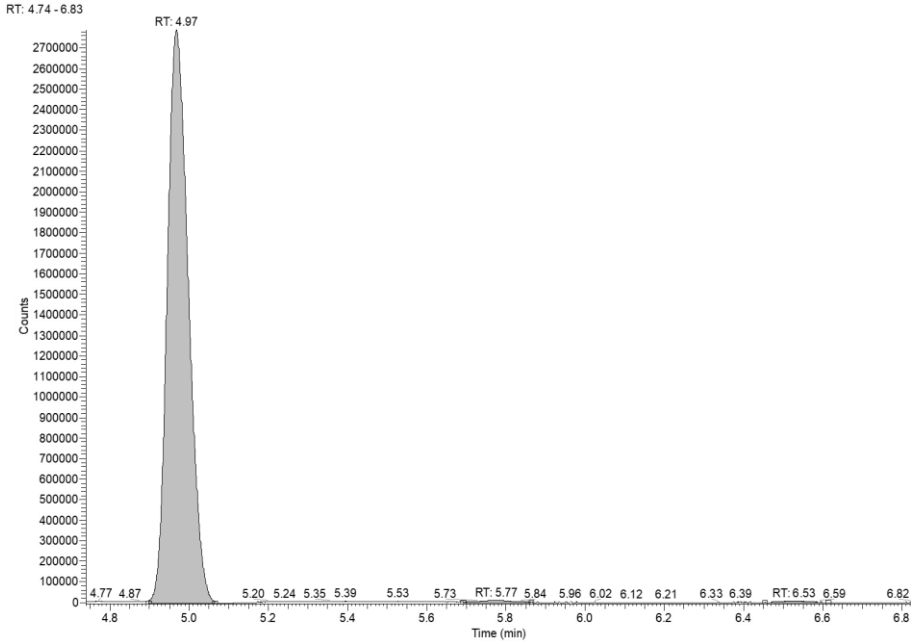

Apex RT	Start RT	End RT	Area	%Area	Height	%Height
4.97	4.9	5.06	10324099.5	99.35	2795050	99.43
5.77	5.69	5.86	40808.419	0.39	9666.297	0.34
6.53	6.45	6.61	27005.314	0.26	6269.647	0.22

40 bar, 20 °C (Val-3, MAA, CD_2Cl_2)

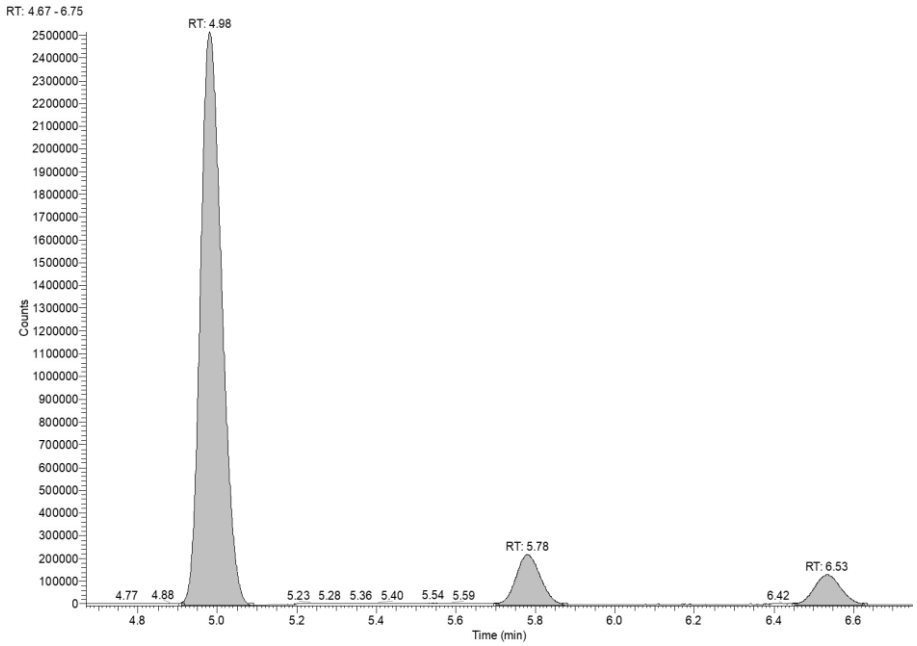

Apex RT	Start RT	End RT	Area	%Area	Height	%Height
4.98	4.91	5.08	9394223.5	85.14	2521200	87.51
5.78	5.7	5.87	980307	8.88	224450	7.79
6.53	6.45	6.63	659036.5	5.97	135350	4.7

40 bar, −20 °C (Val-3, MAA, CD_2Cl_2)

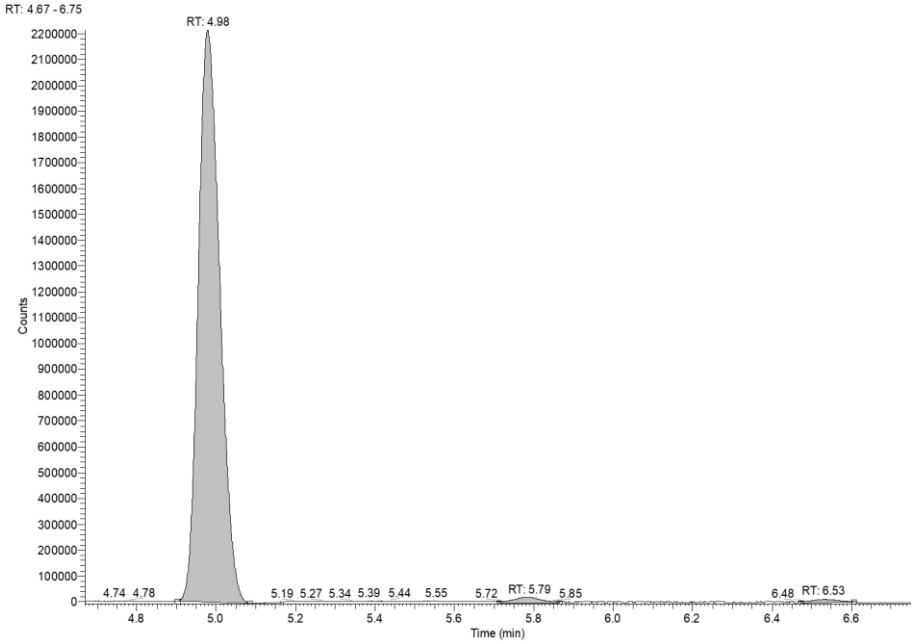

Apex RT	Start RT	End RT	Area	%Area	Height	%Height
4.98	4.91	5.08	9762356.97	96.45	2604972.89	97.48
5.78	5.71	5.87	208892	2.06	40300	1.51
6.54	6.46	6.61	150699.5	1.49	26950	1.01

40 bar, −40 °C (Val-3, MAA, CD_2Cl_2)

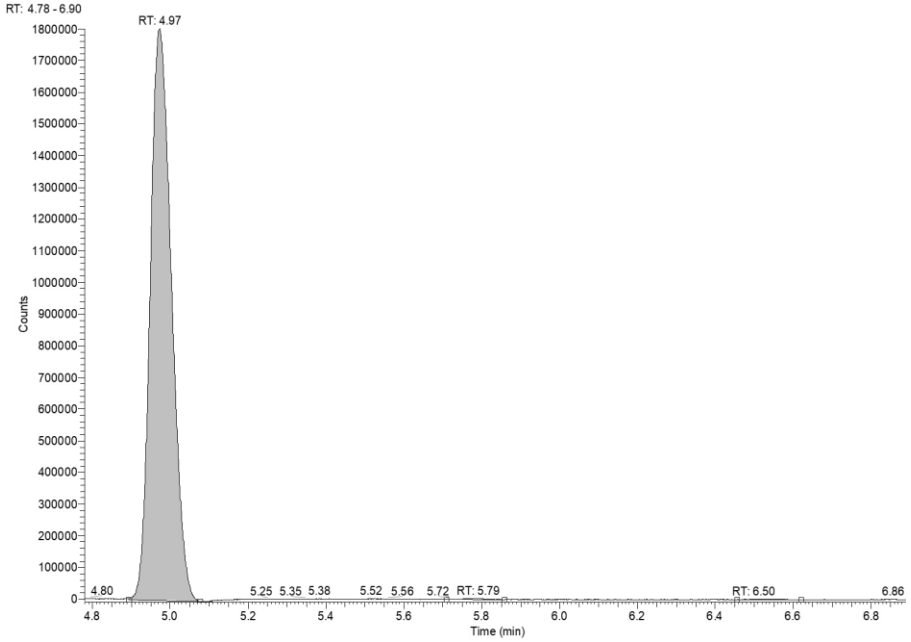

Apex RT	Start RT	End RT	Area	%Area	Height	%Height
4.97	4.9	5.07	7977008.5	99.28	2179541.25	99.38
5.77	5.7	5.86	33967.938	0.42	7783.177	0.35
6.53	6.46	6.61	23971.91	0.3	5741.982	0.26

Substrate and Solvent Screening

MAA, CD_2Cl_2, 20 °C

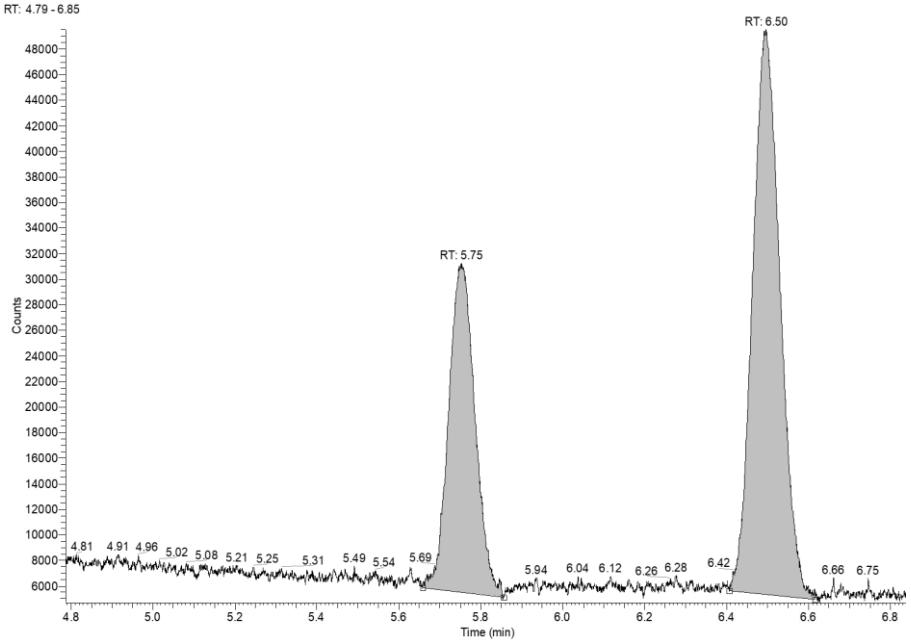

Apex RT	Start RT	End RT	Area	%Area	Height	%Height
5.75	5.66	5.86	114832.207	35.89	25750.173	36.85
6.5	6.41	6.62	205115.966	64.11	44130.799	63.15

MAA, CD_2Cl_2, –20 °C

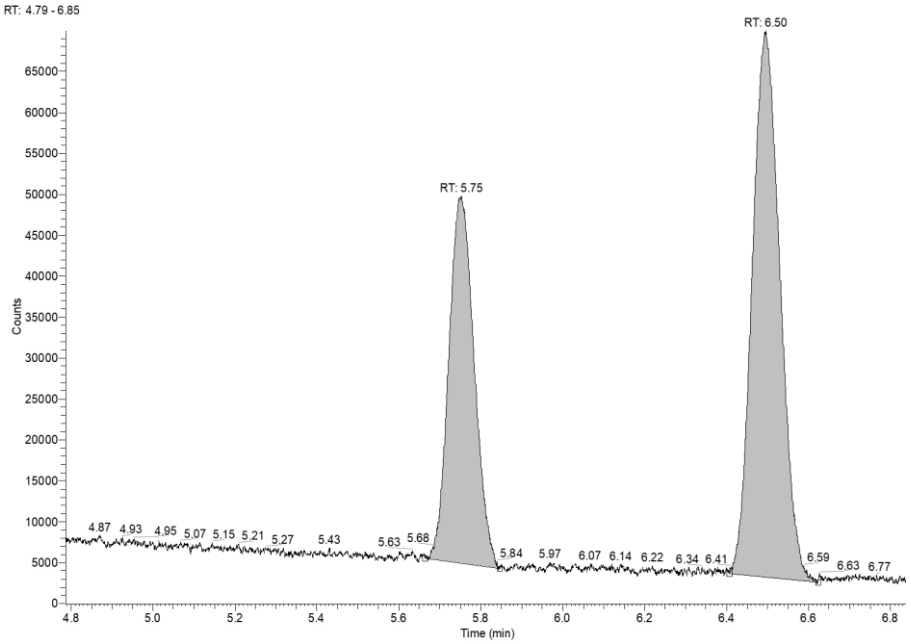

Apex RT	Start RT	End RT	Area	%Area	Height	%Height
5.75	5.66	5.85	192127.10	37.98	44853.088	40.19
6.5	6.41	6.62	313691.03	62.02	66739.694	59.81

MAA, CD_2Cl_2, −40°C

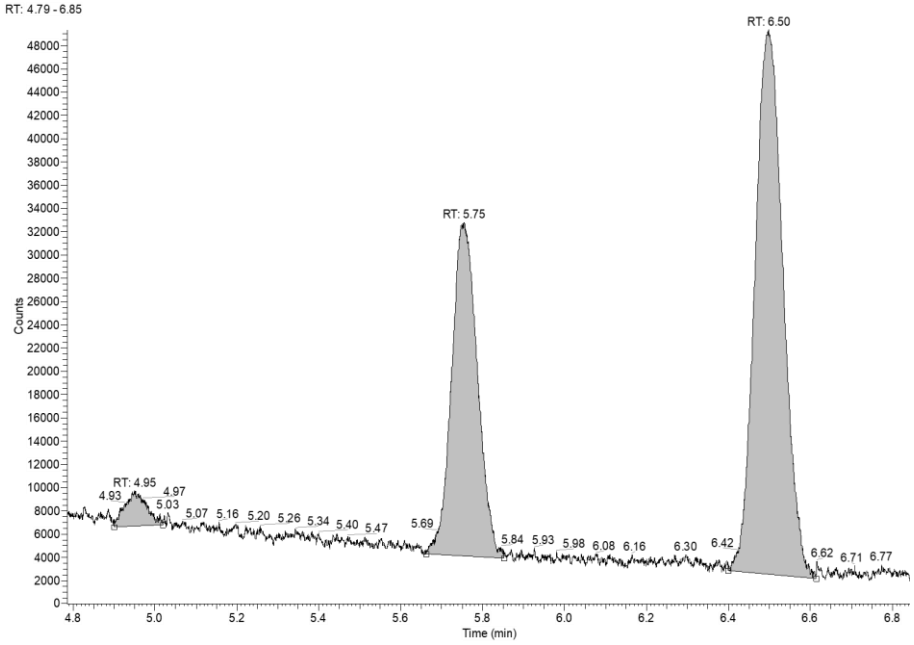

Apex RT	Start RT	End RT	Area	%Area	Height	%Height
4.95	4.9	5.02	11181.156	3.11	3048.502	3.88
5.75	5.66	5.85	125366.582	34.85	28683.93	36.53
6.5	6.4	6.61	223215.709	62.05	46798.355	59.59

MAA, MeCN, 20 °C

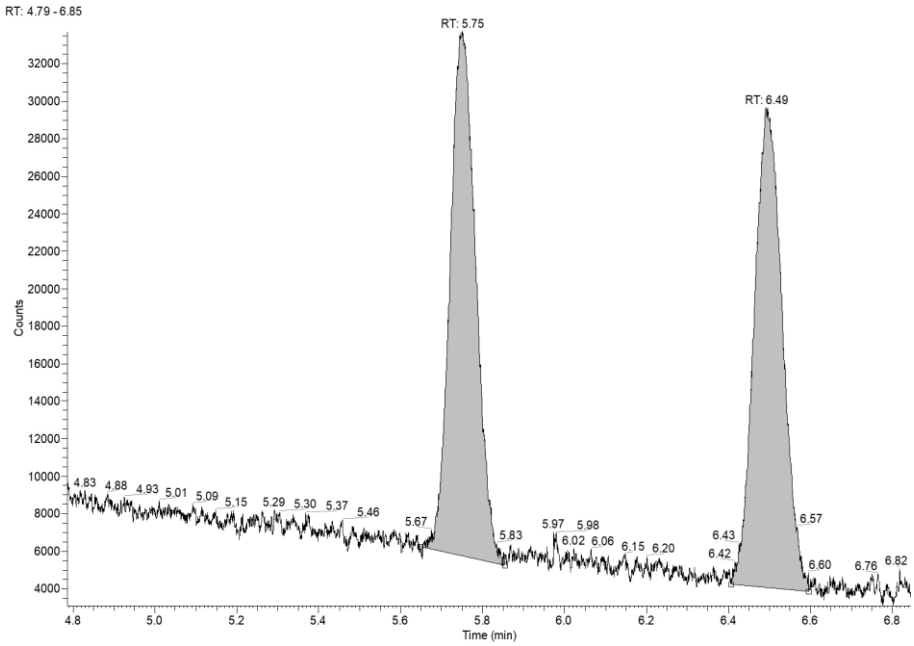

Apex RT	Start RT	End RT	Area	%Area	Height	%Height
5.75	5.65	5.85	121953.046	49.84	27945.552	52.19
6.49	6.41	6.6	122739.479	50.16	25595.429	47.81

MAA, MeCN, −20°C

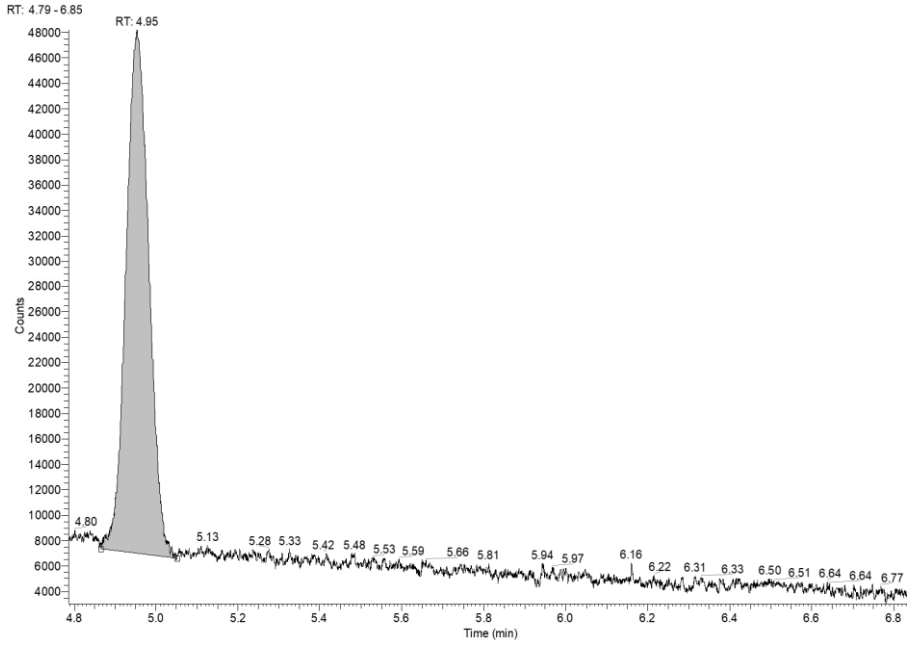

Apex RT	Start RT	End RT	Area	%Area	Height	%Height
4.95	4.86	5.05	159537.681	100	41187.408	100

MAA, MeCN, −40°C

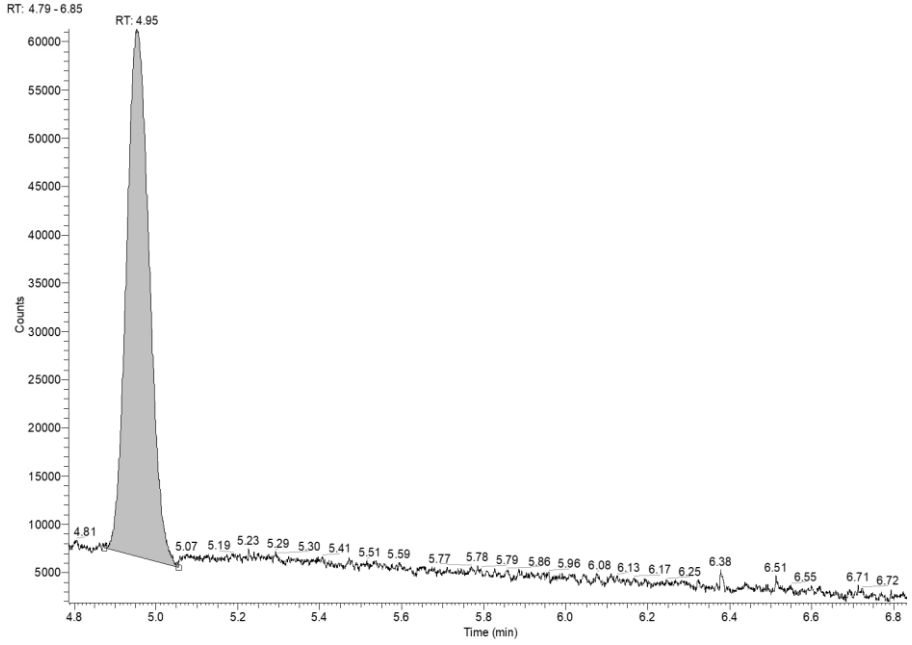

Apex RT	Start RT	End RT	Area	%Area	Height	%Height
4.95	4.87	5.06	212696.988	100	54685.877	100

MAA, $CDCl_3$, 20 °C

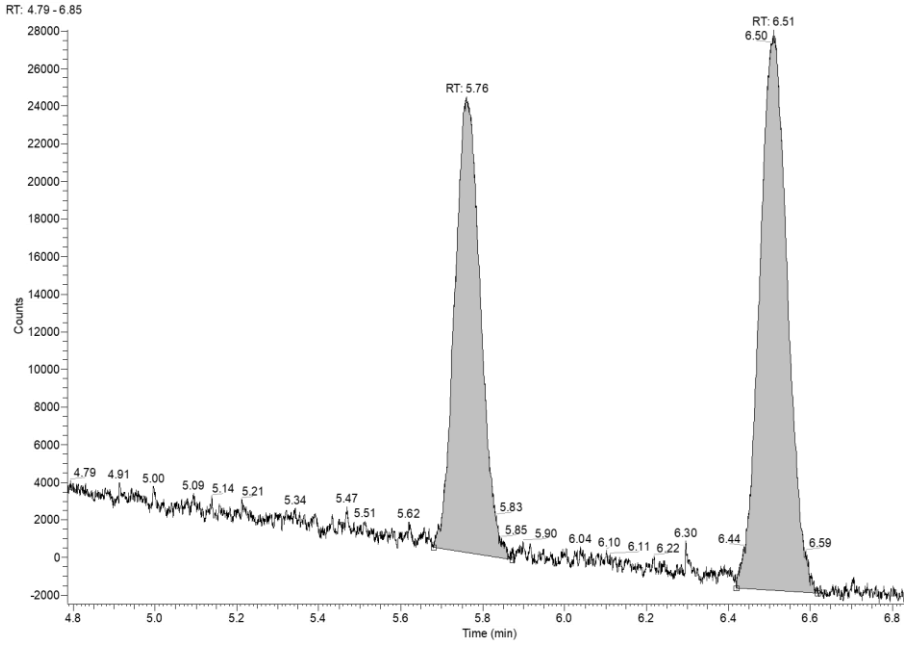

Apex RT	Start RT	End RT	Area	%Area	Height	%Height
5.76	5.68	5.87	105861.983	43.12	24233.08	44.86
6.51	6.42	6.62	139666.144	56.88	29787.518	55.14

MAA, $CDCl_3$, −20°C

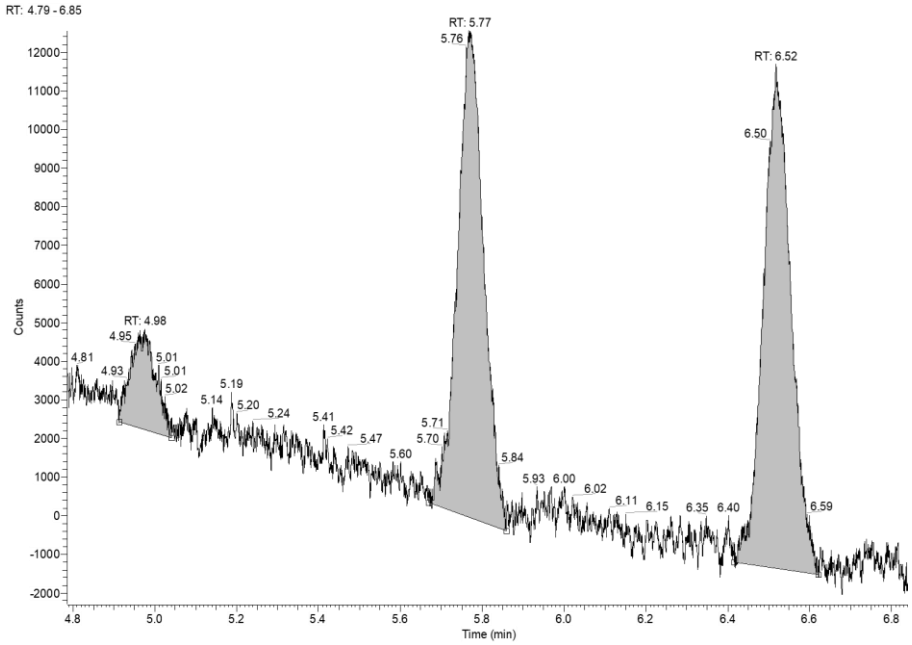

Apex RT	Start RT	End RT	Area	%Area	Height	%Height
4.98	4.91	5.04	10792.52	8.42	2614.885	9.25
5.77	5.67	5.86	56484.35	44.08	12599.151	44.55
6.52	6.42	6.62	60863.466	47.5	13065.662	46.2

MAA, $CDCl_3$, −40°C

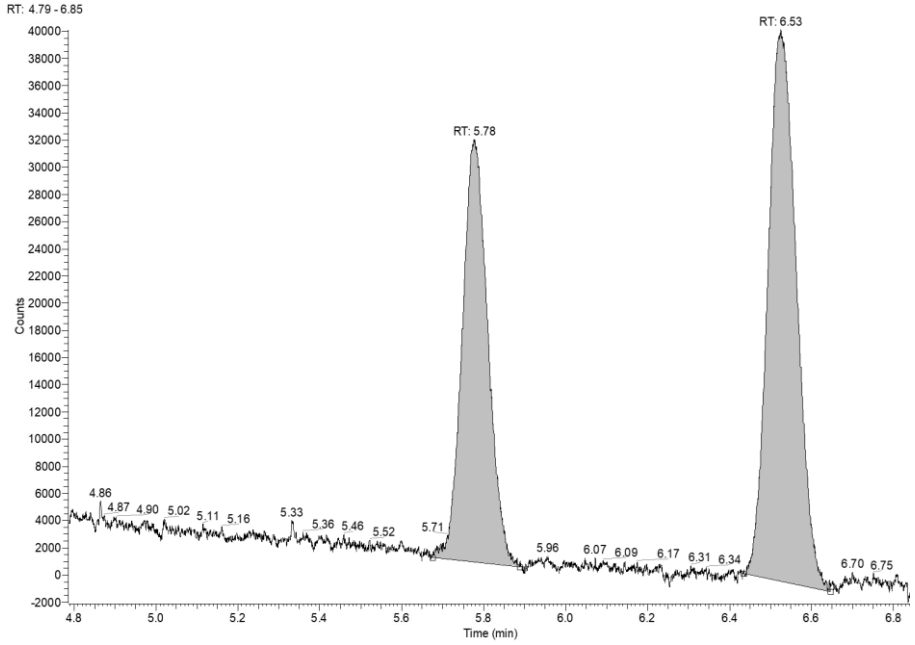

Apex RT	Start RT	End RT	Area	%Area	Height	%Height
5.78	5.67	5.89	134753.183	40.76	31082.278	43.39
6.53	6.43	6.65	195873.91	59.24	40556.788	56.61

Hydrogenation of MAA-Me

MAA-Me, CD_2Cl_2, 20 °C

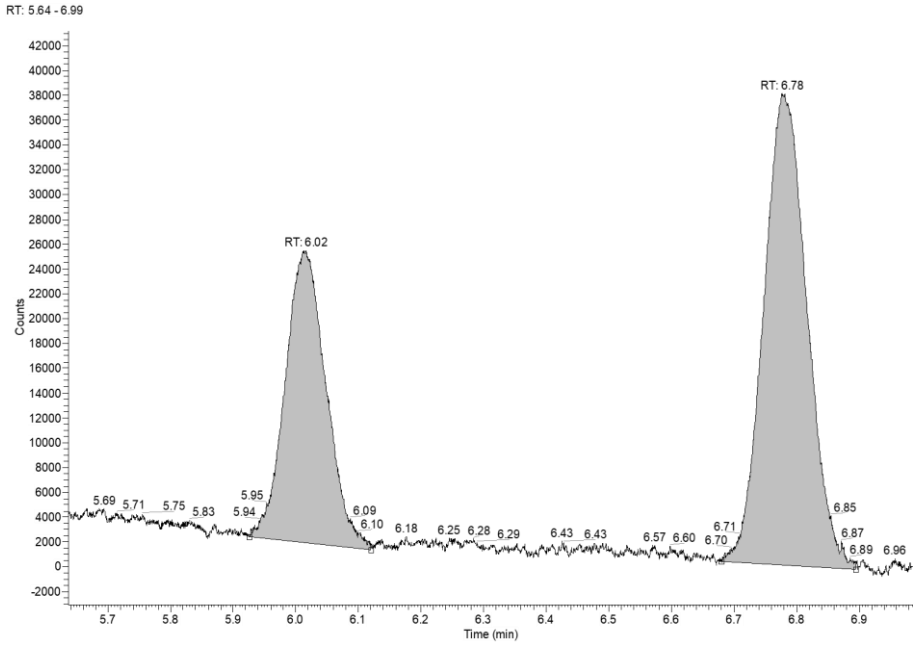

Apex RT	Start RT	End RT	Area	%Area	Height	%Height
6.02	5.93	6.12	106919.727	36.9	23574.88	38.28
6.78	6.68	6.89	182808.202	63.1	38003.14	61.72

MAA-Me, CD_2Cl_2, −20°C

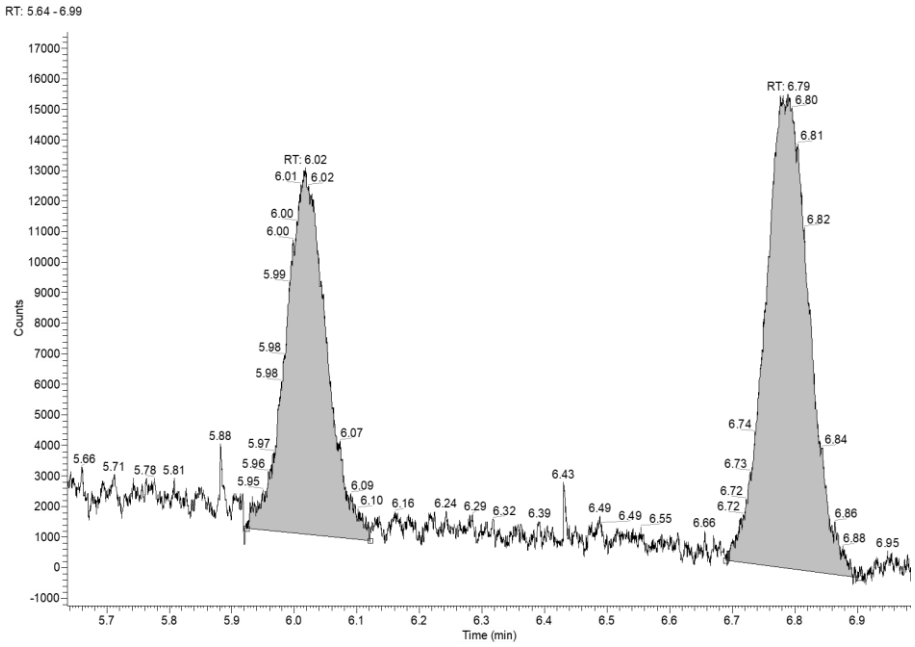

Apex RT	Start RT	End RT	Area	%Area	Height	%Height
6.02	5.92	6.12	53851.245	41.51	11994.398	43.6
6.79	6.69	6.9	75890.062	58.49	15512.953	56.4

MAA-Me, CD_2Cl_2, −40°C

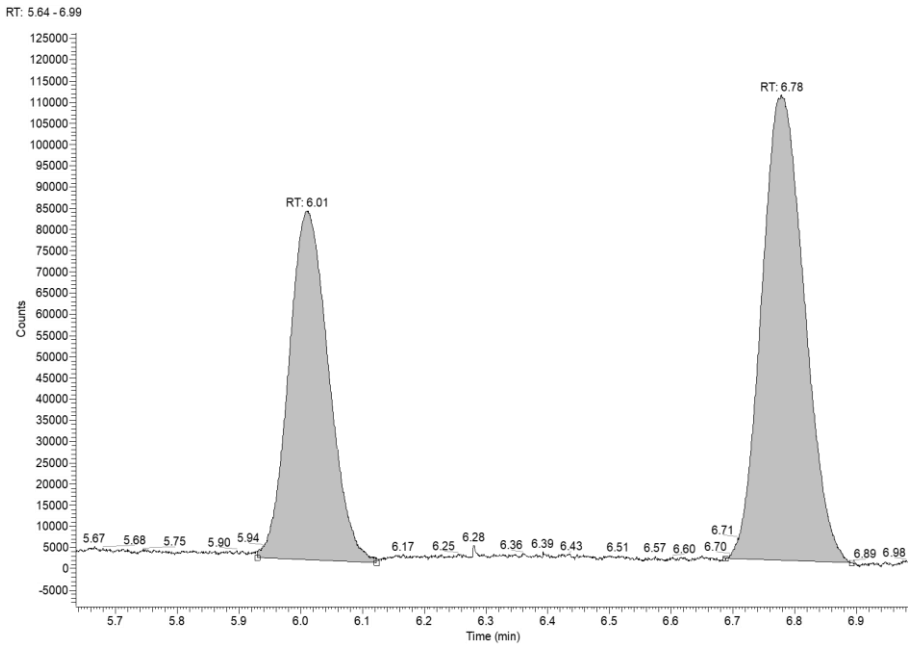

Apex RT	Start RT	End RT	Area	%Area	Height	%Height
6.01	5.93	6.12	368159.832	41.17	82224.842	42.87
6.78	6.69	6.89	526132.536	58.83	109569.163	57.13

MAA-Me, MeCN, 20 °C

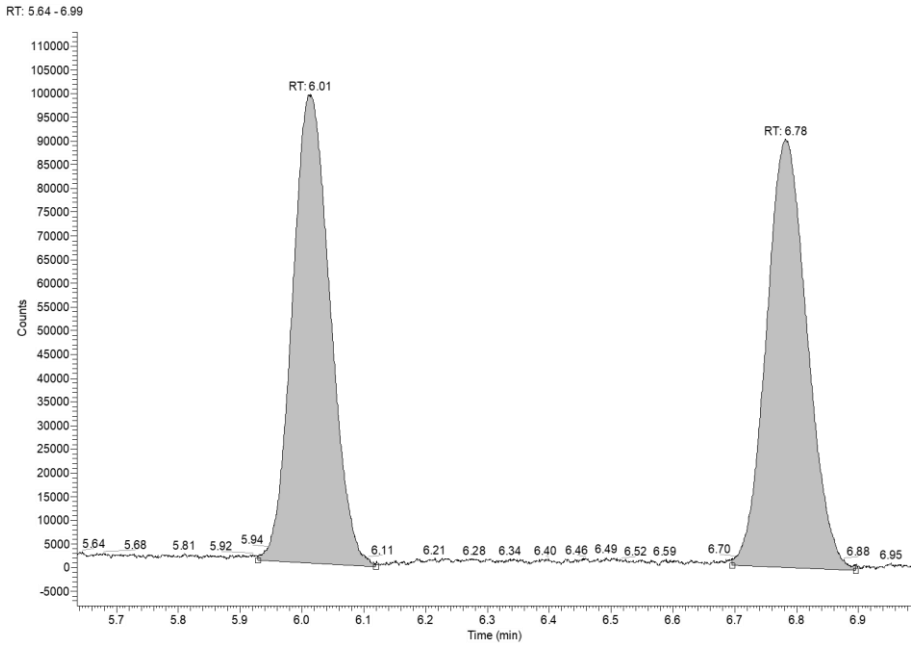

Apex RT	Start RT	End RT	Area	%Area	Height	%Height
6.01	5.93	6.12	419365.699	50.3	98839.366	52.24
6.78	6.69	6.89	414399.836	49.7	90379.482	47.76

MAA-Me, MeCN, −20°C

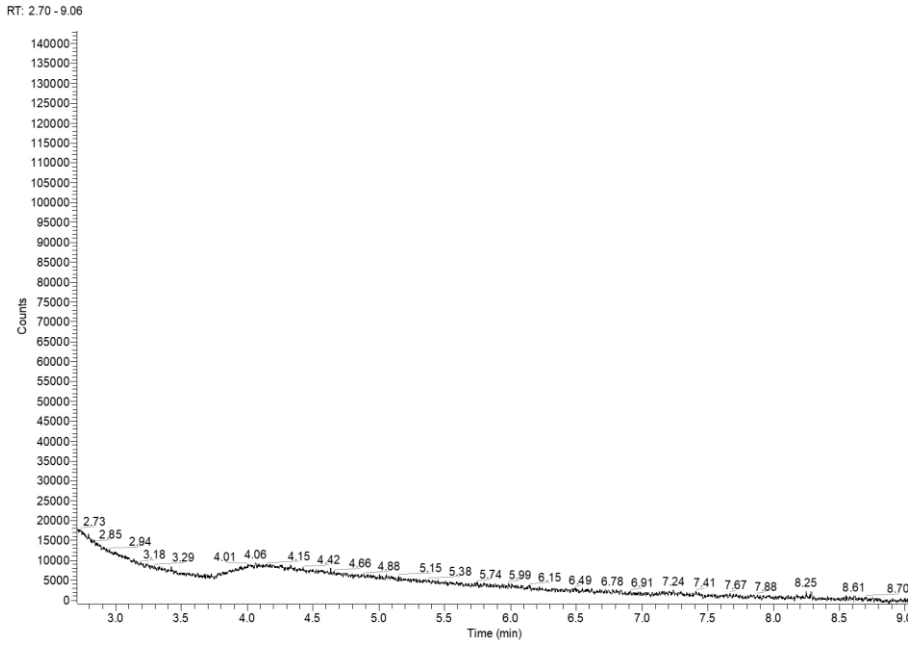

No conversion.

MAA-Me, MeCN, −40 °C

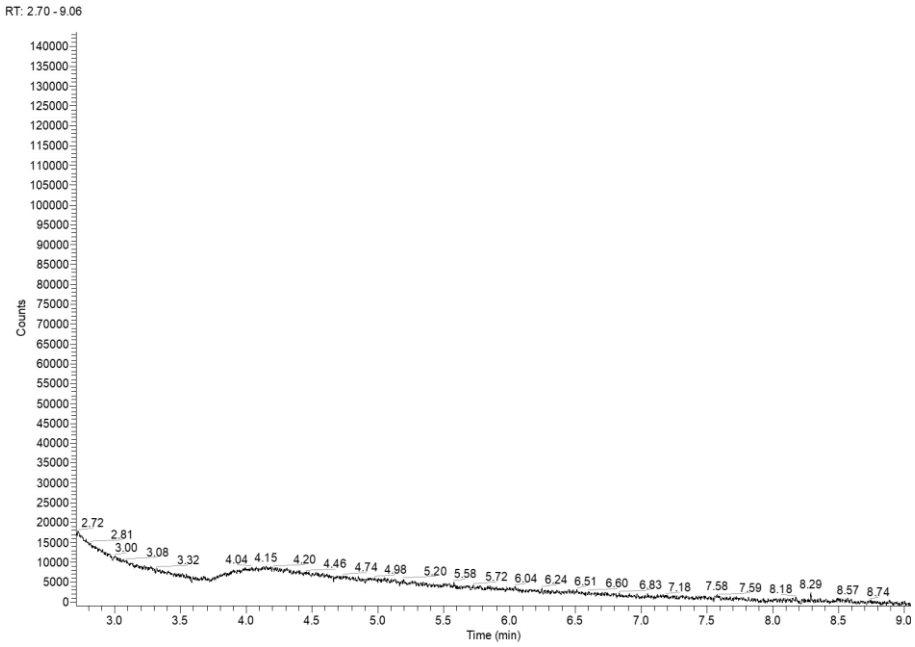

No conversion.

MAA-Me, $CDCl_3$, 20 °C

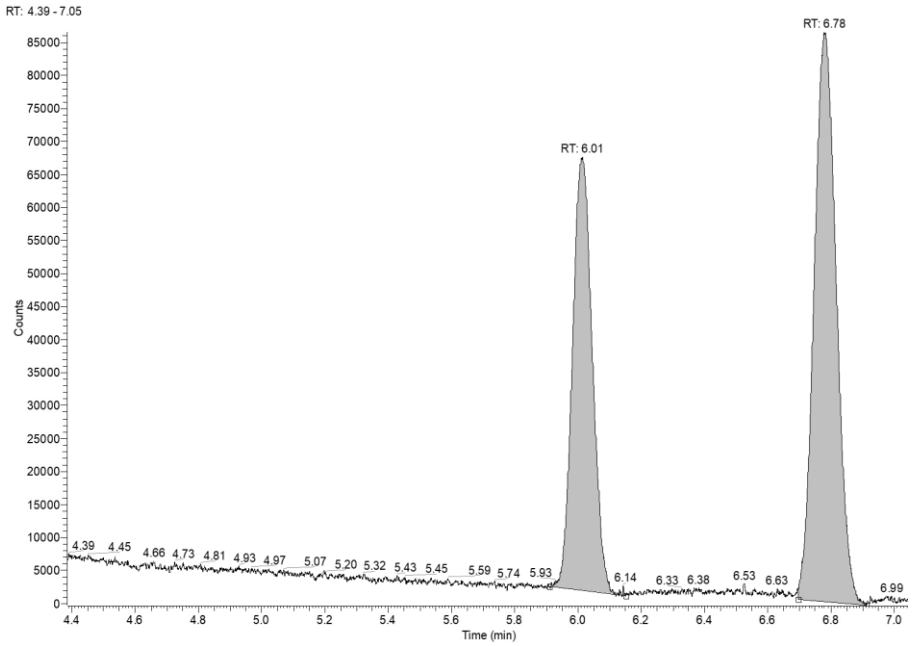

Apex RT	Start RT	End RT	Area	%Area	Height	%Height
6.01	5.91	6.15	285565.267	40.43	65711.696	43.22
6.78	6.7	6.91	420744.15	59.57	86327.057	56.78

MAA-Me, $CDCl_3$, −20 °C

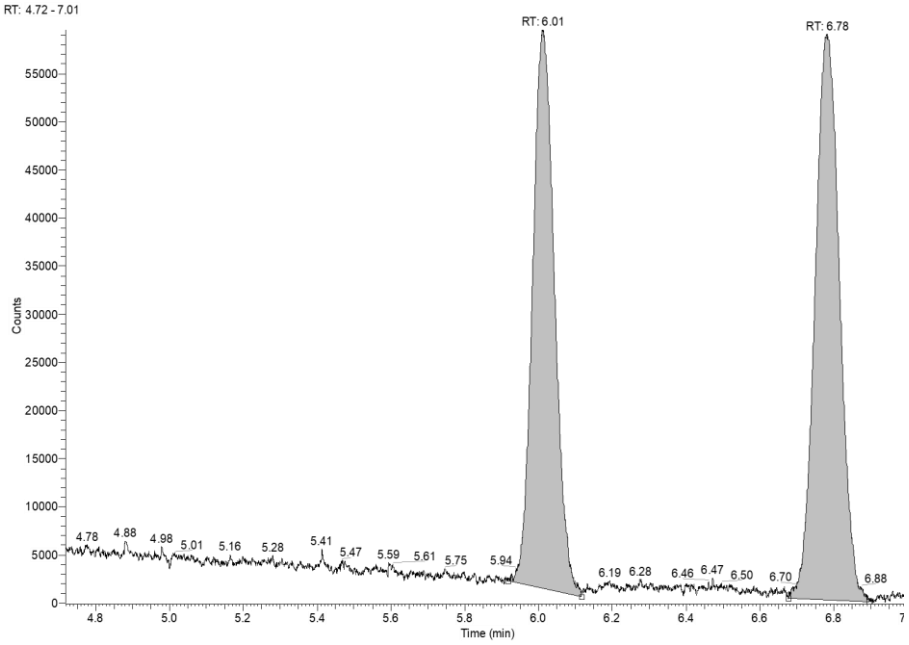

Apex RT	Start RT	End RT	Area	%Area	Height	%Height
6.01	5.92	6.12	238625.307	46.69	58010.243	49.68
6.78	6.68	6.9	272480.177	53.31	58751.309	50.32

MAA-Me, $CDCl_3$, −40 °C

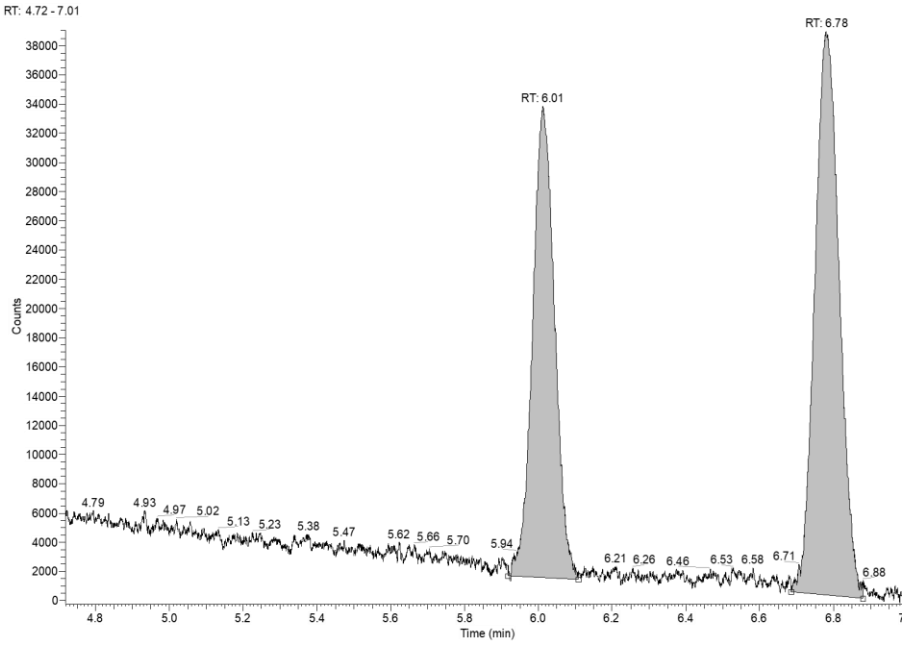

Apex RT	Start RT	End RT	Area	%Area	Height	%Height
6.01	5.92	6.11	133473.34	42.85	32244.649	45.52
6.78	6.68	6.88	178024.071	57.15	38593.047	54.48

Hydrogenation of *p*-(NO_2)-MAC

p-(NO2)-MAC, CD_2Cl_2, 20 °C

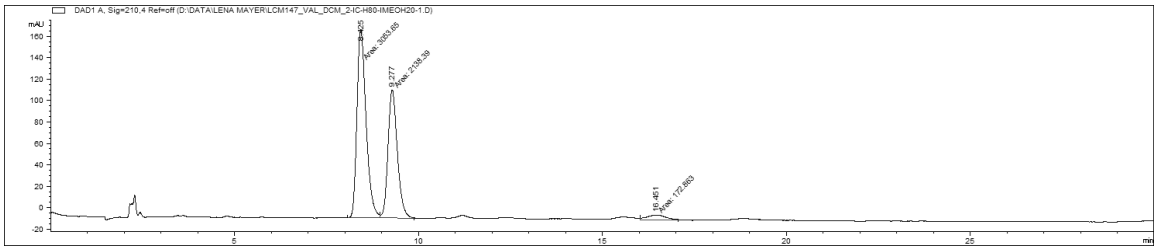

#	Time	Area	Height	Width	Area%	Symmetry
1	8.425	3053.7	175.9	0.2894	56.919	0.694
2	9.277	2138.4	120	0.297	39.859	0.772
3	16.451	172.9	4.7	0.6075	3.222	0.861

p-(NO_2)-MAC, CD_2Cl_2, −20 °C

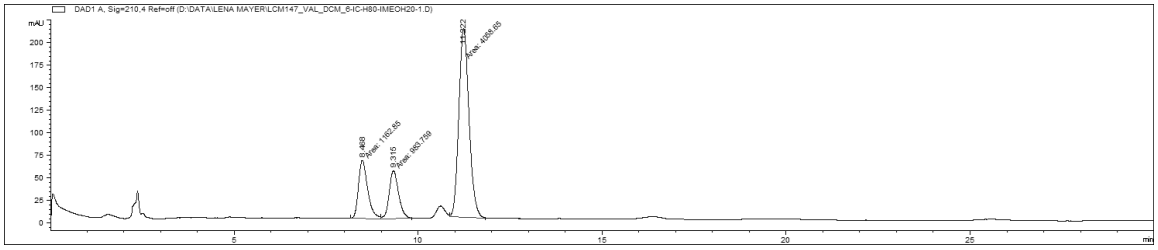

#	Time	Area	Height	Width	Area%	Symmetry
1	8.468	1162.8	65.3	0.2967	18.74	0.679
2	9.315	983.8	54	0.3035	15.854	0.794
3	11.222	4058.7	209.5	0.3229	65.407	0.845

p-(NO_2)-MAC, CD2Cl2, −40 °C

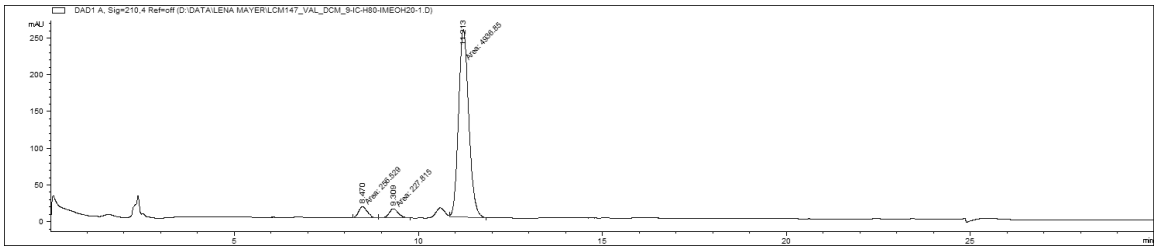

#	Time	Area	Height	Width	Area%	Symmetry
1	8.47	256.5	15.4	0.2784	4.732	0.75
2	9.309	227.8	12.6	0.3018	4.202	0.813
3	11.213	4936.9	255.7	0.3217	91.066	0.858

p-(NO_2)-MAC, MeCN, 20 °C

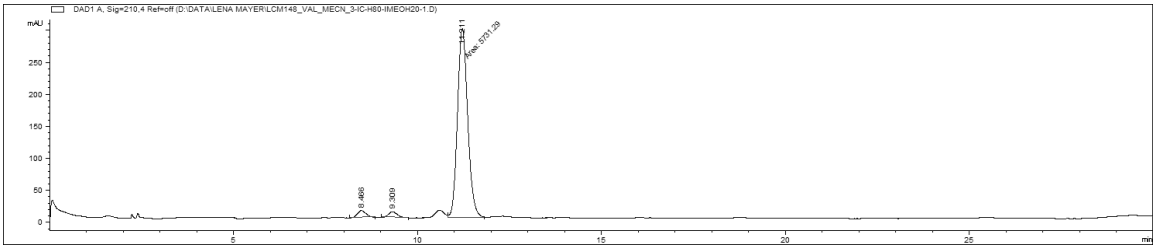

#	Time	Area	Height	Width	Area%	Symmetry
1	8.466	177.5	11	0.2318	2.927	0.77
2	9.309	153.8	9.2	0.2512	2.537	0.748
3	11.211	5731.3	295.6	0.3231	94.536	0.857

p-(NO_2)-MAC, MeCN, −20 °C

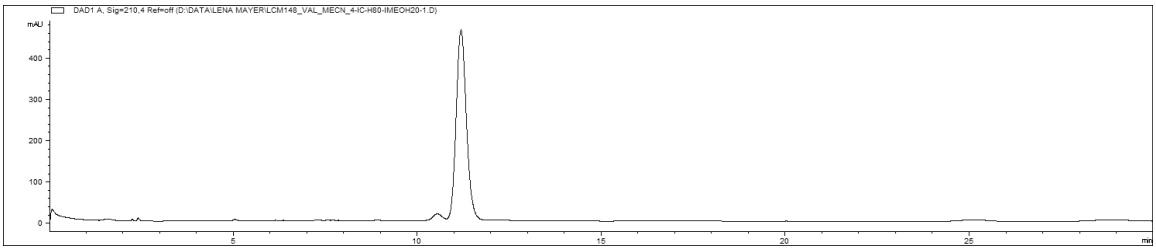

No conversion.

p-(NO_2)-MAC, MeCN, −40 °C

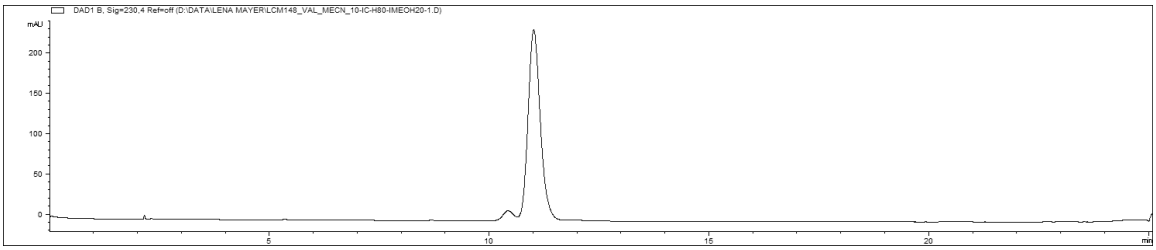

No conversion.

p-(NO_2)-MAC, $CDCl_3$, 20 °C

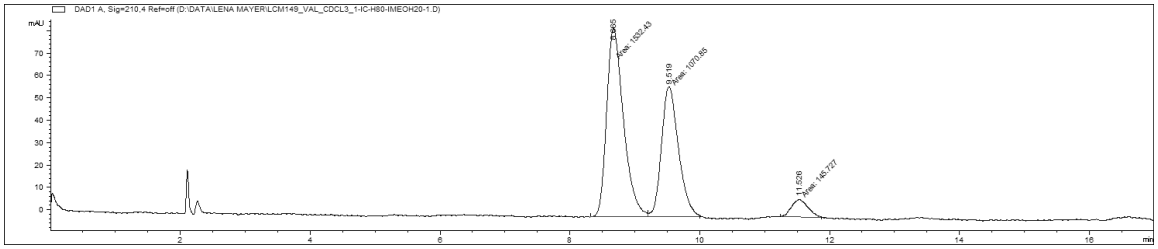

#	Time	Area	Height	Width	Area%	Symmetry
1	8.665	1532.4	84.3	0.3031	55.745	0.663
2	9.519	1070.9	58.3	0.3061	38.954	0.751
3	11.526	145.7	8.1	0.3014	5.301	0.861

p-(NO_2)-MAC, $CDCl_3$, −20 °C

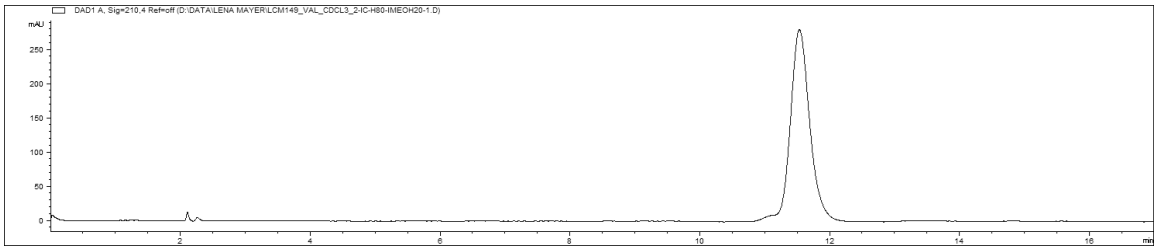

No conversion.

p-(NO_2)-MAC, $CDCl_3$, −40 °C

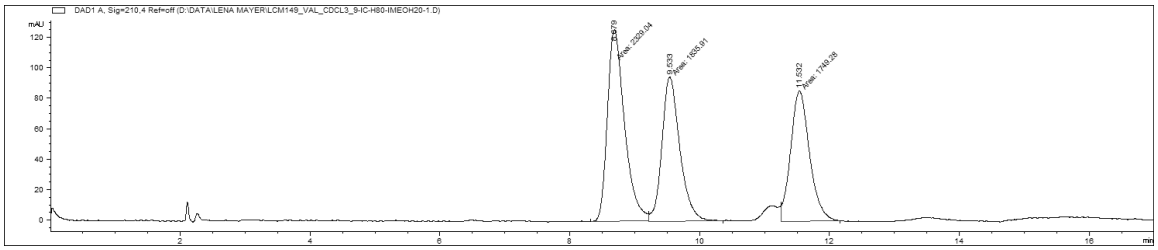

#	Time	Area	Height	Width	Area%	Symmetry
1	8.679	2329	126	0.3082	39.38	0.648
2	9.533	1835.9	95	0.3222	31.042	0.741
3	11.532	1749.3	85.9	0.3396	29.577	0.846

*ee*s for Hydrogenation of MAA with Val-3

Complex. Temp. (1) (0, −20, −40, −60 °C)

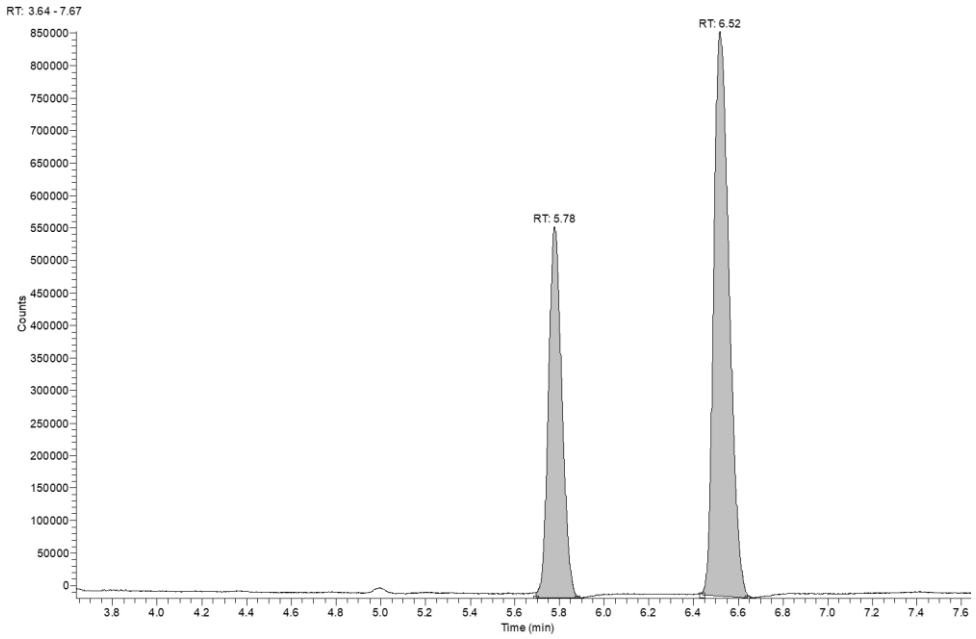

Apex RT	Start RT	End RT	Area	%Area	Height	%Height
5.78	5.7	5.88	2390994	36.29	571400	39.69
6.52	6.44	6.64	4197896.88	63.71	868284.416	60.31

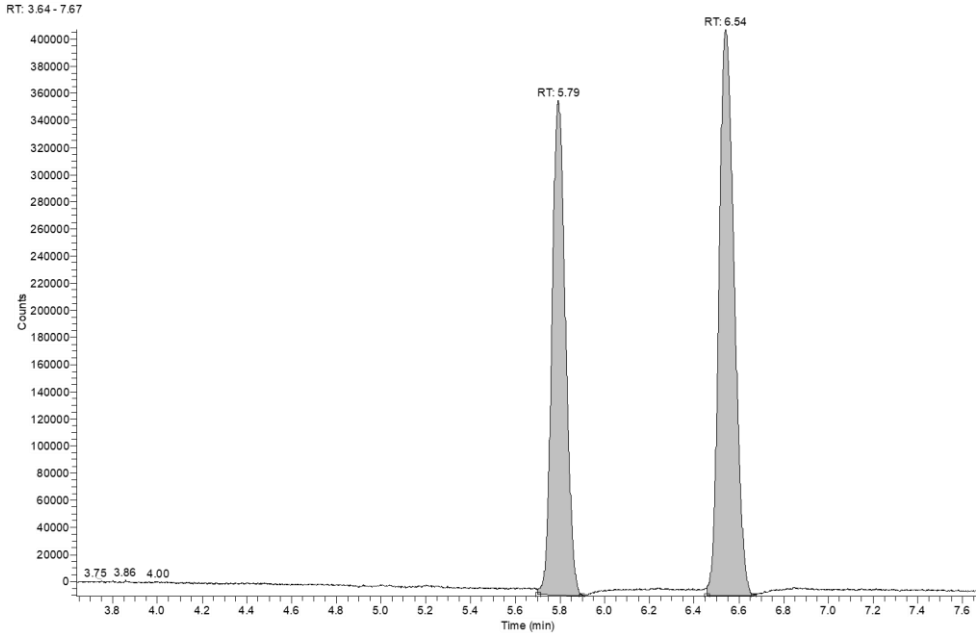

Apex RT	Start RT	End RT	Area	%Area	Height	%Height
5.79	5.7	5.9	1539185.31	43.61	365064.679	46.63
6.54	6.46	6.66	1990285	56.39	417750	53.37

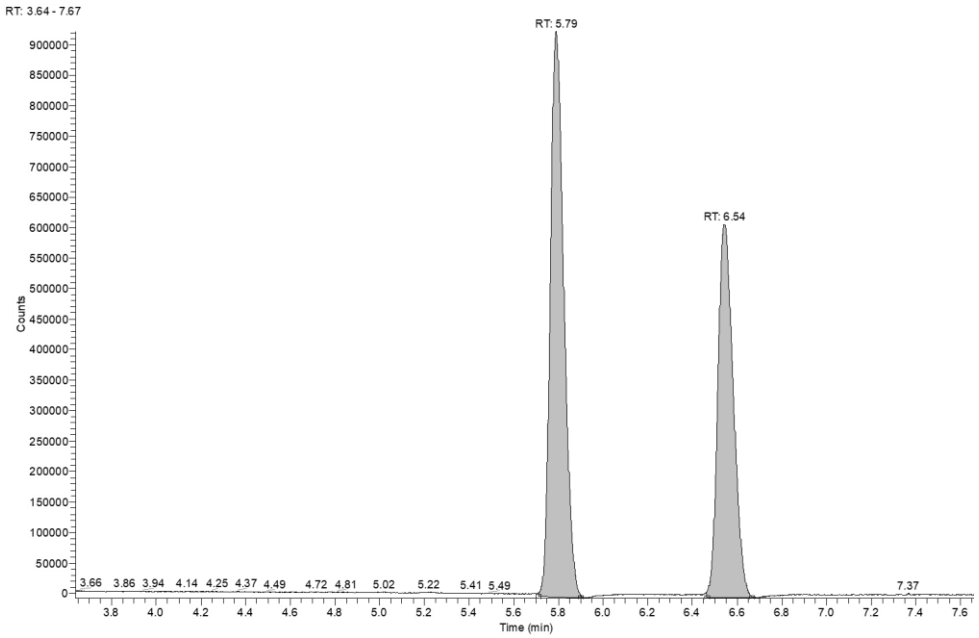

Apex RT	Start RT	End RT	Area	%Area	Height	%Height
5.79	5.71	5.9	3915660.5	57.01	927435	60.2
6.54	6.46	6.67	2952553	42.99	613100	39.8

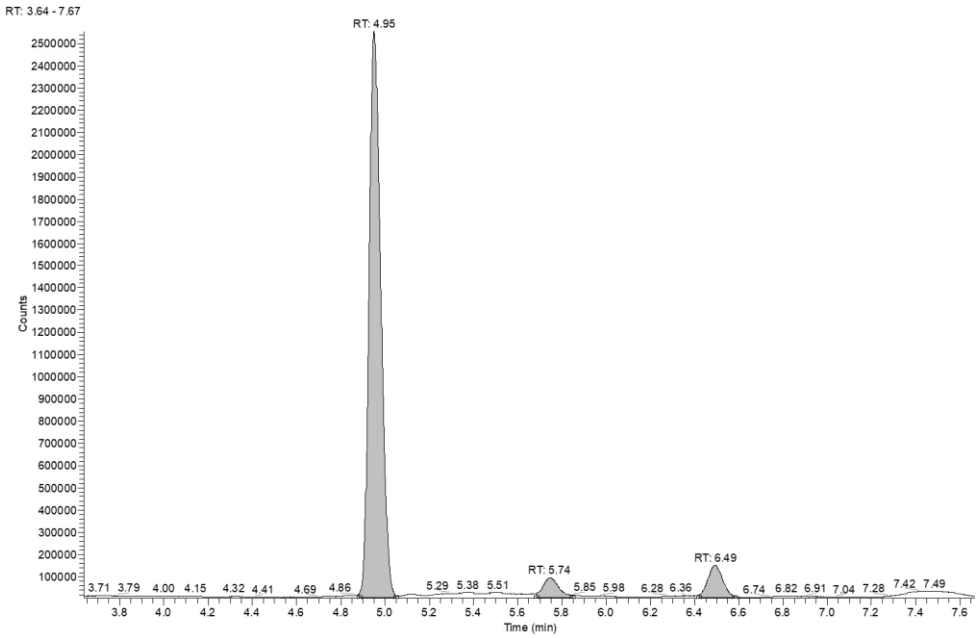

Apex RT	Start RT	End RT	Area	%Area	Height	%Height
5.78	5.7	5.89	3882954.5	54.79	909400	57.14
6.53	6.45	6.65	3203607	45.21	682200	42.86

Complex. Temp. (2) (20, 0, −20, −60 °C)

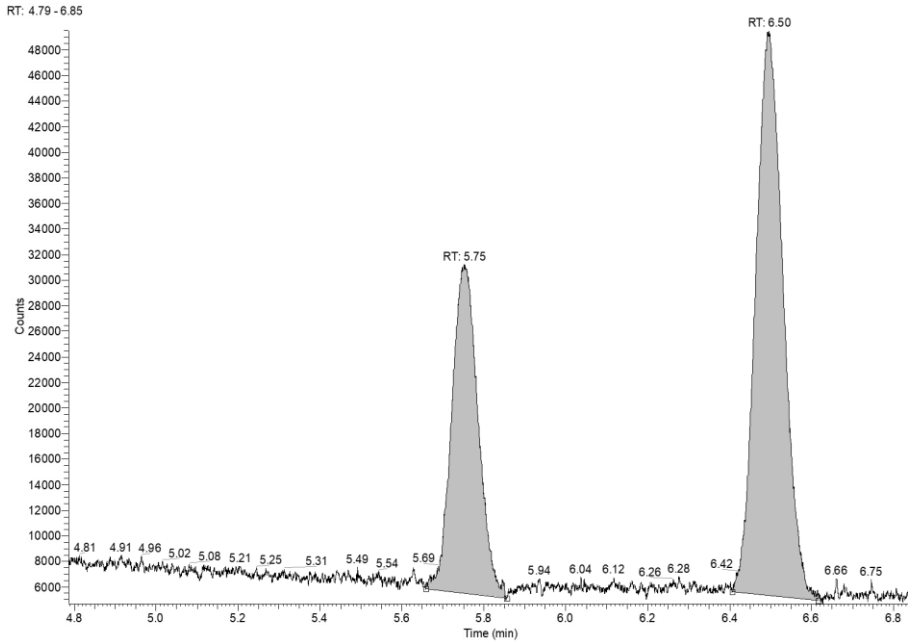

Apex RT	Start RT	End RT	Area	%Area	Height	%Height
5.75	5.66	5.86	114832.207	35.89	25750.173	36.85
6.5	6.41	6.62	205115.966	64.11	44130.799	63.15

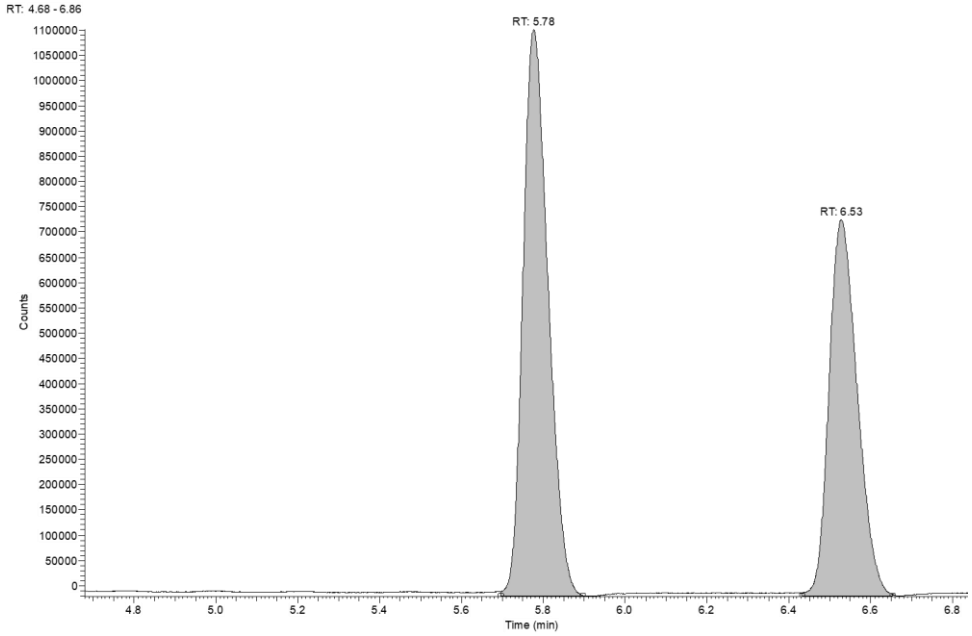

Apex RT	Start RT	End RT	Area	%Area	Height	%Height
5.78	5.7	5.9	4786848.5	57.3	1121700	60.09
6.53	6.43	6.65	3566711	42.7	745100	39.91

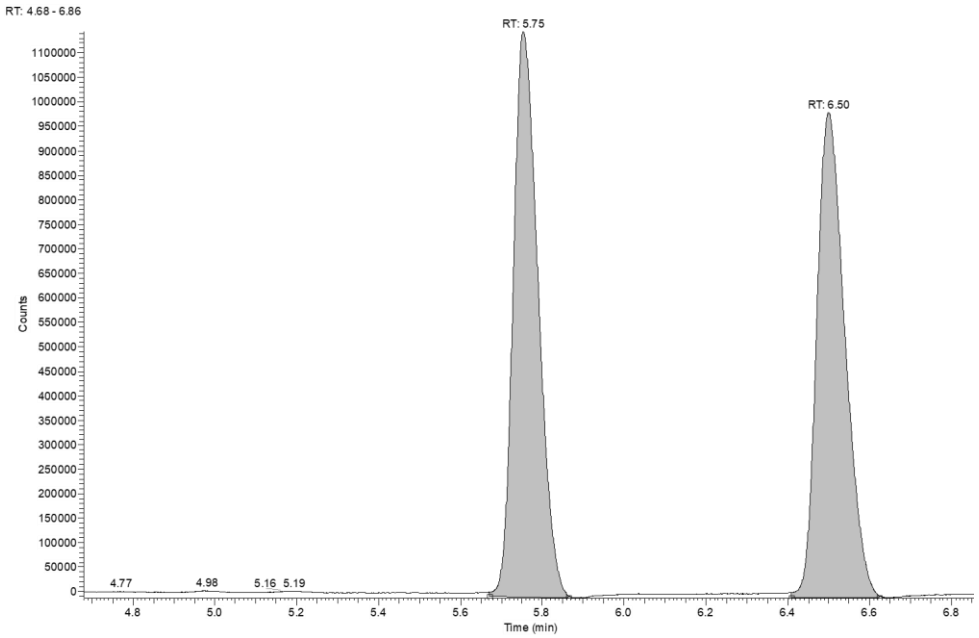

Apex RT	Start RT	End RT	Area	%Area	Height	%Height
5.75	5.67	5.86	4865524.08	50.61	1154657.49	53.8
6.5	6.41	6.62	4747932.5	49.39	991650	46.2

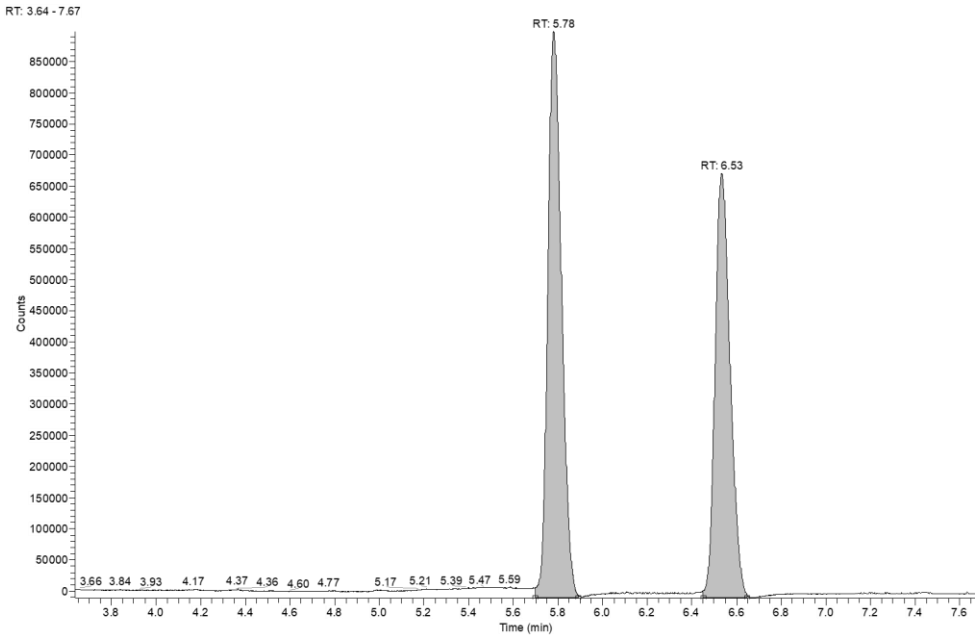

Apex RT	Start RT	End RT	Area	%Area	Height	%Height
5.78	5.7	5.89	3882954.5	54.79	909400	57.14
6.53	6.45	6.65	3203607	45.21	682200	42.86

Comp. Temp. (3) (20, 0, −20, −40, −60 °C

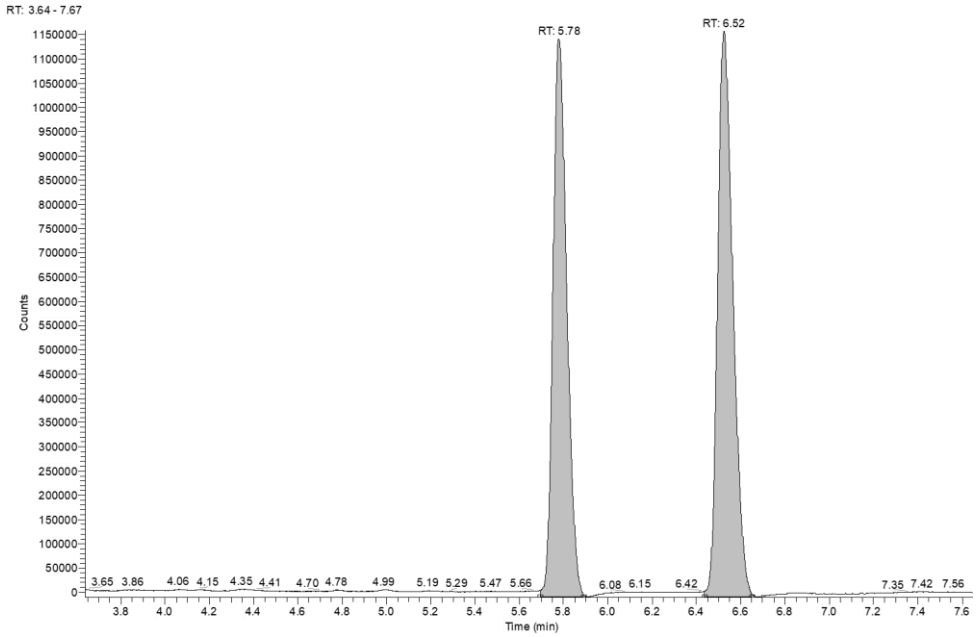

Apex RT	Start RT	End RT	Area	%Area	Height	%Height
5.78	5.7	5.89	5000726	46.98	1151850	49.64
6.52	6.44	6.65	5643640.5	53.02	1168600	50.36

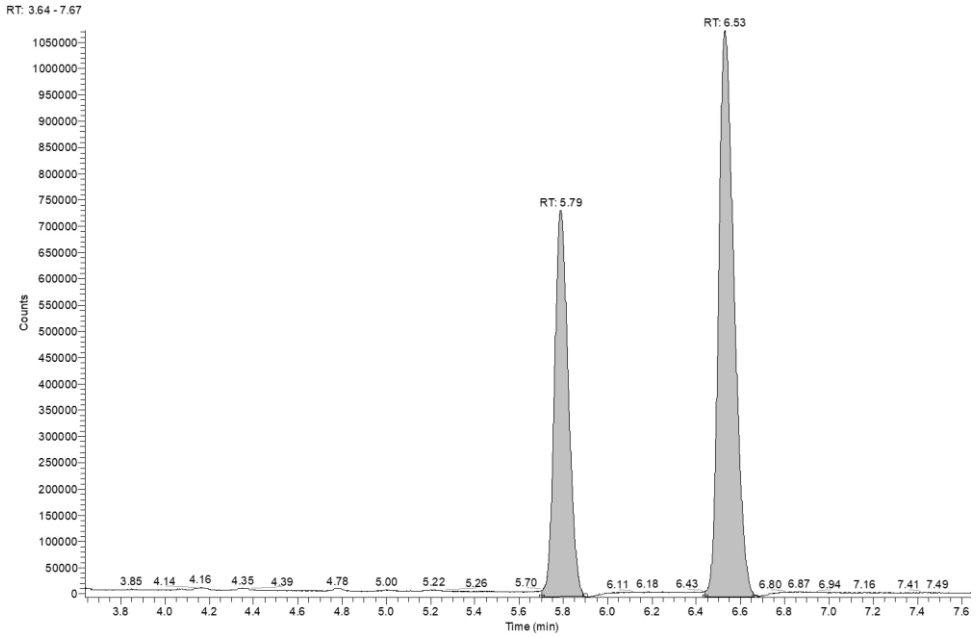

Apex RT	Start RT	End RT	Area	%Area	Height	%Height
5.79	5.7	5.9	3200282	37.71	735157.877	40.55
6.53	6.44	6.66	5286359	62.29	1077950	59.45

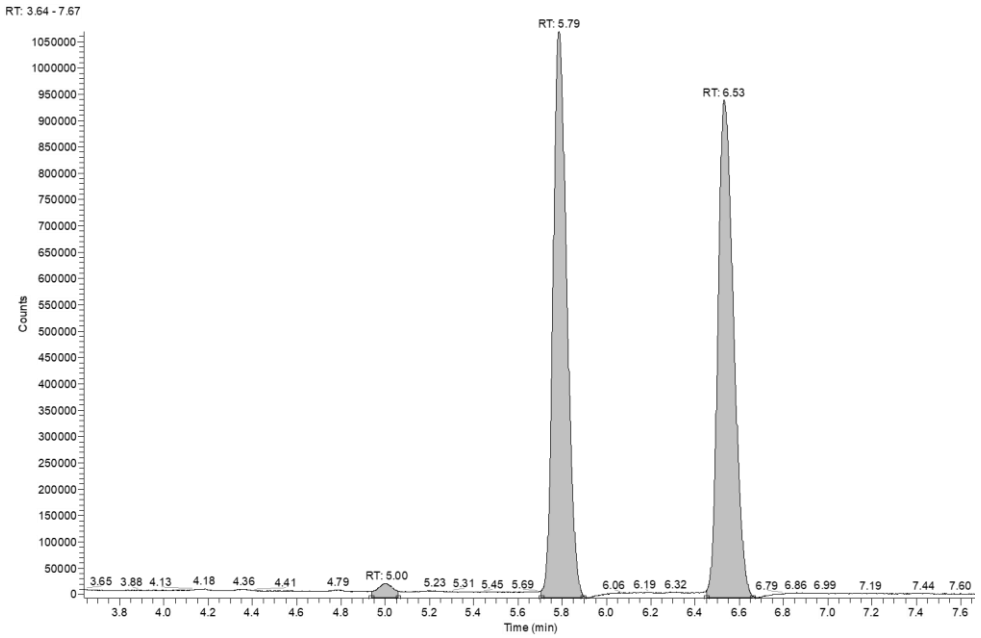

Apex RT	Start RT	End RT	Area	%Area	Height	%Height
5	4.94	5.06	145097	1.53	28200	1.37
5.79	5.71	5.89	4657917.5	49.2	1076450	52.48
6.53	6.45	6.66	4664161	49.27	946400	46.14

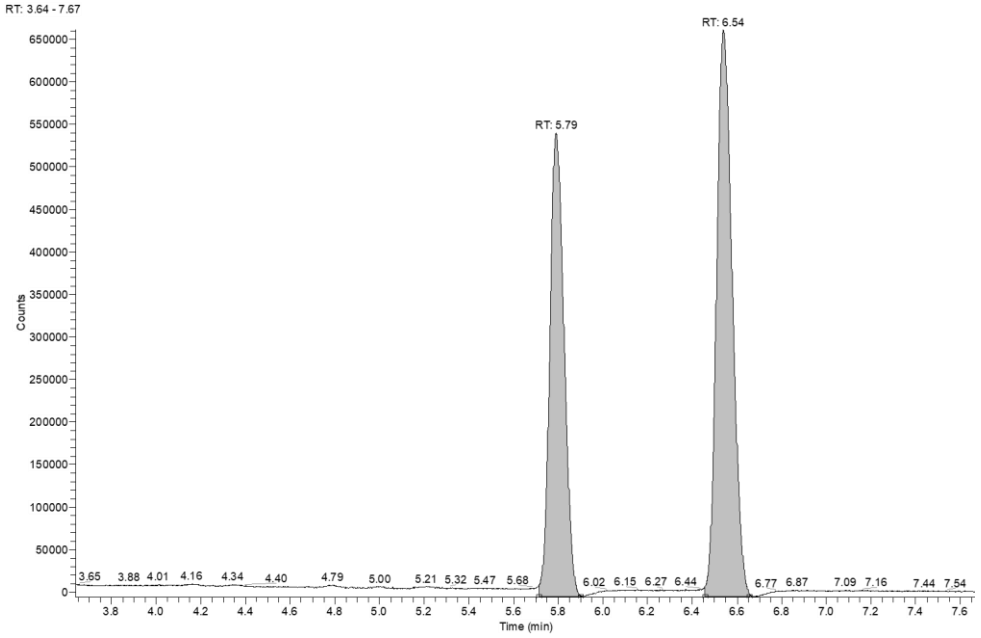

Apex RT	Start RT	End RT	Area	%Area	Height	%Height
5.79	5.71	5.9	2413976	42.56	545450	44.99
6.54	6.46	6.65	3257717.5	57.44	666950	55.01

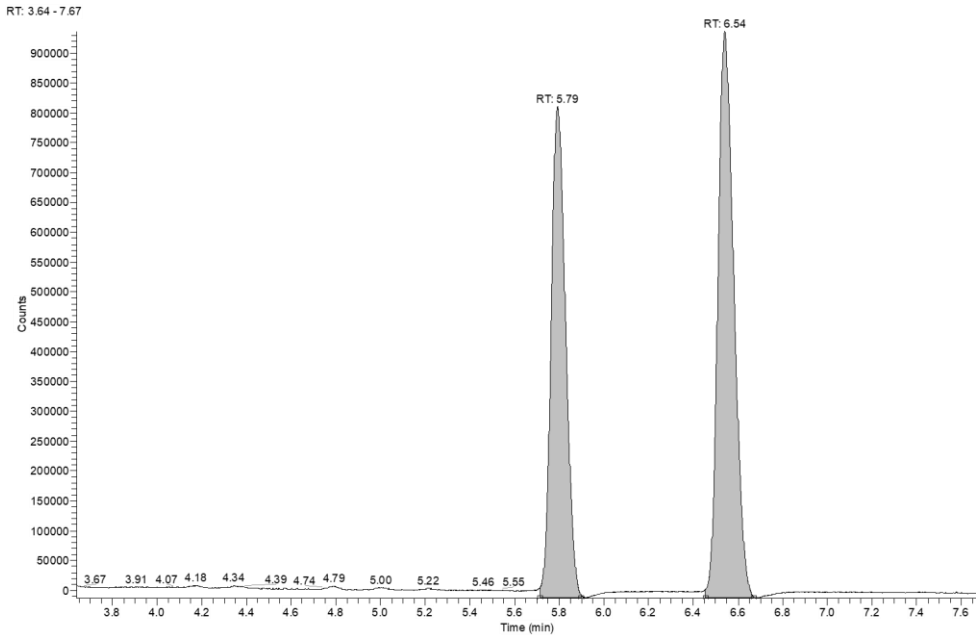

Apex RT	Start RT	End RT	Area	%Area	Height	%Height
5.79	5.71	5.9	3711807	43.99	823600	46.45
6.54	6.45	6.67	4726176.5	56.01	949500	53.55

Const. Temp (0, –20, –40 °C

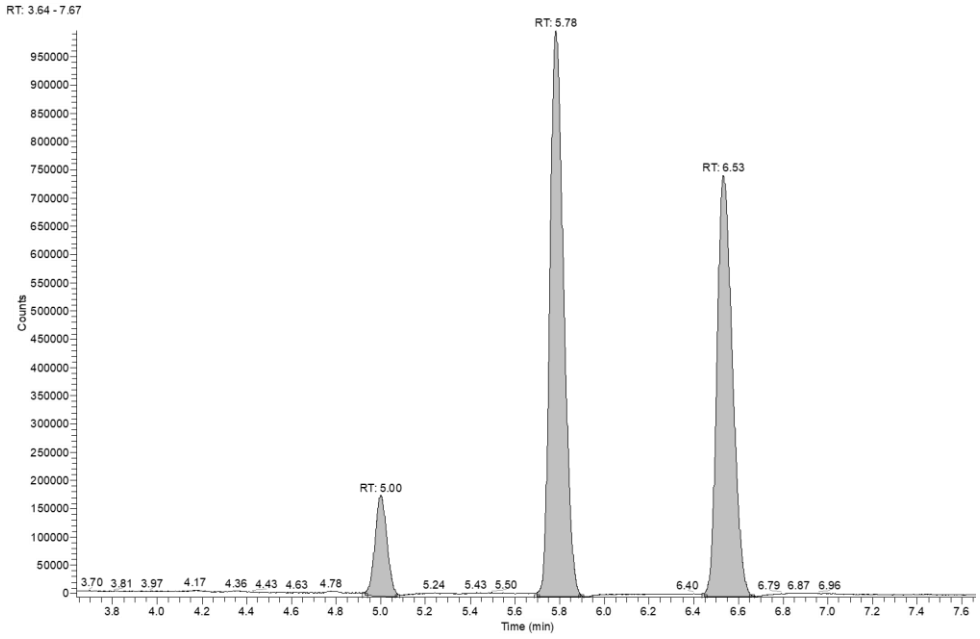

Apex RT	Start RT	End RT	Area	%Area	Height	%Height
5	4.93	5.07	674712.229	7.87	178316.288	9.25
5.78	5.7	5.89	4294278.5	50.08	1002750	52.01
6.53	6.45	6.66	3605373	42.05	746750	38.74

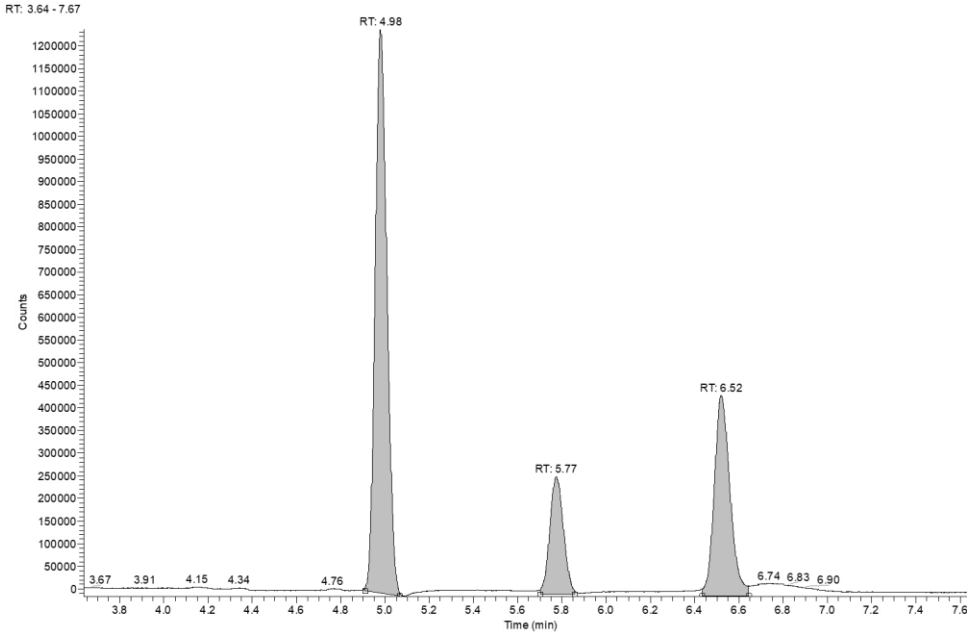

Apex RT	Start RT	End RT	Area	%Area	Height	%Height
4.98	4.91	5.06	4596069.85	57.99	1245113.47	63.9
5.77	5.7	5.86	1125238.4	14.2	260311.503	13.36
6.52	6.43	6.64	2203820.5	27.81	443100	22.74

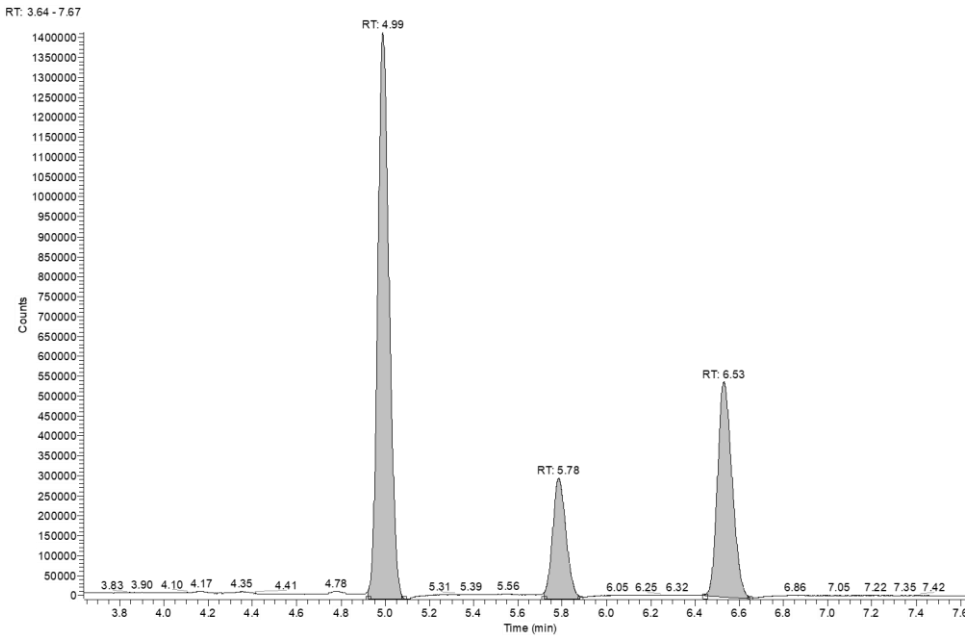

Apex RT	Start RT	End RT	Area	%Area	Height	%Height
4.99	4.92	5.08	5151772.5	57.73	1421450	62.75
5.78	5.72	5.88	1289893.5	14.45	303550	13.4
6.53	6.45	6.65	2482228.07	27.82	540117.244	23.85

Ala-3 temperature dependent experiments with MAA (20 °C, –20 °C, –40 °C):

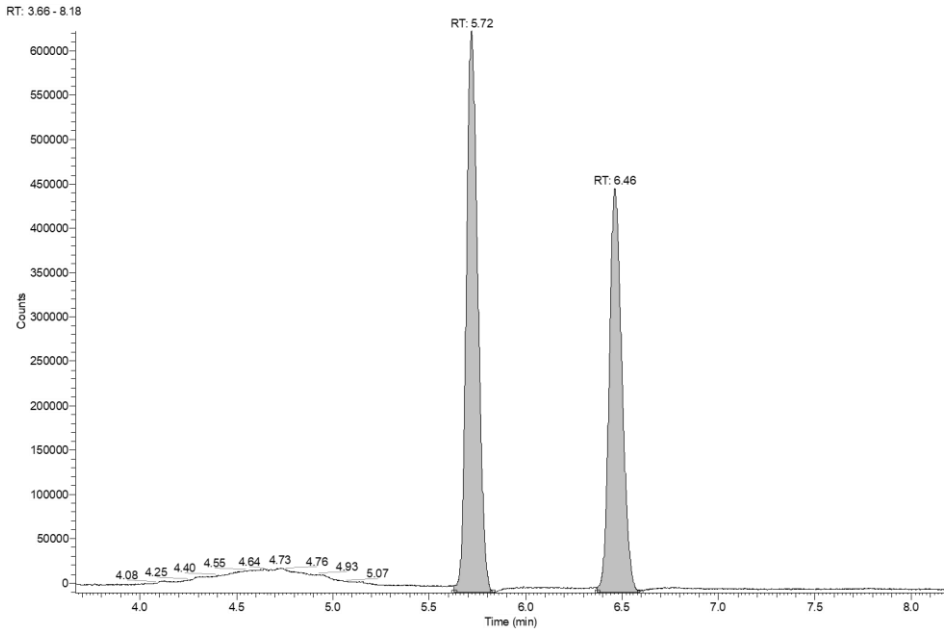

Apex RT	Start RT	End RT	Area	%Area	Height	%Height
5.72	5.63	5.83	2627157	55.73	632550	58.12
6.46	6.37	6.59	2087112.5	44.27	455750	41.88

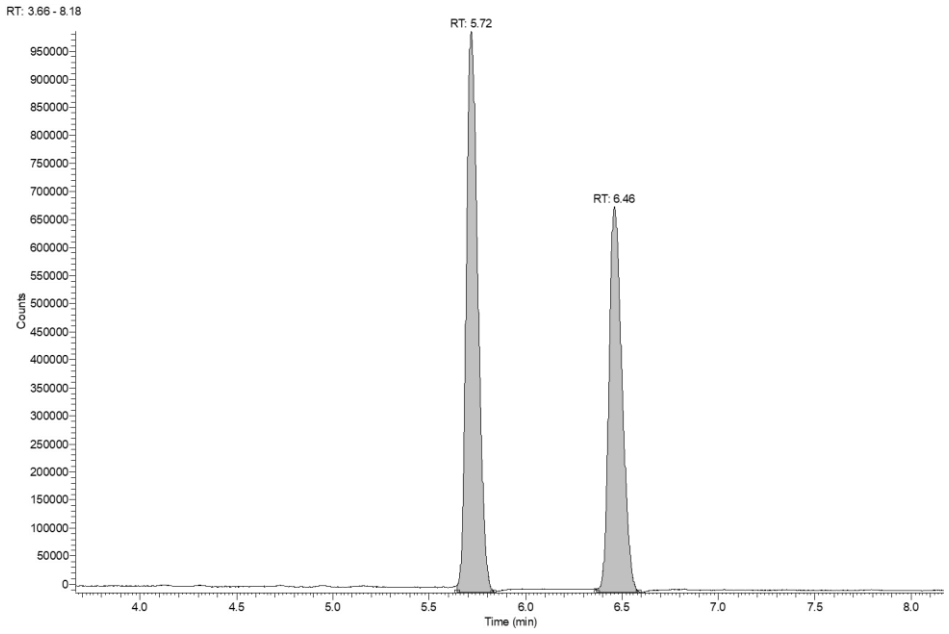

Apex RT	Start RT	End RT	Area	%Area	Height	%Height
5.72	5.64	5.83	4202993	56.42	1000600	59.25
6.46	6.37	6.58	3246051	43.58	688100	40.75

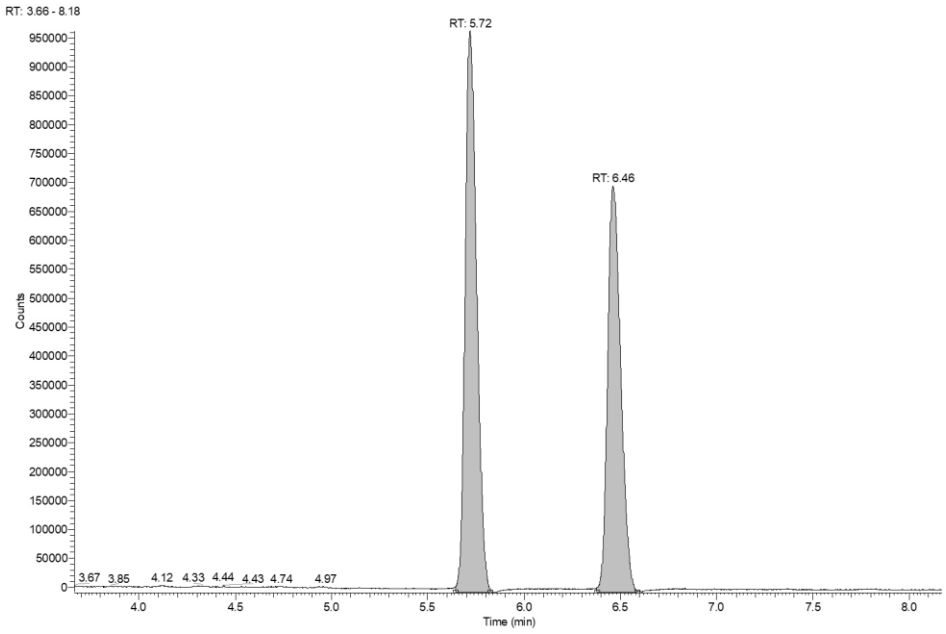

Apex RT	Start RT	End RT	Area	%Area	Height	%Height
5.72	5.64	5.82	4055622	54.92	970300	58.01
6.46	6.38	6.59	3329386	45.08	702450	41.99

Bibliography

[1] G. H. Christie, J. Kenner, *Journal of the Chemical Society, Transactions* **1922**, *121*, 614-620.

[2] R. Kuhn, in *Stereochemie* (Ed.: K. Freudenberg), Franz Deuticke, Leipzig, **1933**, pp. 803-824.

[3] G. Bringmann, A. J. Price Mortimer, P. A. Keller, M. J. Gresser, J. Garner, M. Breuning, *Angew. Chem. Int. Ed.* **2005**, *44*, 5384-5427.

[4] E. H. Woodruff, R. Adams, *Journal of the American Chemical Society* **1932**, *54*, 1977-1982.

[5] K. Mislow, M. A. W. Glass, H. B. Hopps, E. Simon, G. H. Wahl, *Journal of the American Chemical Society* **1964**, *86*, 1710-1733.

[6] E. L. Eliel, *Stereochemistry of organic compounds*, Wiley, New York, **1994**.

[7] E. P. Kyba, G. W. Gokel, F. De Jong, K. Koga, L. R. Sousa, M. G. Siegel, L. Kaplan, G. D. Y. Sogah, D. J. Cram, *The Journal of Organic Chemistry* **1977**, *42*, 4173-4184.

[8] M. Ōki, in *Topics in Stereochemistry, Vol. 14* (Ed.: N. L. A. Ernest L. Eliel, Samuel H. Wilen), John Wiley & Sons, Inc., New York, **1983**, pp. 3-5.

[9] E. Kumarasamy, R. Raghunathan, M. P. Sibi, J. Sivaguru, *Chem. Rev.* **2015**, *115*, 11239-11300.

[10] A. Miyashita, A. Yasuda, H. Takaya, K. Toriumi, T. Ito, T. Souchi, R. Noyori, *Journal of the American Chemical Society* **1980**, *102*, 7932-7934.

[11] J. K. Cheng, S.-H. Xiang, S. Li, L. Ye, B. Tan, *Chem. Rev.* **2021**, *121*, 4805-4902.

[12] B. S. L. Collins, J. C. M. Kistemaker, E. Otten, B. L. Feringa, *Nature Chemistry* **2016**, *8*, 860-866.

[13] S. Erbas-Cakmak, D. A. Leigh, C. T. McTernan, A. L. Nussbaumer, *Chem. Rev.* **2015**, *115*, 10081-10206.

[14] S. P. Fletcher, F. Dumur, M. M. Pollard, B. L. Feringa, *Science* **2005**, *310*, 80-82.

[15] K. Takaishi, M. Yasui, T. Ema, *Journal of the American Chemical Society* **2018**, *140*, 5334-5338.

[16] aD. J. Cram, J. M. Cram, *Science* **1974**, *183*, 803-809; bM. Sapotta, P. Spenst, C. R. Saha-Möller, F. Würthner, *Organic Chemistry Frontiers* **2019**, *6*, 892-899.

[17] J. M. Lavin, K. D. Shimizu, *Org. Lett.* **2006**, *8*, 2389-2392.

[18] A. Ahmed, R. A. Bragg, J. Clayden, L. W. Lai, C. McCarthy, J. H. Pink, N. Westlund, S. A. Yasin, *Tetrahedron* **1998**, *54*, 13277-13294.

[19] S. R. LaPlante, P. J. Edwards, L. D. Fader, A. Jakalian, O. Hucke, *ChemMedChem* **2011**, *6*, 505-513.

[20] L. C. Mayer, S. Heitsch, O. Trapp, *Accounts of Chemical Research* **2022**, *55*, 3345-3361.

[21] M. Reist, B. Testa, P.-A. Carrupt, M. Jung, V. Schurig, *Chirality* **1995**, *7*, 396-400.

[22] L. Meca, D. Řeha, Z. Havlas, *The Journal of Organic Chemistry* **2003**, *68*, 5677-5680.

[23] M. Cavazza, M. Zandomeneghi, A. Ouchi, Y. Koga, *Journal of the American Chemical Society* **1996**, *118*, 9990-9991.

[24] T. Hattori, Y. Shimazumi, H. Goto, O. Yamabe, N. Morohashi, W. Kawai, S. Miyano, *The Journal of Organic Chemistry* **2003**, *68*, 2099-2108.

[25] H. E. Zimmerman, D. S. Crumrine, *Journal of the American Chemical Society* **1972**, *94*, 498-506.

[26] G. Bringmann, D. Vitt, J. Kraus, M. Breuning, *Tetrahedron* **1998**, *54*, 10691-10698.

[27] G. Bringmann, T. Hartung, *Liebigs Ann. Chem.* **1994**, *1994*, 313-316.
[28] C. Yu, H. Huang, X. Li, Y. Zhang, W. Wang, *Journal of the American Chemical Society* **2016**, *138*, 6956-6959.
[29] W. S. Knowles, *Accounts of Chemical Research* **1983**, *16*, 106-112.
[30] J. Wieland, B. Breit, *Nature Chemistry* **2010**, *2*, 832-837.
[31] T. Katsuki, K. B. Sharpless, *Journal of the American Chemical Society* **1980**, *102*, 5974-5976.
[32] D. J. Berrisford, C. Bolm, K. B. Sharpless, *Angewandte Chemie International Edition in English* **1995**, *34*, 1059-1070.
[33] H.-U. Blaser, *Tetrahedron: Asymmetry* **1991**, *2*, 843-866.
[34] J. L. Margitfalvi, P. Marti, A. Baiker, L. Botz, O. Sticher, *Catal. Lett.* **1990**, *6*, 281-288.
[35] K. Mikami, M. Terada, T. Korenaga, Y. Matsumoto, M. Ueki, R. Angelaud, *Angew. Chem. Int. Ed.* **2000**, *39*, 3532-3556.
[36] P. Knochel, R. D. Singer, *Chem. Rev.* **1993**, *93*, 2117-2188.
[37] G. Storch, O. Trapp, *Angew. Chem. Int. Ed.* **2015**, *54*, 3580-3586.
[38] M. Siebert, G. Storch, F. Rominger, O. Trapp, *Synthesis* **2017**, *49*, 3485-3494.
[39] J. A. Osborn, F. H. Jardine, J. F. Young, G. Wilkinson, *Journal of the Chemical Society A: Inorganic, Physical, Theoretical* **1966**, 1711-1732.
[40] L. Horner, H. Winkler, *Justus Liebigs Annalen der Chemie* **1965**, *685*, 1-10.
[41] L. Horner, H. Winkler, A. Rapp, A. Mentrup, H. Hoffmann, P. Beck, *Tetrahedron Lett.* **1961**, *2*, 161-166.
[42] aO. Korpiun, R. A. Lewis, J. Chickos, K. Mislow, *Journal of the American Chemical Society* **1968**, *90*, 4842-4846; bO. Korpiun, K. Mislow, *Journal of the American Chemical Society* **1967**, *89*, 4784-4786.
[43] T. N. Foundation, **2001**.
[44] B. D. Vineyard, W. S. Knowles, M. J. Sabacky, G. L. Bachman, D. J. Weinkauff, *Journal of the American Chemical Society* **1977**, *99*, 5946-5952.
[45] R. Noyori, *Angew. Chem. Int. Ed.* **2002**, *41*, 2008-2022.
[46] S. Mori , T. Vreven , K. Morokuma, *Chemistry – An Asian Journal* **2006**, *1*, 391-403.
[47] G. Zhu, P. Cao, Q. Jiang, X. Zhang, *Journal of the American Chemical Society* **1997**, *119*, 1799-1800.
[48] J. M. Brown, *Chem. Soc. Rev.* **1993**, *22*, 25-41.
[49] C. R. Landis, J. Halpern, *Journal of the American Chemical Society* **1987**, *109*, 1746-1754.
[50] J. M. Brown, P. A. Chaloner, G. A. Morris, *Journal of the Chemical Society, Perkin Transactions 2* **1987**, 1583-1588.
[51] I. D. Gridnev, T. Imamoto, *Accounts of Chemical Research* **2004**, *37*, 633-644.
[52] A. S. S. Chan, J. J. Pluth, J. Halpern, *J. Am. Chem. Soc.* **1980**, *102*, 5954.
[53] P. S. Chua, N. K. Roberts, B. Bosnich, S. J. Okrasinski, J. Halpern, *J. Chem. Soc., Chem. Commun.* **1981**, *1278*, 1280.
[54] B. R. Bender, M. Koller, D. Nanz, W. von Philipsborn, *Journal of the American Chemical Society* **1993**, *115*, 5889-5890.
[55] T. Schmidt, W. Baumann, H.-J. Drexler, A. Arrieta, D. Heller, H. Buschmann, *Organometallics* **2005**, *24*, 3842-3848.
[56] J.-M. Menke, O. Trapp, *The Journal of Organic Chemistry* **2022**, *87*, 11165-11171.

[57] A. C. Mendes, E. T. Baran, R. L. Reis, H. S. Azevedo, *WIREs Nanomedicine and Nanobiotechnology* **2013**, *5*, 582-612.
[58] B. H. Northrop, Y.-R. Zheng, K.-W. Chi, P. J. Stang, *Accounts of Chemical Research* **2009**, *42*, 1554-1563.
[59] D. Mandal, A. Nasrolahi Shirazi, K. Parang, *Organic & Biomolecular Chemistry* **2014**, *12*, 3544-3561.
[60] J. M. Lehn, *Accounts of Chemical Research* **1978**, *11*, 49-57.
[61] D. J. Cram, J. M. Cram, *Accounts of Chemical Research* **1978**, *11*, 8-14.
[62] K. Aikawa, K. Mikami, *Chem. Commun.* **2012**, *48*, 11050-11069.
[63] J. F. Scholtes, O. Trapp, *Synlett* **2020**, *32*, 971-980.
[64] K. Cobos, R. Rodríguez, E. Quiñoá, R. Riguera, F. Freire, *Angew. Chem. Int. Ed.* **2020**, *59*, 23724-23730.
[65] Y. Nagata, S. Ohashi, M. Suginome, *J. Polym. Sci., Part A: Polym. Chem.* **2012**, *50*, 1564-1571.
[66] T. Yamamoto, R. Murakami, S. Komatsu, M. Suginome, *Journal of the American Chemical Society* **2018**, *140*, 3867-3870.
[67] M. Rieger, F. H. Westheimer, *Journal of the American Chemical Society* **1950**, *72*, 19-28.
[68] F. Maier, O. Trapp, *Angew. Chem. Int. Ed.* **2014**, *53*, 8756-8760.
[69] G. Storch, S. Pallmann, F. Rominger, O. Trapp, *Beilstein Journal of Organic Chemistry* **2016**, *12*, 1453-1458.
[70] G. Storch, L. Deberle, J.-M. Menke, F. Rominger, O. Trapp, *Chirality* **2016**, *28*, 744-748.
[71] G. Storch, O. Trapp, *Chirality* **2018**, *30*, 1150-1160.
[72] aH. Frank, G. J. Nicholson, E. Bayer, *Angewandte Chemie International Edition in English* **1978**, *17*, 363-365; bB. Feibush, *Chirality* **1998**, *10*, 382-395; cW. H. Pirkle, W. E. Bowen, *J. High. Resolut. Chromatogr.* **1994**, *17*, 629-633.
[73] P. A. Levkin, A. Levkina, H. Czesla, V. Schurig, *Anal. Chem.* **2007**, *79*, 4401-4409.
[74] J. F. Scholtes, O. Trapp, *Angew. Chem. Int. Ed.* **2019**, *58*, 6306-6310.
[75] aJ. F. Scholtes, O. Trapp, *Chemistry – A European Journal* **2019**, *25*, 11707-11714; bJ. F. Scholtes, O. Trapp, *Chirality* **2019**, *31*, 1028-1042.
[76] J. F. Scholtes, O. Trapp, *Organometallics* **2019**, *38*, 3955-3960.
[77] G. Storch, M. Siebert, F. Rominger, O. Trapp, *Chem. Commun.* **2015**, *51*, 15665-15668.
[78] G. Storch, O. Trapp, *Nature Chemistry* **2017**, *9*, 179-187.
[79] M. Schmitkamp, D. Chen, W. Leitner, J. Klankermayer, G. Franciò, *Chem. Commun.* **2007**, 4012-4014.
[80] P. Oczipka, D. Müller, W. Leitner, G. Franciò, *Chemical Science* **2016**, *7*, 678-683.
[81] P. J. Donoghue, P. Helquist, P.-O. Norrby, O. Wiest, *Journal of the American Chemical Society* **2009**, *131*, 410-411.
[82] K. Mikami, M. Yamanaka, *Chem. Rev.* **2003**, *103*, 3369-3400.
[83] C. Puchot, O. Samuel, E. Dunach, S. Zhao, C. Agami, H. B. Kagan, *Journal of the American Chemical Society* **1986**, *108*, 2353-2357.
[84] M. Terada, K. Mikami, T. Nakai, *J. Chem. Soc., Chem. Commun.* **1990**, 1623-1624.
[85] N. Oguni, Y. Matsuda, T. Kaneko, *Journal of the American Chemical Society* **1988**, *110*, 7877-7878.

[86] M. Kitamura, S. Suga, M. Niwa, R. Noyori, *Journal of the American Chemical Society* **1995**, *117*, 4832-4842.
[87] C. Bolm, *Tetrahedron: Asymmetry* **1991**, *2*, 701-704.
[88] S. Kanemasa, Y. Oderaotoshi, S.-i. Sakaguchi, H. Yamamoto, J. Tanaka, E. Wada, D. P. Curran, *Journal of the American Chemical Society* **1998**, *120*, 3074-3088.
[89] D. A. Evans, J. A. Murry, M. C. Kozlowski, *Journal of the American Chemical Society* **1996**, *118*, 5814-5815.
[90] D. Guillaneux, S.-H. Zhao, O. Samuel, D. Rainford, H. B. Kagan, *Journal of the American Chemical Society* **1994**, *116*, 9430-9439.
[91] T. Satyanarayana, S. Abraham, H. B. Kagan, *Angew. Chem. Int. Ed.* **2009**, *48*, 456-494.
[92] F. C. Frank, *Biochim. Biophys. Acta* **1953**, *11*, 459-463.
[93] M. Kitamura, S. Okada, S. Suga, R. Noyori, *Journal of the American Chemical Society* **1989**, *111*, 4028-4036.
[94] H. Wynberg, B. Feringa, *Tetrahedron* **1976**, *32*, 2831-2834.
[95] B. Feringa, H. Wynberg, *Journal of the American Chemical Society* **1976**, *98*, 3372-3373.
[96] T. Shibata, H. Morioka, T. Hayase, K. Choji, K. Soai, *Journal of the American Chemical Society* **1996**, *118*, 471-472.
[97] W. H. Pirkle, P. G. Murray, D. J. Rausch, S. T. McKenna, *The Journal of Organic Chemistry* **1996**, *61*, 4769-4774.
[98] W. H. Pirkle, P. G. Murray, *J. High. Resolut. Chromatogr.* **1993**, *16*, 285-288.
[99] W. H. Pirkle, P. G. Murray, S. R. Wilson, *The Journal of Organic Chemistry* **1996**, *61*, 4775-4777.
[100] aD. G. Blackmond, *Chem. Rev.* **2020**, *120*, 4831-4847; bL. Huber, O. Trapp, *Origins of Life and Evolution of Biospheres* **2022**, *52*, 75-91.
[101] Y. Geiger, T. Achard, A. Maisse-François, S. Bellemin-Laponnaz, *Nature Catalysis* **2020**, *3*, 422-426.
[102] Y. Geiger, T. Achard, A. Maisse-François, S. Bellemin-Laponnaz, *Chirality* **2020**, *32*, 1250-1256.
[103] T. Buhse, J.-M. Cruz, M. E. Noble-Terán, D. Hochberg, J. M. Ribó, J. Crusats, J.-C. Micheau, *Chem. Rev.* **2021**, *121*, 2147-2229.
[104] aK. Soai, *Tetrahedron* **2022**, *124*, 133017; bK. Soai, S. Niwa, H. Hori, *J. Chem. Soc., Chem. Commun.* **1990**, 982-983.
[105] K. Soai, T. Shibata, H. Morioka, K. Choji, *Nature* **1995**, *378*, 767-768.
[106] C. Romagnoli, B. Sieng, M. Amedjkouh, *Chirality* **2020**, *32*, 1143-1151.
[107] M. Funes-Maldonado, B. Sieng, M. Amedjkouh, *Org. Lett.* **2016**, *18*, 2536-2539.
[108] G. Rotunno, D. Petersen, M. Amedjkouh, *ChemSystemsChem* **2020**, *2*, e1900060.
[109] D. G. Blackmond, *Tetrahedron: Asymmetry* **2006**, *17*, 584-589.
[110] I. D. Gridnev, J. M. Serafimov, H. Quiney, J. M. Brown, *Organic & Biomolecular Chemistry* **2003**, *1*, 3811-3819.
[111] T. Gehring, M. Quaranta, B. Odell, D. G. Blackmond, J. M. Brown, *Angew. Chem. Int. Ed.* **2012**, *51*, 9539-9542.
[112] S. V. Athavale, A. Simon, K. N. Houk, S. E. Denmark, *Nature Chemistry* **2020**, *12*, 412-423.
[113] S. V. Athavale, A. Simon, K. N. Houk, S. E. Denmark, *Journal of the American Chemical Society* **2020**, *142*, 18387-18406.

[114] O. Trapp, S. Lamour, F. Maier, A. F. Siegle, K. Zawatzky, B. F. Straub, *Chemistry – A European Journal* **2020**, *26*, 15871-15880.
[115] O. Trapp, *Frontiers in Chemistry* **2020**, *8*.
[116] Y. Geiger, *Chem. Soc. Rev.* **2022**, *51*, 1206-1211.
[117] S. Heitsch, L. C. Mayer, Y. L. Pignot, O. Trapp, *Chirality* **2023**, *35*, 549-561.
[118] J. Andersen, U. Madsen, F. Björkling, X. Liang, *Synlett* **2005**, *2005*, 2209-2213.
[119] aJ. Sun, J. Vogel, L. Chen, A. L. Schleper, T. Bergner, A. J. C. Kuehne, M. von Delius, *Chemistry – A European Journal* **2022**, *28*, e202104116; bC. Shao, X. Wang, Q. Zhang, S. Luo, J. Zhao, Y. Hu, *The Journal of Organic Chemistry* **2011**, *76*, 6832-6836.
[120] K. Oh, Z. Guan, *Chem. Commun.* **2006**, 3069-3071.
[121] B. C. Boren, S. Narayan, L. K. Rasmussen, L. Zhang, H. Zhao, Z. Lin, G. Jia, V. V. Fokin, *Journal of the American Chemical Society* **2008**, *130*, 8923-8930.
[122] P. S. Donnelly, S. D. Zanatta, S. C. Zammit, J. M. White, S. J. Williams, *Chem. Commun.* **2008**, 2459-2461.
[123] M. Siebert, G. Storch, O. Trapp, *Organic Process Research & Development* **2020**, *24*, 1304-1309.
[124] A. Serra, M. Pineiro, C. I. Santos, A. M. d. A. Rocha Gonsalves, M. Abrantes, M. Laranjo, M. F. Botelho, *Photochem. Photobiol.* **2010**, *86*, 206-212.
[125] T. Ikai, Y. Okamoto, *Chem. Rev.* **2009**, *109*, 6077-6101.
[126] O. Trapp, *Anal. Chem.* **2006**, *78*, 189-198.
[127] O. Trapp, *J. Chromatogr. B* **2008**, *875*, 42-47.
[128] G. R. Fulmer, A. J. M. Miller, N. H. Sherden, H. E. Gottlieb, A. Nudelman, B. M. Stoltz, J. E. Bercaw, K. I. Goldberg, *Organometallics* **2010**, *29*, 2176-2179.
[129] O. Skaff, K. A. Jolliffe, C. A. Hutton, *The Journal of Organic Chemistry* **2005**, *70*, 7353-7363.
[130] K. Verma, T. Zang, T. M. Penning, P. C. Trippier, *J. Med. Chem.* **2019**, *62*, 3590-3616.
[131] D. M. Shendage, R. Fröhlich, G. Haufe, *Org. Lett.* **2004**, *6*, 3675-3678.
[132] M. C. Holland, J. B. Metternich, C. Daniliuc, W. B. Schweizer, R. Gilmour, *Chemistry – A European Journal* **2015**, *21*, 10031-10038.

Danksagung

Als allererstes möchte ich mich bei *Prof. Oliver Trapp* bedanken, dafür mich in seinen wunderbaren Arbeitskreis aufgenommen zu haben. Das Vertrauen das Du mir entgegengebracht hast, sowie deine unvergleichliche Zuversicht, auch bei größeren chemischen Herausforderungen, haben den Rahmen geschaffen diese Arbeit erfolgreich anzufertigen. Mit den Worten unserer Nathalie möchte ich sagen: „Vielen herzlichen Dank!“

Des Weiteren möchte ich *Prof. Hoffmann-Röder* herzlichst für die Zweitkorrektur meiner Arbeit danken. Außerdem danke ich *Prof. Karaghiosoff*, *Prof. Markic*, *Prof. Bracher* und *Prof. Klapötke*, dass sie sich die Zeit genommen haben Teil meiner Promotionskommission zu sein.

Allen Mitarbeitern der Ludwig-Maximilians-Universität, im Besonderen der Feinmechanik, den Glasbläsern, sowie der gesamten Versorgung und vor allem der Analytik Abteilung gilt mein großer Dank.

Dem gesamten AK möchte ich an dieser Stelle noch einmal sagen: ich werde Euch vermissen! Jeder von Euch hat auf seine individuelle Art dazu beigetragen ein super Arbeitsumfeld zu schaffen. Ich bin mir sicher, dass mich die ein oder anderen auch weiterhin begleiten werden! Aber auch der beste Arbeitskreis funktioniert nicht ohne fleißige Helfer wie *Carrie*, die buchstäblich rund um die Uhr das wichtige NMR am Laufen hält, *Brigitte*, die sich um jegliche Bestellungen und Firmeninteraktionen kümmert, (die Neue-) *Nathalie*, die im Labor jetzt für alle eine Helfende Hand ist, *Heike* die auf ihre unverwechselbare Art im Sekretariat alles Wichtige managed und *Claudia*, von der man bei den unterschiedlichsten Problemen volle Rückendeckung erhält. Ihr seid die Basis unseres reibungslosen Alltags, Danke dafür!

Alex, als selbsternanntes „Mädchen für Alles“, durfte mir nicht nur einmal verschiedene analytische Gerät erklären und Fragen dazu beantworten. Danke für Deine Geduld und anhaltende Begeisterung, wenn es um technisch anspruchsvolle Problemlösungen geht! Insgesamt gilt mein Dank allen, die für die Instanthaltung wichtiger Geräte zuständig sind!

Aus dem Labor F3.012 möchte ich mich bei allen ehemaligen und aktiven Doktoranden/Masteranden bedanken. Die Zeit im Labor mit Euch war nie langweilig! Insbesondere *Jan* danke ich dafür, mich ursprünglich in den AK gebracht zu haben. Nicht nur die schönen Weinabende mit Dir haben den Laboralltag gebührend abgerundet! Außerdem danke ich *Flo* (neu), dass er die kleinen „großen“ Fußstapfen in unserer Box auf seine Art hervorragend ausfüllt.

Für das sorgfältige Korrekturlesen dieser Arbeit danke ich Christoph, Simone und Luca von Herzen! So mancher Knoten wurde durch Euer Zutun erst gelöst.

An meine Praktikanten, *Dominik*, *Yanis*, *Alexander*, *Julian*, *Carolin* und *Nadine* geht ein großer Dank für ihre Hilfe. Ihr habt diese Arbeit entschieden weitergebracht (weitergekocht). Durch die Betreuung Eurer Projekte habe ich auch persönlich viel dazugelernt.

In den letzten Jahren durfte ich mit meinen Kollegen auch diverse Abenteuer außerhalb des Labors erleben. Ob musikalische Reisen mit *Flo* (alt), der mich glücklicherweise zurück zur Musik gebracht hat, oder Wanderungen mit *Conny* und *Maren*, es war immer ein Erlebnis.

Für meine kulinarische Weiterbildung bedanke ich mich bei der *Otto-Runde*. Danke, dass ihr so enthusiastisch seid, dass wir es bis nach London geschafft haben! Ich freue mich schon auf das nächste Ottovent mit Euch!

Danke an die Sushi und Sekt „Sekte“ bestehend aus *Anna*, *Jenny* und *Simone*, die mich zuverlässig zum Lachen bringt und jedes Mal aufs Neue einen phänomenalen Abend garantiert. Ihr seid eine einzigartige Kombination!

Danke *Marian*, vom neuen Kollegen zum Mitbewohner zum Marian, der vermutlich immer irgendwie da sein wird. Deine Kreativität sucht ihresgleichen! Ich bin dankbar für deine inspirierenden Eingaben und dein Vertrauen in und außerhalb des Labors.

Danke *Simone*, für unsere gemeinsame Zeit als Bench-Buddys. Ich vermisse Dich schon jetzt! Ich schätze mich glücklich Dich als Laborpartnerin zugeteilt und als enge Freundin gewonnen zu haben. Welch Erfolg unserer Promotion!

Danke *Christoph*, dass du mir nicht nur meine Momente der Ruhe gibst, sondern mich auch immer zum Lachen bringst. Du bist mein Gegenstück, dass mich auf dem Boden der Tatsachen hält. Ich schätze mich glücklich, dass ich auf Deine Unterstützung in allen Lebenslagen bauen kann!

Zu allerletzt möchte ich mich für Eure immerwährende Unterstützung bedanken. Liebe *Mama*, lieber *Papa* und lieber *Felix*, seit ich denken kann, habt ihr immer nur das Beste für mich gewollt und Alles dafür getan. Ich kann gar nicht in Worte fassen was mir das bedeutet. Also sag ich ganz einfach DANKE und versuche es Euch weiterhin gleichzutun!